ANALYSIS OF A CORRUGATED PLATE PHOTOCATALYTIC REACTOR

by Zisheng Zhang

A Thesis
presented to the University of Waterloo
in fulfilment of the
thesis requirement of the degree of
Doctor of Philosophy
in
Chemical Engineering

Waterloo, Ontario, Canada, 1999

The University of Waterloo requires the signatures of all persons using or photocopying this thesis. Please sign below, and give address and date.

ABSTRACT

A new reactor configuration, the corrugated plate reactor, was developed and analyzed through rigorous radiation field simulation, mass transfer measurement and modeling, 4-chlorophenol degradation experiments, as well as degradation kinetics modeling. The novel reactor was then applied to remove 4-chlorophenol, 2,4-dichlorophenol, and 2,4,5-trichlorophenol mixtures from water and to pretreat a contaminated groundwater for subsequent nitrification enhancement. Flat plate as well as slurry reactor systems were also run under otherwise the same operating conditions in order to set up performance benchmarks for the novel reactor.

The radiation fields on TiO_2-coated corrugated and flat plates were modeled based on first principles. A special procedure was developed to calculate the effect of multiple reflection on radiative energy absorption. This allowed for the calculation of the local area-specific rate of energy absorption (LASREA) on the surfaces of catalyst films. Based on the results of the radiation model, the LASREA and the photon absorption efficiency were both found to be quite sensitive to the dimensions of the corrugated plates. Due to the multiple photon reflection between the conjugate wings, corrugated plates possess a superior capability for recapturing longer wavelength photons which would otherwise be reflected out of some classic reactors. This greatly improved the photon absorption efficiency and the uniformity of the radiation distribution on the catalyst films. Compared to the flat plate, corrugations enhanced the radiation absorption efficiency by up to 50% for UV-A fluorescent lamp-powered systems and more than 100% for solar-powered systems.

Mass transfer between the main stream and the surfaces of corrugated as well as flat plates was examined experimentally using the benzoic acid dissolution method. Experimental results were fitted to several relationships which can be used to calculate the average mass transfer coefficients of the tested plates under different flow conditions. A mass transfer model was developed to predict the local mass transfer coefficients on the surfaces of different

corrugated plates. Based on the results of the experiments, mass transfer coefficients were identified to be dependent on not only the flow conditions but also the angle of corrugated plates. Within the flowrate range examined, one corrugated plate showed an enhancement of overall mass transfer rates of up to 400% to 600% over that of the flat plate. This enhancement was due primarily to the large illuminated catalyst surface area in the new reactor. In addition, local mass and photon transfer rates on the corrugated plates correlated positively and therefore are complementary to each other. This result is favorable since a higher local photon absorption rate requires a higher mass transfer rate to avoid mass transfer limitation.

Based on the results of 4-chlorophenol degradation experiments, the corrugated plate reactor was up to 150% more efficient than the flat plate reactor. This energy efficiency was only about 15% lower than that of the slurry reactor. A consistent dependency of the degradation rate on the angle of the corrugated plate was observed. The optimal angle was identified to be near 7°. Under the conditions examined, the reactions in corrugated plate reactors were found to be affected by the transfer of both 4-chlorophenol and oxygen to the catalyst surfaces.

The novel reactor efficiently mineralized mixtures of 4-chlorophenol, 2,4-dichlorophenol, and 2,4,5-trichlorophenol. Photocatalytic mineralization of the groundwater contaminants was slow even after carbonate and bicarbonate were eliminated by lowering the pH. However, nitrification was enhanced significantly after only a short period of pretreatment in the photoreactor. This indicated the potential for using photocatalysis to remove inhibition from biological nitrification systems.

With only three experimentally determined parameters, the new kinetic model incorporates reaction kinetics, mass transfer as well as photon transfer. The performance of the corrugated plate reactors predicted with the model was found to agree with the experimental data reasonably well. Corrugated plates with small angles were predicted to substantially alleviate the mass transfer limitation in flat plate reactors. However, this limitation can never be essentially eliminated unless sufficiently weak radiation sources are adopted. This is probably the bottleneck of aqueous phase photocatalysis.

ACKNOWLEDGMENTS

I would like to express my deepest gratitude to my supervisors, Prof. Murray Moo-Young and Prof. William A. Anderson, for their guidance, support, and encouragement during the entire course of this work. My regards are due to Prof. Jeno M. Scharer, Prof. Robert R. Hudgins, Prof. Peter M. Huck, and Prof. Susan A. Andrews, the members of my advisory committee, for their valuable advice during this study. My sincere thanks is extended to Prof. Hugo I. de Lasa, the external examiner of my thesis, for his time and constructive comments to this thesis.

The author is thankful to Mark Sobon, Siva Ganeshalingam, Jana Otruba, and Ralph Dickhout for their analytical assistance, Frank Wassmer, Rick Hecktus, and Ernie Strutzenberger for their help in the photoreactor set-up, and Jeff Merriman (Uniroyal Chemical in Elmira of Ontario, Canada) for his help during groundwater sampling. I would also like to thank all my friends and colleagues and all staff and faculty members in the department for providing the supportive working environment.

I owe a special debt to my wife, Guiping Li, and my daughters Lisa and Eleen for their support, understanding, and patience throughout my graduate studies.

To:

my beloved wife, Guiping,

and my daughters, Lisa and Eleen

TABLE OF CONTENTS

LIST OF FIGURES

LIST OF TABLES

NOMENCLATURE

Roman Letters

A	total illuminated area of the immobilized catalyst film, m^2
ABS	UV absorbance at 224 nm, dimensionless
$a(\lambda)$	absorption coefficient of the catalyst film as a function of photon wavelength, dimensionless
B	height of the corrugated plates, B=0.05 m
C	bulk 4-chlorophenol concentration, gm^{-3}
C^{in}	Benzoic acid concentration at reactor inlet, $C^{in} = 0\ gm^{-3}$
C^{out}	Benzoic acid concentration at the reactor exit, gm^{-3}
C^*	Benzoic acid solubility in water at 26.6 °C, $C^*=3605\ gm^{-3}$
C_s	4-chlorophenol concentration on the surface of catalyst film, gm^{-3}
C_{is}	concentration of reactant "i" on the catalyst surface, gm^{-3}
C_i	concentration of reactant "i", gm^{-3}
C_j	concentration of reactant "j", gm^{-3}
C_{O2}	concentration of oxygen, gm^{-3}
d	distance between a point on the reactor cover and one on the flat plate, m
d_1	distance between a point on the reactor cover and one on the upper wing of the corrugated plate, m
d_2	distance between a point on the upper wing and one on the lower wing of the corrugated plate, m
D_{4cp}	diffusivity of 4-chlorophenol in water, m^2h^{-1}
D_{O2}	diffusivity of oxygen in water, m^2h^{-1}
Ea	activation energy, $kJmol^{-1}$
Fn_λ	fraction of the UV that go through a quarter inch Plexiglas G-UVT as a function of photon wavelength.

I	radiation intensity, Wm^{-2}
I_0	reference radiation intensity, Wm^{-2}
k_3	extinction coefficient of Plexiglas:G-UVT, m^{-1}
k_4	extinction coefficient of water (k_4=0 for 300 nm<λ<390 nm), m^{-1}
K_0	reaction rate constant, $gh^{-1}m^{-2}$
k_0	model parameter, $gh^{-1}m^{-2}$
K_{4CP}	model parameter for 4-chlorophenol, m^3g^{-1}
K_i	Langmuir adsorption constant of reactant "i", m^3g^{-1}
K_j	model parameter for reactant "j", m^3g^{-1}
K_l	reactor model parameter, m^3g^{-1}
k_L	local mass transfer coefficient at reaction site, mh^{-1}
$\bar{k}_L$	average mass transfer coefficient on the surface of catalyst film, mh^{-1}
k_{4cp}	local mass transfer coefficient of 4-chlorophenol, mh^{-1}
k_{O2}	local mass transfer coefficient of oxygen, mh^{-1}
K_{O2}	model parameter of oxygen, m^3g^{-1}
L	length of the TiO_2-coated corrugated and flat plates, L=0.5 m
n	model parameter, dimensionless
O_b	bulk oxygen concentration, gm^{-3}
P	total lamp power, kW
q	local area-specific rate of energy absorption, Wm^{-2}
q_0	reference value of the local area-specific rate of energy absorption, q_0=1 Wm^{-2}
Re	Reynolds number
Q	flowrate, m^3h^{-1}
Re	Reynolds number
R_i	overall degradation rate of reactant "i", gh^{-1}
R_m	overall mass transfer rate, gh^{-1}
r_i	local degradation rate of reactant "i", $gh^{-1}m^{-2}$

r_{o2} local oxygen consumption rate, $gh^{-1}m^{-2}$

r_{4cp} local degradation rate of 4-chlorophenol, $gh^{-1}m^{-2}$

r_{mi} local rate at which reactant "i" is transferred to the reaction sites, $gh^{-1}m^{-2}$

t reaction time, h

t_{50} time required for 50% reduction of the parent compound concentration, hour

V volume of the reaction medium, m^3

W width of the flat plate, W=0.08 m

w incident radiation on reactor cover, Wm^{-2}

w_λ spectral irradiance, $Wm^{-2}\ nm^{-1}$

$w_{\lambda\psi}$ spectral specific irradiance, $Wm^{-2}\ nm^{-1}Sr^{-1}$

x,y,z rectangular Cartesian coordinate, m

Greek Letters

α half angle of the corrugated plate, degree

δ thickness of reactor cover, m

ϕ quantum yield

λ photon wavelength, nm

ψ solid angle with respect to the reactor cover, Sr

σ constant in Equations (6-1), (A-1), and (A-2), σ=15.575 nm

Subscripts

0 initial

f final

fl flat plate

λ spectral quantities

lw	lower wing of the corrugated plate
m	mass transfer
uw	upper wing of the corrugated plate
s	surface of catalyst film

Superscripts

cv	reactor cover
d	diffuse fraction of the solar UV
p	direct parallel fraction of the solar UV
pn	after penetrating reactor cover
(#)	#th reflections
h	hole or electron vacancy
e	electron
·OH	hydroxyl radical
$HO^{\bullet}_2$	perhydroxyl radical
$O_2^{\cdot}$	superoxide ion radical

Acronyms

4-CP	4-chlorophenol
2,4-DCP	2,4-dichlorophenol
2,4,5-TCP	2,4,5-trichlorophenol
ABS	UV absorbence at 224 nm
AOP	advanced oxidation process
BQ	1,4-benzoquinone
CAS	chemical abstract service
4-CC	4-chlorocatechol

CP	corrugated plate
cv	reactor cover
DO	dissolved oxygen
DOC	dissolved organic carbon
EE/O	electrical energy per order
eV	electron volt
GC/MS	gas chromatography/mass spectra
HQ	hydroquinone
HPLC	high performance liquid chromatograph
IC	ion chromatograph
LCP	the lab version corrugated plate reactor
LASREA	local area-specific rate of energy absorption
LVREA	local volumetric rate of energy absorption
L-H	Langmuir-Hinshelwood
lw	lower wing of the corrugated plate
PTEF	photochemical thermodynamic efficiency factor
SEM	scanning electron microscope
TKN	total Kjeldahl nitrogen
TOC	total organic carbon
UV	ultraviolet
UV-A	photons with wavelengths between 190 and 280 nanometers
UV-B	photons with wavelengths between 280 and 320 nanometers
UV-C	photons with wavelengths between 320 and 380 nanometers
WHO	World Health Organization

CHAPTER 1: INTRODUCTION

One of the major environmental problems facing all of us today is the widespread presence of persistent and toxic chemicals such as chlorinated organics in surface and ground water bodies and drinking water systems. These chemicals enter the hydrosphere through domestic and industrial discharges, chemical spills, and large scale application of pesticides and herbicides. The existence of these chemicals in the environment poses a threat to humans because of their toxicity and the potential pollution to our food chain through bioaccumulation (WHO, 1976). As a result, increasingly stringent restrictions are being imposed on the release of these compounds by various regulatory bodies.

There exist several physical processes available through which water may be purified to different specifications, such as, carbon adsorption, precipitation, air stripping, membrane separation, ion-exchange, and flash evaporation. But none of them is a destructive process, and as a result a further step is required to handle the wastes. In addition, most of these methods are not competitive for the removal of trace amount toxic chemicals from water (Yue, 1993).

Biological treatment has been the most cost-effective and primary means for wastewater contaminant mineralization for many types of effluents. However, persistent and toxic chemicals such as halogenated aromatics, surfactants, herbicides, pesticides, and dyes are known to be non-biodegradable (Vandevivere, Bianchi, and Verstraete, 1998; Tanaka and Ichikawa, 1993; Low, McEvoy, and Matthews, 1991). In addition, there are problems related to the slow nature of biological reactions, strict temperature and pH requirements, and difficult sludge handling.

Advanced oxidation processes (AOPs) typically involve treatment with ultraviolet (UV) light, chemical oxidants (i.e., O_3, H_2O_2, persulfate), catalyst, or their combinations. These processes usually rely on the generation of hydroxyl radicals which are capable of converting a wide spectrum of organic chemicals, including those non-biodegradable ones, to relatively

innocuous end products such as carbon dioxide, water, and inorganic salts (Legrini, Oliveros, and Braun, 1993). In H_2O_2/UV, O_3/UV, and H_2O_2/O_3/UV processes, for example, hydroxyl radicals are generated through the photolysis of H_2O_2 and/or O_3 under the illumination of UV light with wavelengths shorter than 300 nanometers.

Photocatalysis also belongs to the family of AOPs. In photocatalysis, an oxide semiconductor, usually TiO_2, is photo-excited upon absorbing photons with appropriate energy levels (wavelength shorter than 387 nm for anatase). The photo-excited semiconductor produces electrons and holes (i.e., electron vacancy) which can migrate to the solid surface and initiate a series of oxidation and reduction reactions that simultaneously: (1). oxidize toxic organic water/air pollutants; (2). kill microorganisms; and (3). reduce the valence of dissolved metal ions (Turchi and Ollis, 1990).

Photocatalysis is capable of destroying a wide spectrum of water/air pollutants and microorganisms. It has many inherent advantages over other AOPs. For example, it can be driven by solar UV which constitutes 3-5% of total solar energy. It is capable of both oxidation and reduction chemistry through which pollutants such as metal ions can be removed. It proceeds in both air and water phases. And finally, it does not require expensive oxidants (i.e., ozone) and exotic materials (i.e., quartz) for UV-A transmission.

Currently, the major barrier for photocatalysis to obtain wider industrial acceptance is its low overall rate and low energy efficiency due, among other factors, to limited catalyst activity, catalyst poisoning and fouling, scavenging of oxidizing agents by non-target species, low-order dependency of rates on radiation intensity, and limited capacity to deliver photons and reactants to catalyst surfaces (Parent et al., 1996).

Research into photocatalysis has been very active for the last 15 years. This interesting process has been explored for potential use in indoor air purification and disinfection (Goswami, Trivedi, and Block, 1997), precious metal recovery (Ollis, Pelizzetti, and Serpone, 1991), soil remediation (Holden et al., 1993), ultrapure water (Prairie et al., 1993) and drinking water

(Matthews and McEvoy, 1992) production, industrial water (Lin and Rajeshwar, 1997; Blanco and Malato, 1994) and groundwater (Mechos and Turchi, 1993) detoxification, and removing inhibition to biodegradation (Bolduc and Anderson, 1997). However, most of the previous work was on the degradation of different substances, reaction mechanisms, kinetics, activities of different catalysts, and effects of a few selected environmental conditions. Research with potential use in the development and scale-up of energy-efficient reactor systems is scarce. A commercially competitive full-scale photocatalytic water detoxification system has not yet been generally accepted in practice.

The objective of this research is to make some contributions to the development of cost-effective photocatalytic water detoxification systems and to gain some insight into the engineering issues related to the design and operation of such photocatalytic reactors.

As presented in the following chapters, the above-mentioned objective was achieved by analyzing a newly-proposed novel reactor configuration through rigorous radiation simulation, mass transfer measurement and modeling, model compound degradation experiments, as well as reaction kinetics modeling. This new reactor configuration is a compact immobilized system with low pressure drops, offers a large illuminated catalyst surface area, possesses superior capability to recapture reflected photons, has superior mass transfer rates, and can be designed for efficient solar UV utilization.

CHAPTER 2: LITERATURE REVIEW

2.1 Fundamentals of Photocatalysis

2.1.1 Semiconductor Photocatalysts

Band-Gap Theory

According to the band theory in solid state physics, the energy levels available for valence electrons of single atoms within a crystalline solid are quantized into discrete bands, and these bands are separated by regions of forbidden energy, also referred to as band gaps. A band filled or partially filled with electrons with ground level energy is called a valence band, while an empty higher energy band is called a conduction band. Conductor materials possess continuous electronic energy states since their valence bands are either incompletely filled or overlapped with a conduction band. Insulators are characterized by a completely filled valence band and an essentially insurmountably great band gap to the conduction band (Wang, 1989). The electronic structure of a semiconductor lies between those of a conductor and an insulator and valence band electrons can usually be excited to the conduction band when certain level of energy is absorbed. This unique characteristic of semiconductors makes them good potential photocatalysts.

Based on laws of photochemistry, only photons with energies greater than the band gap energy can result in the excitation of valence band electrons and possible reactions. Absorption of photons with lower energies or longer wavelengths usually causes vibrations or rotations of semiconductor atoms in the crystalline lattice which leads to energy dissipation in other forms such as heat.

Semiconductor Photocatalyst

In addition to a high photoactivity upon illumination, a desirable photocatalyst for the destruction of water contaminants should be (1) resistant to chemical attack over appropriate ranges of temperature and pH; (2) non-toxic; (3) insoluble in water; and (4) inexpensive.

Many semiconductors, including TiO_2, have been examined as candidate photocatalysts (Fox and Dulay, 1993; Turchi, 1990). Of these solids, $BaTiO_3$, WO_3, SiO_2, MgO, SnO_2, Cr_2O_3, MoS_2, In_2O_3, $SrTiO_3$, MgO, Kaolin, Al_2O_3 and α-Fe_2O_3 all show activities lower than that of TiO_2 (Palmisano et al., 989; Harada, Hisanaga, and Tanaka, 1990; Tanaka and Hisanaga, 1994). Only ZnO was more active than TiO_2 in photocatalytic oxidation of phenol and nitrophenol but a chemical test for Zn^{++} in the solution was positive (Palmisano et al., 1989).

Because of its high activity, desirable physical and chemical properties, low cost, and availability, TiO_2 has been the most frequently used catalyst in photocatalysis (Domènech, 1993). This metal oxide is a n-type semiconductor and also a widely used pigment. The three crystalline forms of titanium dioxide includ brookite, rutile and anatase. The specific grativities of brookite, rutile and anatase are 4170, 4260 and 3840 kgm^{-3} (Perry, Green, and Maloney, 1984). Both rutile and anatase have been extensively studied as photocatalysts. The lattice structure of both rutile and anatase is given in the literature (Linsebigler, Lu, and Yates, 1995). The rutile form has a band gap of 3.0 eV and can be excited by light with wavelengths shorter than 414 nm, while the anatase form has a band gap of 3.2 eV and can be excited by light with wavelengths shorter than 387 nm (Nair, Luo, and Heller, 1993).

2.1.2 Reaction Mechanism

As shown in Figure 2-1, in response to illumination by photons with sufficient energy, electrons in the valence band of TiO_2 are excited to the conduction band and leave electronic vacancies in the valence band, called holes. These conduction band electrons and holes may

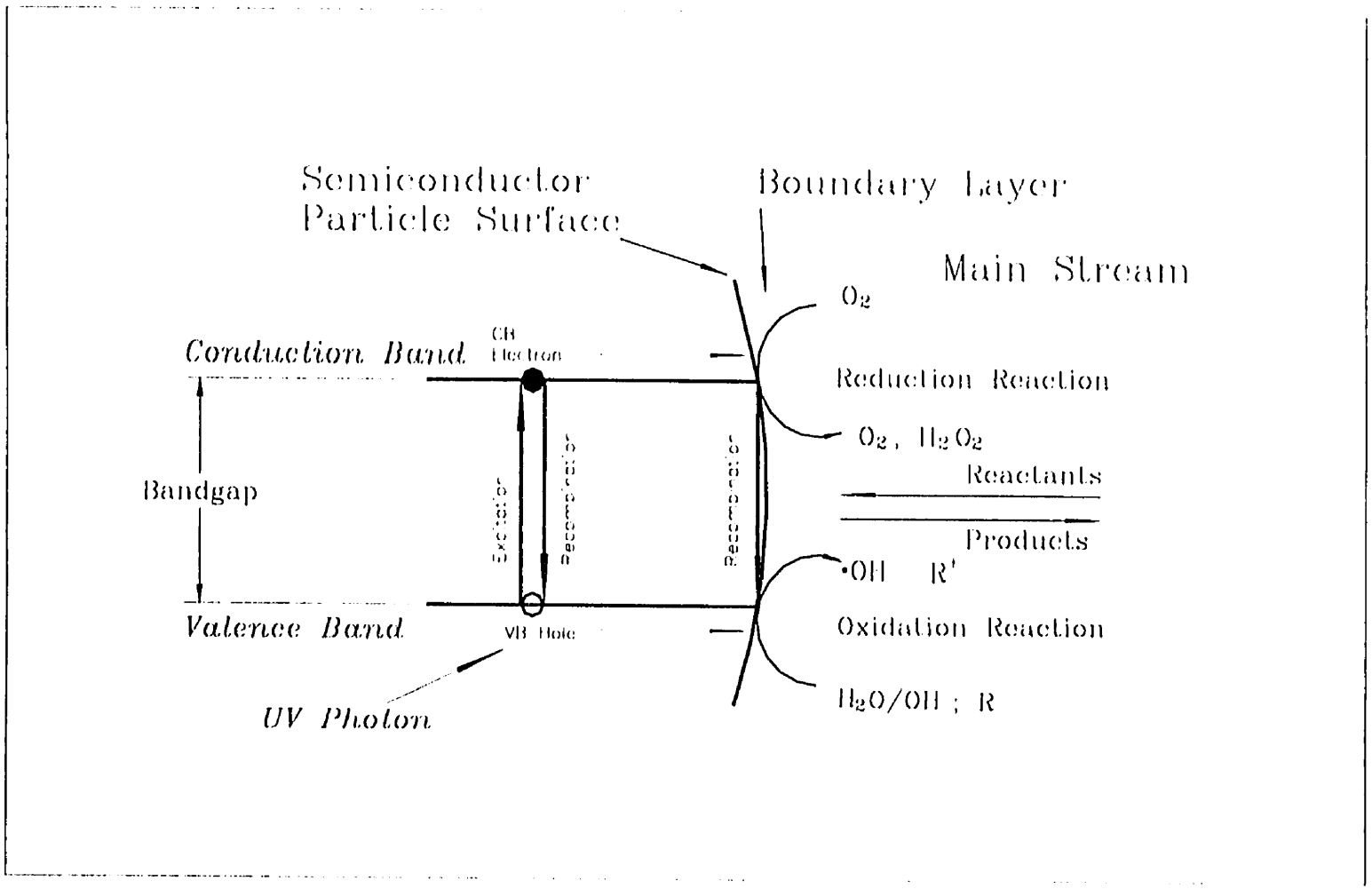

Figure 2-1: Simplified Mechanism for Photocatalysis

recombine with each other and release the energy as heat, or migrate to the catalyst surface and initiate redox reactions which result in the generation of active radicals (i.e., hydroxyl radicals, superoxide ion radicals, and perhydroxyl radicals) and the destruction of pollutants (Turchi and Ollis, 1990).

Based on the band-gap and band edge positions of titanium dioxide, conduction band electrons possess a redox potential of -0.2 eV (Mao, Schoneich, and Asmus, 1991) and are capable of reducing substances with potentials lower (or more positive) than -0.2 eV. Valence band holes possess a redox potential of 2.6-2.8 eV (Schiavello, 1993) and are capable of oxidizing species with potentials higher (or more negative) than 2.6 eV. For comparison, the redox potential of perhydroxyl radical is 1.7 eV.

Primary Oxidizer

With an oxidizing potential of 2.85 eV (vs. NHE), hydroxyl radical is one of the most powerful oxidizing agents and is believed to be the primary oxidant responsible for the heterogeneous photocatalytic oxidation of many chemicals (Schiavello, 1993; Lawless, Serpone, and Meisel, 1991; Terzian et al., 1991; Draper and Fox, 1990; Pelizzetti et al., 1990; Al-Ekabi and Serpone, 1988; Okamoto et al., 1985a; Matthews, 1984; Izumi et al., 1980; Jaeger and Bard, 1979). Evidence supporting this opinion includes (Turchi and Ollis, 1990): (1). ESR and photoluminscence work identified hydroxyl radical as the most abundant radical during photocatalysis; (2). Necessity of catalyst hydroxylation to allow complete oxidation of organic chemicals; (3). The importance of the hydroxyl radical step showed up in kinetic isotope studies; and (4). Formation of intermediates similar to those produced in reactions where hydroxyl radical is known to be the oxidizing agent.

Although the current prevailing view favors hydroxyl radical as the primary oxidizer, the contributions of direct hole oxidation, superoxide ion radical oxidation, and electron reduction to photocatalysis have also been noted. Kesselman and co-workers (1995) obtained evidence

showing direct hole oxidation of acetate and chlorinated acetates accounts for as much as 30% of the total degradation. Through quantitatively analyzing the intermediates during photocatalytic treatment of quinoline, Cermenati and colleagues deduced that superoxide ion radicals were the primary oxidizer. In the photocatalytic decolorization of textile dyes (Vinodgopal et al., 1994) and degradation of 2,4,6-trinitrotoluene (Bahnemann et al., 1995), electron reduction was reported as the initial reaction step.

Actually, the hydroxyl radical, hole, superoxide ion radical, perhydroxyl radical, and electron generated directly or indirectly in photocatalysis, all have oxidizing power, reducing power or both. Under thermodynamically favorable conditions, they are all capable of contributing to the photocatalytic degradation of water contaminants. The actual reaction scheme and also the primary pollutant attacking agent are dependent upon factors such as the chemical bond and the redox potential of the pollutant, the pH and temperature of the system, as well as the types and concentrations of electron donors and acceptors. For example, since hydroxyl radical is relatively incapable of attacking carbon-chlorine bonds (Legrini, Oliveros, and Braun, 1993) and possibly the reducing power of photo-generated electrons is not sufficiently high, carbon tetrachloride could not be mineralized without the addition of extra electron donors (Ollis, Pelizzetti, and Serpone, 1991). This chemical could be mineralized with the addition of alcohols, carboxylic acids, and benzene derivatives as electron donors through a reductive pathway (Choi and Hoffmann, 1995).

An Oxidation Reaction Scheme

Turchi and Ollis (1990) proposed a reaction scheme that is believed to be applicable to the photocatalytic mineralization of most of the organic water pollutants. This mechanism could be simplified into the following six elementary steps:

1. electron-hole pair generation upon the absorption of near UV light (Equation 2-1);
2. TiO_2 particle surface hydroxylation and hydration through the adsorption of water

molecules (Equations 2-2 and 2-3);

3. hydroxyl radical formation through the trapping of holes at the hydroxylated and hydrated sites (Equations 2-4 and 2-5);
4. adsorption of organic chemicals onto catalyst surface sites (Equation 2-6);
5. attack of the hydroxyl radical to organic chemicals near the catalyst surface (Equation 2-7); and,
6. recombination of electron-hole pairs (Equation 2-8).

$$TiO_2 + hv \rightarrow h^+ + e^- \quad (2\text{-}1)$$

$$O_L^{2-} + Ti^{IV} + H_2O \rightleftarrows O_LH^- + Ti^{IV}\text{-}OH^- \quad (2\text{-}2)$$

$$Ti^{IV} + H_2O \rightleftarrows Ti^{IV}\text{-}H_2O \quad (2\text{-}3)$$

$$Ti^{IV}\text{-}H_2O + h^+ \rightleftarrows Ti^{IV}OH^{\bullet} + H^+ \quad (2\text{-}4)$$

$$Ti^{IV}\text{-}OH^- + h^+ \rightleftarrows Ti^{IV}OH^{\bullet} \quad (2\text{-}5)$$

$$site + R_i \rightleftarrows R_{i,ads} \quad (2\text{-}6)$$

$$Ti^{IV}OH^{\bullet} + R_1 \rightarrow Ti^{IV} + R_2 \quad (2\text{-}7)$$

$$h^+ + e^- \rightarrow heat \quad (2\text{-}8)$$

$$Ti^{IV} + e^- \rightleftarrows Ti^{III} \quad (2\text{-}9)$$

$$Ti^{III} + O_2 \rightleftarrows Ti^{IV}\text{-}O_2^- \quad (2\text{-}10)$$

$$e^- + Ti^{IV}\text{-}O_2^- + 2(H^+) \rightleftarrows Ti^{IV}(H_2O_2) \quad (2\text{-}11)$$

$$Ti^{IV}\text{-}O_2^- + H^+ \rightleftarrows Ti^{IV}(HO^{\bullet}_2) \quad (2\text{-}12)$$

$$(H_2O_2) + (^{\bullet}OH) \rightleftarrows (HO^{\bullet}_2) + (H_2O) \quad (2\text{-}13)$$

Reactions (2-2) and (2-3) are both thermodynamically possible, with reaction 2-2 more favored at high pH and the other at low pH. In addition to hydroxyl radicals, interactions between the photo-generated electrons and holes and adsorbed oxygen can also lead to the formation of superoxide ion radicals, hydrogen peroxide, and perhydroxyl radicals (Equations 2-9 through 2-13). The ultimate fate of these active oxygen species was not discussed in the report (Turchi and Ollis, 1990).

2.1.3 Reaction Kinetics

Since the primary oxidizer, hydroxyl radical, is too reactive to travel far away from the catalyst surface (Turchi and Ollis, 1990) before reaction occurs, the redox (electron transfer) reactions between hydroxyl radicals and the reactants occur primarily (if not completely) at the catalyst surface. The most favorable situation would be with the reactants adsorbed onto the catalyst surface since the redox reaction requires orbital overlap of the electron donors and acceptors. In addition, trapping of the electrons and holes also requires the adsorption of oxygen and water. Therefore, adsorption is one of the critical processes determining the photocatalytic reaction rate. Based on the Langmuir isotherm, considering the adsorption of reactant "i", solvent water, as well as other species (i.e., other reactants, intermediates, inhibitive ions), the reaction rate of reactant "i" can be expressed by a modified Langmuir-Hinshelwood (L-H) equation (adapted from Turchi and Ollis, 1989):

$$-R_i = -V\frac{dC_i}{dt} = \frac{AK_0K_iC_i}{(1 + K_iC_i + \sum_{j \neq i} K_jC_j)} \qquad (2\text{-}14)$$

For the photocatalytic oxidation of organics where oxygen is an electron acceptor, the reaction rate and Langmuir adsorption constants "K_i and K_j" are dependent on radiation

intensity on the catalyst surface, oxygen concentration in the reaction medium, nature of the species "i", catalyst form, temperature, and pH (Turchi, 1990). The rate constant, "K_0", can be expressed by Equation (2-15) below (Chen and Ray, 1998; Turchi and Ollis, 1989; Ollis, 1985; Okamoto et al., 1985a,b):

$$K_0 = \frac{k_0 K_{O_2} C_{O_2}}{1 + K_{O_2} C_{O_2}} \frac{I^n}{I_0^n} \qquad (2\text{-}15)$$

The exponent n is dependent, among other factors, on the radiation intensity on the catalyst surface. At low radiation intensities, n equals "1" while at high radiation intensities it is 0.5 (Blake et al., 1991; Ollis, Pelizzetti, and Serpone, 1991). When the radiation intensity is so high that the limiting factor becomes the transfer of reactants to the reaction sites (i.e., the catalyst surface), an increase in radiation intensity will not result in any increase in reaction rates (Ollis, Pelizzetti, and Serpone, 1991). The radiation intensity at which n changes from "1" to "0.5" is a function of the redox system being examined (Parent et al., 1996) and has been reported to be between 2 and 170 Wm^{-2} (Okamoto et al, 1985b; Blake et al., 1991; D'Oliveira, Al-Sayyed, and Pichat, 1990; Reeves et al., 1992).

In addition to the power relationship, the rate coefficient and radiation intensity data were also fitted into other types of expressions such as (Ray and Beenackers, 1997):

$$K_0 = \frac{k_s a I^b}{1 + a I^b} \qquad (2\text{-}16)$$

In this equation, a, b, and k_s are constants. As discussed earlier, the reactants need to be provided from the bulk of the liquid to the reaction site, the catalyst surface. This requires that at steady state the mass transfer rate of any reactant "i", r_{mi}, equal the consumption rate of that reactant due to the reaction:

$$r_{mi} = r_i = k_L (C_i - C_{is}) \qquad (2\text{-}17)$$

Most photocatalytic reactions follow the modified L-H relationship as presented above (Gerischer and Heller, 1992; Lawless, Serpone, and Meisel, 1991; Turchi and Ollis, 1989; Mao, Schoneich, and Asmus, 1991). However, there are a few reports in which first order kinetics could correlate the data satisfactorily (Lee, 1995; Alberici and Jardim, 1994; Matthews, 1991; Al-Ekabi and Serpone, 1988; Matthews, 1987a,b; Augugliaro et al., 1993; Okamoto et al., 1985b). In addition, Tseng and Huang (1991) found zero order kinetics in their research.

The disagreement in kinetics does not seem to be related to the nature of the chemicals degraded since for the same chemical, phenol, an L-H relationship (Matthews, 1988), 1st order (Okamoto et al., 1985b) as well as zero order kinetics were reported. It may due to the different experimental conditions the authors employed. Actually, the L-H kinetics will become pseudo first order when the reactant concentration is sufficiently small (Lee, 1995). On the other hand, zero order kinetics could approximate L-H kinetics given sufficiently high reactant concentration (Sabin, Turk, and Vogler, 1992). Specific operating problems also seem to have interfered with the interpretation of the data. In at least three cases, it is not clear whether or not the first order kinetics reported were due to mass transfer limitation (Matthews, 1987b; 1991; Al-Ekabi and Serpone, 1988).

2.1.4 Energy Efficiencies

In photocatalysis, terms available for the evaluation of energy efficiencies include, the Electrical Energy per Order (EE/O), the quantum yields, the quantum efficiencies, and the Photochemical Thermodynamic Efficiency Factor (PTEF). The EE/O refers to the electrical energy consumption for an order of magnitude destruction of the pollutants and it is based on the implicit assumption of 1st order kinetics in terms of pollutant concentration (Bolton, Cater, and Safarzadeh-Amiri, 1992). The quantum yield is defined as the number of molecules reacted divided by the number of photons incident on the catalyst surface (Bockelmann et al., 1993),

while the quantum efficiency represents the number of molecules reacted divided by the number of photons absorbed (Valladares and Bolton, 1993). The PTEF was defined by Serrano and de Lasa (1997) as the fraction of the absorbed radiative energy that is used for hydroxyl radical generation. Based on the principles of chemical engineering thermodynamics, the upper limits of the PTEF were calculated to be between 0.237 and 0.308, depending on the energy levels of the absorbed photons (between 300 and 390 nanometers). The PTEF can provide guidance to the evaluation of the energy efficiencies of any hydroxyl radical-initiated non-chain photochemical reactions.

As discussed in Section 2.12, photocatalysis consists of several physical and chemical steps (i.e., generation, recombination, and trapping of conduction band electrons and valence band holes; recombination of trapped electrons and holes; redox reactions at the catalyst surface; and adsorption/desorption of species on the catalyst surface) which determine its quantum yield (Parent et al., 1996). Depending on the particular redox system being investigated, the quantum yield has been reported to be more sensitive to different factors governing one or more steps. These factors included: the nature and concentrations of the target compound and other species in the system (Turchi and Ollis, 1989; Lindner, Theurich, and Bahnemann, 1997), the catalyst (Ha and Anderson, 1996; Lindner et al., 1995), electron donors/acceptors (Lindner, Theurich, and Bahnemann, 1997), the wavelength of the photons (Stafford, Gray, and Kamat, 1997a) and the rate at which photons are absorbed by the catalyst (Hoffmann et al., 1995). For aqueous phase photocatalysis, the quantum yields have been found to be very low and are usually lower than 5% (Legrini, Oliveros, and Braun, 1993).

Several researchers have determined that the dependence of quantum yields on photon flux is zero order at low radiation intensities and negative half order at higher radiation intensities (Ollis, Pelizzetti, and Serpone, 1991). This is believed to occur because the recombination of conduction band electrons and valence band holes follow higher order kinetics in terms of the concentrations of these charge-carriers (Linsebigler, Lu, and Yates, 1995). The

radiation intensity at which the order changes depends, among other factors, on how fast the redox reactions proceed. Low order dependence on radiation intensity is observed when the redox reactions are slow and cannot use electrons and holes as fast as they are generated (Parent et al., 1996). Consequently, adding photons too rapidly results in high concentrations of electrons and holes in the catalyst and high recombination rates. For example, a single wavelength irradiation at 330 nm with an adsorbed radiation intensity of 1.7 Wm^{-2} yielded a quantum yield of 56% for $CHCl_3$ degradation. On the other hand, under same conditions the quantum yields was reduced to 2% as the radiation intensity increased to 151 Wm^{-2} (Hoffmann et al., 1995).

For the degradation of 4-chlorophenol, the quantum yield was found to have increased from 1% to 7% as the wavelength of the absorbed photons changed from 360 nm to 300 nm (Stafford, Gray, and Kamat, 1997a). This indicates that photons with different energy levels have different capacity in initiating the redox reactions. Unfortunately, photon incidence rates were not kept constant for different runs. In addition, it was difficult to judge from the report whether the photon absorption rates were calculated correctly.

Although photocatalysis is capable of both oxidative and reductive chemistry, it is important to remember that these two processes tend to proceed such that electrons and holes are consumed at the same rate to keep electrical neutrality. Accumulation of either charge-carrier, electron or hole, will result in higher recombination rates and therefore lower quantum yields (Kennedy and James, 1996). For the degradation of many organic chemicals using TiO_2 as the catalyst and dissolved oxygen (DO) as the oxidant, quantum yields have been found to be limited by the accumulation of electrons. Therefore, addition of superior electron acceptors, such as H_2O_2, can usually result in higher reaction rates and also higher quantum yields (Martin, Lee, and Hoffmann, 1995).

2.1.5 Intermediates and Extent of Mineralization

The destruction of essentially every type of chemical, including, halogenated hydrocarbons, aromatic hydrocarbons, nitrogen-containing heterocycle compounds, hydrogen sulfide, surfactants, herbicides, metal complexes, have been demonstrated repeatedly in recently years. Lists of these chemicals have been documented by several researchers (Lee, 1995; Hoffmann et al., 1995; Legrini, Oliveros, and Braun, 1993).

Reaction Intermediates

Information on reaction intermediates is important because their properties will directly affect the applicability of photocatalysis as a water decontamination method as well as the possibility of a combined approach. For example, a toxic or recalcitrant intermediate may prohibit the use of biological treatment as a polishing step in a combined process. Unfortunately, information on reaction intermediates is very limited to date. This may be because of the low levels of some intermediates, or the experimental difficulties. After all, the photocatalytic degradation of some chemicals may not result in stable intermediates.

In Table 2-1 lists the identified reaction intermediates during the degradation of a few selected chemicals. Of these intermediates, trichloroacetic acid, an intermediary product for the degradation of perchloroethylene, is known to be toxic to animals (Glaze, Kenneke, and Ferry, 1993). Actually, the reaction intermediates for pentachlorophenol, and 2,3,5-trichlorophenol have been proven to be more toxic to microorganisms than their parent compounds (Jardim, Moraes, and Takiyama, 1997; Manilal et al., 1992).

Table 2-1: Examples of Intermediates During Photocatalytic Degradation

Chemical	Intermediate	Reference
tetrachloroethylene	dichloroacetic acid, trichloroacetic acid	Glaze, Kenneke, and Ferry, 1993
trichloroethylene	dichloroacetaldehyde	Ollis et al., 1984
	dichloroacetic acid, dichloroacetaldehyde	Glaze, Kenneke, and Ferry, 1993
pentachlorophenol	tetrachlorobenzoquinone, tetrachlorohydroquinone	Mills and Hoffmann, 1993
	2,3,5,6-tetrachlorophenol, 2,3,5,6-tetrachloro, 1,4-benzoquinone, 2,3,5,6-tetrachloro,1,4-hydroquinone,	Jardim, Moraes, and Takiyama, 1997
2,3,5-trichlorophenol	2,3,5-trichloro,1,4-hydroquinone	Jardim, Moraes, and Takiyama, 1997
3,5-dichlorophenol	2,5-dichloro,1,4-hrdroquinone	Jardim, Moraes, and Takiyama, 1997
2,4-dichlorophenol	detected but not identified	Jardim, Moraes, and Takiyama, 1997
	detected but not identified	Ku and Hsieh, 1992
	chlorohydroquinone, chlorophenol	Trillas, Peral, and Domènech, 1996
4-chlorophenol	benzoquinone, 4-chlorocatechol, hydroxyhydroquinone, 2,5,4-trihydroxybiphenol, phenol, hydroquinone	Lindner, Theurich, and Bahnemann, 1997
	hydroquinone, 4-chlorocatechol	Stafford, Gray, and Kamat, 1997b
	hydroquinone,benzoquinone, 4-chlorocatechol	Al-Ekabi et al., 1989
	hydroquinone, 1,4-benzoquinone	Al-Sayyed, D'Oliveira, and Pichat, 1991

As can be noted from Table 2-1, for the photocatalytic degradation of the same chemical (i.e., trichloroethylene, pentachlorophenol, 4-chlorophenol), different intermediates were reported by different researchers. This may indicate (1) different sensitivity of the intermediates to different analysis methods, and/or correlations between reaction pathways and the experimental conditions (i.e., radiation source, catalyst, electron donors/acceptors) and/or (3) different adsorption capabilities of the systems examined.

For the degradation of 4-chlorophenol, aromatic hydroquinone was identified as the major intermediate in studies in which HPLC was used (Al-Sayyed, D'Oliveira, and Pichat, 1991; Mills and Morris, 1993). However, Haarstrick and co-workers failed to detect this chemical with GC/MS in their investigation into the photocatalytic degradation of 4-chlorophenol and *p*-toluenesulfonic acid mixture (Haarstrick, Kut, and Heinzle, 1996). In another study (Lindner, Theurich, and Bahnemann, 1997), different forms of the TiO_2 catalyst resulted in the detection of different reaction intermediates. Due to the different adsorption capacity of reaction intermediates on the catalyst surface, one research group observed a change in the relative level of the reaction intermediates by simply changing the catalyst quantity in a slurry system (Stafford, Gray, and Kamat, 1997b)

Extent of Mineralization

Of all the compounds examined to date, the only one that was reported to be resistant to complete photocatalytic mineralization is atrazine, a representative of s-triazine herbicides (Pugh et al., 1995; Chester et al., 1993; Pelizzetti, Minero, and Grätzel, 1991; Pelizzetti et al., 1990). Addition of peroxydisulfate and periodate did not result in any destruction of the final product, cyanuric acid. This was explained by the super-inert nature of cyanuric acid which is characterized as a symmetric structure with three nitrogen atoms on the aromatic ring and three hydroxyl groups attached to the three carbons on the ring. Fortunately, atrazine could be

essentially detoxified in photocatalysis since cyanuric acid possesses low toxicity (Pelizzetti et al., 1990).

Ollis and co-workers (1984) failed to observe the release of CO_2 for the degradation of 1,3-dichlorobenzene,1,2-dichlorobenzene, 1,4-dichlorobenzene, and trichloroacetic acid. These chemicals were mineralized later in other labs (Chemseddine and Boehm, 1990; Lee et al., 1993; Glaze, Kenneke, and Ferry, 1993). Titanium dioxide of different grades was used in the two studies. The results from these studies indicate that for the photocatalytic degradation of some chemicals, the right experiment conditions (i.e., the catalyst, electron donors/acceptors, pH, photon wavelength) are essential.

Degradation of Compound Mixtures

Wastewaters are usually contaminated with more than one kind of pollutant. It is therefore important to examine the influence of other pollutants to the photocatalytic degradation of the chemical in question. To date, very few studies have been reported in this area.

Ollis and Turchi (1989) investigated a system of benzene and perchloroethylene (PCE) and found that compared to the degradations of the two single compounds, PCE inhibited the degradation rate of benzene but the mineralization of PCE was unchanged. Al-Ekabi and co-workers (1989) studied the degradation of 4-CP, 2,4-dichlorophenol, and a mixture of these two chemicals. It was reported that in the mixed system, the disappearance rate of 4-CP was significantly reduced. Wilkinson (1994) reported results on the photocatalytic degradation of phenol and 2-chlorobenzoic acid system. Compared to the reaction rates for single component systems, the reaction rates dropped approximately 30% for each chemical.

Since photocatalytic reactions rely on both the photo-generated radicals and the adsorption sites on the catalyst surface, it is unlikely to see the oxidation rate of one compound enhanced by the existence of another reactant to be oxidized because of the competition of limited adsorption sites and oxidizing radicals. The multi component systems investigated above all belong to this situation. However, if different chemicals could go through different pathways

(i.e., oxidative and reductive), a synergistic effect is possible. Prairie and co-workers (1993) reported results on the photocatalytic decontamination of an artificial wastewater with both organic chemicals and metal ions. Based on the results, it was concluded that efficient designs of photocatalytic systems for wastewater treatment must consider both oxidation and reduction processes.

2.1.6 Degradation of Chlorophenols

The photocatalytic degradation of 4-chlorophenol (4-CP) has been examined extensively in both slurry systems (Lindner, Theurich, and Behnemann, 1997; Stafford, Gray, and Kamat, 1997a,b; March, Martin, and Saltiel, 1995; Martin, Lee, and Hoffmann, 1995; Martin et al., 1995; Cunningham and Sedlák, 1994; Mills and Morris, 1993; Al-Sayyed, D'Oliveira, and Pichat, 1991; Tseng and Huang, 1991; Barbeni, Pramauro, and Pelizzetti, 1986; 1984) and immobilized systems (Peill and Hoffmann, 1997, 1996, 1995; Hofstadler et al., 1994; Al-Ekabi et al., 1989; Al-Ekabi and Serpone, 1988; Matthews, 1990, 1988, 1987a). Hydroxyl radical was believed to be the major oxidizer although hole capture by 4-CP is also thermodynamically favorable (Al-Sayyed, D'Oliveira, and Pichat, 1991). The initial reaction of a photo-generated hydroxyl radical with 4-CP occurs through the following parallel pathways (Mills and Morris, 1993; Al-Sayyed, D'Oliveira, and Pichat, 1991):

$$\text{4-CP} + {}^{\bullet}\text{OH} \rightarrow \text{hydroquinone} \qquad (2\text{-}18)$$

$$\text{4-CP} + {}^{\bullet}\text{OH} \rightarrow \text{4-chlorocatechol} \qquad (2\text{-}19)$$

$$\text{4-CP} + {}^{\bullet}\text{OH} \rightarrow \text{1,4-benzoquinone} \qquad (2\text{-}20)$$

$$\text{4-CP} + {}^{\bullet}\text{OH} \rightarrow \text{unidentified intermediates} \qquad (2\text{-}21)$$

Table 2-2: Previous Studies on 4-Chlorophenol

Source	Experimental Conditions	Major Findings
Peill and Hoffmann, 1997	optimized Degussa P25-coated fibre optic cable reactor; 1 kW Xe arc lamp; 190 mL water; C_0= 13 mgL^{-1}	t_{50}=4.5 hours; measured Φ=0.012; 50% UV left after travel 1cm along the fibre
Hofstadler et al., 1994	Degussa P25-coated glass fibre bundles as reactor; irradiated from one end with 400 W high pressure Hg lamp; C_0= 134 mgL^{-1}	E_a=20.6 $kJ.mol^{-1}$; Φ=0.002; no mass transfer limitation; reaction rate decrease when pH increase from 3 to 11; H_2O_2 enhance reaction rate
Matthews, 1988	spiral glass tube reactor with Degussa P25 coated inside of the tube; 20 W black light lamp at spiral center; pH=3.6; 40 °C; Re=1600; 40 mL water; C_0= 1 to 100 mgL^{-1}	L-H kinetics; Φ=0.01
Al-Ekabi et al., 1989	spiral glass tube reactor with Degussa P25 coated inside of the tube, 6-black light lamps around spiral tube; Re=660; Tygon tubing	L-H kinetics; [4-CP]<8 mgL^{-1}: close to1st order; [4-CP]>25 mgL^{-1}: close to zero order
Al-Ekabi and Serpone, 1988	spiral glass tube reactor with Degussa P25 coated inside of the tube, 6-black light lamps around spiral tube; TiO_2-coated beads packed in an annulus, black light lamp at the centre; C_0=2 mgL^{-1}; Tygon tubing	1st order kinetics; mass transfer limited; higher radiation intensity resulted in dependency of rate on flowrate in a larger range
Stafford, Gray, and Kamat, 1997b	annular slurry reactor with black light lamp or 450 W medium pressure Hg lamp; Degussa P25; 0.8 L water; C_0=32 mgL^{-1}	4-chlorocatechol is better adsorbed than 4-CP; 4CC concentration depended on light intensity TiO_2 loading, photon wavelength, and pH
Lindner, Theurich, and Bahnemann, 1997	slurry reactor; TiO_2 of different grades	Φ<0.0035; Pt doping and oxidant (i.e., H_2O_2, $K_2S_2O_2$) addition had no effect

Table 2-2 cont'd

Source	Experimental Conditions	Major Findings
Martin, Lee, and Hoffmann, 1995	25 mL water with 1 gL^{-1} Degussa P25,C_0= 13 mgL^{-1} 4-CP	addition of ClO_2^-, ClO_3^-, IO_4^-, $S_2O_8^{2-}$, and BrO_3^- enhanced reaction rate
March, Martin, and Saltiel, 1995	shallow pond reactor; 1 gL^{-1} TiO_2; I=35 Wm^{-2}	1st order kinetics, rate coefficient=0.11 min^{-1}; reactor performance simulation
Cunningham and Sedlák, 1994	30 mL slurry with 2 gL^{-1} Degussa P25; photon flux $1.7x10^{16}$-$2x10^{18}$ @360 nm	very low catalyst adsorption capacity; Ag+ addition enhanced rate; zero order to [4-CP]
Mills and Morris, 1993	125 mL cylindrical reactor irradiated with 6-16 W black light lamps; 0.5 gL^{-1}; Degussa P25; 30 °C; C_0 = 128 mgL^{-1}; pH=2	L-H kinetics; E_a=16 $kJ.mol^{-1}$; Φ=1.1%; rate$\propto I^{0.74}$ for I=2.7-32.7 Wm^{-2} ; rate$\propto I^{0.5}$ for I>22 Wm^{-2}; rate depends on oxygen level.
Al-Sayyed, D'Oliveira, and Pichat, 1991	90 mL cylindrical reactor; 2gL^{-1} Degussa P25; 125 W high pressure Hg lamp radiated from reactor bottom; 20 °C; C_0=20 mgL^{-1}; pH=3 to 6	L-H kinetics with K=0.13 $L.mg^{-1}$ and k=0.15 $mgL^{-1}.min^{-1}$ Φ=1%; E_a=5.5 $kJ.mol^{-1}$; pH=3.4-6.0 no significant change in reaction rate; r$\propto I^{0.5}$ for I>10-20 Wm^{-2}
Matthews, 1990b	spiral glass tube reactor; 1 gL^{-1} Degussa P25; 20 W black light lamp at spiral center; pH=3.5; 40 °C; Re=1400; 40 mL water	L-H kinetics

Results of a recent study suggest that the unidentified reaction intermediates in Equation (2-21) are hydroxyhydroquinone, phenol, and 2,5,4-trihydroxybiphenol (Lindner, Theurich, and Bahnemann, 1997). This agrees with the results of another study (Al-Sayyed, D'Oliveira, and Pichat, 1991) in terms of the total number of detected reaction intermediates. Table 2-2 is a summary of the experimental conditions and major findings of selected studies on 4-CP.

Other chlorophenols that have been examined for photocatalytic degradation are 2,4-DCP, 3,5-DCP, 2,3,5-TCP, 2,4,5-TCP, and pentachlorophenol (Jardim, Moraes, and Takiyama, 1997; Malato et al., 1997; Trillas, Peral, and Domènech, 1996; Alberici and Jardim, 1994; Mills

and Hoffmann, 1993; Ku and Hsieh, 1992; Manilal et al., 1992; Tseng and Huang, 1991; Barbeni, Pramauro, and Pelizzetti, 1986).

2.2. Factors Affecting TiO_2/UV Process Efficiency

Heterogeneous photocatalysis can be broken into seven unit processes. They are: i. transfer of radiation energy from the light source to the catalyst; ii. photo-induced electron-hole generation in the catalyst; iii. travel of the reactants from bulk of the fluid to the vicinity of catalyst surface; iv. adsorption of reactants to sites on catalyst surface; v. redox reactions in the vicinity of catalyst surface; vi. desorption of products; and vii. mass transfer of the products back to bulk of the fluid. Factors affecting any of these unit processes contribute to photocatalysis.

2.2.1 Catalyst Forms and Modification

In photocatalysis, the catalyst plays an essential role. It absorbs radiation energy, transforms photons into chemical energy in the form of active radicals, provides the environment (the orbital overlap of electron donors and acceptors through adsorption of the reactants and trapping of the radicals) for the redox reactions which result in the degradation of water contaminants. Factors governing the quality of a photocatalytic catalyst include not only the type of substances and its crystalline structures but also many others such as specific surface area, surface hydration, surface ionic condition, surface defectiveness, and impurities.

TiO_2 Form

Of the three crystalline structures of TiO_2, anatase has been shown to be more active as a photocatalyst than rutile (Tanaka, Capule, and Hisanaga, 1991; Sclafani, Palmisano, and Davis,

1990). Anatase will undergo transformation into rutile at temperatures above 610°C (Wilkinson, 1994). This adds the effect of preparation temperature on the catalyst activity. Surface defective sites at the surface can also alter the adsorption sites of this semiconductor and therefore its performance (Linsebigler, Lu, and Yates, 1995).

A few commercial TiO_2 products have been examined for their performance as a photocatalyst for water decontamination, including Degussa P-25 (Suri et al., 1993, Nair, Luo, and Heller, 1993), Fischer Certified Grade (Ollis et al., 1984), and Hombikat UV-100 (Lindner et al., 1995). Reeves and co-workers (1992) conducted photocatalytic chemical decomposition with several commercially available TiO_2 samples and found that Degussa P-25 gives the highest reaction rates. This product is a mixture of non-porous rutile (30%) and anatase (70%) particles and possesses a specific surface area of approximately 55 m^2g^{-1} (Lee, 1995). This corresponds to an average particle diameter of about 30 nm. For the degradation of 4-CP, Degussa P-25 was recently proven to be the best TiO_2 catalyst (Lindner, Theurich, and Bahnemann, 1997). For the degradation of dichloroacetic acid in a slurry system, however, Hombikat UV-100 was reported to be 4 times more active than P-25 (Lindner et al., 1995). Hombikat UV-100 consists of pure anatase particles of 10 nm and possesses a specific surface area of approximately 200 m^2g^{-1}.

So far most researchers used slurry systems in which TiO_2 particles or aggregates are suspended in contaminated water. In such systems, there exists an optimal catalyst loading in terms of maximum reaction rates as a result of the compromise between surface area and the shielding effect (Augugliaro et al., 1991). This optimal loading is apparently correlated with other system parameters and has been reported to be around 0.6 to 3.0 gL^{-1} for Degussa P-25 (Mehrvar, 1998; Augugliaro et al., 1991; Wei and Wan, 1991; Ahmed and Ollis, 1984) and around 4-5 gL^{-1} for UV-100 (Mehrvar, 1998; Lindner et al., 1995). Slurry systems offer very large catalyst surfaces that may be activated through vigorous mixing. This type of system is unlikely to suffer from mass transport-related limitations (Assink and Koster, 1995). Under similar conditions, therefore, slurry systems usually provide higher reaction rates compared to

immobilized systems. Unfortunately, a further step is required after treatment for the separation of the catalyst from the treated water.

TiO_2 has also been used as immobilized on many kinds of materials using evaporation of TiO_2 aqueous slurries (Matthews, 1988; Sabate et al., 1991; Al-Ekabi and Serpone, 1988), high-temperature thermal decomposition of titanium alkoxides (Serpone et al., 1986), or drying and calcination of alcohol solutions of titanium tetraisopropoxide (Murabayashi et al., 1993). No immobilization related deactivation was observed to date (Fujishima, 1995). Table 2-3 is a summary of the materials on which TiO_2 has been coated successfully.

Post-treatment catalyst-water separation is not required for immobilized systems. However, this type of system may suffer from a few other limitations. Compared to slurry systems, immobilized systems usually possess much lower catalyst surface areas. This is particularly true for conventional photoreactor configurations. In addition, mass transfer may become the limiting factor, especially at low pollutant concentrations, under high radiation intensities, or under unfavorable hydraulic conditions (Ollis, Pelizzetti, Serpone, 1991; Lepore, Pant, and Langford, 1993). Actually, a few mass transfer limited cases have been encountered (Matthews and McEvoy, 1992; Matthews, 1991; Al-Ekabi and Serpone, 1988; Turchi and Ollis, 1988). Mass transfer limitations could be alleviated by proper design and operation of the immobilized systems (Sabate et al., 1991).

Table 2-3: Materials TiO_2 Immobilized On

Parent Material	Reference
activated carbon	Uchida, Itoh, and Yoneyama, 1993
alumina	Fujishima, 1995
ceramic	Fujishima, 1995; Aguado, Anderson, and Hill, Jr., 1994
quartz	Tada and Tanaka, 1997; Fernández et al., 1995
silica gel	Zhang et al., 1994
fibre optic cable	Peill and Hoffmann, 1997; Hofstadler et al., 1994; Marinangeli and Ollis, 1980; 1977
fibre glass	Serrano and de Lasa, 1997; Pugh et al., 1995; Zhang et al., 1994; Al-Ekabi et al., 1993; Pacheco, Watt, and Turchi, 1993
glass	Krýsová et al., 1998; Ray and Beenackers, 1998; Ohko, Hashimoto, and Fujishima, 1997; Freudenhammer et al., 1997; Lichtin and Avudaithai, 1996; Trillas, Peral, and Domènech, 1996; Ogata et al., 1995; Fernández et al., 1995; Zhang et al., 1994; Zeltner, Hill, Jr., and Anderson, 1993; Sabate et al., 1991; Al-Ekabi and Serpone, 1988; Matthews, 1987a
glass wool	Zhang et al., 1994
sand	Lee, 1995; Zhang et al., 1994; Matthews, 1991; Haarstrick, Kut, and Heinzle, 1996
stainless steel	Ha et al., 1996; Wilkinson, 1994; Fernández et al., 1995; Pacheco, Watt, and Turchi, 1993
teflon	Low and Matthews, 1990

Immobilized TiO_2 particles form a porous film on the parent material. These films are usually less porous at the two interfaces with the parent material and with the reaction medium. Aguado, Anderson, and Hill (1994) studied the degradation of formic acid over TiO_2 ceramic membranes and reported the following findings:

i. Only the mass of the TiO_2 membrane influenced its capacity for radiation absorption;

ii. Neither the size of the precursor colloid particles from which the membrane is formed nor the porosity of the membrane affected UV absorption significantly;

iii. Lambert-Beer relationship can be used to describe UV absorption in TiO_2 membranes; and,

iv. For a given radiation intensity and membrane porosity, there is a membrane thickness which gives the optimal quantum yield.

This optimal membrane thickness was found to be 0.6 μm for a radiation intensity of approximately 1.0 Wm^{-2} (Aguado, Anderson, and Hill, 1994). Ogata and co-workers investigated the effect of TiO_2 coating thickness on the photodegradation of beef extract and peptone (Ogata et al., 1995). They reported that the reaction rate increased proportionally with increases in the thickness of the TiO_2 coating within a range of from 0.2 to 1.0 microns. The radiation source emits photons at 254 and 185 nm and provided illumination which is equivalent to about 100 Wm^{-2}.

Catalyst Modification

Low energy efficiency has been the major problem with the commercialization of UV/TiO_2 water decontamination (Parent et al., 1996; Saltiel, Martin, and Goswami, 1992). Catalyst activity improvement through modifications of the TiO_2 surface is one possibility to enhance this efficiency. Three methods have been shown to be effective, including, doping of metals and other species, surface chelation, and photosensitization. In terms of catalyst doping,

two precautions should be exercised. First, additional water pollutant should not be introduced into the system. Secondly, dopants are not universally effective in different redox systems (Parent et al., 1996).

Metal ion doping can improve trapping of the photo excited conduction band electrons at the surface whereby suppressing charge carrier recombination (Hoffmann et al., 1995). Many kinds of metals have been tried as dopants. Among others, gold (Gao et al., 1991), silver (Chen and Chou, 1994; Konda and Jardim, 1991), palladium (Papp et al., 1993), platinum (Harada, Hisanaga, and Tanaka, 1990; Izumi, Fan, and Bard, 1981; Suri et al, 1993) were found to enhance quantum yield substantially for the systems examined. 1%Pt- doped Aldrich TiO_2 enhanced the activity of Aldrich TiO_2 by 200% to 400% (Suri et al., 1993). Harada and co-workers enhanced the degradation rates of two organophosphorus insecticides by a factor of 10 through doping of platinum on TiO_2 (Harada, Hisanaga, and Tanaka, 1990).

Some adsorbents, such as activated carbon, clay, or silica (Yoneyama et al., 1994; Uchida, Itoh, and Yoneyama, 1993) could also enhance photocatalysis by improving the adsorption at the catalyst surface. Fu and co-workers (1996) improved TiO_2 photoactivity by a factor of 300% using silica and ziroconia. Another way to enhance organic adsorption on catalyst surface is to render the solid surface hydrophobic (Langford, Lepore, and Persaud, 1997).

2.2.2 Radiation Wavelength and Intensity

The probability for a photon to be absorbed by TiO_2 and utilized in electron-hole pair generation is dependent on its energy level. In order to account for the different capability of photons with different energy levels in generating charge-carriers when incident on the catalyst surface, a parameter, called the absorption coefficient, has been introduced (Crittenden and Zhang, 1995). The absorption and scattering coefficients of titanium dioxide suspensions have

also been measured (Cabrera, Alfano, and Cassano, 1996).

The rate of photon absorption by the catalyst should be directly proportional to the electron-hole pair generation rate if the fraction of the radiation energy lost due to light transfer barriers does not change with radiation intensity. However, as discussed in previous sections, this does not necessarily mean that the reaction rate is directly proportional to radiation intensity, due to an enhanced charge-carrier recombination rate and possible mass transfer limitation. Actually, photocatalytic reaction rates were usually found to be proportional to radiation intensity for low level radiations and to approximately the square root of radiation intensity for high level radiations. This relationship is supported by the results of many systems where transport was not limited (Ollis, 1991; D'Oliveira, Al-Sayyed, and Pichat, 1990; Okamoto et al., 1985b). The transition between these two regions is dependent upon the experimental conditions and has been reported to be between 2-170 Wm^{-2} (Okamoto et al, 1985b; Blake et al., 1991; D'Oliveira Al-Sayyed, and Pichat, 1990; Reeves et al., 1992). Therefore, large catalyst surface areas illuminated by radiation with intensities lower than the transitional level should be used to obtain a moderate reaction rate as well as a high energy efficiency.

Based on the idea that illumination is not a necessity for all the steps in photocatalysis except for photoexcitation, Sczechowski tried to use periodic instead of continuous illumination to enhance quantum yield (Sczechowski, 1995). Some researchers have operated fluidized bed reactors to take advantage of the large catalyst surface area that may be activated as a result of the mixing in such systems (Haarstrick, Kut, and Heinzle, 1996; Lee, 1995).

2.2.3 Water, Electron Acceptors and Donors

In photocatalysis, catalyst surface hydroxylation is an essential step and the base for subsequent redox reactions (Hoffmann et al., 1995; Linsebigler, Lu, and Yates, 1995). Studies show that water dissociatively adsorbs onto the TiO_2 surface and reacts with the bridging oxygen

atoms to form two hydroxyl groups. This adsorption is a function of temperature and will drop substantially at 77 to 127 °C (Linsebigler, Lu, and Yates, 1995). The results of one study indicated that at temperatures above 250 °C, all the hydroxyl groups on TiO_2 surface will be removed and the catalyst activity reduced substantially (Munuera, Rives-Arnau and Saucedo, 1979).

For the photocatalytic oxidation of water pollutants, electron acceptors adsorbed on catalyst surface are required to trap the excited electrons and thereby free the valence band holes which initiate the generation of oxidative radicals and the redox reactions on the catalyst surface. Oxygen is the most common electron acceptor as it exists naturally and is available at no additional cost. In addition, in many cases oxygen is required stoichiometrically as a reactant for complete mineralization (Hsiao, Lee, and Ollis, 1983). Without oxygen, complete oxidation of chloro-organics could not be realized (Sabate et al., 1991; Matthews, 1988; Okamoto et al., 1985b; Barbeni, Pramauro, and Pelizzetti, 1984; Hsiao, Lee, and Ollis, 1983). The dependence of the reaction rates on DO level has been given in Equation (2-15). Desired oxygen levels in photocatalytic reactors are system specific and depend on, among other factors, radiation intensity and the type and amount of the chemical to be degraded. Turchi and Ollis reported that sufficient oxygen could be furnished by purging the reactor with air (Turchi and Ollis, 1989). Augugliaro and co-workers found that their system required an oxygen pressure of at least 0.5 atmosphere in the reactor head space (Augugliaro et al., 1991). In another case, the reaction rate was still oxygen limited even after the system was purged with oxygen of one atmosphere (Okamoto et al., 1985a). Oxygen molecules adsorb onto TiO_2 surfaces through partial charge transfer from the surface adsorption site to the oxygen molecule. This adsorption decrease with an increase in temperature and the maximum desorption rate occurs at 75 °C (Linsebigler, Lu, and Yates, 1995).

One of the methods to enhance the quantum yield of photocatalytic oxidation processes is to add to the reactor electron donors that are superior to oxygen. This could result in faster

trapping of the electrons, leaving more holes available to continue the oxidation process (Hoffmann et al, 1995). Apparently, a desirable electron acceptor should have a strong oxidizing power and cause no need for additional treatment after use. Many kinds of oxidizers have been examined as potential electron acceptors. Hydrogen peroxide is the one that has been examined the most (Matthews, 1991; Tanaka, Hisanaga, and Harada, 1989). Hydrogen peroxide enhances the reaction in two ways. First, it can split to produce hydroxyl radical directly by absorbing radiations with wavelengths shorter than 300 nm (Peyton and Glaze, 1988). Second, it can produce hydroxyl radical through the following reactions:

$$H_2O_2 + e^- = {}^{\bullet}OH + OH^- \qquad (2\text{-}22)$$

$$H_2O_2 + O_2^{\bullet -} = {}^{\bullet}OH + OH^- + O_2 \qquad (2\text{-}23)$$

The $O_2^{\bullet -}$ in Equation (2-22) is produced through the interaction between adsorbed oxygen and trapped electrons as expressed by Equation (2-10) in section 2.12. H_2O_2 was found to enhance the reaction rates substantially in many studies (Matthews, 1991; Tanaka, Hisanaga, and Harada, 1989). However, Chemseddine and Boehm (1990) found that H_2O_2 inhibits the photocatalytic degradation of acetic acid and chloroacetic acids. This was explained to be that H_2O_2 occupied the adsorption site for oxygen as well as for the reactants.

Martin, Lee, and Hoffmann (1995) examined ClO_2^-, ClO_3^-, IO_4^-, BrO_3^-, and $S_2O_8^{-2}$ as electron acceptors and found that they were all capable of increasing the photodegradation rate of 4-CP. Their effectiveness followed the order: $ClO_2^- > IO_4^- > BrO_3^- > ClO_3^-$. Other oxidants that have been examined as electron acceptors include: peroxydisulfate and periodate (Pelizzetti et al., 1991) and Oxone® (Al-Ekabi et al., 1993). They were all reported to be better electron acceptors than oxygen with Oxone® (a potassium peroxymonosulphate compound) being the best.

For those photocatalytic reactions through reductive pathways, the existence of oxidizers may be detrimental to the reaction and electron donors may be necessary to initiate or enhance

the reaction (Choi and Hoffmann, 1995; Bahnemann et al., 1995). For example, Choi and Hoffmann used alcohols, carboxylic acids, and benzene derivatives as electron donors and mineralized carbon tetrachloride successfully.

2.2.4 Temperature Effect

Temperature affects photocatalytic reaction rates by affecting adsorption of water, oxygen, and other reaction- related species on the catalyst surface, transport of reactants and reaction products to and from the catalyst surface, the solubility of reaction related species in water, and the performance of artificial light sources.

Within certain temperature ranges, photocatalytic reaction rates were found to increase with increases in temperature (Bahnemann, Bockelmann, and Goslich, 1991; Hofstadler et al., 1994; Al-Ekabi et al., 1989; Matthews, 1987b; Okamoto, 1985b). The upper limits of these temperature ranges are believed to be associated with the substantial desorption of water and oxygen which occurs around 75°C (Linsebigler, Lu, and Yates, 1995). Compared to conventional chemical reactions, photocatalytic reactions have been reported to be less sensitive to temperature (Fox and Duely, 1993). As can be seen from Table 2-2, the activation energy of 4-CP was found to be as low as 16 kJ. The output of artificial radiation sources is also dependent on temperature, with 30°C being the optimal one for fluorescent lamps (Roche, 1993). Therefore, appropriate commercial reactor design must allow for suitable temperature control.

2.2.5 Mass Transfer Effect

Photocatalysis involves the transfer of reactants, reaction products between the bulk liquid and the reaction sites (i.e., the catalyst surfaces). For slurry systems, no effect of mass transfer has been reported so far. This is due to the large interfacial areas of the water and the

catalyst in such systems. When TiO_2 is immobilized on stationary solid substrates, the area of the water/catalyst interface will usually be substantially reduced. In addition, reactants have to travel a relatively distances and also a thick stagnant layer before they can reach the reaction sites. Under high-level radiation, low reactant concentrations, and/or low turbulence conditions, the process may be limited by mass transfer. It can be deduced from Equation (2-16), mass transfer controlled-processes should follow first order kinetics with respect to the limiting reactant concentration in the bulk liquid. Al-Ekabi and Serpone examined the photocatalytic degradation of chlorinated phenols in two types of reactors. The first reactor included a coiled glass tube with TiO_2 immobilized on the inner surfaces and a fluorescent lamp placed at the center. The second reactor was annular one packed with TiO_2-coated glass beads and illuminated with a fluorescent lamp at the axis. The results from both reactors showed dependency of the reaction rate on the liquid flow rates and first order kinetics was reported (Al-Ekabi and Serpone, 1988). Matthews also reported flow-dependent reaction rates and "first order kinetics" with a film reactor (Matthews, 1987b). These reactions were considered to be mass transfer limited (Turchi and Ollis, 1992). Sabate and co-workers (1991) reported results obtained from an annular reactor with catalyst immobilized on the inner wall and illuminated from the center. Mass transfer problems were not identified and the reaction followed the L-H relationship. Mass transfer limitation potential in photocatalytic reaction systems was analyzed carefully (Assink and Koster, 1995). It was concluded that unless low radiation intensity and/or very high liquid velocities are adopted, particles on which TiO_2 is coated should be kept smaller than 50 μm to avoid mass transfer limitation. Therefore, it is obvious that mass transfer should not be overlooked in considering immobilized photoreactors.

2.2.6 Reaction Inhibition

All species in the reaction medium, including water, reaction intermediates, reaction products, other reactants, and nonreactive components, may simultaneously adsorb onto catalyst surfaces and therefore occupy active reaction sites on a competitive basis (Ollis, Pelizzetti and Serpone, 1989). The adsorption of species other than target reactants may therefore inhibit photocatalytic reaction rate because those active sites would have been occupied by reactants without those other species. Results obtained with multicomponent systems and practical wastewaters have clearly confirmed the inhibition as a result of other known compounds (Wilkinson, 1994; Turchi and Ollis, 1990), COD and suspended solids (Watts et al., 1994), and inorganic ions (Hisao, Lee, and Ollis, 1983; Fujihira, Satoh, and Osa, 1982; Augugliaro et al., 1991; Mechos and Turchi, 1993; Pacheco, Prairie, and Yellowhorse, 1993; Low, McEvoy, and Matthews, 1991).

Turchi and Ollis (1989) studied the degradation kinetics of perchloroethylene (PCE) and benzene mixtures. Their findings indicated that PCE did not affect benzene degradation but benzene and its intermediates significantly inhibited the degradation kinetics for PCE. Watts and co-workers (1994) found that photocatalytic degradation of chloroether was completed quenched at a soluble COD of 164 mgL^{-1}. They also found that ammonia-nitrogen of up to 70 mgL^{-1} showed no apparent inhibition. Perchlorates, and nitrates of 0.1 M showed little inhibition, and sulphate and phosphates exhibited noticeable inhibition at 0.001 M (Abdullah, Low, and Matthews, 1990; Augugliaro et al., 1991; Low, McEvoy, and Matthews, 1991). Chloride ion has been identified as an inhibitive species by many researchers (Fujihira, Satoh, and Osa, 1982; Hsiao, Lee, and Ollis, 1983; Augugliaro et al., 1991). As one of the common ions in natural water bodies, bicarbonate also inhibits photocatalytic reactions (Pacheco, Prairie, and Yellowhorse, 1993; Methos and Turchi, 1993; Glaze, Kenneke, and Ferry, 1993). Fortunately this inhibition could be substantially alleviated by operating the reactor at a lower

pH value (i.e., 5.0). This occurs because that the bicarbonate equilibrium shifts to dissolved carbon dioxide at lower pH.

2.2.7 pH Effect

The pH of the reaction medium affects surface chemistry and solution kinetics. The overall effect is usually case specific and it is difficult to draw any general relationship based on the results available to date (Vohra and Davis, 1993). Augugliaro and co-workers (1993) examined the effect of pH on the degradation kinetics of nitrophenol isomers. Okamoto and co-workers (1985a) studied the effect of pH on the degradation of phenol and identified an optimal pH of 3.5. However, sulfuric acid was used for pH adjustment and therefore it is not clear whether or not the pH dependency was correlated with sulphate, an inhibitory ion. Ku and Hsieh (1992) found that the photocatalytic degradation rate of 2,4-DCP was not apparently affected within a pH range from 3 to 11. For ammonia degradation, on the other hand, pH was found to be a critical parameter (Bonsen et al., 1997). Up to a pH of 7.2, no reaction was observed. For pH values from 7.2 to 9.9, higher pH resulted in higher reaction rates. Within a range of 3-11, Augugliaro and co-workers (1993) reported that the degradation of nitrophenols was enhanced at lower pH values. The chemicals used for pH control were sodium hydroxide and sulfuric acid. It is suggested here that acids and bases that do not have inhibitive effects (i.e., sodium hydroxide, nitric acid) to photocatalytic reactions should be used in examining the effects of pH.

2.3 Photochemical Reactors

2.3.1 Illumination Sources and Radiation Transfer Materials

The radiation source is a critical component of photoreaction systems (Stevens and

Mourad, 1995). For heterogeneous reactors utilizing artificial lamps, the type of lamp which gives the highest efficiency in the spectrum of interest, yet is compatible with other parts of the system, should be of first choice.

Many different UV sources have been used in previous investigations into photocatalysis, including different types of lamps and solar radiation. Artificial UV lamps can be classified into low pressure mercury lamps, medium pressure mercury lamps, high pressure mercury lamps, high pressure xenon lamps, as well as fluorescent lamps (i.e., low pressure mercury lamps with phosphorus powders deposited on the inner surface of the lamp tube). Low pressure mercury lamps irradiate rays of 185 and 254 nm (Philips Lighting Company, 1998). This type of lamp is not a good candidate in photocatalysis because of the ozone generation risk and the difficulty in UV-C transmission. High pressure mercury lamps irradiate primarily in the UV-A and visible light region (Philips Lighting Company, 1998). Compared to low pressure mercury lamps, they are usually more powerful but may need high voltage for lamps of tubular shape. Medium pressure mercury lamps possess characteristics between low and high pressure mercury lamps. The high pressure xenon lamps are powerful and irradiate with a near continuous spectrum over a wide range, comparable to that of solar radiation (Philips Lighting Company, 1998). Since only the UV part could result in photocatalytic reactions, this type of lamp would not be energy efficient.

Fluorescent lamps usually have outputs from 5 to 100 watts and irradiate in UV-B, UV-A, or visible region, depending on the phosphor powders applied. Their energy efficiencies are typically from 15 to 30%. Fluorescent lamps have been popular among photocatalysis researchers. In UV-A region, the solar radiation intensity is typically from 15 to 50 Wm^{-2}, depending on the location, the cloud cover, and the humidity (Goswami, 1997; Curcó et al.,1996; Turchi and Mehos, 1994).

Factors that need to be considered in selecting light transmission materials include, light transmission efficiency in the interesting wavelength range, chemical and thermal stability, cost,

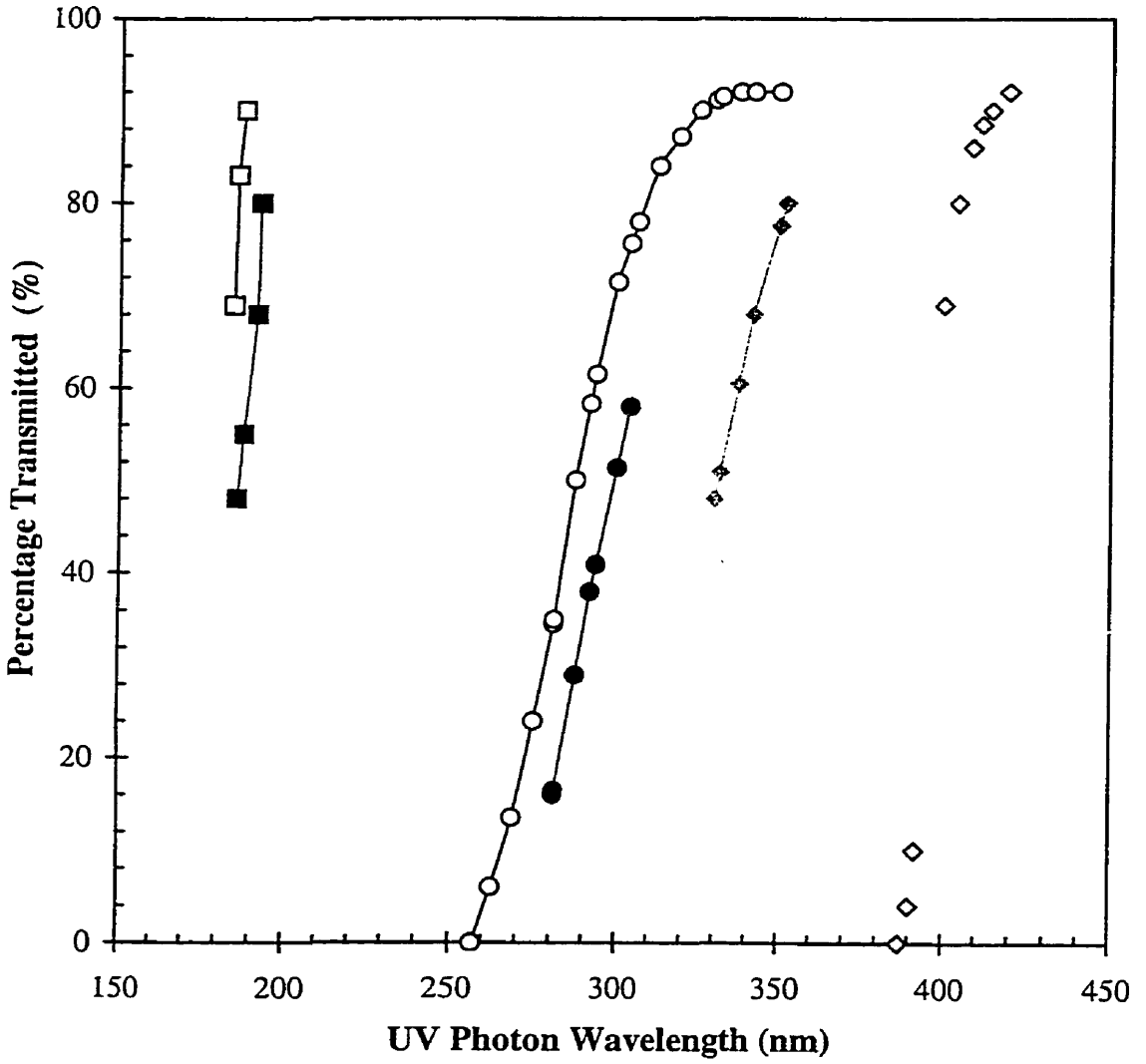

Figure 2-2: UV Transmission Characteristics of Selected Materials
Thickness:3.175 cm (Rohm and Haas Co., 1985 and Rabek, 1983);
▯distilled water; ■ fused quartz; ○ UVT acrylic; ● Pyrex glass;
◆ window glass; ◇ UVA acrylic

fabrication potential, and durability. Figure 2-2 shows the optical properties of a few commonly used materials (Rohm and Haas Co., 1985; Rabek, 1983). Quartz is one of the most "transparent" solid materials for UV light, but it may be too expensive to be used in full-scale water treatment systems. Compared to Pyrex glass, acrylic materials could offer low cost, appropriate optical properties, and superior fabrication potential, but they are chemically and thermally less stable (Pugh et al., 1995).

To date, most researchers used Pyrex glass in their studies. In these systems most radiation in UV-C and UV-B regions is absorbed by the Pyrex glass wall and dissipated as heat, allowing most of UV-A to reach the catalyst surface. However, there are situations in which the synergistic effect of photolytic- photocatalytic reactions is significant (Puma and Yue, 1994; Matthews and McEvoy, 1992). In these cases, quartz should be considered.

2.3.2 Mixing of Reactant and Catalyst

The effects of mixing on the performance of slurry photoreactors have been examined by Hacker and Butt (1975). It was reported that mixing will increase the reaction rate if the local reaction rate is dependent upon the absorbed radiation energy, the reaction slurry is optically thick, and the relative time scale of chemical process to the mixing process is small. This result applies to photocatalytic water treatment systems in which TiO_2 is suspended in the aqueous phase or immobilized on mobile particles. In this type of system, mixing will enhance reaction rates since more uniform activation of the catalysts and higher mass transfer rates could be expected.

Because high quantum yield is only possible for radiation of low levels, distribution of radiation to a large catalyst surface is actually the central problem in scaling-up a photocatalytic reactor (Ray and Beenackers, 1998). Lee (1995) tried to enhance the degradation of phenol by utilizing the mixing effect in a fluidized bed photoreactor. Karpel, Sczechowski and co-workers

operated a Taylor Vortex photoreactor with lamps located at the center (Karpel et al., 1997; Sczechowski, 1995). It was reported that the photocatalytic reaction rate could be enhanced by a factor of 3 because of the mixing induced by Taylor Vortex.

For systems with TiO_2 immobilized on stationary surfaces, mixing could enhance heat transfer and the transport of reactants to catalyst surface and the products to liquid bulk. These may result in better temperature control and increases in reaction rates for reactions with kinetics of higher than zero order. For reactions that suffer from product inhibition (Lepore, Pant, and Langford, 1993), proper mixing may also alleviate this inhibition. For this type of reactor, mixing cannot significantly change the radiation distribution on the catalyst surfaces and the effect of mixing would be limited provided that the system is not transport limited.

2.3.3 Radiation Models

In photoreactors, transfer of heat and mass, transfer and absorption of photons, photocatalytic reactions and other possible reactions (i.e., photolytic) are closely interrelated processes. Reaction rates contribute to and also depend on the temperature field, the radiation field, as well as the concentration field (i.e., the distribution of pollutants, inhibitory ions, products, electron donors and acceptors such as O_2 and H^+ in the reactor). As most photochemical reactions are not sensitive to small temperature changes, the performance of a photoreactor could be approximately determined by mass and radiation balances (Alfano, Romero, and Cassano, 1986a). The effect of the Local Volumetric Rate of Energy Absorption (LVREA) on reaction rates is the peculiar feature of all homogeneous photochemical processes. Therefore, effective modeling of the emission, transfer, and absorption of photons is usually the key in photoreactor modeling.

The first step in radiation modeling is the choice of an appropriate radiant energy source model. This source model could be a distribution of radiant energy in the vicinity of the reactor

(i.e., reactor wall) or a lamp emission algorithm. Radiation models developed using the first approach are classified as incidence models. Those developed using the other approach are classified as emission models. Incidence models always contain one or more experimentally adjustable parameters which need to be fitted using lab data. For polychromatic radiation sources, the absorbed photons at different wavelengths are additive (Cassano et al., 1995).

Photon transfer in a heterogeneous medium may follow Rayleigh theory, Mie theory, or geometric optics, depending on the physical dimensions of the inhomogeneities as compared to the wavelength of the photons (Cassano et al., 1995). A heterogeneous medium may be regarded as optically homogeneous provided that the smallest inhomogeneities (i.e., catalyst particle diameter) are sufficiently small as compared to the wavelength of the radiation. Transfer of photons through (optically) homogeneous media could usually be modeled accurately with the Lambert-Beer's law (Rizzuti, 1985) and the principles of geometric optics (Roger and Villermaux, 1979). In this case, reflection, refraction, and to some extent diffraction should be addressed. Scattering should usually be considered in analyzing photon transfer in heterogeneous media.

Previous work on radiation field modeling in both homogeneous and heterogeneous media have been reviewed in detail (Cassano et al., 1995; Alfano, Romero, and Cassano, 1986a,b). The majority of the previous work was performed in homogeneous (Tsekov and Smirniotis, 1997; Yokota et al., 1976; Akehata and Shirai, 1972) and heterogeneous (Romero, Alfano, and Cassano, 1997; Pasquali et al., 1996) annular reactors. Romero, Alfano, and Cassano (1997) rigorously simulated the photon absorption and scattering in an annular slurry photocatalytic reactor illuminated with a mercury arc lamp placed at the center. It was observed that the calculated profile of the LVREA along the radial coordinate was very steep for TiO_2 loadings commonly adopted in photocatalysis studies. The lamp was modeled as an extense source with volumetric emission as recommended in the literature (Alfano, Romero, and Cassano,1986a). Pasquali and co-workers (1996) evaluated the radiation field in another annular

slurry photocatalytic reactor. The illumination source was either mercury arc or metal halide fluorescent lamps, which was modeled as a linear source with diffuse emission. The catalyst used was TiONAVC grade with an average particle diameter of 11.9 microns. These solid particles were modeled as diffusely reflecting spheres. Experimental results fitted the model well. Compared to the results due to Romero, Alfano, and Cassano (1997), the profile of the LVREA along the radial coordinate was not steep at all. In addition, the radiation field was found to be insensitive to the scattering distribution function (i.e., angularly dependent phase function). Cabrera, Alfano, and Cassano (1994) calculated the LVREA in a slurry type planar reactor illuminated with a medium pressure mercury lamp positioned at the focal axis of a parabolic reflector. The volumetric absorption and scattering coefficients were determined experimentally. The scattering distribution function were obtained from a model derived from geometric optics that was assumed to respond to a specular, partial reflection process (Siegel and Howell, 1992). Maruyama and Nishimoto (1992) demonstrated the use of two-flux model to illustrate the radiation intensity profile in heterogeneous photochemical reactors. Compared to the rigorous models, this model is simple but semi-empirical in nature. Marinangeli and Ollis (1977) modeled the radiation intensity profile in a catalyst-coated cylindrical optical fibre.

2.3.4 Reactor Configuration

Dozens of classical and novel photocatalytic reactor configurations have been proposed and/or examined to date. Selected information on these photocatalytic reactors are summarized in Table 2-4.

Several groups conducted researches on solar-radiated pilot-scale tubular reactor systems (Blanco and Malato, 1994; Mehos and Turchi, 1993; Pacheo, Prairie, and Yellowhorse, 1993). In these systems, aqueous TiO_2 slurries were pumped through horizontal borosilicate glass tubes located at the foci of solar concentrators. For the treatment of an effluent from a resin plant

(contains phenol, toluene, xylene, phthalic acid, fumaric acid, phenylethylene, etc.), photocatalytic method was found to be fully competitive compared with other AOPs being currently used in industry (Pacheo, Prairie, and Yellowhorse, 1993). However, fine TiO_2 particles may exist in the treated water due to the incomplete separation of the catalyst from the treated water (through pond settling). Two major limitations were identified with these concentrated solar systems. They are, (1) concentrated solar radiation at the expense of concentrators results in higher reaction rates but lower photo-efficiency, and (2) TiO_2-water separation is required after treatment.

Table 2-4: Previously Studied Photoreactor Configurations

Reactor I.D.	**UV Source /TiO_2 Form**	**Reference**
tubular reactor	solar, slurry	Blanco and Malato, 1994; Mehos and Turchi, 1993; Pacheo, Prairie, and Yellowhorse, 1993
annular reactor	artificial at center immobilized or slurry	Chester et al., 1993;Wei and Wan, 1991; Okamoto et al., 1985a
flat plate reactor	side, solar/artificial, immobilized	Augugliaro et al., 1995; Wilkinson, 1994; Pugh et al., 1995
spiral glass tube reactor	artificial at center, immobilized	Al-Ekabi and Serpone, 1988; Matthews, 1987b
falling film reactor	side, solar/ artificial, immobilized	Krýsová et al., 1998; Freudenhammer et al., 1997; Puma and Yue, 1994
double skin reactor	solar, slurry	Well et al., 1996
packed bed reactor	solar or artificial at center or outside, immobilized	Dong and Berman, 1996; Zhang, 1994; Robertson and Henderson, 1990; Al-Ekabi and Serpone, 1989; Matthews, 1987a

Table 2-4 cont'd

Reactor I.D.	UV Source /TiO_2 Form	Reference
monolithic reactor	artificial at one end	Luo, 1994
fibre optic bundle reactor	artificial at end, immobilized	Peill and Hoffmann, 1995; Hofstadler et al., 1994
Taylor vortex reactor	artificial at center, slurry	Karpel et al., 1997; Sczechowski, 1995
fluidized bed reactor	artificial at center or outside, immobilized	Haarstrick, Kut, and Heinzle, 1996; Lee, 1995; Brucato et al., 1992; Raupp and Dibble, 1991
PHOTO-CREC reactor	artificial at center, immobilized	Valladares, 1995; de Lasa and Valladares, 1997
accordion folded mesh and flutter fibre strand	solar, immobilized	Pacheco, Watt, and Turchi, 1993
multiple tube reactor	artificial at end, immobilized	Ray and Beenackers, 1998
tube light reactor	TiO_2-coated thin tube lights	Ray, 1998
turbulent slurry reactor	center, slurry / filtration	Butters and Powell, 1995
helical plate /wave guide	artificial at center, immobilized	Dong and Berman, 1996
finned structure reactors	artificial, immobilized	Say et al., 1998
membrane type reactors	artificial or solar, immobilized	Bischoff, Fain, and Stockdale, 1999; Berman and Grayfer, 1998; Cooper, 1998; Gonzalez-Martin, Murphy, and Hodko, 1998

Chester, Okamoto and co-workers examined the photocatalytic degradation of organic pollutants in annular reactors with the lamp tubes at the center and with TiO_2 suspended in the reaction medium (Wei and Wan, 1991; Okamoto et al., 1985a) or immobilized on the reactor wall (Chester et al., 1993). Augugliaro (1995), Wilkinson (1994), and Pugh (1995) used flat plate reactors in their studies. Matthews (1987b) used a TiO_2-coated spiral tube wound around a lamp in his research. No superior photo-efficiency and reactor capacity was reported in these studies.

In falling film reactor systems, the catalyst was immobilized on slabs (Krýsová et al., 1998; Freudenhammer et al., 1997; Puma and Yue, 1994) or walls of columns (Puma and Yue, 1994) along which liquid films descend. The immobilized catalyst can be illuminated by either solar or artificial radiation sources from one side of the slab (Krýsová et al., 1998; Freudenhammer et al., 1997; Puma and Yue, 1994), or by artificial lamps at the center or surrounding the column (Puma and Yue, 1994). Puma and Yue (1994) found that the configuration with TiO_2 coated on the internal wall of a column and with the lamp in the middle of the column was the most efficient one. Although falling film reactors enjoy many advantages such as possible efficient utilization of solar power, they all suffer from low reactor capacity as a result of the limited activated catalyst surface area per unit volume of reactors.

Well and co-workers (1996) developed a solar powered photocatalytic reactor, called double-skin reactor. This is a slurry type reactor in which water flows through a thin slit between two acrylic sheets. While it is capable of utilizing both the direct and diffuse solar UV rays, some problems were also experienced (Well, Dillert, and Bahnemann, 1997).

Several versions of the packed bed reactors have been reported, differing in the reactor body as well as the packings. Robertson and Henderson (1990) patented a packed bed reactor which included an annular packed with TiO_2-coated glass mesh and radiated by a lamp located at the center. Al-Ekabi, Serpone (1989), and Matthews (1987a) also performed experiments in annular beds but the packings used in their study were TiO_2-coated glass wool and glass beads

respectively. Zhang (1994) examined the degradation of trichloroethylene (TCE) using solar irradiated acrylic tubes packed with various TiO_2-coated solid particles. The supported catalysts were optimized with respect to catalyst type, catalyst loading, silica-based support material, particle size, catalyst/support bonding, and calcination temperature. The best packing, silica gel coated with Pt-dopted anatase, was claimed to be as high as 4 times more active than Pt-dopted anatase slurries (Zhang et al., 1994). Since the diameters of the silica gel particles and the tubular bed were both very small, scale-up potential and maintenance cost may become a problem. Generally speaking, packed bed reactors tend to suffer from limited effective catalyst surface area per reactor volume due to the opaque nature of TiO_2 films. Mehrvar (1998) tested the degradation of 1,4 dioxane in a column packed with TiO_2-coated stainless steel Tellerette.

At least two TiO_2-coated optical fibre bundle type photoreactors have been examined (Peill and Hoffmann, 1995; Hofstadler et al., 1994). For a TiO_2-coated fused-silica fibre with a diameter of 2 mm and a length of 480 mm, 10% of the initial radiation intensity was obtained at the other end when illuminated at one end with a beam of collimated light (Hofstadler et al., 1994). For the degradation of 4-CP, Peill and Hoffmann reported a quantum yield enhancement of 90% over that of a slurry reactor. This type of reactor may not be competitive due to problems such as, high cost of optical fibre bundles and radiation energy loss in photon transfer.

Taylor vortex photoreactors have been reported in several sources (Karpel et al., 1997; Sczechowski, 1995). This type of reactor consists of two co-axis columns (i.e., a stationary outer one and a rotating inner one) with a lamp placed at the axis of the columns. Taylor vortex flow pattern of the TiO_2 slurries in the annulus induced by the rotating inner column, allows the suspended TiO_2 particles periodic exposure to radiation. Since illumination of the active sites of the catalyst is necessary only for the electron/hole pair generation and the rest of the reaction steps can proceed in the dark, periodic illumination has the potential to effectively activate more catalyst particles and therefore enhance quantum yields. Compared to slurry reactors at similar conditions, a factor of three increase in quantum yields was reported possible by using Taylor

vortex (Sczechowski, 1995). An optimal illumination period of approximately 0.15 seconds has been documented in a recent patent (Sczechowski, Koval, and Noble, 1995). Apparently, Taylor vortex reactors have disadvantages such as the added complexity due to the need for moving parts and catalyst recovery from water.

Haarstrick and Lee reported results on annular fluidized bed photoreactors in which TiO_2-coated sand (Lee, 1995) and quartz (Haarstrick, Kut, and Heinzle, 1996) particles were "fluidized" when wastewater was introduced at the bottom of the reactor at certain rates. For the degradation of a mixture of 4-CP and *p*-toluenesulfonic acid, the energy efficiency was found to be higher than 100 mg of TOC per kWh of power input. However, catalyst activity reduction associated with attrition was experienced (Lee, 1995). The random mixing of both fluid and TiO_2-coated particles in fluidized beds could allow more catalysts to be illuminated periodically, whereby enhancing the quantum yield. Compared to the mixing in Taylor vortex reactors, mixing in fluidized bed reactors should usually be less intensive and more random than controlled. Therefore, the mixing-associated quantum yield enhancement in a fluidized bed reactor is not expected to be greater than that in a Taylor vortex reactor. On the other hand, there is no catalyst-water separation problem with fluidized bed reactors.

Valladares (1995) studied the degradation of phenol and methylene-blue in a new reactor configuration (i.e., PHOTO-CREC II). This system is actually an annular reactor with a lamp placed at the center and 15 conical baskets positioned in the annular. These conical baskets were made of perforated stainless steel plates and their surface possess an angle of 45° with respect to the axis of the annular and the fluorescent lamp tube. TiO_2-coated glass meshes were fixed on the conical surfaces. For the degradation of Methylene blue, quantum yields of up to 0.63% were reported. This reactor configuration has been described in more detail in a recent patent (de Lasa and Valladares, 1997).

Pacheco and co-workers investigated the solar detoxification of trichloroethylene-spiked water and compared the performances of an accordion folded mesh (AFM) reactor and a flutter

strand (FS) reactor (Pacheco, Watt, and Turchi, 1993). The AFM reactor consisted of a tubular accordion shaped TiO_2-coated stainless steel screen in a Pyrex glass tube. The FS reactor consisted of a Pyrex glass tube in which TiO_2-coated fiberglass strands were fixed in position at the upstream end. These strands flutter in fluid flow. Both reactors were placed at the focus of a large parabolic trough for illumination. The AFM reactor was reported to perform better than the FS reactor.

Ray and Beenackers (1998) developed and tested a bench scale multiple tube reactor (MTR) for the degradation of a soluble acid dye, Special Brilliant Blue (SBB). The structure of this reactor resembles that of a shell and tube heat exchanger with the reaction liquid flow through the shell side over the outside surfaces of the TiO_2-coated quartz tubes while the photons travel along the tube side via multiple internal reflection. The illumination source, a low voltage halogen lamp, was optically positioned in an aluminum reflector at one end of the reactor. Compared to classical reactors, this reactor provides a large activated catalyst areas per unit reactor volume. This means potential for higher quantum yield and higher reactor capacity. However, the overall energy efficiency of this reactor may not be high due to the absorption of effective photons by the aluminum reflector and the tubes (if quartz not used). In addition, capital cost also tends to be high because of the necessity to use many tiny, thin, and exotic tubes.

Ray (1998) reported another novel reactor configuration, the tube light reactor (TLR). This reactor is essentially a tank in which numerous custom-designed U-shaped tiny fluorescent lamps are elaborately packed. Catalysts were immobilized on the surface of these tiny lamps. This reactor offers a very large illuminated catalyst surface area per reactor volume and was predicted to be effective for absorbing/scattering fluids (Ray, 1998). Unfortunately, these tiny lamps require a voltage as high as 1020 volts. Replacement of these lamps may well be costly for capital, labour, as well as down-time reasons. In addition, mercury contamination potential due to lamp failure may also be a concern for such a system.

In the US alone, there exist more than ten patents on different photocatalytic reactor systems (Bischoff, Fain, and Stockdale, 1999; Berman and Grayfer, 1998; Cooper, 1998; Gonzalez-Martin, Murphy, and Hodko, 1998; Say et al., 1998; de Lasa and Valladares, 1997; Dong and Berman, 1996; Butters and Powell, 1995; Raupp and Dibble, 1991; Robertson and Henderson, 1990). Several of these patented reactor configurations involve the use of catalyst-coated porous elements which are arranged to surround the lamps (Bischoff, Fain, and Stockdale, 1999; Berman and Grayfer, 1998; Cooper, 1998; Gonzalez-Martin, Murphy, and Hodko, 1998) and/or to form a flat structures for solar UV utilization (Gonzalez-Martin, Murphy, and Hodko, 1998). As one alternative, flat sheets of catalyst-coated porous elements were arranged to assume a "sandwich" together with the lamp arrays (Berman and Grayfer, 1998).

The turbulent slurry reactor due to Butters and Powell (1995) consists of a turbulent slurry reaction system and catalyst recovery/recycle system in which tiny TiO_2 particles are separated from water through ceramic membrane filtration. The membrane is cleaned periodically with backflow air. The systems patented recently by Say and co-workers (1998) are claimed to be compact and efficient for photocatalytic pollutant conversion, although no experimental data were reported. These reactors, called finned structure reactors, use catalyst-coated structures placed in the optical proximity of the illumination source. As one reactor configuration, the catalyst supporting structure includes multiple non-intersecting fins oriented parallel to the general flow direction of the fluid stream. These fins may be flat, pleated, perforated, or porous plates. The light source includes one or more lamps that may penetrate the fins. As another configuration, the catalyst supporting structure includes one or more cylinders having pleated inner surfaces with longitudinal lamps disposed in the cylinders. The reactors due to Dong and Berman (1996) consist of three distinct configurations. The first configuration is actually an annular reactor with a catalyst-coated and curved helical plate positioned in the annular space and a lamp at the center. The second configuration is an annular bed packed with

catalyst-coated particles and a lamp at the center. The packing was arranged such that the greater the distance from the lamp, the greater the fraction of the UV that is absorbed per unit penetration. The third configuration (wave guide reactor) involves the use of multiple flat catalyst supports, placed parallel to each other and at a small angle with respect to the array of the tubular lamps.

2.3.5 Photoreactor Modeling

Strictly speaking, the modeling of a photocatalytic reactor based on the first principles requires the simultaneous solution of the momentum, thermal energy, mass, as well as radiation balance equations. In contrast to photocatalytic reaction processes, reports on photocatayltic reactor modeling are rare. To date, there exist only several relatively complete works on photocatalytic reactor modeling. Cassano and co-workers (1995) presented a critical review on the fundamentals and applications of photoreactor analysis and design. Tubular and annular reactor configurations were analyzed as examples for simplicity. It was shown that the state of the art allows for the precise design of homogeneous photoreactors, if the mass and thermal energy fluxes as well as the intrinsic reaction kinetics can be predicted with sufficient accuracy. However, an equivalent state of the art for heterogeneous photoreactor design is not developed yet (Cassano et al., 1995).

Cabrera, Alfano, and Cassano (1994) performed rigorous radiation modeling and trichloroethylene degradation in a slurry type planar reactor. Model predictions were unfortunately not presented together with the experimental data. Ollis and Turchi (1990) developed models for the analysis of combined photolytic and catalytic reactions of TiO_2 slurries in annular and falling film reactors. The results of this study gave very interesting guidance to photoreactor design. However, experimental data were not available for quantitive model validation. Marinangeli and Ollis (1977) modeled photocatalysis in cylindrical optical fibres

based on fundamental principles. Again, no experimental work was reported.

There exists in the literature many photoreactor modeling works in which radiation field modeling was not performed. Crittenden and co-workers (1995) modeled the degradation of trichloroethylene in a fixed bed reactor. In their mathematical model, L-H kinetics was assumed. The Langmuir rate constant was assumed to be a function of radiation intensity and influent organic concentration. Radiation intensity was assumed to be constant throughout the bed. Saltiel, Martin, and Goswami (1992) modeled the performance of four types of solar-powered photocatalytic reactors (i.e., flat plate, compound parabolic concentrator, east-west and north-south one-axis tracking parabolic trough reactors). Reaction kinetics was modeled with L-H kinetics and a power law relationship was used to relate illumination to chemical destruction. March, Martin, and Saltiel (1995) simulated a solar-powered recirculation type flat plate slurry reaction.

2.4. Real Wastewater, Engineering Scale Studies and Cost Estimates

Photocatalysis has been shown to be effective in treating many types of non-biodegradable real wastewaters, including, contaminated groundwaters (Preis, Krichevskaya, and Kharchenko, 1997; Enzweiler et al., 1994; Pacheco, Prairie, and Yellowhorse, 1993; Mechos and Turchi, 1993), resins factory effluent (Blanco and Malato, 1994), textile wastewater (Freudenhammer et al., 1997), pharmaceutical plant wastewater (Anheden, Goswami, and Svedberg, 1995), distillery wastewater (Zaidi, Goswami, and Wilkie, 1993), and pulp and paper wastewater (Turchi, Edmundson, and Ollis, 1989). The results of these studies are important since the effects of the non-target species (i.e., background COD, inhibitory ions) were considered.

Of these real wastewater treatment demonstrations, four were performed in engineering scale systems (Enzweiler et al., 1994; Blanco and Malato, 1994; Pacheco, Prairie, and

Yellowhorse, 1993; Mechos and Turchi, 1993). Enzweiler and co-workers (1994) examined the photocatalytic destruction of benzene, ethyl benzene, toluene, and xylene in contaminated groundwater in three different types of commercially available systems. The first two systems were actually the same annular reactors illuminated by fluorescent lamps placed at the axis. The annular space was either packed with TiO_2-coated fibre glass mesh (first system, immobilized) or kept empty (second system, slurry). The third system was a solar-powered slurry one and consisted primarily of a glass tube array. Membrane filtration was used to recover the catalyst from treated water. It was found that the reaction in the second system was about three times faster than in the first system under otherwise identical conditions. In addition, the fixed bed (first system) caused a nine-fold increase in the pressure drop over that of second system. Solar radiation was estimated to be a cheaper UV source for photocatalysis.

Mechos (1993), Pacheco and co-workers (1993) demonstrated ground water treatment using solar-concentrating parabolic troughs with tubular slurry reactors mounted at the foci. Blanco and Malato (1994) treated effluent from a resin factory in a similar system. The results of a cost estimate indicated that the photocatalytic treatment systems tested are fully competitive compared to other best available technologies (Blanco and Malato,1994; Mechos and Turchi, 1993). Non-concentrating solar reactors were believed to be more cost-effective due to the elimination of the costly parabolic troughs as well as the enhanced energy efficiency of photocatalysis under lower level radiations (Mehos and Turchi, 1993). Some issues closely related to the economics of photocatalytic water treatment have been discussed (Goswami, 1997; Ollis, 1988). For systems using artificial lamps, most of the cost is associated with UV generation (i.e., purchasing, powering and servicing the lamps).

2.5 Combined Chemical and Biological Treatment

Every wastewater treatment process has its strengths and limitations in terms of

applicability, cost, and effectiveness. For example, biological processes are known to be very economic and reliable for treating most wastewaters (i.e., municipal wastewater, food and farm processing water). However, these processes suffer from a lack of effectiveness for recalcitrant and inhibitory organics. Chemical oxidations have been proven to be capable of destroying a wide spectrum of contaminants, including recalcitrant and inhibitory organics. But they can be very costly due to the non-selective nature, low energy efficiency, and/or the use of oxidants. For a certain water treatment tasks, sequential use of chemical and biological methods could result in reductions in overall treatment cost (Scott and Ollis, 1996). For wastewaters that are toxic, inhibitory, or refractory to biological cultures, chemical pretreatment can degrade the inhibitory, toxic, and refractory compounds and thereby alleviate or eliminate the toxicity and inhibition. It can meanwhile produce smaller, less aromatic, more polar, or more oxygenated fragments as intermediates which are mostly biodegradable (Jochimsen and Jekel, 1997). Conversely, economic biological pretreatment can remove the biogenic water pollutants and thereby reduce the oxidant and reactor requirement in the chemical oxidation step that follows.

As a potentially cost-effective water treatment strategy, combined biological and (photo)chemical oxidation is becoming increasingly popular among the researchers in recent years. Heinzle and co-workers (1992) studied the ozonation and biotreatment of pulp bleaching effluents. Cyclic activated sludge pretreatment and ozonation were believed to be cost-effective options. Tanaka and Ichikawa (1993) reported significant reduction of the toxic effects of cationic, anionic, and nonionic surfactants to methanogenic bacteria through pretreatment with TiO_2 photocatalysis. Yu and Hu (1994) enhanced the biodegradability of chlorophenols through ozone treatment. The authors also found that the biological cultures acclimated to the parent compounds did not have an advantage in degrading chemical treatment intermediates. Karrer, Ryhiner, and Heinzle (1997) demonstrated a procedure for evaluating the applicability of combined biological-chemical treatment. Chemical consumption per unit removal of dissolved organic carbon (chemical and biological steps combined) was recommended as the parameter

for cost estimation. Bolduc, Hess and co-workers reported the effectiveness and optimal photocatalytic pretreatment times in enhancing the biodegradabilities of 2,4,6-trinitritoluene (Hess et al., 1998) and m-dichlorobenzene, diphenylamine, and resorcinol (Bolduc and Anderson, 1997). Jochimsen and Jekel (1997) investigated the effect of ozonation on the subsequent biological treatment of tannery wastewater. The optimal ozone dosage was found to be between 1 and 3 grams of ozone per gram of DOC. Relevant issues for the integration of biological and chemical oxidation processes have been critically reviewed (Scott and Ollis, 1995).

2.6 Concluding Remarks

Photocatalysis has been proven to be capable of oxidizing organic water/air pollutants, killing microorganisms, and reducing the valence of dissolved metal ions. Important process parameters include catalyst form, illumination wavelength and intensity, nature and level of the target compound, electron acceptors and donors, inhibition due to inorganic ions and non-target chemicals, temperature, pH, and mass transfer. Photocatalytic reaction rates typically follow L-H type kinetics with the rate constant behaving with lower order dependency (usually between 0.5 and 1) on the radiation intensity on the catalyst surface.

Limited pilot-scale results indicate that photocatalysis could be as cost-effective as other best available water treatment technologies. Current state of the art suffers from low energy efficiency and relatively low fraction of solar energy that can be used (approximately 4%).

More work on the development of superior photocatalysts, photoreactors, and oxidizing agents (i.e., H_2O_2) could lead to fruitful results. Combined photocatalytic and biological approach could potentially result in overall cost savings. There is a shortage of studies on the development, modeling, and design of novel photocatalytic treatment systems. No experimentally tested photoreactor model, if there is one, is yet published in the literature.

CHAPTER 3: 4-CHLOROPHENOL DEGRADATION

In order to set-up benchmarks for the evaluation of different reactor configurations and to collect system-specific data for use in reactor modeling, photocatalytic degradation of 4-CP in two classic reactor configurations, immobilized flat plate reactor and slurry reactors, were performed. The results are summarized in the following sections of this chapter.

3.1 Materials and Methods

3.1.1 Chemicals and Catalyst

Reagent grade 4-chlorophenol from BDH Ltd. (England) was used as the model pollutant. This compound is also known as 1-chloro-4-hydroxybenzene or p-chlorophenol. Its CAS registry number is 106-48-9. Other chemicals used for HPLC analysis, intermediate identification, and pH control include: methanol (99.8%), acetonitrile (99.9%), phenol (99%), nitric acid, and potassium hydroxide from BDH Inc. (Canada), hydroquinone (99%) and resorcinol (99%) from Sigma Chemicals Co. (US), catechol (98%) from BDH Chemicals (England), 1,4-benzoquinone (98%) from Aldrich Chemical Company (US), and 4-chlorocatechol (95-99%)from Helix Biotech (Canada). The water used for all the runs was deionized water filtered with a Milli-Q system. Degussa P25 TiO_2 (Arkon, OH, USA) was used as the catalyst either suspended in water or immobilized on stainless steel plates. Based on information from the supplier, this product consists of non-porous particles of anatase (70%) and rutile (30%) and has a density of 3800 kg m^{-3}, a primary diameter particle of 21 nanometers, and a specific surface area of from 36 to 65 m^2g^{-1}.

4-CP was selected as the primary model compound based on the following considerations:

(1). Chlorinated phenols are a class of common water pollutants originated from industrial operations such as coal gasifying, coking, and oil refining (Verschueren, 1983).

(2). Biodegradation of 4-CP is slow and often requires a long lag period (Mikesell and Boyd, 1985). In addition, it is not easy to strip 4-CP out of water since this chemical has a very low Henry's law constant, which is listed in Table 4-4 (Howard, 1989).

(3). As a water pollutant, 4-CP can cause taste at a concentration as low as 0.25 mgL^{-1} and odour at 6.4 mgL^{-1}. Water with 4-CP will be toxic to microorganisms and fish if the concentration of this compound exceeds 5 mgL^{-1}. In addition, 4-CP contaminates the environment through bioaccumulation (Verschueren, 1983; Howard, 1989).

(4). 4-CP has been photocatalytically degraded by several research groups. Valuable background information makes it possible for the current research to concentrate on reactor engineering.

(5). 4-CP does not absorb electromagnetic radiation with wavelengths longer than 300 nm. Therefore, photolytic reactions would be negligible in systems illuminated by fluorescent lamps. This makes it possible to examine photocatalytic reactions alone.

3.1.2 Catalyst Immobilization

A procedure for the immobilization of TiO_2 on stainless steel plate was developed based on information from the literature (Ha and Anderson, 1996; Valladares, 1995; Wilkinson, 1994). It can be summarized into the following steps: (1) Clean thoroughly the steel plate with 20% hydrochloric acid and allow it to air dry; (2). Bake the cleaned plate in an oven at 200 °C for two hours; (3). Add gradually Degussa P-25 TiO_2 into a beaker containing 25% (v/v) aqueous methanol solution until the catalyst loading reaches approximately 180 gL^{-1}; (4). With a brush, paint the slurry onto the baked clean steel plate so that it forms as thin as possible a layer but opaque to UV light; (5). Bake the coated plate in an oven at 300°C for about 5 hours and then

allow it to cool in the air. The purpose of step (2) is the generation of an oxidized layer on the steel plate surface which was reported to improve the binding between TiO_2 and the plate (Ha and Anderson, 1996). The opaqueness of the film was examined by painting the same slurry onto a UV transmitting acrylic plate and measuring for UV transmission with a radiometer.

3.1.3 Photoreactor and System Set-up

Degradations were carried out in reactors created by placing different internals in a rectangular Plexiglas acrylic plastic chamber. The reactor cover was made from a UV transmitting Plexiglas (G-UVT). Its spectral UV transmission is plotted in Figure 2-2 (Rohm and Haas Canada Inc., 1985). A stainless steel screen enclosure packed with glass beads was used as a water distributor in the entrance zone of the plastic chamber (before the reaction zone). The flat plate reactor consisted of the plastic chamber, the distributor, and a TiO_2-coated flat plate (Figures 4-2 and 4-3) in the chamber placed 2.5 cm from the cover. The dimension of the catalyst coating was 80 mm by 500 mm. The plate was made from 3/64 inch stainless steel sheets (SS-314). The slurry system was formed when the artificial wastewater was spiked with 1 gL^{-1} TiO_2.

Figure 3-1 shows the experimental system set-up. Illumination was provided with three 40-watt fluorescent lamps (Philips, TLK 40W/10R) placed above the reactor and in parallel with the reactor cover. These lamps are built with reflection coatings on half of their inner surfaces and illuminate only one side. Their emission power at different wavelengths was obtained from the supplier and is plotted in Appendix A (Figure A-1). The pump was a centrifugal magnetically-coupled type and all the water-contacting parts were made from polypropylene. The reservoir was made from a 1000 mL-Erlenmeyer flask with ports for inlet, outlet, sampling, pH probe, dissolved oxygen (DO) probe, and thermometer. Oxygen required for the reactions was admitted into the reservoir through an opening to the ambient air. The reservoir

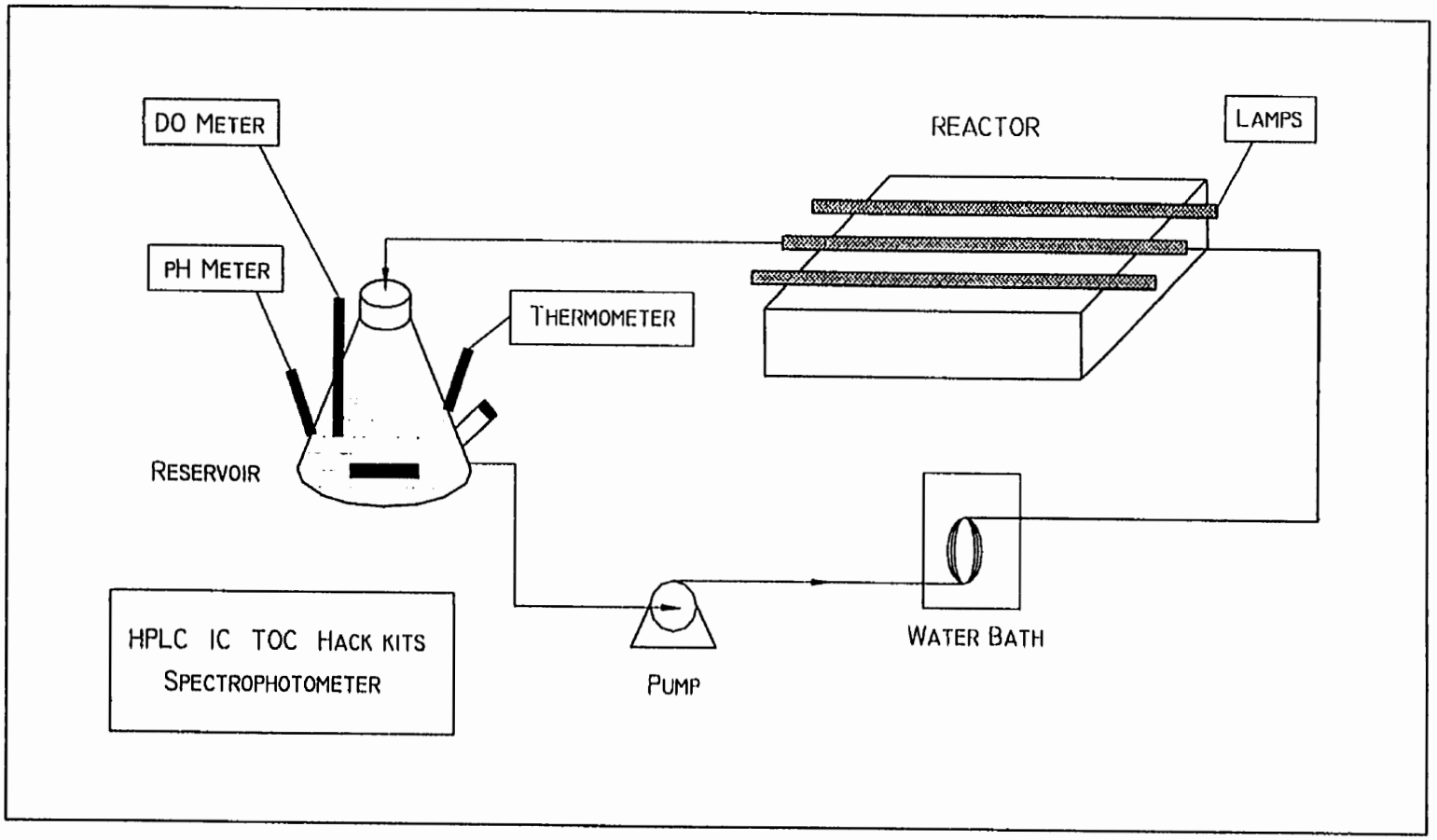

Figure 3-1: Schematic of the Experimental System Set-up

inlet was built to be tangential to its wall so that sufficient air could be entrained through the water/air interface. Temperature was controlled with a water bath. Half-inch C-flex tubing (Cole-Parmer 6424-81) was used to connect the components together.

3.1.4 Experimental Procedure

During all the experimental runs, temperature was kept constant at approximately 26.6+-0.5 °C (converted from a reading of 80 F). The pH of the reaction medium was monitored but not regulated unless otherwise indicated. The dissolved oxygen level in the reaction medium was constant at approximately 7.0 mgL^{-1}.

Before each experimental run, the reactor system was cleaned by pumping deionized water through it for about 10 minutes without illumination. As indicated by the optical densities of the water, this procedure allowed the removal of any residual compounds from previous runs. The system was then drained and 4 litres of premixed 30 mgL^{-1} 4-CP solution was introduced. The newly charged water was pumped in the system for 1-5 minutes and then the lamps were switched on. This was recorded as time zero. Samples were then taken at different times from the reservoir and analysed for UV absorbance at 224 nm, for compositions, and/or for total organic carbon (TOC). All the samples were analysed as they were taken without any pretreatment except that those from the slurry run were centrifuged at a speed of 6000 rpm for 10 minutes to remove the TiO_2 particles before analysis.

3.1.5 Analysis Methods

UV absorbencies of the samples at 224 nm was measured using a Spectronic UV/visible wavelength spectrophotometer (Genesys 2, Milton Roy). At the beginning of the reaction, the absorbance was due to the parent chemical alone but afterwards it also included the absorbance

of the intermediate compounds. Therefore, a linear relationship between the UV absorbance of the reaction medium and the parent chemical concentration does not exist during the course of the reaction. However, for a given reaction pathway the time course of the UV absorbance of the reaction medium does provide a measure of the overall degradation rate of the UV absorbing species.

Composition of the reaction medium was determined with an HPLC system, consisting of an LKB Bromma 2249 Gradient Pump, a Gilson Model 401 Diluter, a Gilson Model 231 Sample Injector, a Regis ODS II Reversible Column (15 cm x 4.6 mm i.d., 5 microns), and a Gilson Model 116 UV detector. Integration was done on a Spectra-Physics SP4270 Integrator. The eluent contained 45% water, 50% methanol, and 5% acetonitrile and was pumped through the system at a flowrate of 0.5 $mLmin^{-1}$. The detector was set at 225 to 230 nm with sensitivities of 0.05 to 0.1 AUFS.

TOC (TC-IC) was determined with an Astro 2001 UV-persulphate TOC analyzer or a combustion-type TOC analyzer with an infrared detector (TOC-500, Shimadzu Corporation, Japan). Radiation intensity was determined with a Spectroline digital radiometer (DRC-100X, Spectronics Corporation, New York) equipped with a DIX-365 sensor. The pH was monitored with a pH meter manufactured by Barnant Company in Barrington, IL and a VWR gel-filled combination electrode produced by TAI Orion Research. DO in the water was determined with a YSI Oxygen Meter (Model 57). The microstructures of the catalyst films were observed under a scanning electron microscope manufactured by Joel Ltd., Japan. All calibration curves are attached in Appendix D at the end of the report.

3.2 Results and Discussions

3.2.1 System and Catalyst Film Checkup

In order to obtain reliable experimental results, interactions other than photocatalytic reactions between the model pollutant and the system must be insignificant. For example, the irreversible reactions between the pollutant and system components such as the tubing and the reactor wall must be negligible. A few simple tests (i.e., reactor material screening tests, tubing selection tests, photolysis and catalysis checkups, tracer tests) were therefore performed before the start of formal experiments. C-flex tubing and acrylic plastics were selected as the connection tubing and reactor material since these two materials showed insignificant physical and chemical interaction with 30 mgL^{-1} 4-CP aqueous solution. Tygon tubing was found to react irreversibly with the artificial wastewater. The 4-CP disappearance due to dark processes (i.e., reactions with and adsorption by the system components, volatilization) was found to be less than 5% in a time interval of 10 hours. Tracer test results indicated that the velocity profile in the reactor was close to that of the plug flow due to the effects of the flow distributor.

The catalyst films on stainless steel plates were examined for mechanical stability, porosity, thickness, surface roughness, and surface metal ions that might have diffused from the parent metal during immobilization.

Two experimental runs were carried out in the flat plate reactor using deionized water under two representative flowrates. The UV absorbance of the samples at 300 nm was found to be constant at zero during the course of these runs, indicating that the catalyst film is mechanically stable in the system.

The average immobilized catalyst weight per unit surface area was evaluated by weighing the plate before and after immobilization and was found to be about 1 mg TiO_2 per square centimetre of the coating. Figure 3-2 shows three typical SEM images of the catalyst

(a)

(b)

(c)

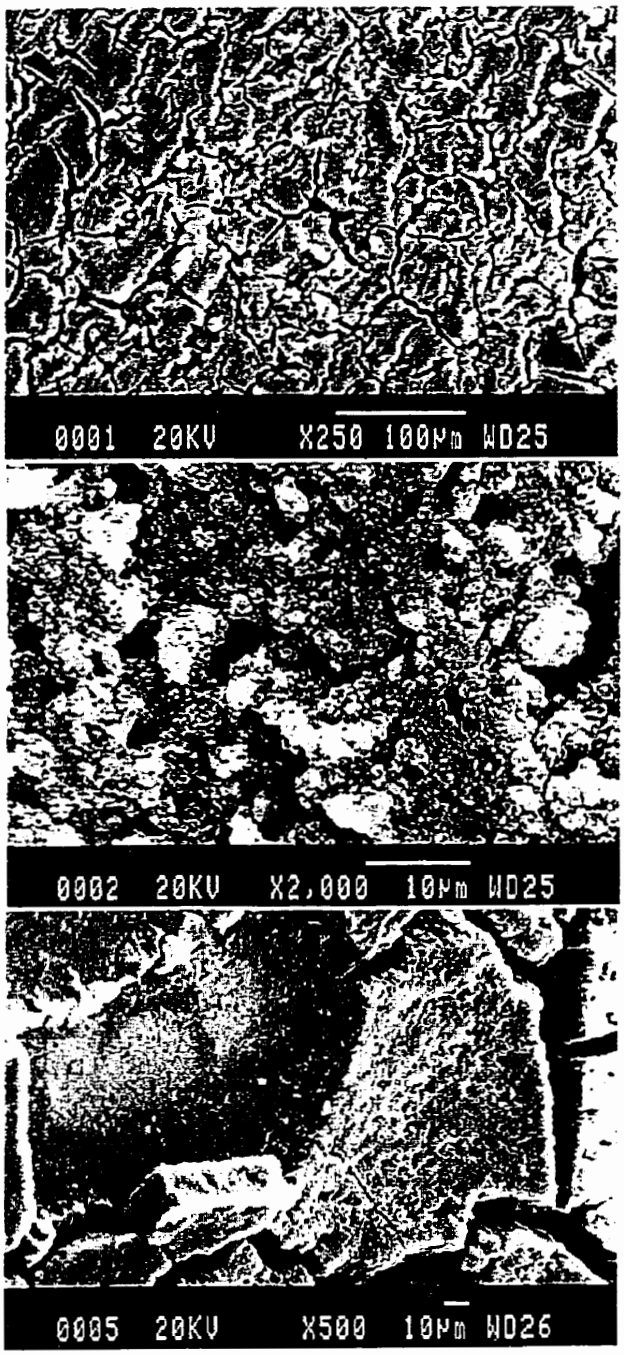

Figure 3-2: SEM Images of the TiO_2 Film

films. Figure 3-2a (magnified 250 times) shows the primary cracks of the film resembling dry pond mud. Figure 3-2b shows the pores between the relatively dense clusters of the solid TiO_2 particles. Figure 3-2c shows that the thickness of the film is around 10 microns. Based on the density and the mass balance of the semiconductor catalyst, the porosity of the film could be estimated to be around 80%. Elemental analysis of the films indicated the existence of a trace amount of iron on their surfaces.

Figure 3-3 depicts the normalized UV absorbance profiles for runs under the same experimental conditions with different catalyst coatings. This figure indicates that the activity of the catalyst films is stable.

3.2.2 Flat Plate Reactor

During most of the runs, the pH of the reaction medium was monitored and it usually dropped from an initial value of around 5.5 to about 3.8 near the completion of the reaction. In addition, two constant-pH (4 and 5.5) runs were also performed. In these two runs, the pH was controlled with potassium hydroxide and nitric acid. Information regarding these two chemicals are given in Section 3.3.1. The reaction kinetics of these two runs was comparable to that of the runs without pH control. Therefore, the pH effect is negligible over a range from 4 to 5.5.

The degradation kinetics (in terms of UV absorbance, 4-CP concentration, and sample TOC) was found to follow an L-H type relationship. In terms of concentration, this could be expressed by the following two equations, where Equation (3-2) is the integrated form of the rate model (3-1).

$$\frac{V}{A}\frac{dC}{dt} = \frac{K_0 K C}{(1 + KC)} \qquad (3\text{-}1)$$

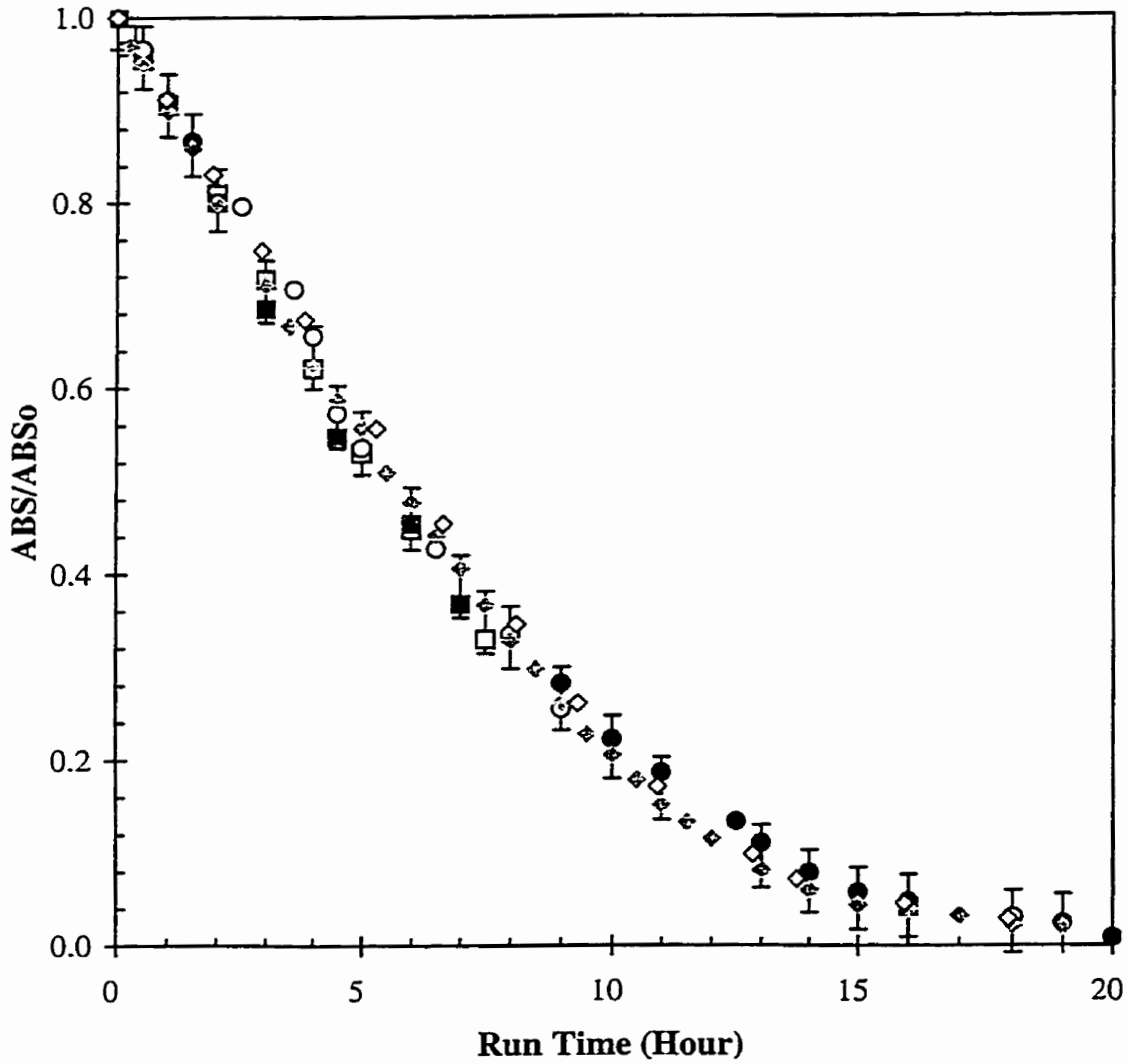

Figure 3-3: Repeated 4-CP Degradation, as Measured by Normalized UV Absorbance, for Three Different TiO_2 Coatings
Flat plate; C_0=30 mgL^{-1}; I=122 Wm^{-2}; Re=4313
□ 1st coating, 1st run; ■ 2nd coating, 1st run; Bars: confidence interval; ○ 2nd coating, 2nd run; ● 2nd coating, 3rd run
◆ 3rd coating, 1st run; ◇ 3rd coating, 10th run

$$C = C_0 + \frac{1}{K}\ln\frac{C}{C_0} - \frac{A}{V}K_0 t \qquad (3\text{-}2)$$

In order to examine their chemical compositions, samples were injected into the HPLC and detected for UV absorbance at multiple wavelengths between 200 and 300 nm. Since all aromatic compounds should absorb in this wavelength range (Jacob, 1992), all aromatic reaction intermediates should be detected in this way, within the detection limits of the HPLC system. Five UV absorbing reaction intermediates were detected. 4-chlorocatechol, hydroquinone, 1,4-benzoquinone, catechol, resorcinol, and phenol standards were prepared to identify these intermediates. The analysis results rejected the existence of catechol, resorcinol, and phenol in the samples. 4-chlorocatechol, hydroquinone, and 1,4-benzoquinone were identified as three of the intermediates based on retention time match up with standards and reaction mechanisms proposed in previous studies (Al-Sayyed, D'Oliveira, and Pichat, 1991; Al-Ekabi et al., 1989).

Figures 3-4 through 3-7 depict the typical experimental results. The TOCs due to the parent compound as well as those of the intermediates were calculated based on the concentrations of these compounds. The results are plotted in Figure 3-4. The TOC of the unknown intermediates was obtained by subtracting the TOCs due to 4-CP, 4-chlorocatechol, hydroquinone, and 1,4-benzoquinone from the measured TOC of the samples. Typical 4-CP concentrations and TOC data are shown in Figure 3-5 together the lines fitted from Equation (3-1). Since the levels of all the intermediates were much lower than that of the parent compound until 95% of the 4-CP were degraded (see Figure 3-4), they were considered kinetically negligible in the rest of the report. This allowed the acquisition of 4-CP concentrations from the relatively less-scattered UV absorbance data. Figures 3-6 and 3-7 depict the effects of Reynolds number and radiation intensity on reaction rates.

Under high level radiation (i.e., 122 Wm^{-2} on reactor cover), the reaction was mass transfer dependent over the entire flow regime examined. It is interesting to note that deviations

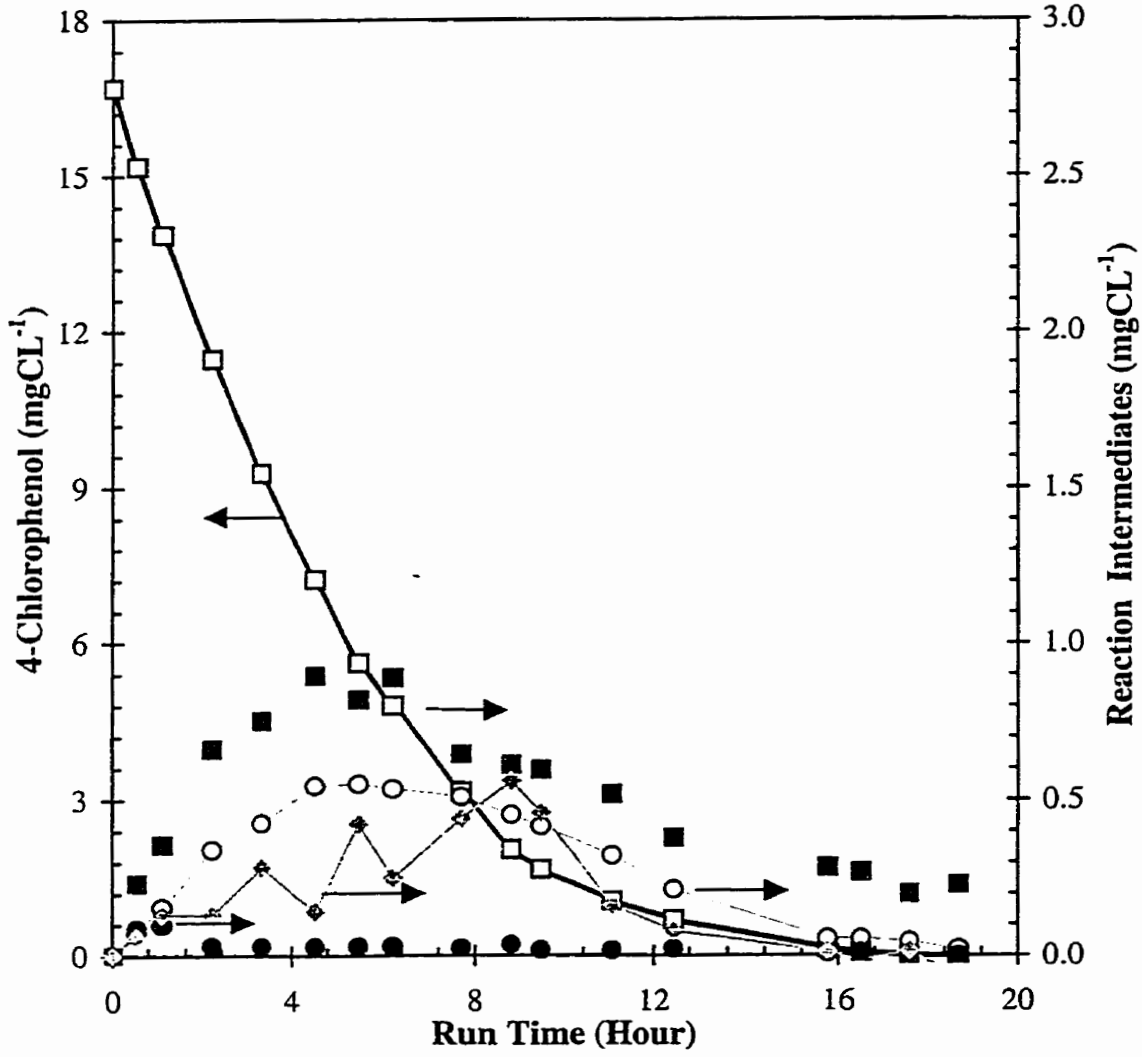

Figure 3-4: Reactant and Intermediates Profiles, Expressed on a Carbon Basis

Flat plate; I=122 Wm^{-2}; Re=5813

□ 4-CP; ■ 4CC; ○ HQ; ● BQ; ◆ Other

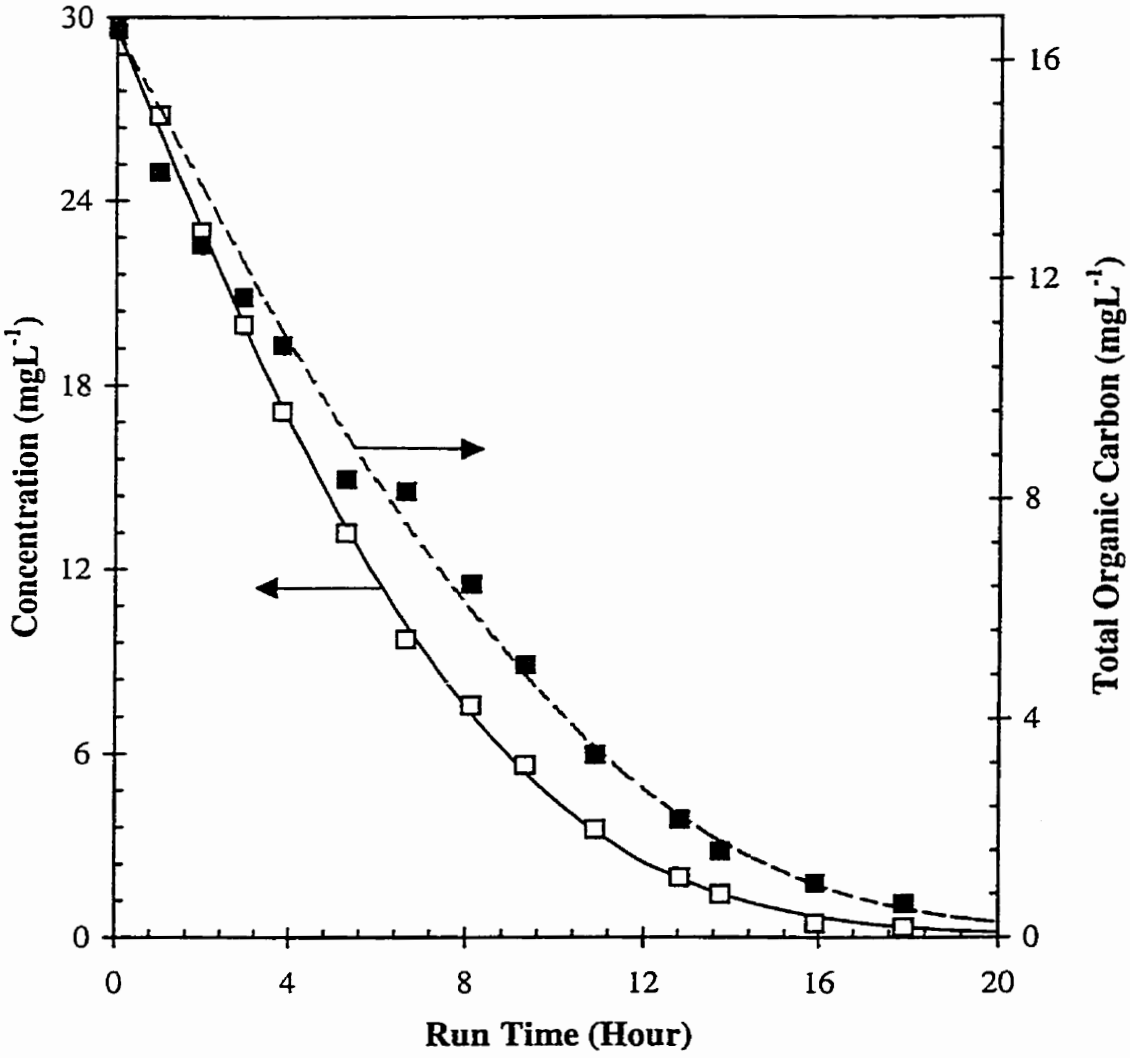

Figure 3-5: 4-CP Degradation Kinetics: Flat Plate Reactor
Re=4313; I=122 Wm^{-2};
□ concentration data; ■ TOC data; Lines: L-H fittings

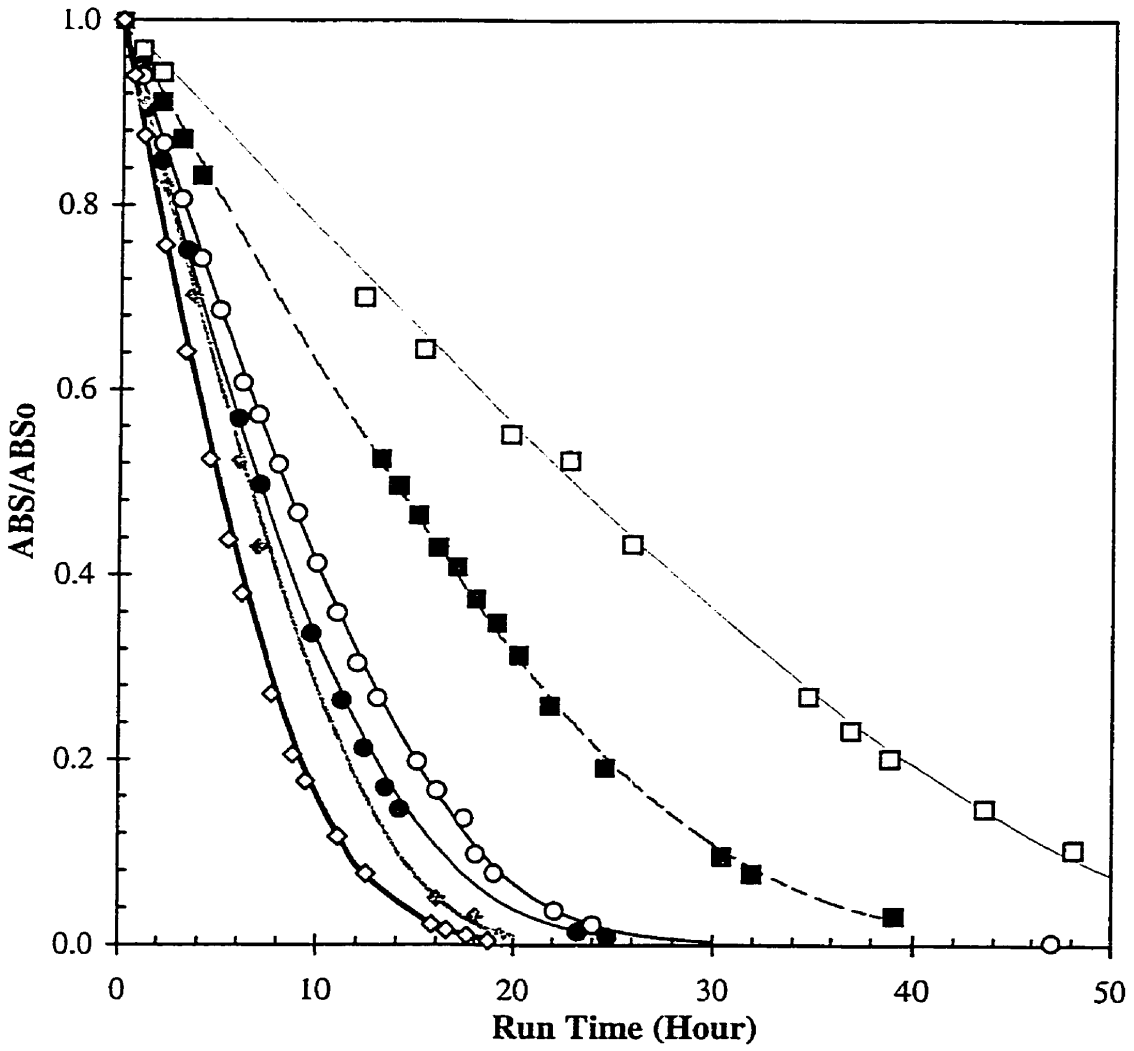

Figure 3-6: Effect of Reynolds Number on Degradation Kinetics, as Measured by Normalized UV Absorbance
Flat plate; C_0=30 mgL^{-1}; I=122 Wm^{-2}
□ Re=431; ■ Re=782; ○ Re=1633; ● Re=2550
◆ Re=3411; ◇ Re=5813; Lines: L-H fittings

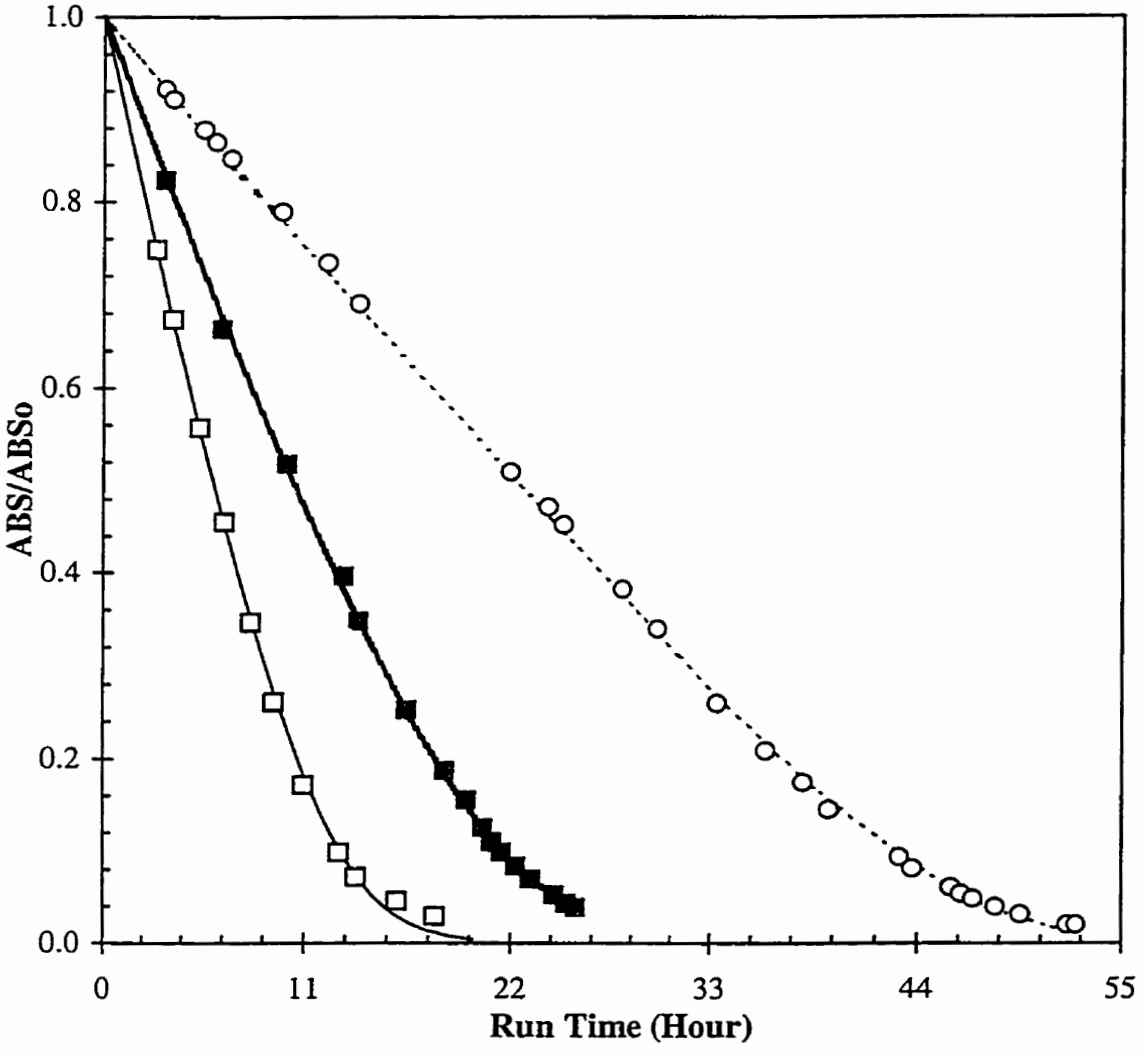

Figure 3-7: Effect of Radiation Intensity on Degradation Kinetics
Flat plate; Re=4313; C_0=30 mgL^{-1}; Lines: L-H fittings
□ I=122 Wm^{-2}; ■ I=43 Wm^{-2}; ○ I=15 Wm^{-2};

from zero order kinetics occur at approximately the same 4-CP concentration although the mass transfer rates were different. This is because that the transfer of both 4-CP and oxygen (two reactants) affect the reaction rate. As 4-CP concentration was initially much higher than that of oxygen (7 mgL^{-1}), the process was actually limited by the transfer of oxygen until the concentrations of 4-CP was reduced to such a level that the ratio of their mass transfer rates is equal to the stoichiometrically defined one. Based on correlations available (Calderbank and Moo-Young, 1961; McCabe, Smith, and Harriott, 1993) and the diffusivities of these two substances, this corresponds to a 4-CP concentration of around 8.7 mgL^{-1}. Since oxygen concentration was kept constant, the degradation should therefore behave zero order kinetics with respect to 4-CP when its concentration is higher than about 8.7 mgL^{-1}, and change gradually to first order as the reaction proceeded further.

As indicated in Figures 3-5 through 3-7, Equation (3-2) fits the kinetic data for all the individual runs exceptionally well. Therefore, parameters obtained in fitting the kinetic data into Equation (3-2) can be conveniently used to calculate reaction rate profiles for the individual runs. Based on the calculated reaction rates, measured mass transfer rates (see Chapter 7), and reaction stoichiometry (neglecting all the intermediates) average 4-CP and oxygen concentrations on the surface of the catalyst film were calculated and plotted in Figures 3-8 and 3-9 against the main stream concentrations of 4-CP and oxygen. These results agree well with the discussions in the last paragraph. Under high radiation level (i.e., 122 Wm^{-2} on reactor cover), the reaction was severely limited by the transfer of oxygen from liquid to catalyst films.

Although Equation (3-2) fits the kinetic data exceptionally well, one should be cautious in assigning fundamental meanings to the parameters obtained in fitting the data due to the interference of mass transfer and parameter correlation. In addition, this model cannot be used for reactor scale-up since neither radiation transfer nor mass transfer was considered. Therefore, a new model is required.

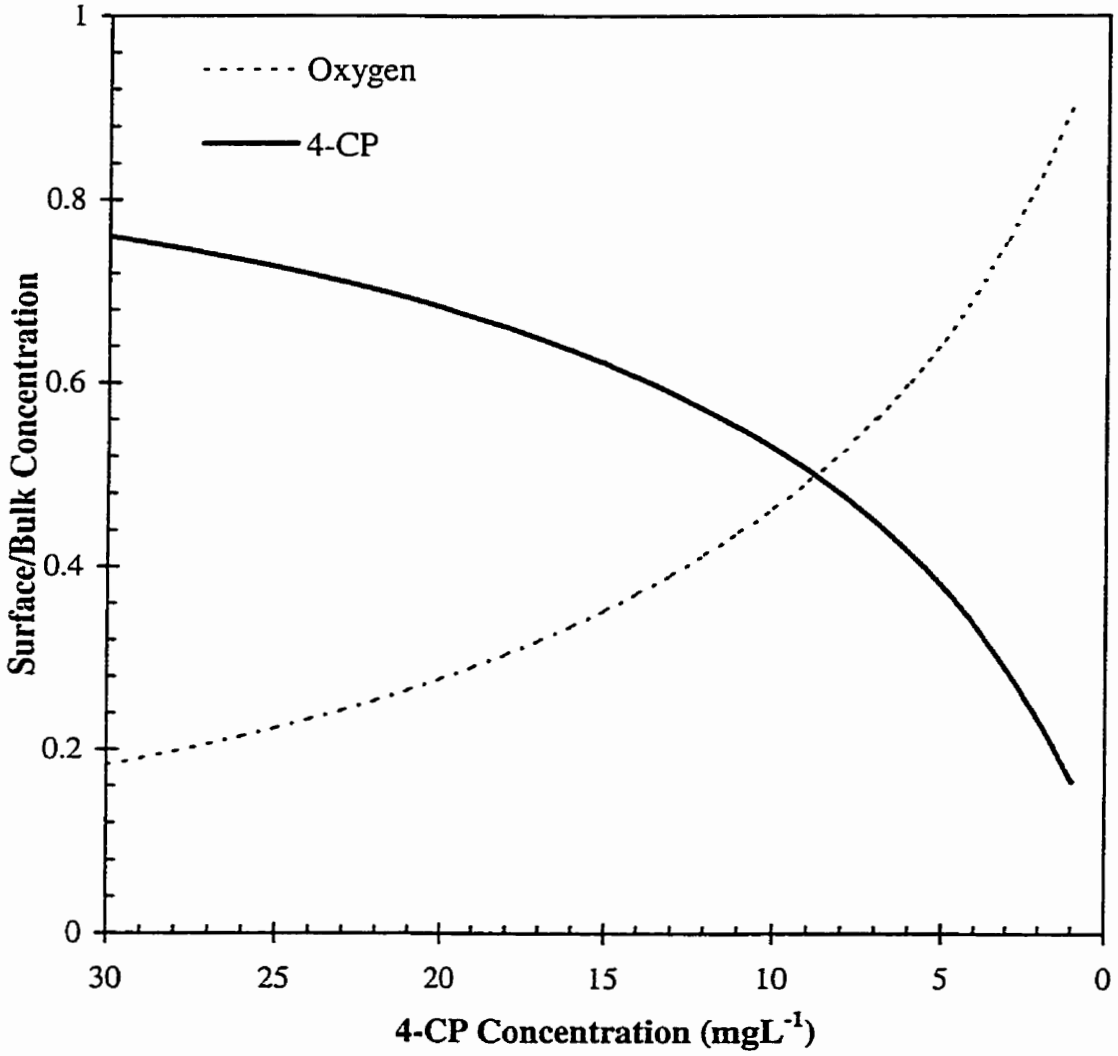

Figure 3-8: Relative Surface Concentration of Reactants as a Function of Bulk 4-CP Concentration at High-level Radiation
Flat plate; Re=5813; I=122 Wm^{-2}

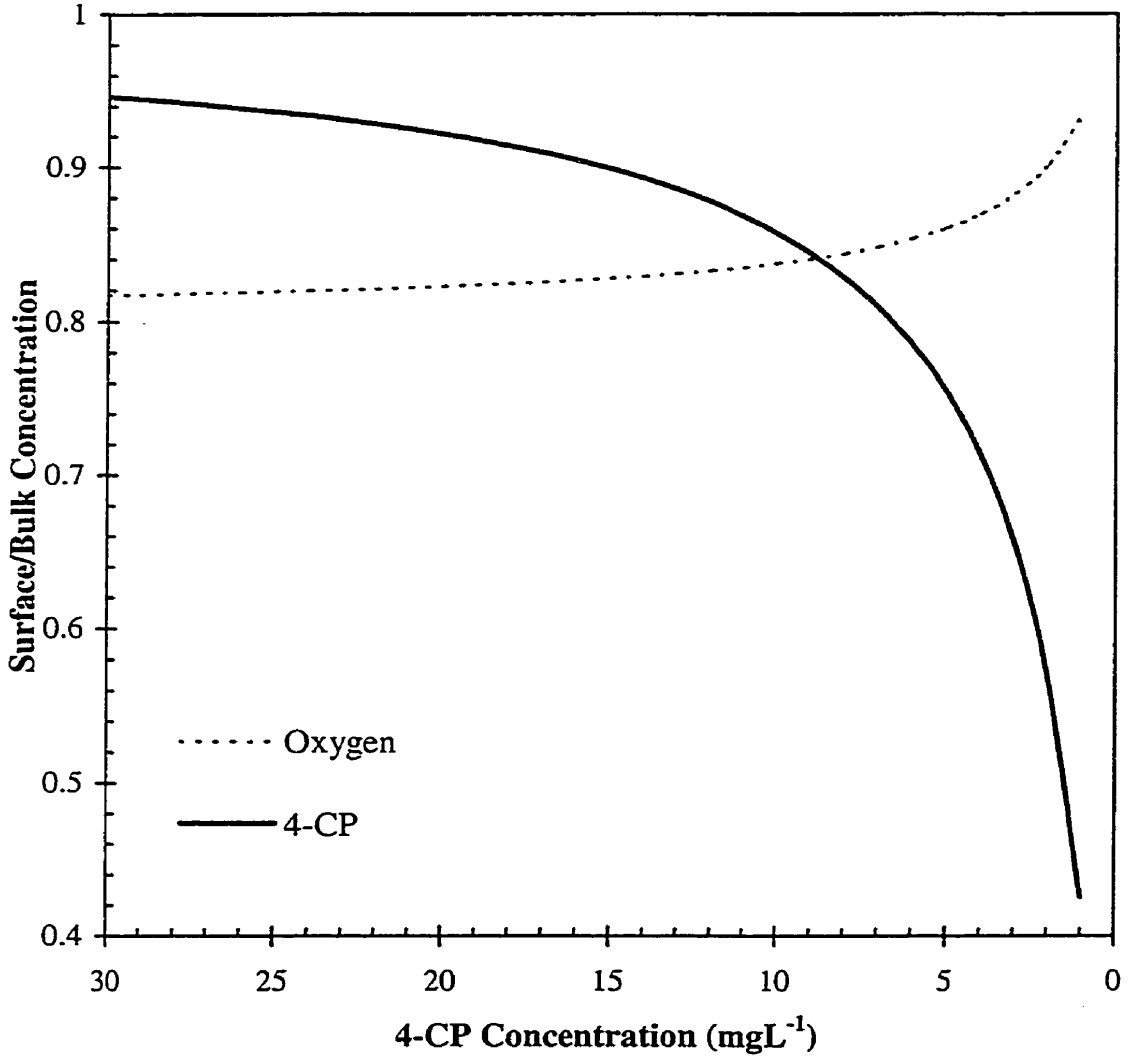

Figure 3-9: Relative Surface Concentration of Reactants as a Function of Bulk 4-CP Concentration at Low-level Radiation
Flat plate; Re=5813; I=15 Wm^{-2}

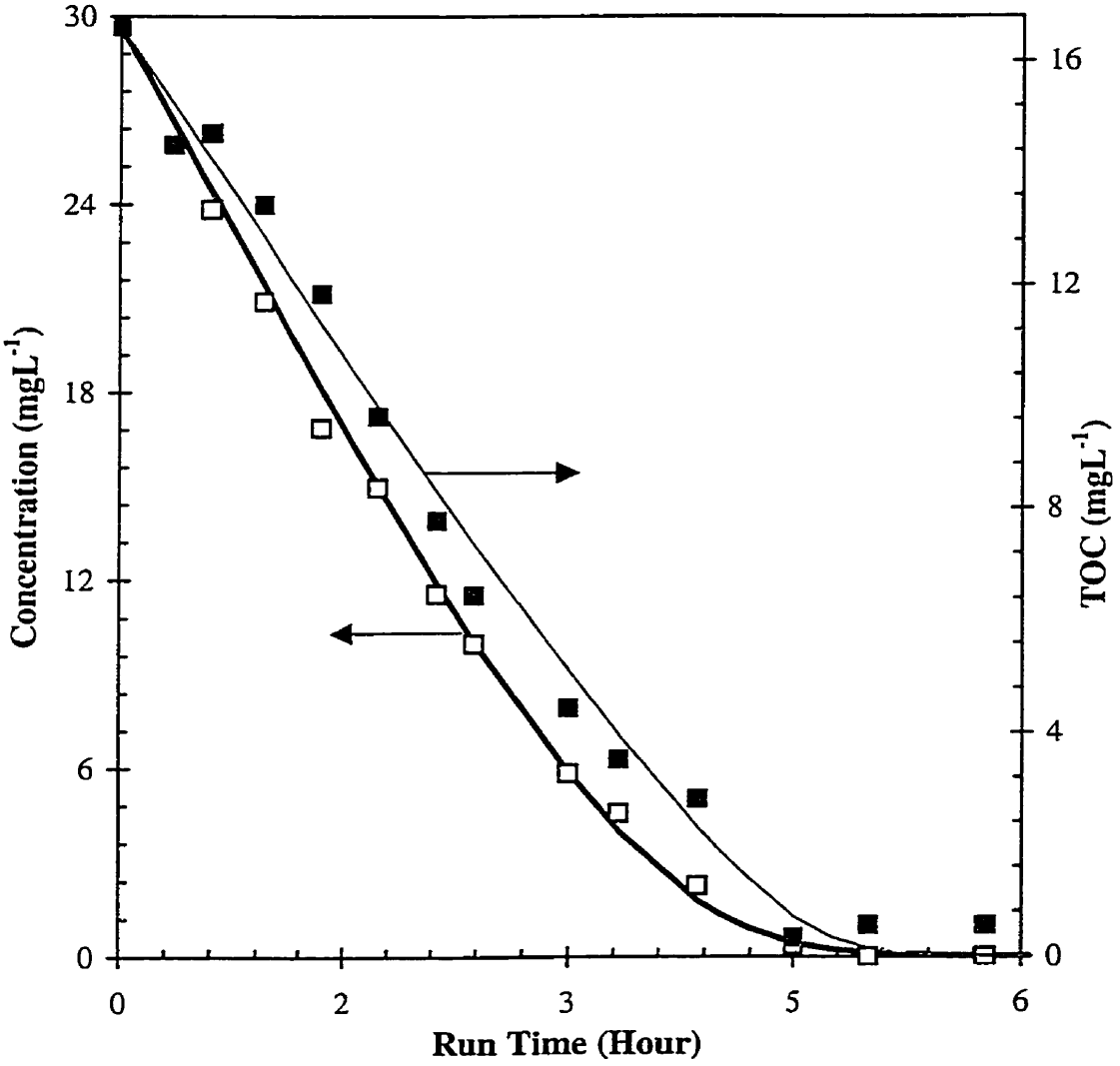

Figure 3-10: 4-CP Degradation Kinetics: Slurry System
1 gL^{-1} TiO_2 slurry; Re=4313; I =122 Wm^{-2}
□ concentration data; ■ TOC data; Lines: L-H fittings

3.2.3 Slurry Reactor

The slurry run was conducted under experimental conditions exactly the same as the one presented in Figure 3-5. The results are plotted in Figure 3-10. By comparing Figures 3-5 and 3-10, we can see that the slurry run was approximately 200% faster. Similar findings have been reported previously (Enzweiler et al., 1994). This is due to the enormous difference of the illuminated catalyst surface area between the two systems. Based on the loading, the density, and the size of the catalyst particle aggregates (Ray, 1997), the total surface area of the catalyst aggregates was estimated to be over 21 m^2 in the slurry system. All catalyst particles may be illuminated in a slurry system as they pass through the reactor with the water being treated. Therefore, the slurry reactor enjoyed an illuminated TiO_2 surface area which is up to 525 times higher than that in the flat plate reactor tested.

Based on the model-determined photon absorption rates (see Chapter 6), the initial quantum efficiency of the flat plate reactor was calculated to be 0.47%. Similar information for the slurry system was not obtained since the corresponding photon absorption rate was not available. It is very difficult to correctly quantify the light absorption in a slurry system.

3.3 Concluding Remarks

30 mgL^{-1} 4-CP contaminated artificial wastewater was mineralized in both immobilized flat plate and slurry reactors. Five reaction intermediates that absorb UV in the range of 200 to 300 nm were detected. Three of them were identified to be 4-chlorocatechol, hydroquinone, and 1,4-benzoquinone. The concentrations of these intermediates were all lower than approximately 3% of the initial 4-CP concentration.

L-H kinetic model fitted the photocatalytic 4-CP degradation data very well and was therefore used to extract the reaction rates from the concentration data. However, one should

be cautious in assigning fundamental meanings to the parameters fitted using immobilized system data. This model cannot be used for photoreactor scale-up either.

Under otherwise identical experimental conditions, the slurry system was found to be 200% faster than the immobilized system due to its great TiO_2 surfaces that can be illuminated.

Photocatalysis on immobilized TiO_2 films can be limited by the transfer of either the oxidant (i.e., oxygen), the substances being oxidized (i.e., 4-CP), and/or the reaction products between the reaction sites and the main flow stream. Based on the experimental results, the photocatalytic reactions in the flat plate reactor were initially limited by oxygen transfer and shifted to 4-CP transfer as the reactions proceeded.

The TiO_2 films immobilized on the stainless steel plate were physically and chemically stable during the course of the experiments. They possess a thickness of approximately 10 microns and a porosity of approximately 80%. Elemental analysis of films indicated the existence of a trace amount of iron on its surface.

CHAPTER 4: CORRUGATED PLATE REACTOR

4.1 Materials and Methods

2,4-dichlorophenol (2,4-DCP) and 2,4,5-trichlorophenol (2,4,5-TCP) used in this part of the work were both from Sigma Chemical Company. Their CAS numbers are 120-83-2 and 95-95-4 respectively. Dechlorination was examined by analyzing chloride ion concentrations in the samples using a Dionex ion chromatograph (IC) equipped with an IONPAC AS4A-SC 4 mm column and a Dionex CDMII conductivity detector. The eluent was composed of 1.8 mM Na_2CO_3 and 1.7mM $NaHCO_3$ (volume ratio of 1:1) and was pumped through the system at a flowrate of 2 mL min^{-1}. The reagent was 50 mN H_2SO_4. Its flowrate was 4 mL min^{-1}. The sample loop volume was 10 μL. Other materials and methods are described in Section 3.1. The operating temperature was kept constant at 26.6 °C.

4.2 Considerations in Photoreactor Development

Based on the results in previous studies, photocatalytic reactions follow L-H kinetics in terms of the concentrations of the chemicals being degraded with the rate constants showing lower order (usually between 0.5 and 1) dependency on radiation intensities. Here, both the chemical concentrations and the radiation intensities refer to those at the catalyst surface. The overall reaction rate can therefore be obtained by integrating the rate expression over the catalyst area in a reactor.

As a result of the kinetic characteristics of photocatalytic reactions, a powerful and efficient photoreactor must possess: (1) a large catalyst surface area per unit reactor volume, (2) the capability to illuminate with relatively low intensities a large catalyst surface continually, and (3) sufficient mass transfer capacity between the liquid bulk and all the reaction sites. In

addition to catalyst surface area and radiation/mass transfer, other issues needing to be considered in photocatalytic reactor development include: (1) reactor configuration and radiation source positions; (2) types and capacities of the lamps (if solar energy is not to be used); (3) radiation energy absorption, refraction, scattering, and reflection; (4) catalyst mixing for systems with TiO_2 suspended or immobilized on mobile particles; (5) heat transfer and temperature control; (6) types and concentrations of target pollutants; (7) materials for light transmission, reactor wall, and catalyst immobilization; and (8) ease of fabrication, operation, and maintenance.

For heterogeneous reactors utilizing artificial lamps, the type of lamp which gives the highest efficiency in the spectrum of interest, yet is compatible with other parts of the system, should be of the first choice. Factors needing to be considered in selecting light transmission materials include, light transmission efficiency in the wavelength range of interest, chemical and thermal stability, cost, fabrication potential, and durability. Quartz is one of the most "transparent" solid materials for UV light but it is also quite expensive. Pyrex is less expensive but this type of glass absorbs UV-C (190 - 280 nm) and UV-B (280 - 320 nm), allowing only UV-A (320 - 380 nm) to reach the catalyst surface. The dissipation of UV-B could be of a great loss in the overall energy efficiency since rays in this wavelength range may be more effective than UV-A rays in activating photocatalytic reactions (Stafford, Gray, and Kamat, 1997a). Compared to glass, UV-transmitting acrylic plastics could offer low cost, appropriate optical properties (transparent to both UV-B and UV-A), and superior fabrication potential. This material may be subject to attack by some organic chemicals if their concentrations are high. Fortunately, photocatalysis is most suitable for detoxifying waters contaminated with chemicals at low levels, which may not attack acrylic plastics noticeably.

For systems with TiO_2 immobilized on stationary surfaces, the effect of mixing on light distribution is limited. However, it could still enhance the reaction rates owing to increased mass and heat transfer. These could in turn improve temperature control and alleviate product

inhibition if it exists (Lepore, Pant, and Langford, 1993).

Cost, fabricatability, and chemical stability are among the major considerations in reactor construction material selection. Ordinary materials such as stainless steel, carbon steel, aluminum, and plastic could all be used for the reactor wall.

4.3 Reactor Configuration and Characteristics

Figure 4-1 is a sketch of the photoreactor developed and examined in this study. In this reactor, the catalyst is immobilized on both sides of the corrugated plates. For the treatment of a given wastewater stream, primary parameters that may affect the performance of a CP reactor include, construction material, lamps, catalyst film characteristics, "angle" and "depth" of the corrugated plates, radiation intensity, temperature, and flowrate through the reactor (Reynolds number). The advantages of this reactor configuration are summarized as follows:

(i). It could provide a high illuminated catalyst surface area per unit volume of the reactor and therefore a high capacity.

(ii). As an immobilized system, post treatment catalyst-water separation is not required.

(iii). Sufficiently high mass transfer rates could hopefully be obtained by adopting an appropriate angle of the corrugated plates, by eliminating the narrow corners of these plates, by the use of flow-spoilers such as screens, or by operating the reactor in (pseudo)turbulent flowrate ranges.

(iv). Temperature in the lamp sleeves could be controlled conveniently through the use of forced air venting or natural convection, allowing optimal function of the radiation sources.

(v). It requires relatively low capital costs. Only the lamp sleeves need to be built with UV transmitting material such as glass or acrylics. Stainless or carbon steel or plastics could be used for all other parts. The fabrication will be relatively easy since the reactor wall

and lamp sleeves require little machining and the corrugated plates could be formed conveniently using a press.

(vi). It could be operated at relatively low costs. The system does not contain any moving parts. Since the total illuminated surface area of the catalyst films would not be affected in case some lamps break down, the maintenance requirement is not strict. Since the catalyst is immobilized on stationary surfaces, deactivation due to factors such as attrition does not exist and a long catalyst lifetime is possible. The pressure drop of the reactor will be relatively low since the whole reactor simulates multi-triangular tube bundles. Based on an estimation using the hydraulic radius method, the pressure drop was as low as 40 pascals per meter of the flow channels (B=0.05 m, α=3.5°, Re=930, resistance due to the distributor was not included).

(vii). Maintenance cost will be low since there are no moving parts in the reactor. In addition, the corrugated plates and lamps could be pulled out of the reactor easily for catalyst regeneration or lamp replacement when required.

(viii). It is structurally flexible. Desired catalyst surface areas and radiation intensities could be easily obtained by using TiO_2-coated corrugated plates with different angles and by adjusting the number of lamps in each lamp sleeve. The reactor could be built as long as desired for optimal effluent quality.

(ix). It is operationally flexible. The velocity profile across the reactor will be similar to that of a packed bed (packed with corrugated plates) which could be close to plug flow at relatively high Reynolds numbers. Meanwhile, if the reactors are used in series, controlled back-mixing could be realized by recycling the fluid at certain stages.

(x). Solar UV could be used to illuminate a corrugated plate.

The illuminated catalyst film areas per unit reactor volume of a few selected reactor configurations were estimated and the results are listed in Table 4-1. Based on the estimation

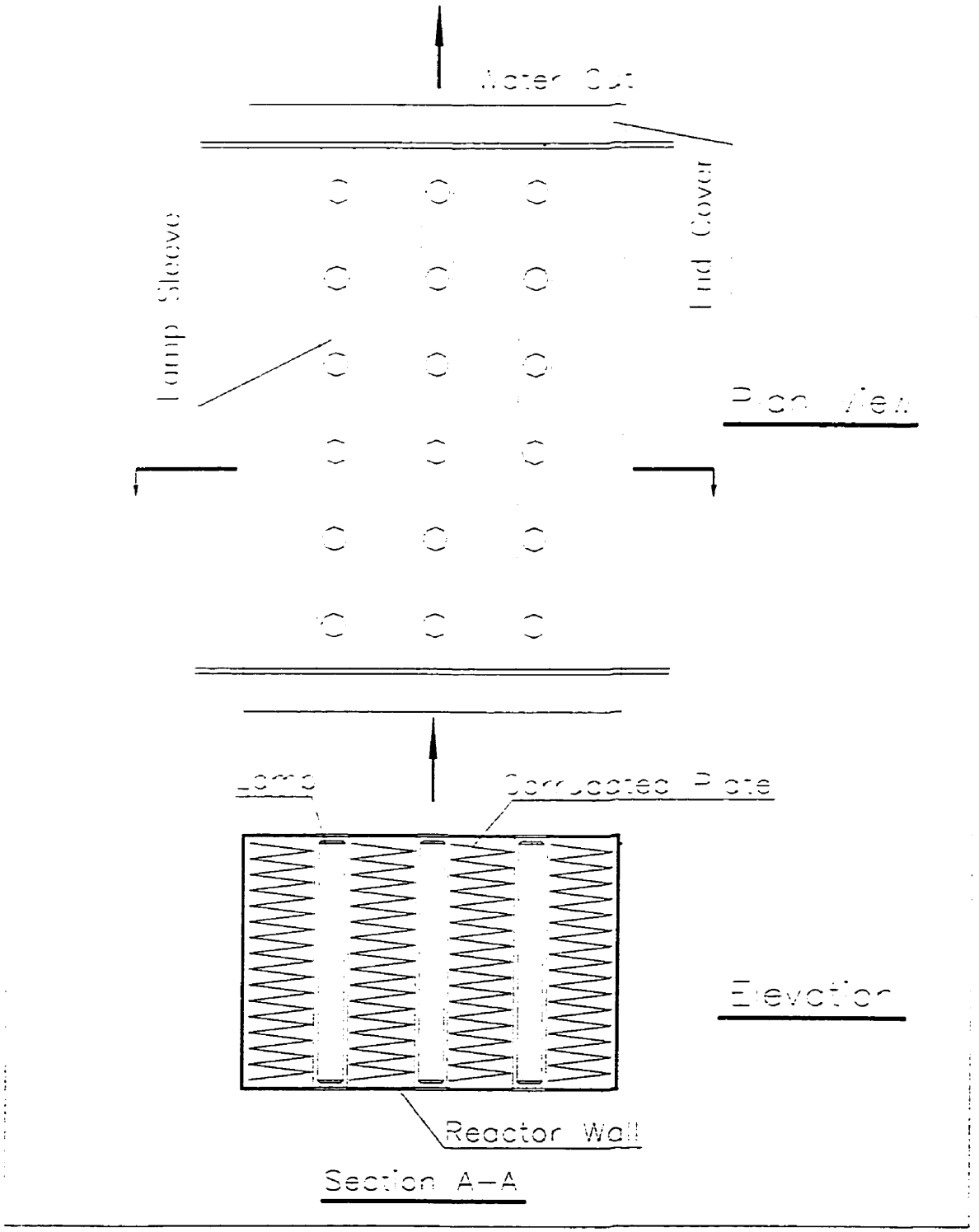

Figure 4-1: Schematic of the Corrugated Plate Reactor

results, only the tube light reactor (Ray 1997) possesses illuminated catalyst film area that is higher than those of the CP reactors. However, the tube light reactor may not be attractive because of the high voltage requirement of the special lamps, the expected high cost to purchase and replace the lamps, and the mercury contamination risk in case of a lamp failure.

Table 4-1: TiO_2 Film Area per Unit Reactor Volume for Selected Reactors

Reactor Configuration	A/V_R (m^2m^{-3})	Notes
multiple tube reactor[2,3]	up to 45	reactor structure based on Ray and Beenackers (1998); assumed distance between lamp-sleeve assembly: 0.01 m; catalyst immobilized on outer wall of the lamp sleeves
packed bed reactor[2,3]	up to 80	assumed distance between the lamp-sleeve assembly: 0.01 m; catalyst immobilized on spherical packing
tube light reactor[1]	> 1000	based on Ray (1997); catalyst immobilized on the walls of the lamps; lamps take 75% of the reactor volume
CP reactor[2,3] (α=10°, B=5 cm)	up to 115	reactor structure shown in Figure 4-1; catalyst immobilized on the surfaces of the corrugated plates
CP reactor[2,3] (α=7°, B=5 cm)	up to 165	
CP reactor[2,3] (α=5°, B=5 cm)	up to 230	
CP reactor[2,3] (α=3.5°, B=5 cm)	up to 330	

1 special lamps with a diameter of 0.0045 m in direct contact with contaminated water.
2 assumed illumination source: regular tubular lamp with a diameter of 0.036 m.
3 exterior diameter of the lamp sleeve: 0.056 m.

As a result of the physical restrictions in a laboratory environment, a lab version corrugated plate (LCP) reactor, as shown in Figure 4-2, was used to collect the data for research into the CP reactor. This reactor consists of a plastic chamber, a distributor, and a TiO_2-coated corrugated plate. Since the LCP and CP reactors are hydraulically similar, data collected using

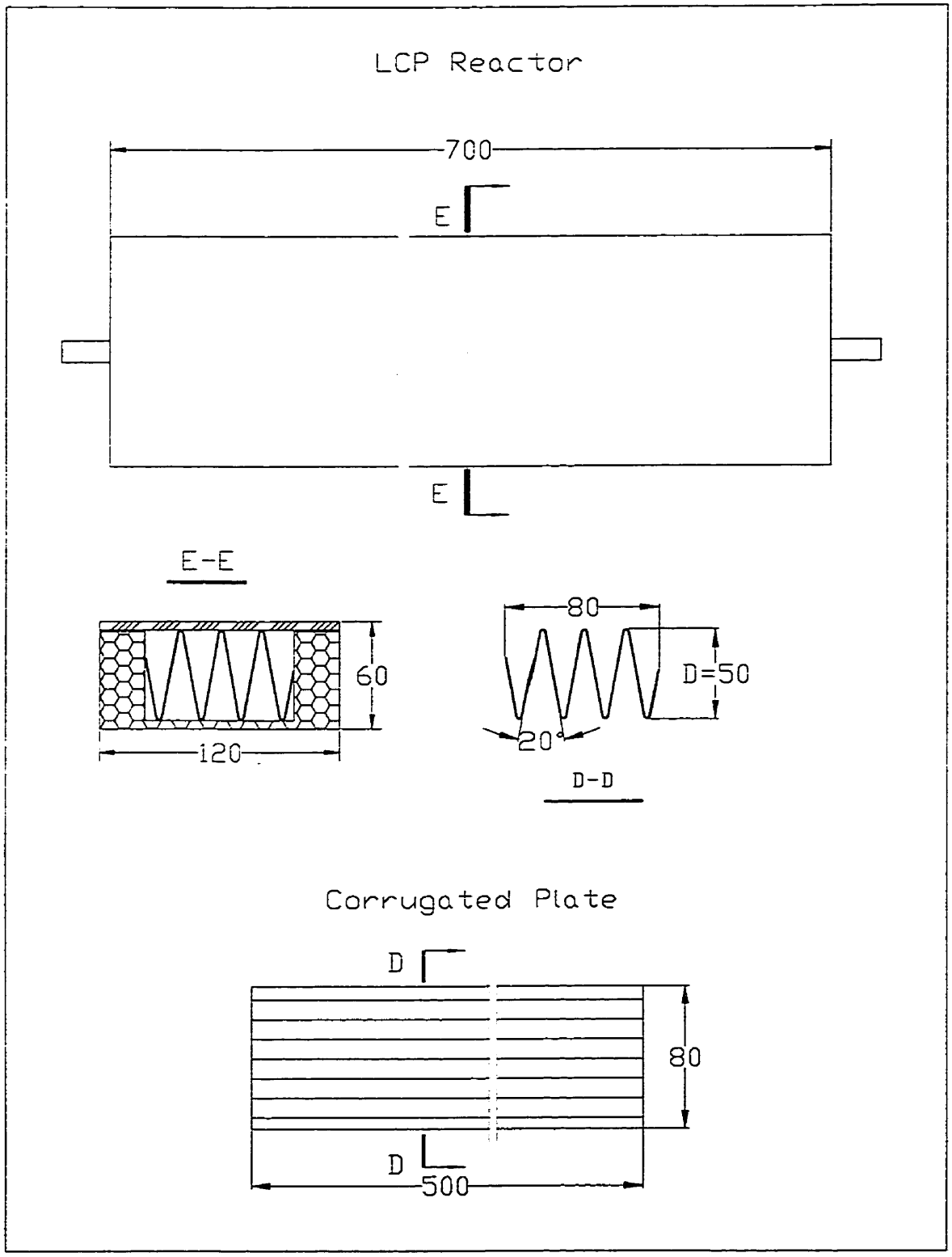

Figure 4-2: LCP Reactor Dimensions (mm)

the LCP reactor can be used to predict the performance of the CP reactor as long as the differences in radiation intensity and catalyst film area are considered.

4.4 Degradation of 4-Chlorophenol

As the key component of the CP reactor, a corrugated plate has three important structural parameters. They are the "depth" B, the "half angle" α, and the "cap". These parameters all affect the performance of the unit. For example, the deeper the corrugated plate the larger the surface area provided but the less uniform the radiation on its surface. A smaller "cap" will result in larger surface area but there are limitations due to fabrication and mass transfer considerations. Based on the Lambert's Cosine Law, the "angle" is strongly correlated with the radiation distribution over the corrugated surface. In this research, the "depth" B, and the "cap" were both fixed. The effect of the angles of the corrugated plates and the radiation intensities on the photocatalytic reactions was examined experimentally. Corrugated plates examined in this study are shown in Figure 4-3. 4-CP degradation with each of these plates was performed under three different flowrates to determine the mass transfer effect. Some typical experimental results are summarized in Figures 4-4 and 4-5 together with the lines fitted by Equation (3-2). Again the Langmuir Hinshelwood relationship fitted the data very well.

As can be seen from Figure 4-4 that the performance of a CP reactor is indeed strongly dependent on the angle of the corrugated plate. The 90% degradation times of the flat plate, the LCP, and the slurry reactors are calculated based on the experimental data. The results are summarized in Table 4-2, together with the surface areas of the illuminated catalyst films in these reactors. As can be seen from this table that one LCP reactor was 150% more efficient than the flat plate reactor (i.e., 100-13/5.2*100). However, it is still about 15% less efficient than the slurry reactor (i.e., 100-4.5/5.2*100). The illuminated catalyst film area of the best LCP reactor (α=3.5°) was 10 times greater than that of the flat plate reactor. As shown in Figure 4-5,

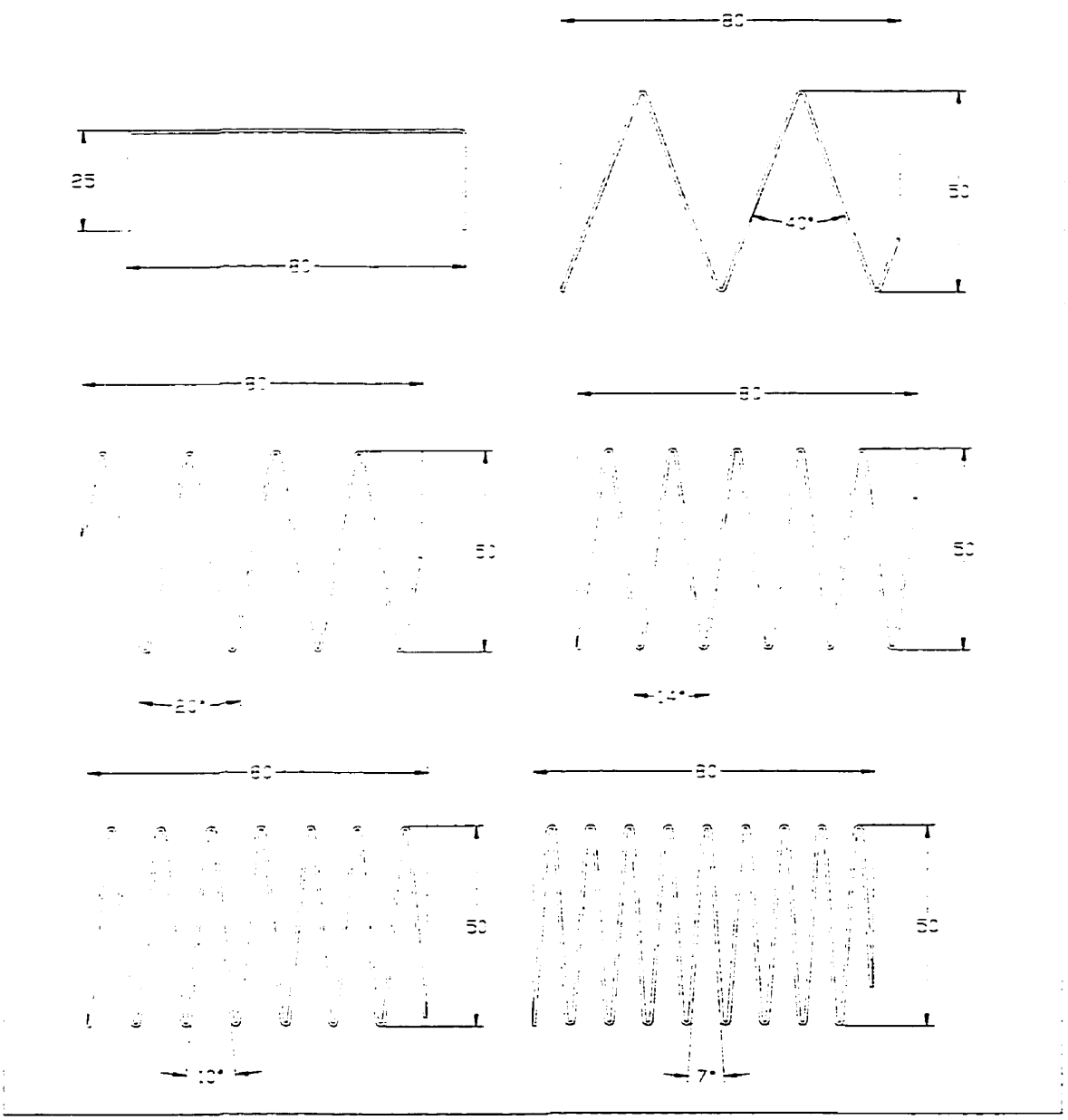

Figure 4-3: Flat and Corrugated Plate Dimensions (mm)

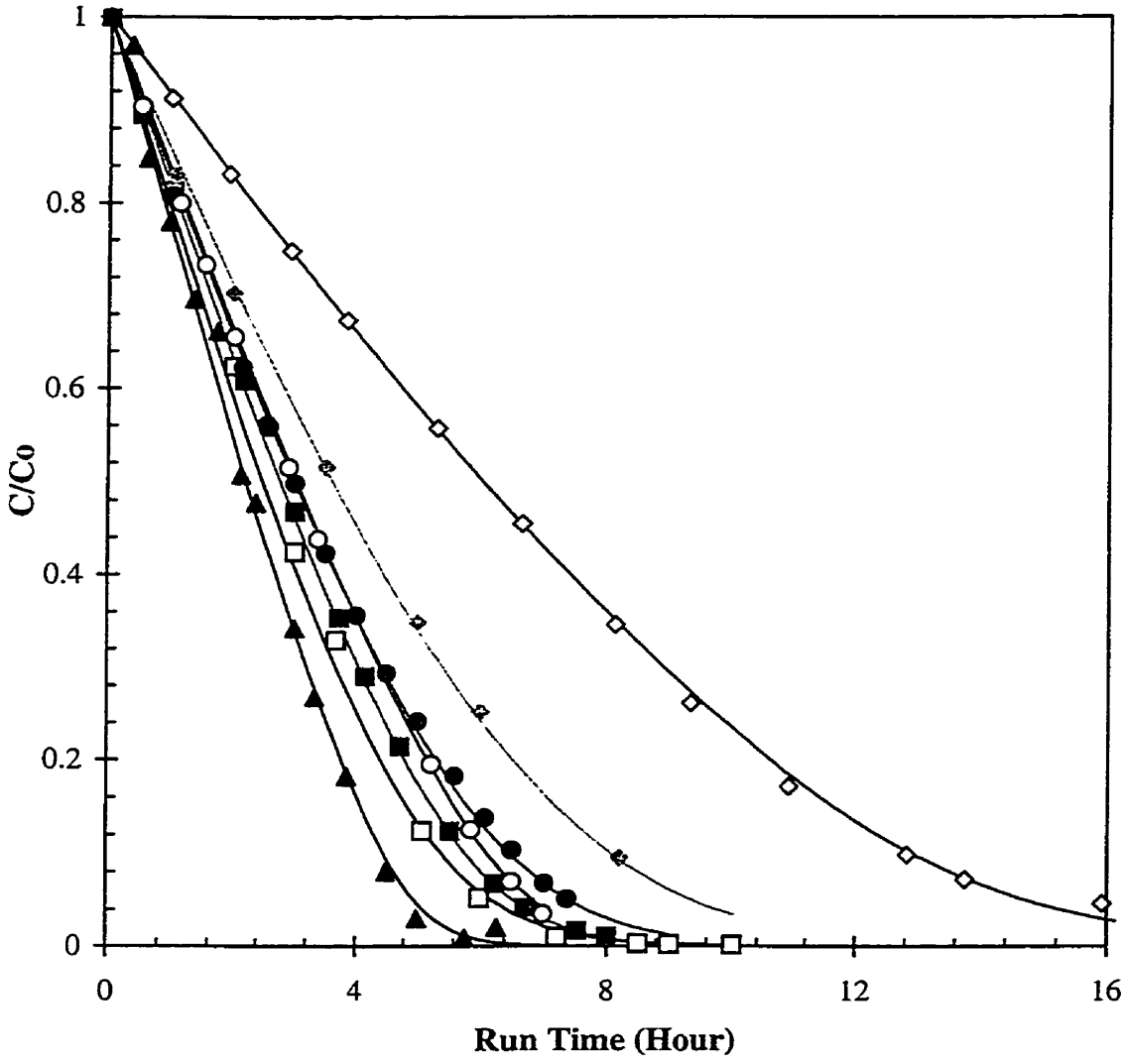

Figure 4-4: 4-CP Degradation in Corrugated Plate Reactor at Five Different Angles, Compared to Flat Plate and Slurry Reactors

Flowrate=23 $Lmin^{-1}$; C_0=30 mgL^{-1}; I=122 Wm^{-2}

□ α=3.5°; ■ α=5°; ○ α=7°; ● α=10°; ◆ α=20°

◇ flat plate reactor; ▲ slurry reactor; Lines: L-H fittings

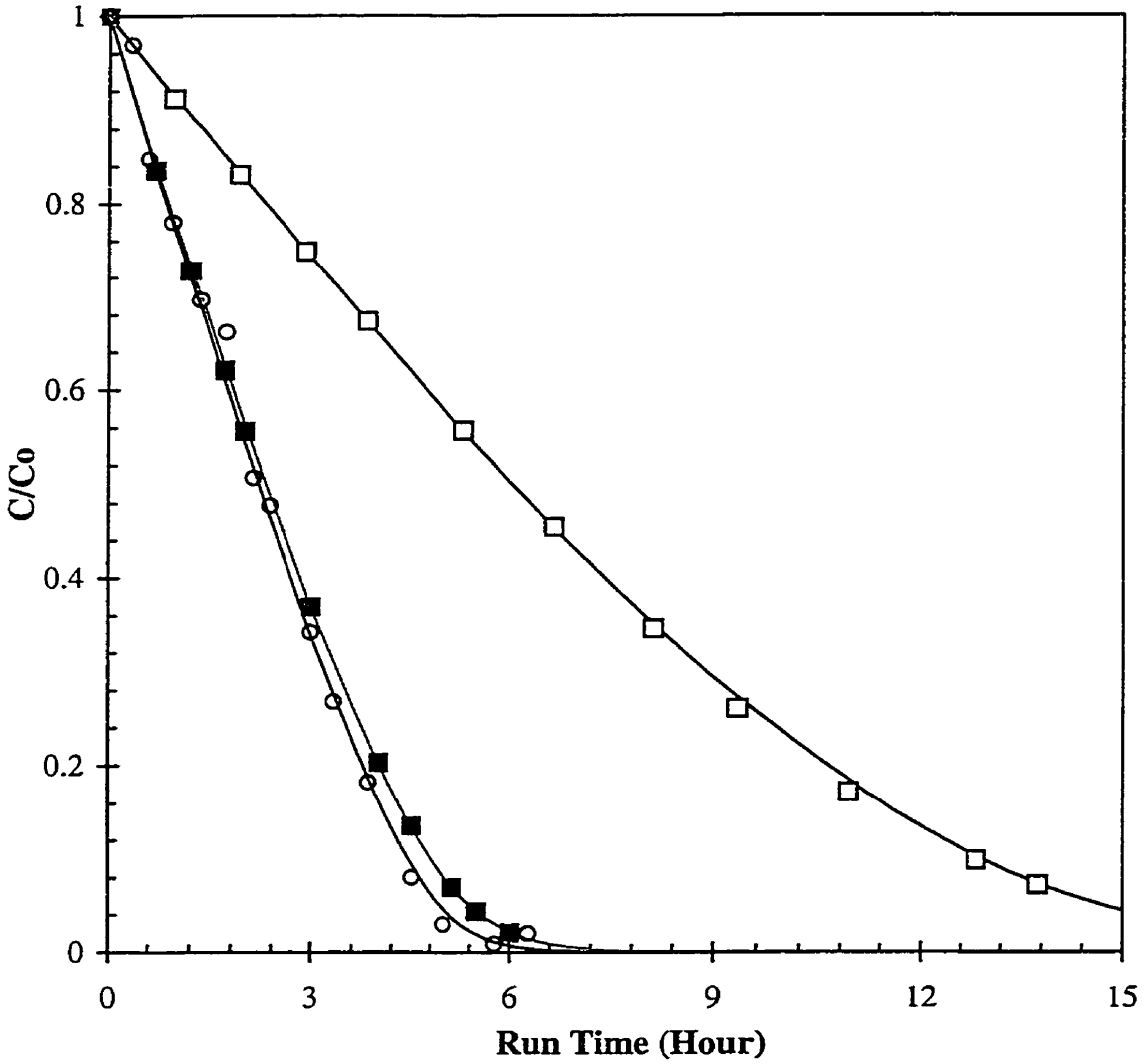

Figure 4-5: Comparison of 4-CP Degradations in Flat, Slurry and Corrugated Plate Reactors

C_0=30 mgL^{-1}; I=122 Wm^{-2}; □ flat plate, flowrate=23 $Lmin^{-1}$
■ α=3.5°, flowrate=30 $Lmin^{-1}$; ○ slurry reactor, flowrate=23 $Lmin^{-1}$
Lines: L-H fittings

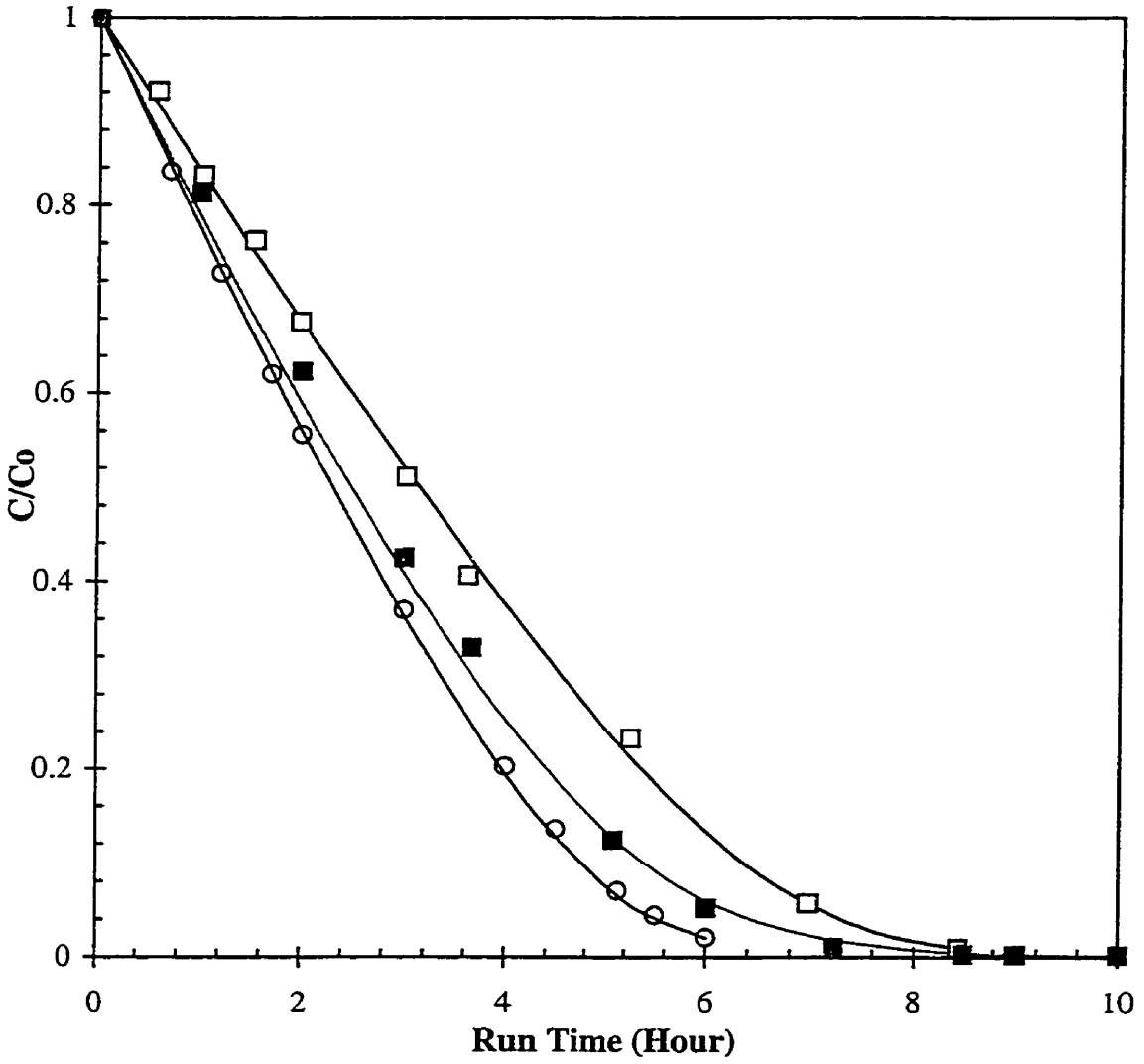

Figure 4-6: Effect of Reynolds Number on Reaction Rate
α=3.5°; C_0=30 mgL^{-1}; I=122 Wm^{-2}
□ Re=730; ■ Re=930; ○ Re=1220; Lines: L-H fittings

the performance of the LCP reactor was found to approach that of the slurry reactor at a higher flowrate. This indicates mass transfer limitations in the LCP reactor. Mass transfer limitation is also reflected by the results presented in Figure 4-6.

Table 4-2: Comparison of Reactor Performance and Illuminated TiO_2 Areas

Reactor	Area of TiO_2 Film (m^2)	Area Ratio	T_{90} (h)	T_{90} Ratio
flat plate	0.04	1	13	1
LCP (α=20°)	0.115	2.9	8.2	1.6
LCP (α=10°)	0.203	5.1	6.6	2
LCP (α=7°)	0.271	6.8	6.2	2.1
LCP (α=5°)	0.349	8.7	5.8	2.2
LCP (α=3.5°)	0.445	11.1	5.2	2.5
slurry reactor	**21.1	525	4.5	2.9

**: Estimated based on a catalyst loading of 1 gL^{-1}, a catalyst specific gravity of 3800 kgm^{-3}, and an assumed diameter of the catalyst aggregates of 0.3 μm.

In order to alleviate mass transfer limitations, stainless steel screens (14 mesh, TiO_2-coated and bare) were attached onto the flat plate. Screens may enhance the degradation rate through enhancing the mass transfer between the catalyst surface and liquid bulk and providing more immobilized TiO_2 surface. On the other hand, mass transfer resistance also affects adversely the activation of the catalyst immobilized on the flat plate surface by blocking the light transfer route. The results in Figure 4-7 indicate that bare screen resulted in a decrease of the reaction rate by approximately 35%. While the TiO_2-coated screen enhanced the reaction rate by approximately 50% (based on time required for 90% 4-CP reduction). The piece of the screen used possess a TiO_2-coated surface area of 0.067 m^2, 1.65 times that of the flat plate. The effect of TiO_2-coated screens on the performance of CP reactors was also examined briefly. Two runs were performed. Based on the results of these two runs, the effect of the screen on the

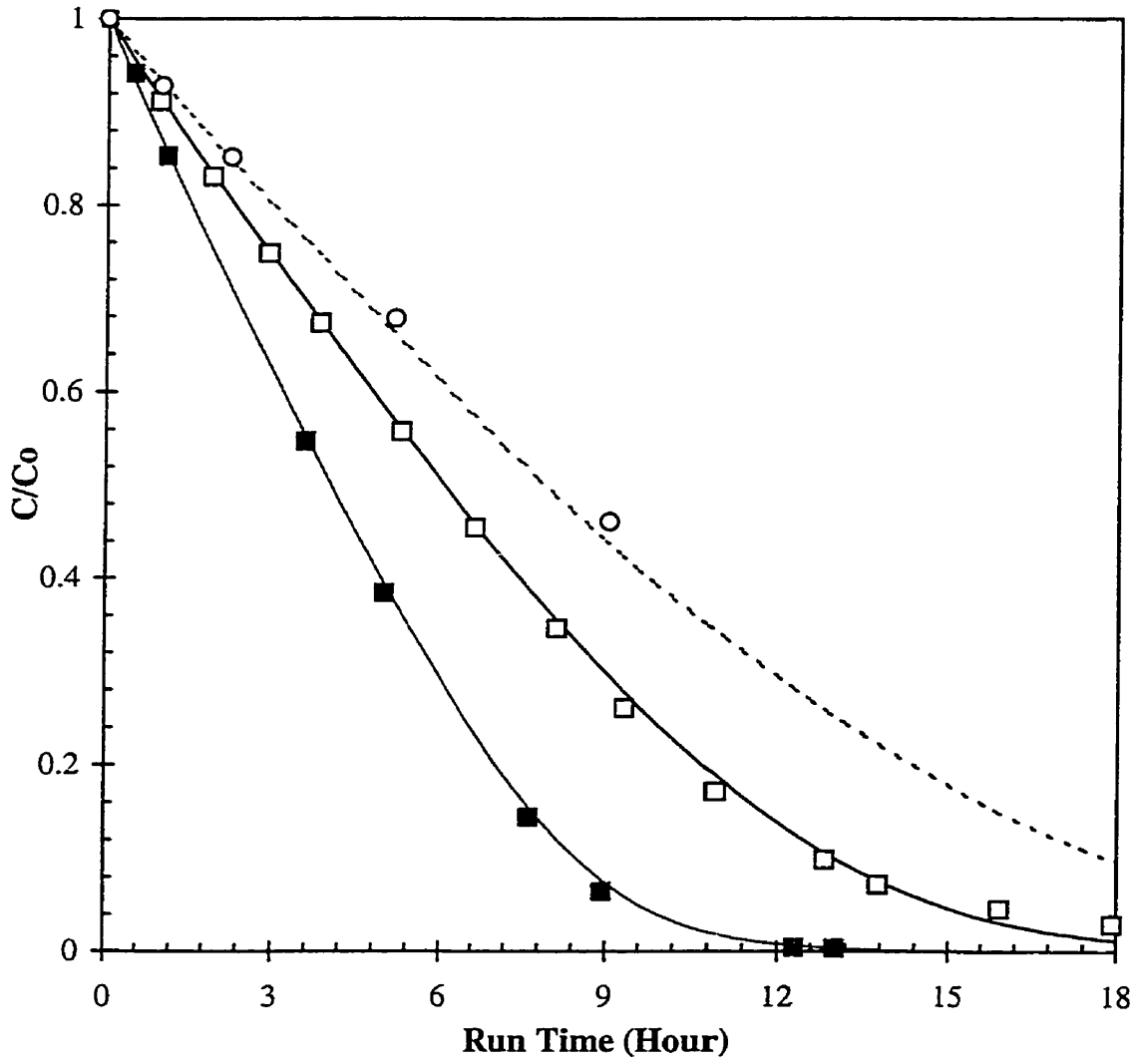

Figure 4-7: Effect of Screen on Reaction Rate
Flat plate; Re=4313; C_0=30 mgL^{-1}; I=122 Wm^{-2}; □no screen
■coated screen; ○ uncoated screen; Lines: L-H fittings

performance of the LCP reactor was not significant. It was very difficult to attach the screens on the corrugated plates without losing a noticeable amount of TiO_2 film.

As a method of estimating the energy efficiencies of the processes in which light is an input, Electrical Energy per Order (EE/O) has been used widely (Bolton et al., 1996). The EE/O was defined as the electrical energy (in kilowatts hour) required to mineralize the pollutant in one cubic meter of contaminated water by one order of magnitude. Generally speaking, the higher the energy efficiency of a system, the lower the EE/O. The EE/O can be calculated with Equation (4-1) based on the total lamp power (P, in kW), the reaction time (t, in hour), the total volume of the water in the system (V, in m^3), and the initial and final pollutant concentrations (C_0 and C_f, in mgL^{-1}). For reactions with first order kinetics, the EE/O offers an unbaised evaluation of the energy efficiency of a reactor system. For reactions with other types of kinetics, the EE/O becomes a function of the initial pollutant concentration and can only be used for rough estimation purposes.

$$EE/O = \frac{P \times t}{V \times \log(C_0 / C_f)} \qquad (4\text{-}1)$$

Table 4-3 shows the EE/O values calculated based on this and previous work on the degradation of chlorinated phenols. Although the photocatalytic degradability of all phenolic compounds is comparable (Al-Ekabi et al., 1989 and next Section), these values can only be used as a rough guidance to the novelty of the reactor systems examined due to the inconsistency of the experimental conditions in different studies. As can be seen from this table, the newly proposed CP reactor offered the best energy efficiency.

Table 4-3: Reported Energy Efficiencies of a Few Reactor Configurations

Reactor, Illumination Source, compound	Int. Conc. (mgL^{-1})	EE/O ($kWh\text{-}m^{-3}$)	References
annular slurry, fluorescent lamp, phenol	94	106	Okamoto et al., 1985a
spiral glass coil, fluorescent lamp, 4-CP	1.3	74	*Matthews, 1987a
spiral glass coil, fluorescent lamp, phenol	76	360	Al-Ekabi and Serpone, 1988
fibre optics bundle, high pressure mercury, 4-CP	13	25000	Peill and Hoffmann, 1995
fluidized bed, medium pressure mercury, 4-CP + p-toluenesulfonic acid	64 + 64	9300	Haarstrick, Kut, and Heinzle, 1996
annular slurry, fluorescent lamp, 4-CP	32	155	Stafford, Gray, and Kamat, 1997a
flat plate, fluorescent lamp, 4-CP	30	93	**This study
flat plate with screen, fluorescent lamp, 4-CP		62	
CP reactor, fluorescent lamp, 4-CP		37	
slurry reactor, fluorescent lamp, 4-CP		32	

*: Reactive Tygon tubing was used.
**: Lamp efficiency was assumed to be 17%.

Based on the model-determined photon absorption rates (see Chapter 6), the initial quantum efficiencies of the flat as well as the CP reactors (α=3.5°) were calculated to be 0.47% and 0.70% respectively. Since as many as 26 hydroxyl radicals are required to mineralize each 4-CP molecule (Stafford, Gray, and Kamat, 1997b), there exists a quantum efficiency upper limit of 3.85% for 4-CP. This indicates that more than 80% of the photo-generated hydroxyl radicals

were dissipated as waste in the CP reactor.

By comparing the EE/O values and the quantum efficiencies, we can see that the CP reactor (α=3.5°) enhanced the EE/O of the flat plate reactor by 150%. However, the corresponding enhancement of the quantum efficiency was only about 50%. This is because that the different photon capture capabilities of the flat and corrugated plates were not considered in quantum efficiency calculation.

4.5 Degradation of Chlorophenol Mixtures

Chlorinated phenol mixtures are a class of widely existing water pollutants in the environment due to industrial discharges and widespread applications of herbicide and fungicide (Al-Ekabi et al., 1989; Verschueren, 1983). In order to examine the photocatalytic degradation of highly chlorinated phenols as well as their mixtures, 4-CP, 2,4-DCP, and 2,4,5-TCP were degraded as single compound or equimolar mixtures (with the same initial TOC) in one CP reactor (α=3.5°). Selected information about these three compounds is summarized in Table 4-4.

An equimolar mixture of these three compounds was examined previously (Al-Ekabi et al., 1989). However, Tygon tubing was used to connect the components of their system. As presented in Chapter 3, this material was found in our tubing screening tests to react irreversibily with 4-CP. A total of four runs was performed in this study. The experimental results are presented in Figures 4-8 through 4-12.

Figure 4-8 shows the degradation kinctics of 4-CP and 2,4-DCP as single compounds, Figure 4-9 shows the degradation kinetics of 4-CP and 2,4-DCP mixture, and Figure 4-10 shows the concentration profiles of 4-CP, 2,4-DCP, and 2,4,5-TCP during the degradation their mixture. Figures 4-11 and 4-12 present the TOC reduction and chloride ion production during these four experimental runs.

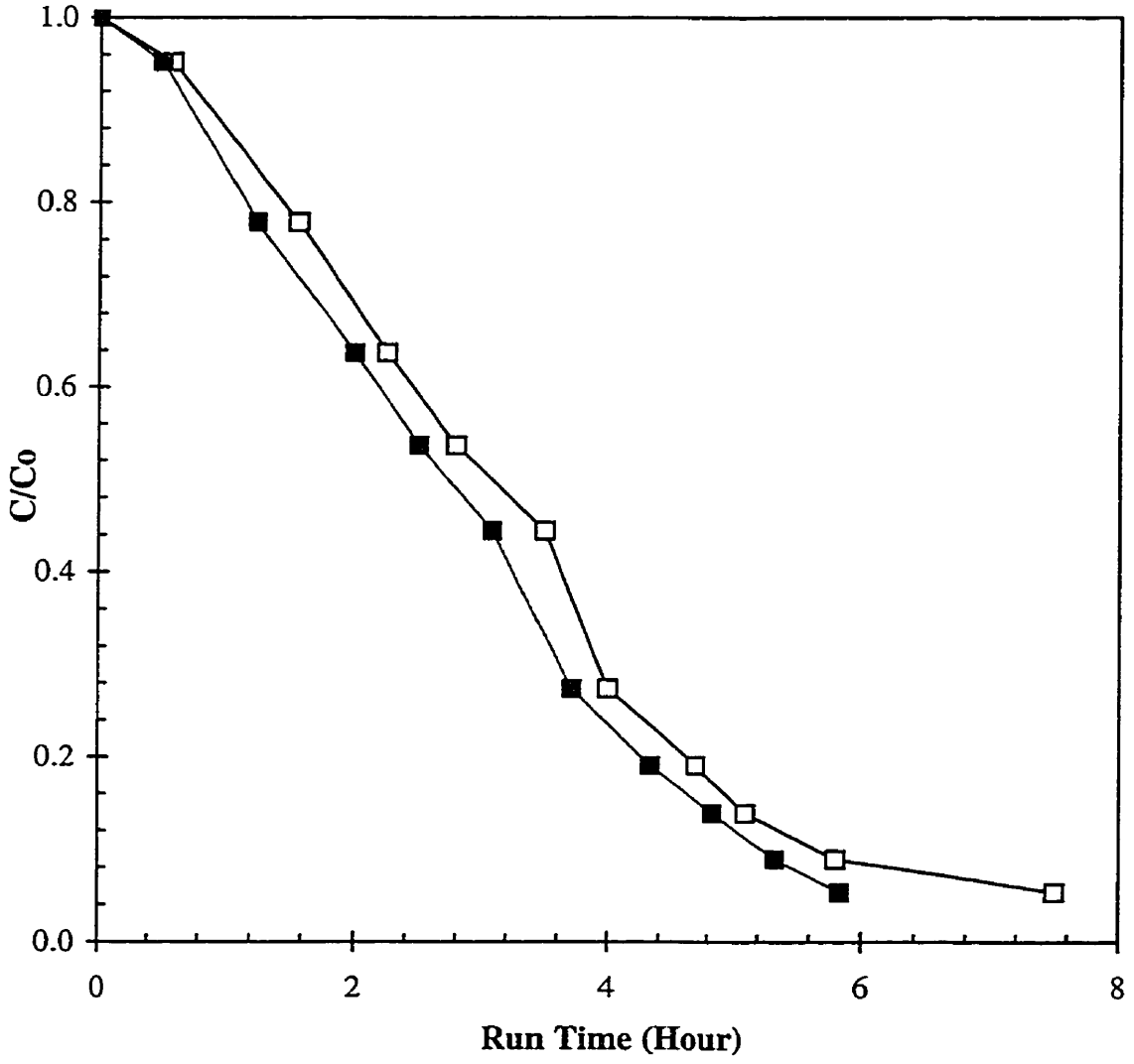

Figure 4-8: Degradation Kinetics of 4-CP and 2,4-DCP as Individual Compounds
CP reactor with α=3.5°; Re=930; C_0=234 μM
I=122 Wm^{-2}; □ 2,4-DCP; ■ 4-CP

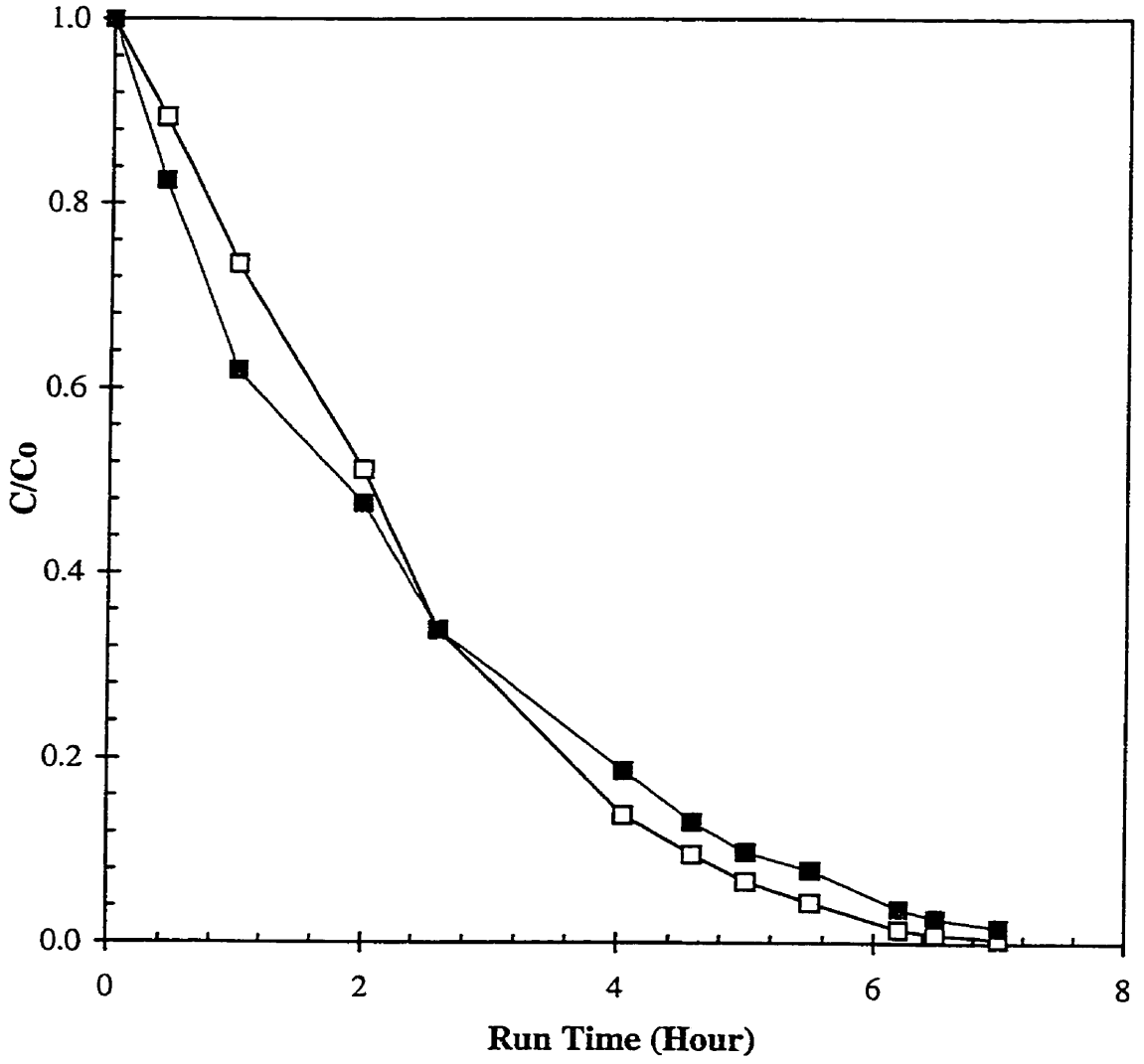

Figure 4-9: Degradation Kinetics of a 4-CP and 2,4-DCP Mixture
CP reactor with α=3.5°; Re=930; C_0=117μM each
I=122 Wm^{-2}; □ 4-CP; ■ 2,4-DCP

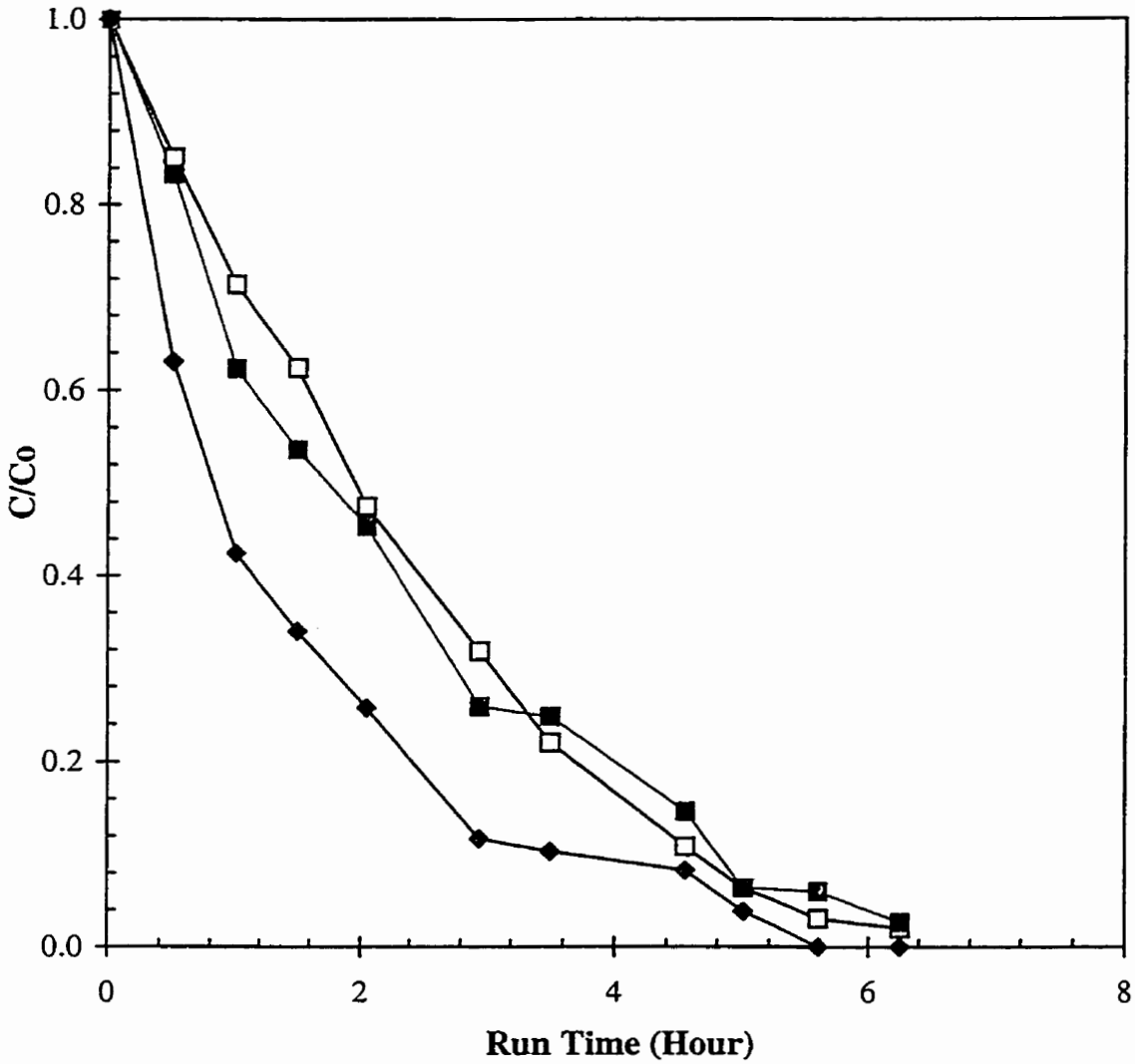

Figure 4-10: Degradation Kinetics of a 4-CP, 2,4-DCP, and 2,4,5-TCP Mixture: Concentration Profiles
CP reactor with α=3.5°; Re=930; I=122 Wm^{-2};
C_0=77.8μM each; □ 4-CP; ■ 2,4-DCP; ○ 2,4,5-TCP

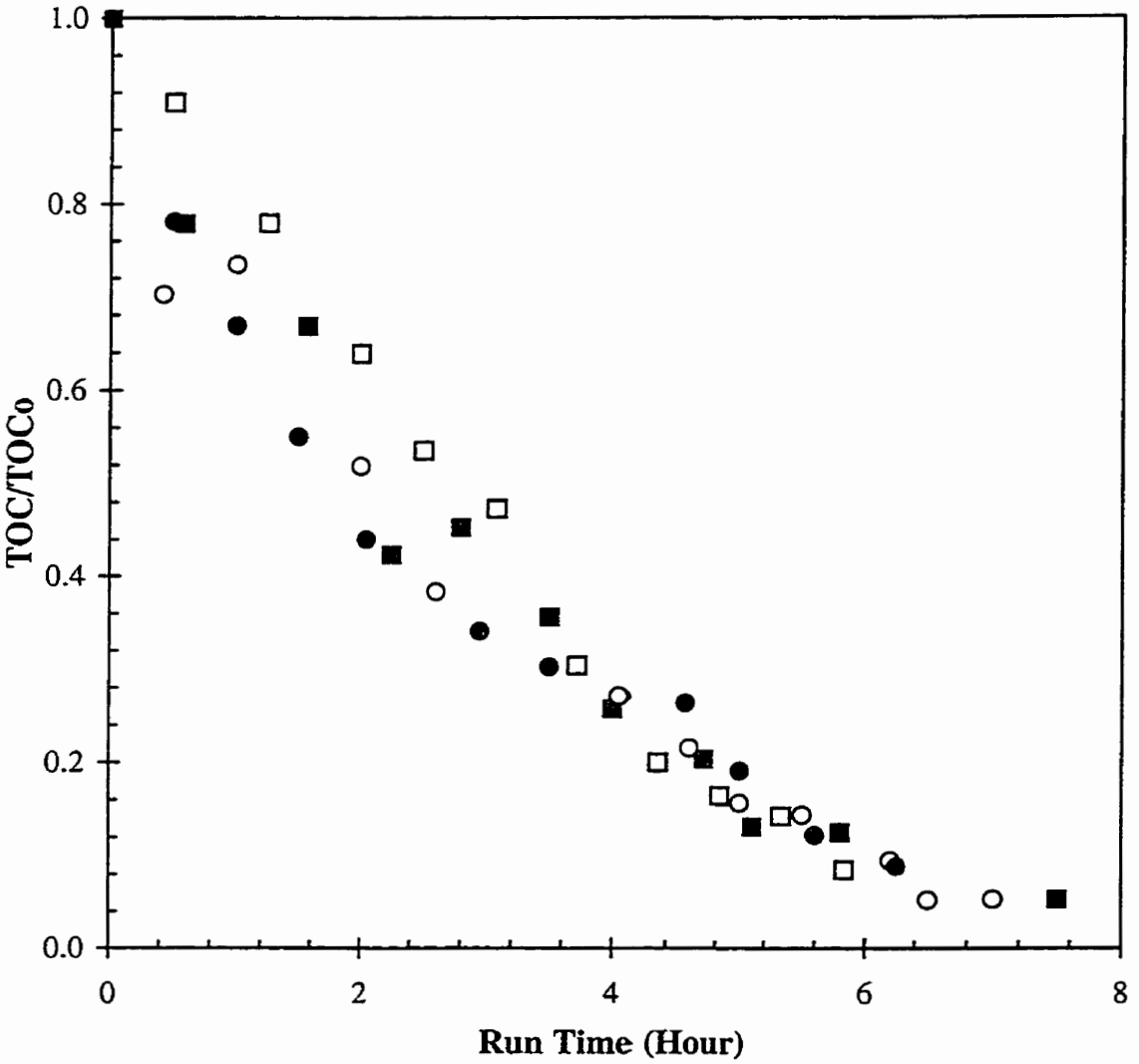

Figure 4-11: Degradation Kinetics of Different Chlorophenol Mixtures: TOC Profiles

CP reactor with α=3.5°; Re=930; I=122 Wm^{-2};
TOC_0=16.8 mgL^{-1}; □ 4-CP only; ■ 2,4-DCP only; ○ mixture of 4-CP and 2,4-DCP; ● mixture of 4-CP, 2,4-DCP and 2,4,5-TCP

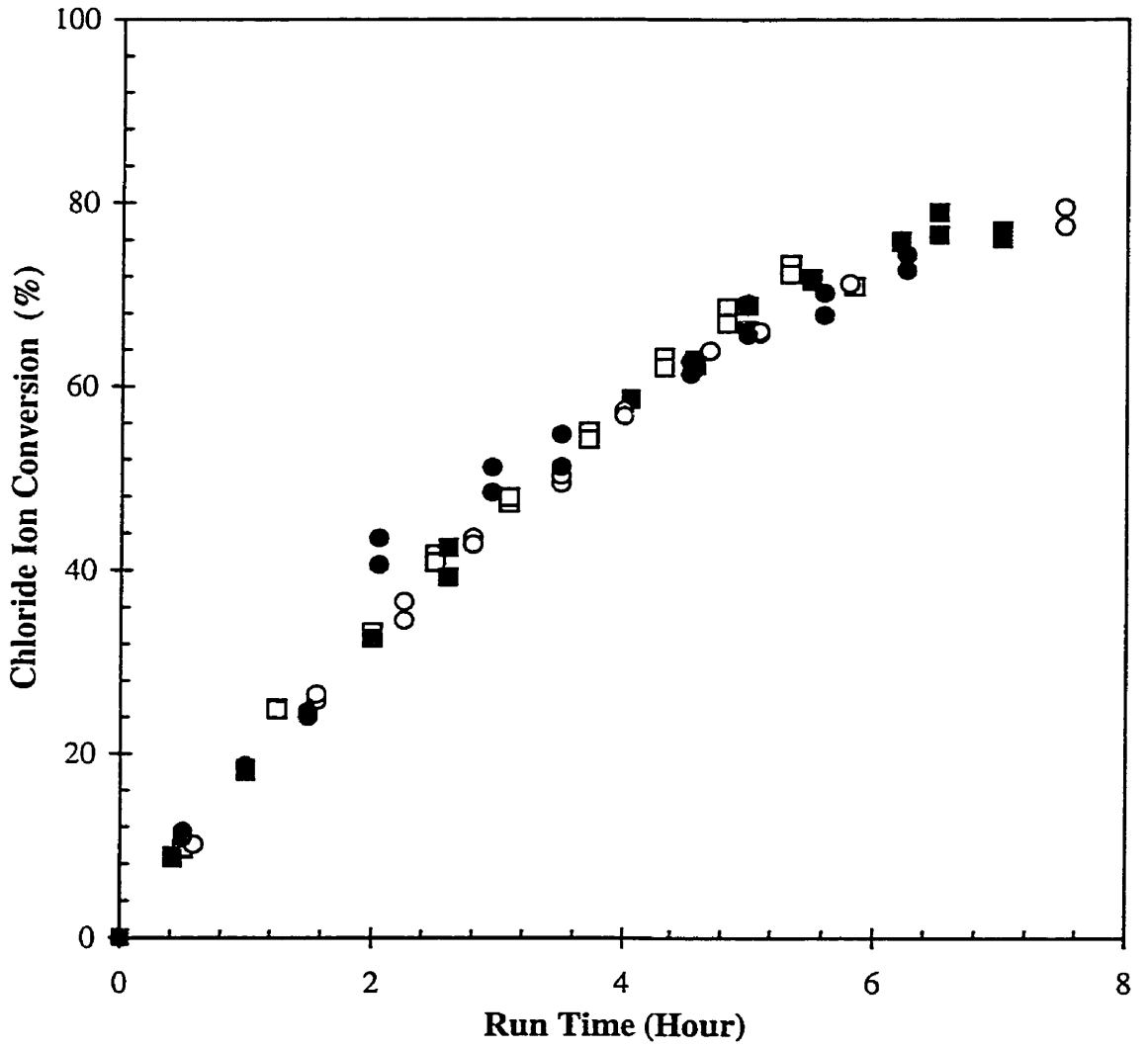

Figure 4-12: Dechlorination Kinetics of Different Chlorophenol Mixtures
CP reactor with α=3.5°; Re=930; I=122 Wm^{-2};
TOC_0=16.8 mgL^{-1}; □ 4-CP only; ○ 2,4-DCP only; ■ mixture of 4-CP and 2,4-DCP; ● mixture of 4-CP, 2,4-DCP and 2,4,5-TCP

Table 4-4: Physical and Hazardous Properties of the Model Compounds (Mackay et al., 1993; Verschueren, 1983; Howard, 1989)

Chemical Name	4-chlorophenol (4-CP)	2,4,- dichlorophenol	2,4,5- trichlorophenol
Synonyms	1-chloro-4-hydroxybenzene *p*-chlorophenol	2,4-DCP	2,4,5-TCP
Molecular Weight	128.56	163.01	197.46
Melting Point (°C)	43	45	62
Boiling Point (°C)	220	210	252
Henry's Law Constant ($Pa\ m^3\ mol^{-1}$)	0.0567	0.435	0.521
Odour Threshold (mgL^{-1})	1.24	0.21	0.06
Taste Threshold (mgL^{-1})	1.16	0.012	0.001
Bioconcentration Factor	1.0 -1.5	1.0 - 2.5	2.0 - 8.4

The results in Figures 4-8, 4-9, 4-11, and 4-12 all indicate that the degradation rates of these three chlorinated phenols are similar in terms of phenol concentration or TOC, regardless of the degree of chlorination. This finding is favorable since it indicates the advantage in using photocatalysis to detoxify highly chlorinated phenols. In addition, experimental data collected with less toxic phenolic compounds may be used to assess the photocatalytic degradation of highly toxic chlorinated phenols. This will certainly provide convenience during the experiment. The relatively fast rate of 2,4,5-TCP reduction shown in Figure 4-10 may be due to the adsorption of this compound to the system components.

4.6 Concluding Remarks

For the degradation of 4-CP, the newly proposed CP reactor resulted in a 150% enhancement in capacity and energy efficiency over that of the flat plate reactor. This enhancement was due primarily to the large illuminated surface area of the catalyst films in the new reactor. The energy efficiency of the CP reactor was only about 15% lower than that of the slurry reactor. A catalyst-coated screen was also found to enhance the photocatalytic degradation of 4-CP in the flat plate reactor by about 50%. The CP reactor still suffers from mass transfer limitation.

For the degradation of phenolic compounds, the CP reactor has the highest energy efficiency compared to all other immobilized systems examined previously. The CP reactor configuration is promising due to its potentially low capital, and O&M costs, its capability for efficient solar UV utilization, and its proven superior performance.

The photocatalytic degradation rate of 4-CP, 2,4-DCP, and 2,4,5-trichlorophenol were found to be similar in terms of phenol concentration or TOC, regardless of the degree of chlorination. Based on this observation, photocatalysis should be more advantageous for use in the dechlorination of highly chlorinated phenols.

Photon efficiency is not as suitable as the EE/O in evaluating the energy efficiencies of photoreactor systems as it does not incorporate the efficiency in converting electricity or sunlight to absorbed photons. However, it could be used to estimate how far the energy efficiency of a particular system is from its upper limit.

CHAPTER 5: COMBINED PHOTOCATALYTIC AND BIOLOGICAL GROUNDWATER TREATMENT

Biological wastewater treatment processes (i.e., activated sludge) are relatively less expensive but subject to inhibition from toxic compounds. Photocatalysis is capable of degrading essentially all toxic chemicals but suffers from high cost and competitive inhibition from many species. Therefore, for the treatment of a real wastewater contaminated by biodegradable as well as recalcitrant/toxic chemicals, the two treatment processes may be complementary to each other if used in series (Scott and Ollis, 1995). The biological step could degrade the biodegradable compounds so that in the next photocatalytic step competitive inhibition due to these species is reduced and the oxidation rate of the recalcitrant/toxic compounds increased. Alternatively, the photocatalytic step could enhance the subsequent biological step by breaking-down compounds which would otherwise be toxic to the microorganisms. In addition, the photocatalytic step could also provide substrates to the next biological step in the form of photocatalytic reaction intermediates. A prerequisite to the success of such a combined system is that the photocatalytic step does not increase the toxicity of the wastewater to the microorganisms in the bioreactor. Oxidation reactions usually go through the sequence (Bolduc and Anderson, 1997):

$$\text{Organics} \longrightarrow \text{Aldehydes} \longrightarrow \text{Carboxylic acids} \longrightarrow \text{Carbon dioxide}$$

The competitiveness of photocatalysis as a wastewater treatment method can therefore be improved by enhancing its energy efficiency as well as by using it as a step in a combined photocatalytic/biological treatment system (Scott and Ollis, 1995). In addition to the efficiencies of the individual steps, another factor affecting the efficiency of a combined photocatalytic/biological treatment process is the relative extent of treatment in each step. The optimal extent of treatment in the photocatalytic step should be such that it destroys a relatively

large fraction of the toxic compounds and provide relatively more biodegradable reaction intermediates. For the treatment of a given wastewater in a given set of photo- and bio- reactors, there should be an optimal residence time in the photoreactor at which the overall treatment cost is minimized.

In order to examine the potential for use of the CP reactor in treating real wastewaters as a stand-alone method or in combination with bioprocesses, a contaminated groundwater from the Uniroyal Chemical plant site in Elmira, Ontario, was studied. The groundwater contained high levels of ammonia and lower levels of organic and inorganic species. Biological nitrification could not be used directly to convert ammonia to nitrate because of the inhibition from the toxic organics. At present, the Uniroyal Chemical plant uses activated carbon adsorption to remove the nitrification inhibitors, yielding a groundwater which can then be sent for biotreatment. The specific objectives of these tests were, to identify suitable operating conditions for the CP reactor using the contaminated groundwater, to determine whether nitrification inhibition could be removed or reduced using photocatalysis, and to look for a relationship between the length of photocatalytic pretreatment and the extent of the subsequent nitrification. The results are described in the following sections of this chapter.

5.1 Materials and Methods

5.1.1 Characteristics of the Groundwater

Table 5-1 is a summary of the typical characteristics of this water as provided by Uniroyal Chemical. In addition to the species listed here, it is believed that the water also contains dozens of other substances (especially organic compounds) at levels lower than the detection limits.

Table 5-1: Characteristics of the Contaminated Groundwater

Organics and Surrogate Parameters	**Concentration**	**Metals and Inorganics**	**Concentration**
VOCs (μgL^{-1})		Hardness ($CaCO_3$)	523
chlorobenzene	14000		
formaldehyde	15	Conductivity (μSm^{-1})	4500
Extractables (μgL^{-1})			
		pH	7.36
aniline	450		
benzothiazole	81	**Metals (mgL^{-1})**	
carboxin (oxethiin)	320		
2-chlorophenol	33	Arsenic (As)	0.011
4-chloro-3-methylphenol	17	Barium (Ba)	0.136
2,4-dichlorophenol	34	Calcium (Ca)	119
2,6-dichlorophenol	20	Iron (Fe)	1.93
di-n-butyl phthlate	16	Lead (Pb)	0.002
2-mercaptobenzothiazole	4400	Magnesium (Mg)	62.7
nitrosodiphenylamine /diphenylaime	170	Manganese (Mn)	0.167
2,4,5-trichlorophenol	6.5	Potassium (K)	90.2
2,4,6-trichlorophenol	8.8	Sodium (Na)	566
		Strontium (Sr)	2.02
Herbicides (μgL^{-1})		Zinc (Zn)	0.05
2,4,5-T	0.72	**Inorganics (mgL^{-1})**	
2,4,5-TP (Silvex)	0.29		
Dicamba	15	Ammonia (N)	117
Surrogate Parameters (mgL^{-1})		Chloride (Cl)	748
		Nitrate (N)	14.5
		Nitrite (N)	0.2
Alkalinity ($CaCO_3$)	632	Sulfates (SO_4)	723
COD	103	Sulphide	0.02
DOC	18.6	Total Cyanide (CN)	0.036
TOC	19.3	TKN	114

5.1.2 Experimental Method

Contaminated groundwater was collected in head space-free glass containers, stored at 4°C, and used within one or two days of collection. The groundwater was treated in the photoreactor under three Scenarios:

Scenario A: groundwater charged into the photoreactor as it was

Scenario B: groundwater charged into the photoreactor after its pH lowered to 4.5

Scenario C: groundwater charged into the photoreactor after its pH lowered to 4.5 and addition of hydrogen peroxide (60 mgL^{-1} initially).

Concentrated sulfuric acid instead of nitric acid was used for pH adjustment for nitrogen balance considerations. The flowrate through the corrugated photoreactor was constant at 23 $Lmin^{-1}$. This corresponds to a Reynolds number of 930 for the corrugated plate reactor used (α=3.5°). The radiation intensity at the reactor cover was constant at 122 Wm^{-2}. More detailed information on the photoreactor, the experimental set-up, and the experimental procedure are described in Section 3.1.

In order to examine the effect of the extent of photocatalytic pretreatment on subsequent biological nitrification, the groundwater was treated in the photoreactor for different lengths of time under Scenario B and sample were taken for various analyses and for nitrification tests. The pH was adjusted to 7.5 prior to biotreatment.

Nitrification was carried out in 250 mL Erlenmyer flasks within a shaker at 25°C, using an inoculum of nitrifying sludge from the existing treatment system. Sludge was added to make a concentration of approximately 1000 mgL^{-1}. Samples were taken for desired analyses 72 hours after the start of nitrification.

5.1.3 Analysis Methods

Samples were analyzed using a UV spectrophotometer, a TOC analyzer, HPLC, HACH kits (HACH, 1998), and/or a IC for spectral UV absorption, TOC, chemical analysis, total nitrogen (HACH method #10022), nitrate (HACH method #8039), nitrite (HACH method #8507), chloride, and sulfate. Ammonia was measured using an Orion ammonia electrode (Model 95-12). Information about the spectrophotometer, the TOC analyzer, the IC, and the HPLC system is provided in Sections 3.1.5 and 4.1. All samples from the bioreactors (i.e., flasks) were centrifuged before analyses were performed.

5.2 Results and Discussions

5.2.1 Photocatalytic Treatment

The experimental results are presented in Figures 5-1 through 5-4. TOC (Figure 5-1) and pH (Figure 5-3) of the samples and concentrations of nitrate (Figure 5-4) and a selected compound (the one corresponds to the largest HPLC peak, see Figure 5-2) were recorded during the photocatalytic degradation of the groundwater under the three Scenarios described above. As can be seen from Figure 5-1, TOCs of the groundwater and concentrations of the selected compound decreased less than 20% after 7 hours in the photoreactor under Scenario A. Considering the fact that vaporization to the environment may have also contributed to this decrease, the photocatalytic reactions must have been sluggish. This is primarily due to the inhibition from the carbonate and bicarbonate ions in the groundwater. Similar phenomena have been experienced by several researchers (Pacheco, Prairie, and Yellowhorse, 1993; Methos and Turchi, 1993; Glaze, Kenneke, and Ferry, 1993). Adjusting the initial pH from around 7 to a value of 4.5 (Scenario B) effectively alleviated this inhibition by driving off the alkalinity.

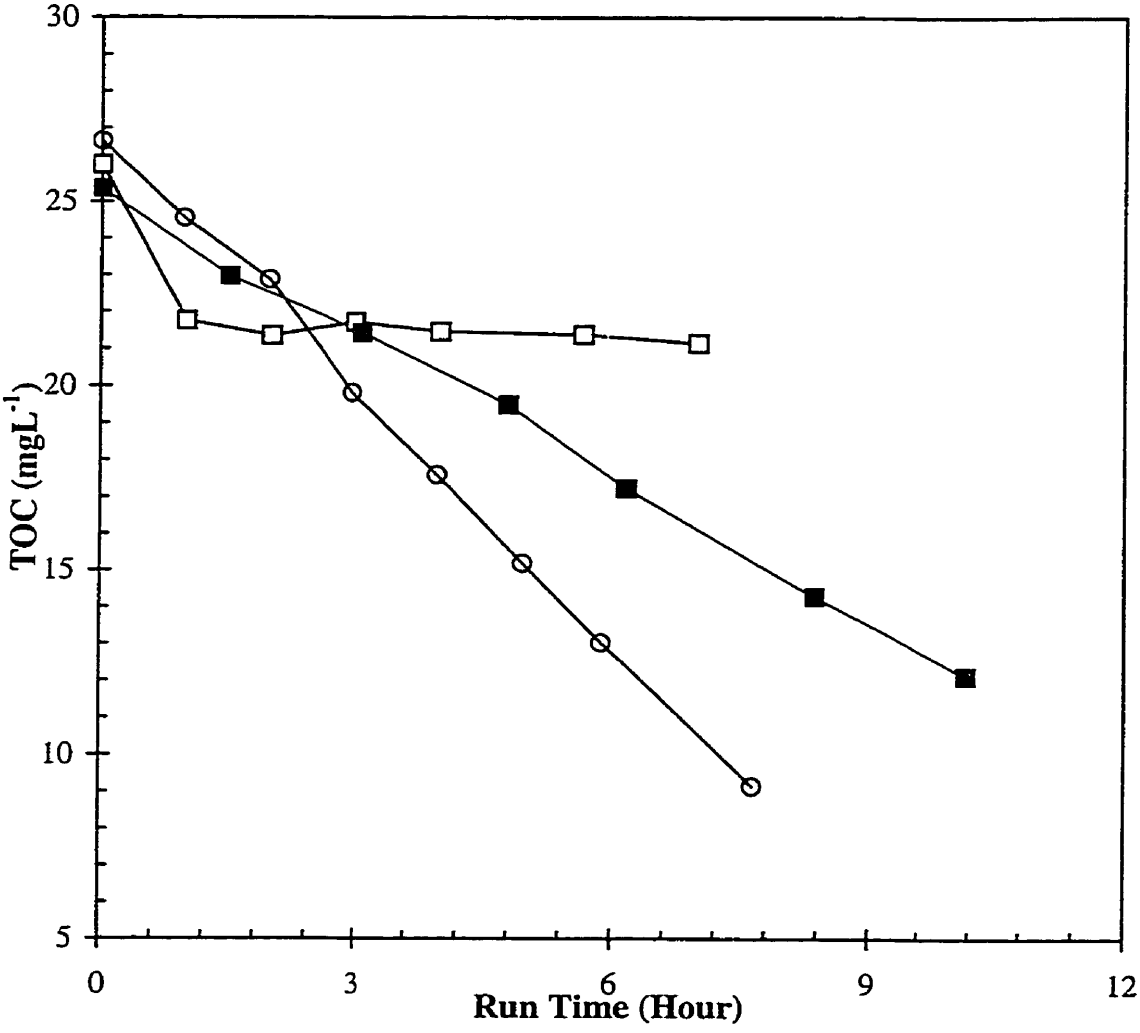

Figure 5-1: TOC Reduction During Photocatalytic Groundwater Treatment

CP reactor with α=3.5°; Re=930; I=122 Wm^{-2}

□ Water used as was; ■ with pH adjustment

○ with pH adjustment and H_2O_2 addition

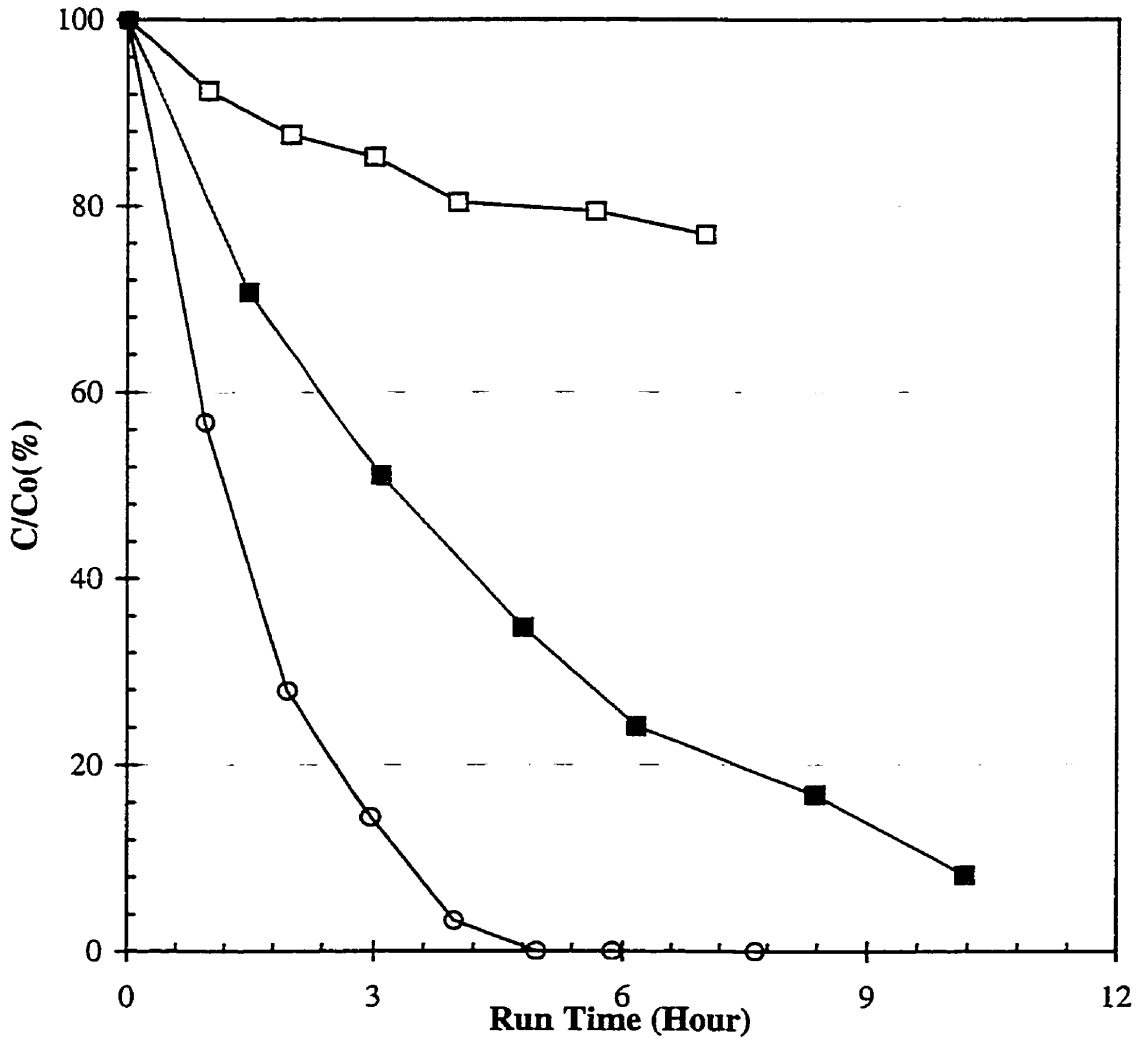

Figure 5-2: Degradation of a Selected, Unidentified Compound During Groundwater Pretreatment

CP reactor with α=3.5°; Re=930; I=122 Wm^{-2}

□Water used as was; ■ with pH adjustment

○ with pH adjustment and H_2O_2 addition

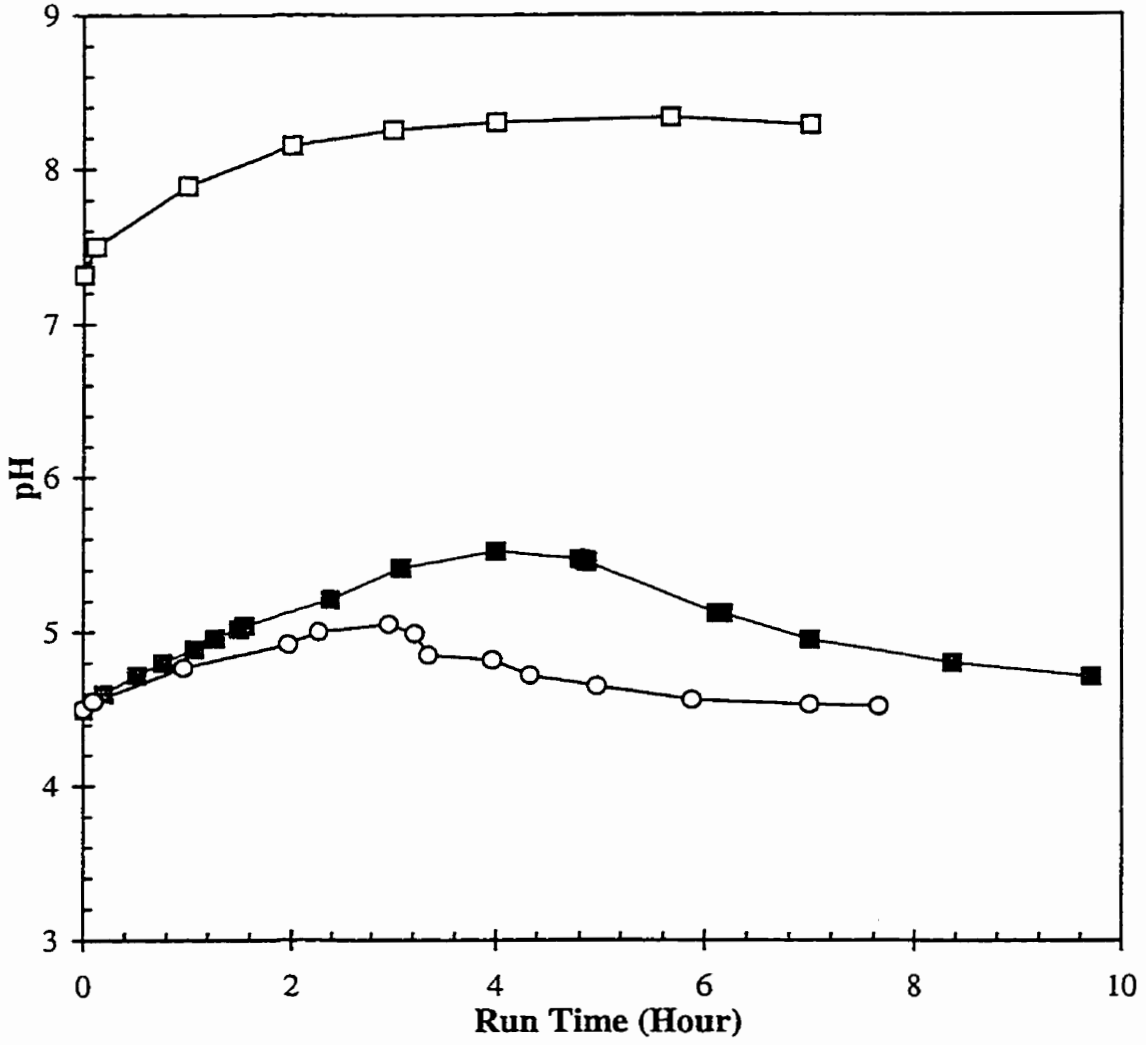

Figure 5-3: Groundwater Pretreatment: pH Profiles
CP reactor with α=3.5°; Re=930; I=122 Wm^{-2}
□ Water used as was; ■ with pH adjustment
○ with pH adjustment and H_2O_2 addition

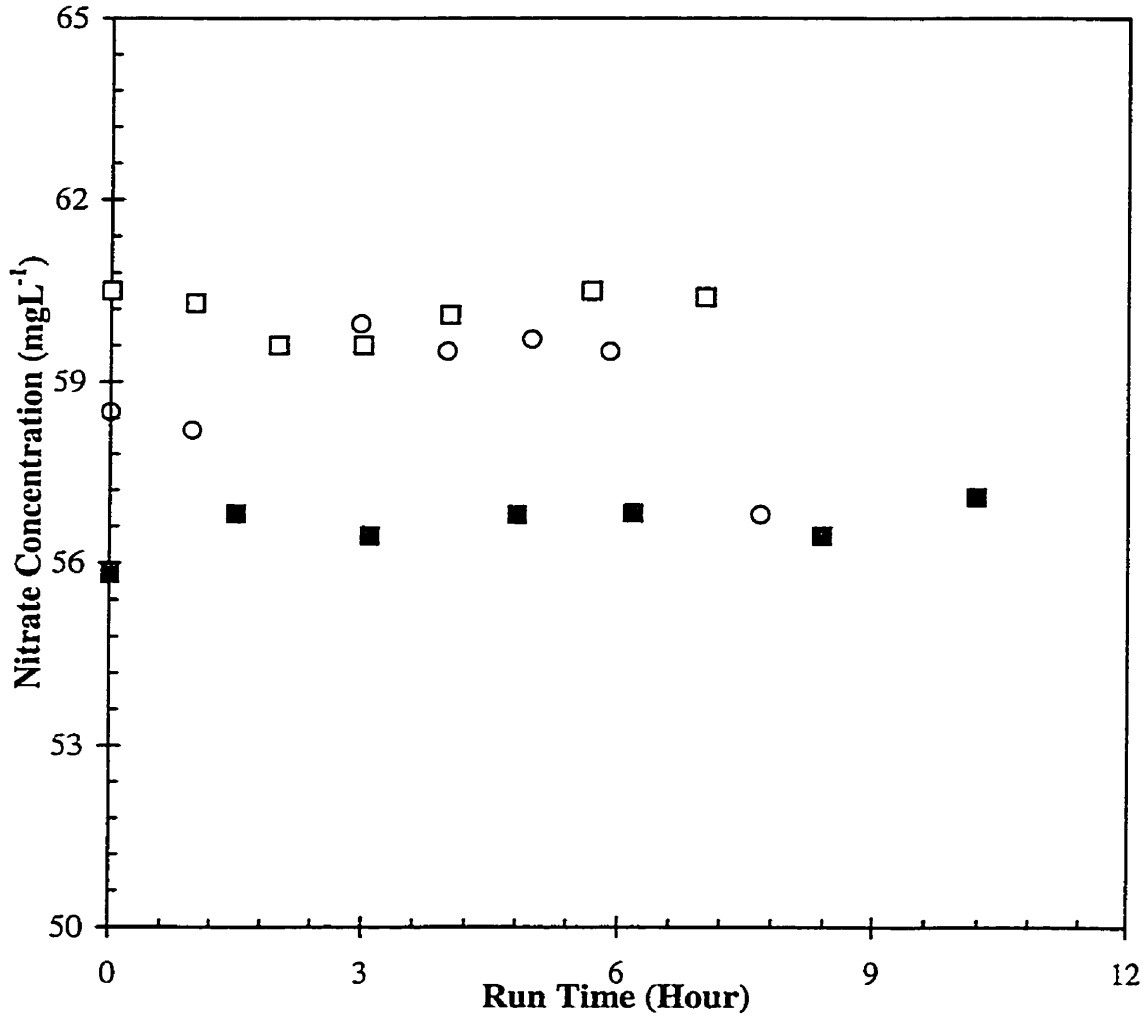

Figure 5-4: Groundwater Pretreatment: Nitrate Profiles
CP reactor with α=3.5°; Re=930; I=122 Wm^{-2}
□ Water used as was; ■ with pH adjustment
○ with pH adjustment and H_2O_2 addition

Using pH adjustment plus the addition of hydrogen peroxide (Scenario C) enhanced the reactions further. By comparing the results in Figures 5-1 and 5-2, we can also observe that when the unidentified target compound disappeared after 5 hours in the photoreactor (open circles in Figure 5-2) the TOC of the groundwater was reduced by only about 40% (open circles in Figure 5-1). This phenomenon is indicative of the formation of acidic reaction intermediates. Existence of species other than the selected compound may also have contributed to this phenomenon.

The pH patterns shown in Figure 5-3 are quite interesting. As the organic water pollutants are oxidized, the pH pattern should usually be characterized by a relatively fast initial drop followed by slow decrease due to the formation of acidic reaction intermediates and the change in the ionic strength of the water as the reactions proceed. Such patterns were observed during the degradation of 4-CP spiked de-ionized water (as presented in Chapter 4). However, during the photocatalytic degradation of the groundwater the pH increased for the first couple of hours and then decreased as the reaction proceeds. Specific reasons for this particular pH pattern are unknown and should be examined during further work on this groundwater..

Nitrate concentrations of the samples as functions of the run time are presented in Figure 5-4. Based on the sensitivity of the analytical method (IC) used, the nitrate levels were essentially constant during these experimental runs and photocatalytic conversion of ammonia to nitrate did not happen. This result agrees with the findings by another research group, where photocatalytic nitrification was demonstrated to proceed under basic conditions only (Bonsen et al., 1997). The levels of sulfate and chloride ions were also examined and they were both not found to change significantly during the photocatalytic degradation of the groundwater.

5.2.2 Biological Nitrification

The results of biological nitrification tests are presented in Figures 5-5 through 5-10. Control nitrification tests with untreated water, NH_3-spiked pure water, and ground water treated with the photoreactor lights turned off, were performed for comparative purposes. The effects of photocatalytic pretreatment extent (expressed as times in the photoreactor) on ammonia conversion (Figure 5-5), TOC levels (Figure 5-6), nitrate and nitrite production (Figures 5-7 and 5-8), and levels of total nitrogen and a selected compound (Figures 5-9 and 5-10) are discussed below. The keys in these figures are:

"NH_3 only" : tap water containing only NH_3 (as NH_4Cl) with no pretreatment, as a benchmark test of the sludge's nitrifying capability.

"3 Off": groundwater pretreated for 3 hours in the photoreactor with the lamps off, including pH adjustments.

"0 Off": groundwater with pH adjustment only.

"Original": groundwater used as was.

"1 On, etc.": groundwater pretreated in the photoreactor with lamps on for indicated length of time (i.e., 1 hour), including pH adjustments.

As can be seen in Figure 5-5 that photocatalytic pretreatment has a demonstrable and significant effect in improving the extent of biological nitrification. This effect is sensitive to the length of pretreatment time, up to a certain point. Beyond this point there appears to be no additional benefit to further pretreatment. With a pretreatment time of 6 hours, the extent of nitrification was enhanced by a factor of 600%. Biological TOC removal was approximately the same under all test conditions, but there is a trend towards higher removal with longer pretreatment times. As expected, the formation of nitrate (Figure 5-7) appears to be consistent with ammonia disappearance. Figure 5-8 shows a tendency to accumulate nitrite when

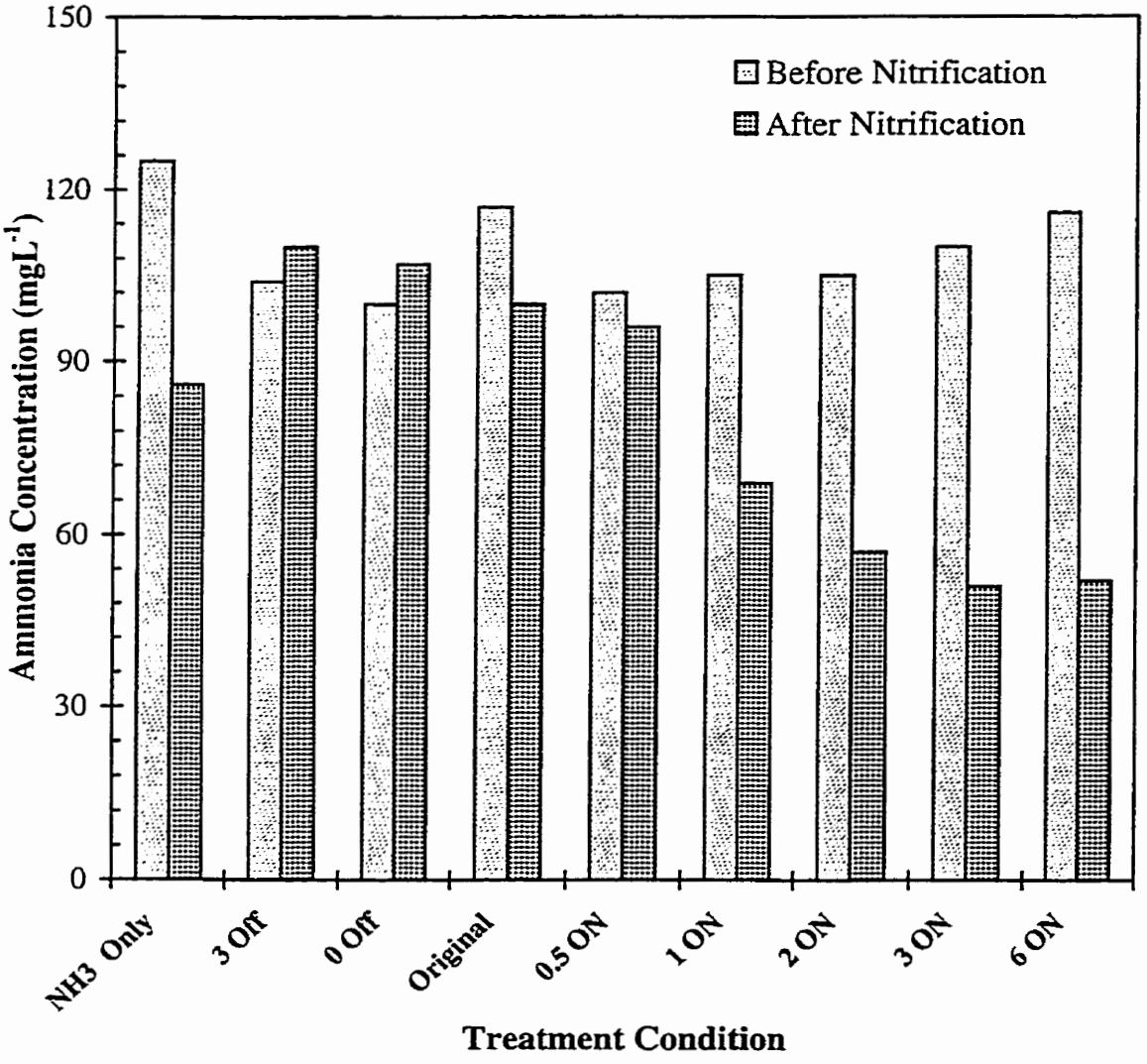

Figure 5-5: Effect of Photocatalytic Pretreatment on Subsequent Nitrification: Ammonia Profiles
CP reactor with α=3.5°; Re=930; I=122 Wm^{-2}

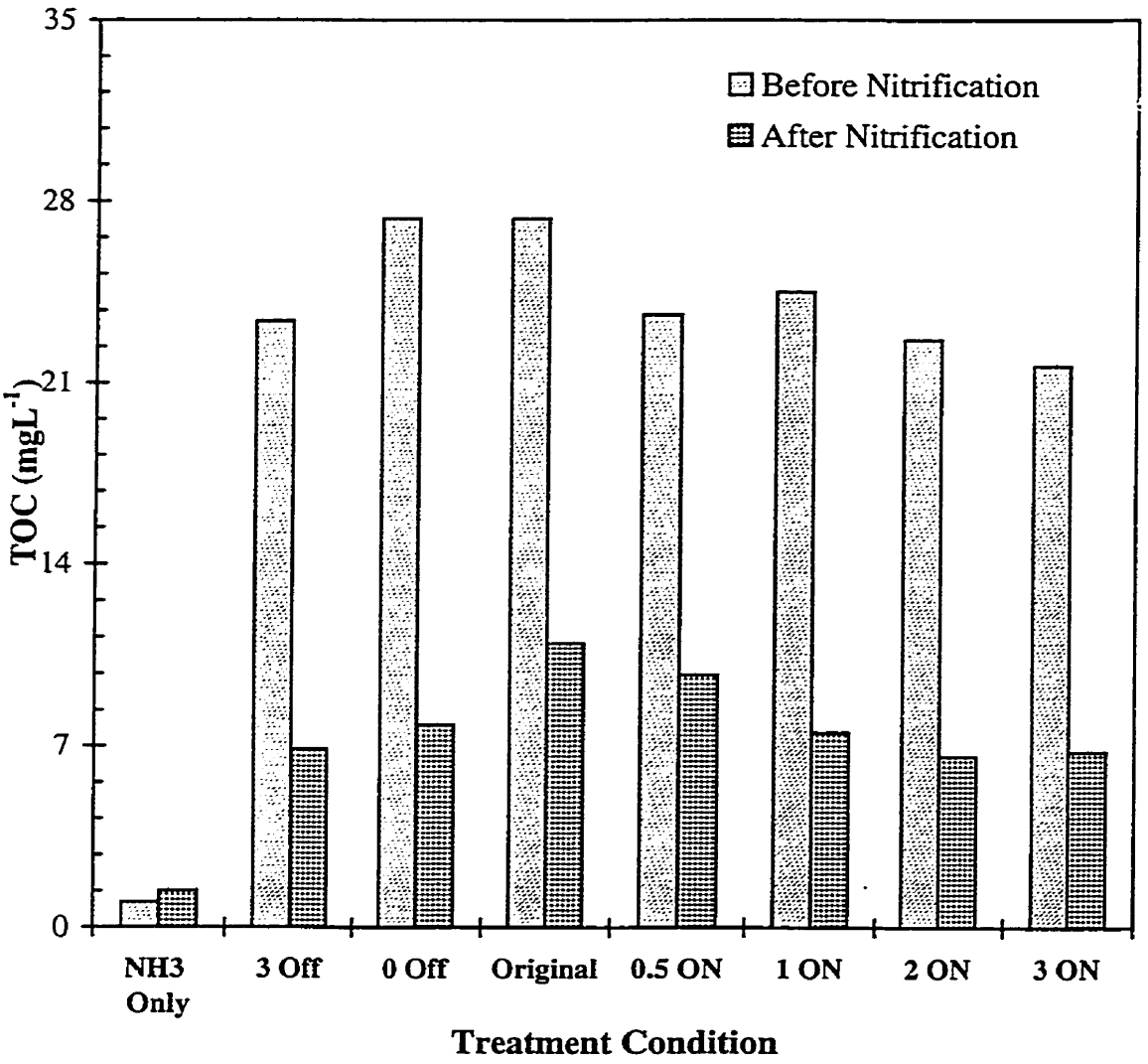

Figure 5-6: Effect of Photocatalytic Pretreatment on Subsequent Nitrification: TOC Profiles
CP reactor with α=3.5°; Re=930; I=122 Wm^{-2}

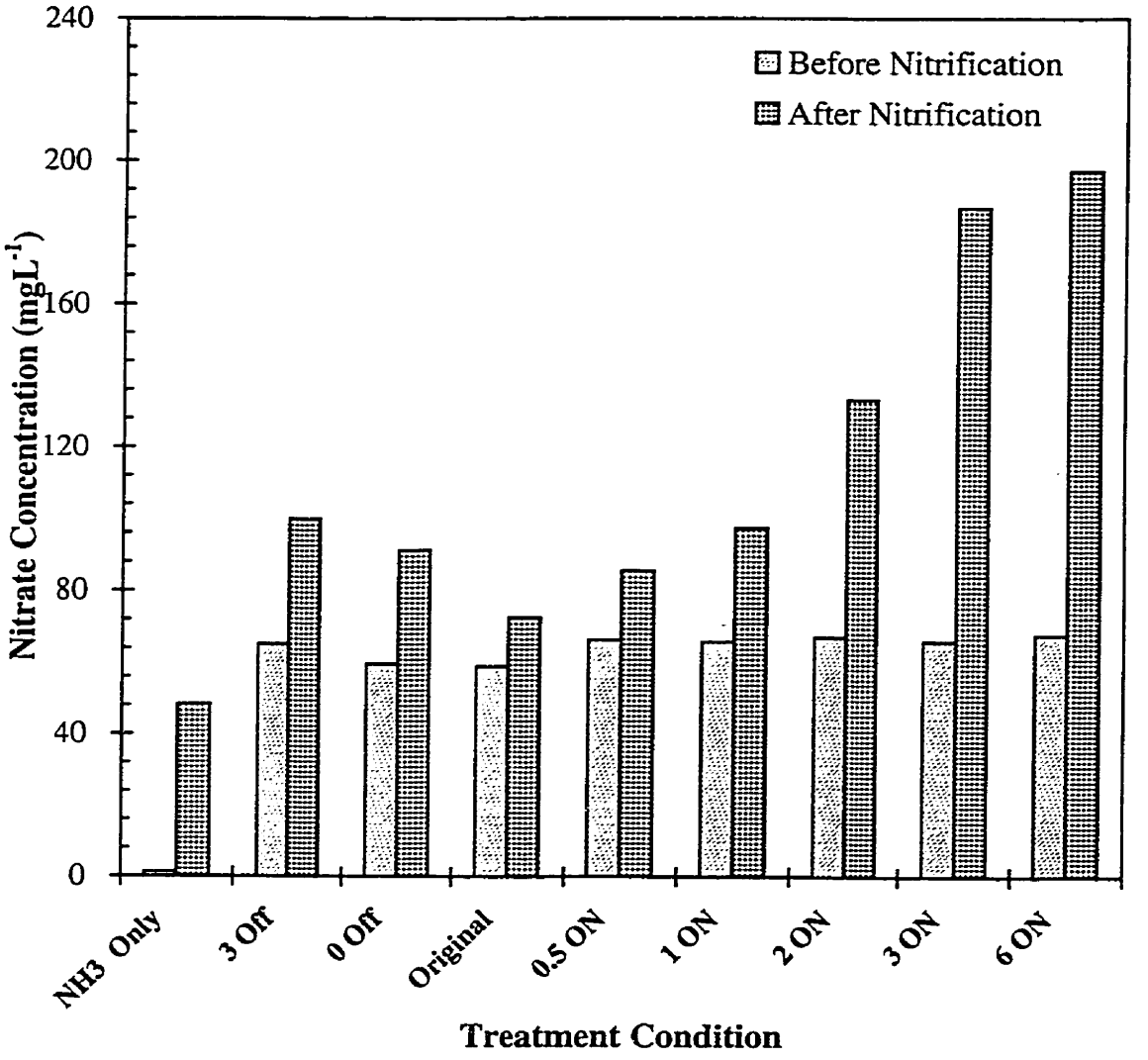

Figure 5-7: Effect of Photocatalytic Pretreatment on Subsequent Nitrification: Nitrate Profiles
CP reactor with α=3.5°; Re=930; I=122 Wm^{-2}

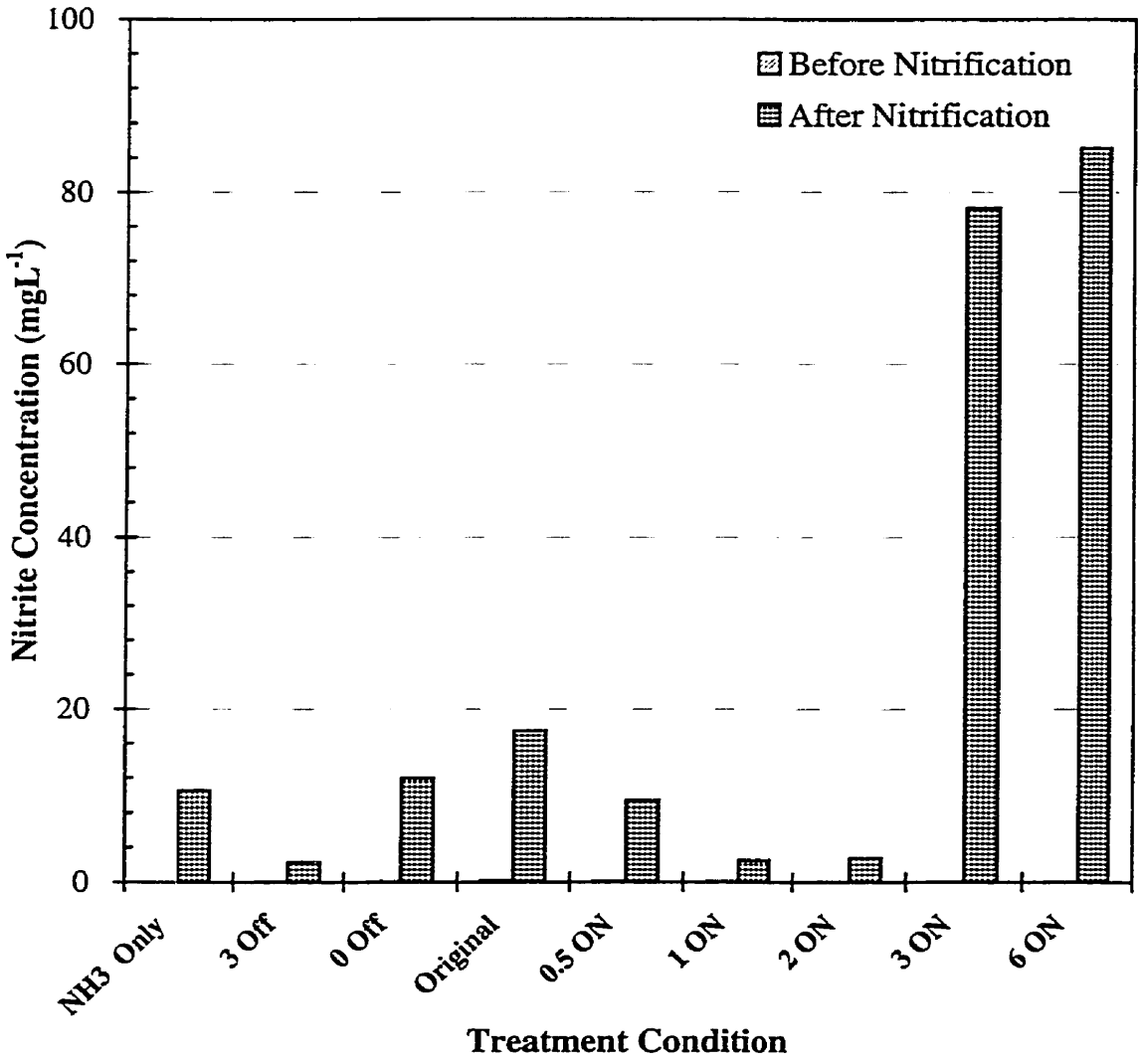

Figure 5-8: Effect of Photocatalytic Pretreatment on Subsequent Nitrification: Nitrite Profiles
CP reactor with α=3.5°; Re=930; I=122 Wm^{-2}

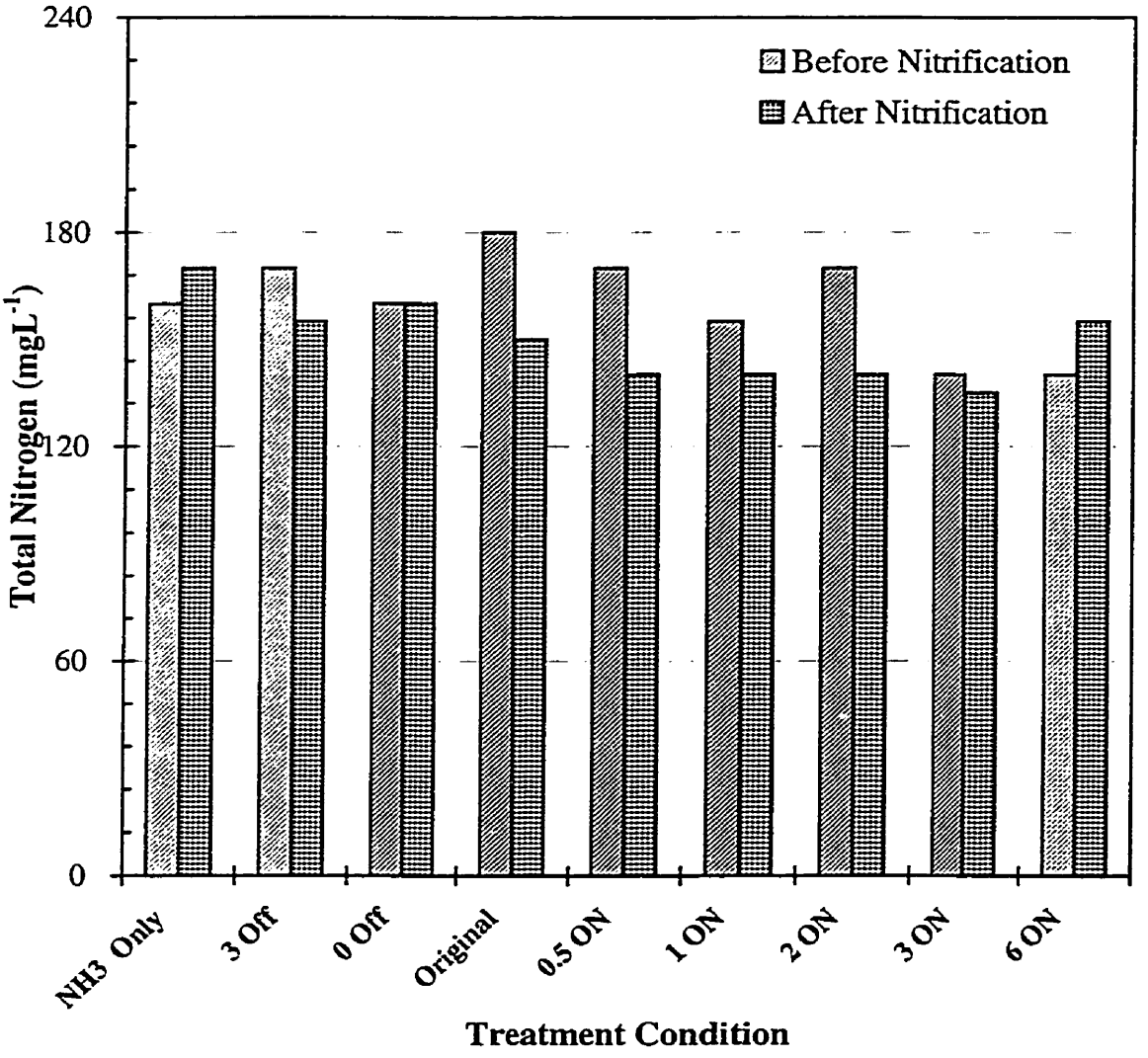

Figure 5-9: Effect of Photocatalytic Pretreatment on Subsequent Nitrification: Total Nitrogen Profiles
CP reactor with α=3.5°; Re=930; I=122 Wm^{-2}

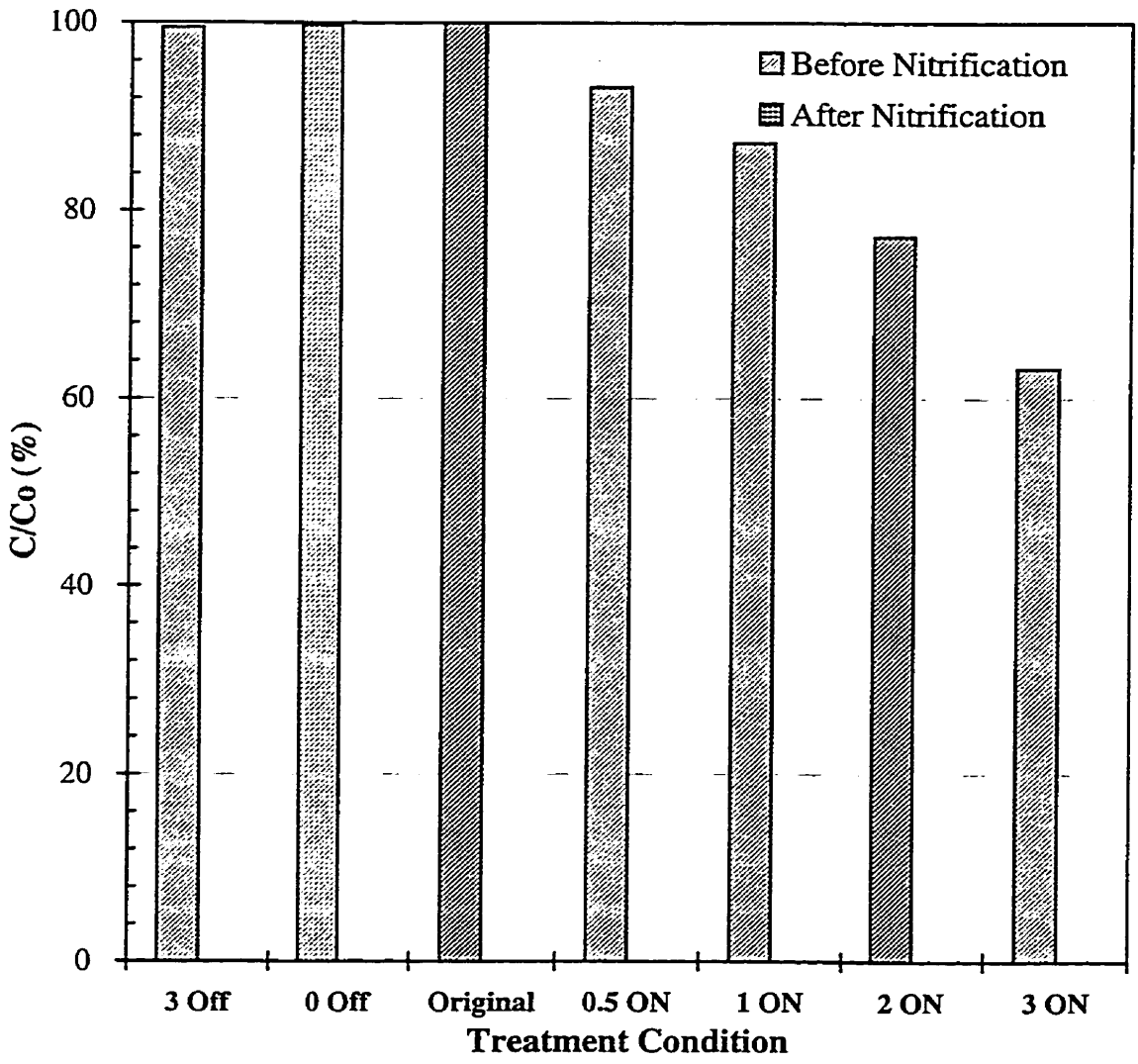

Figure 5-10: Effect of Photocatalytic Pretreatment on Subsequent Nitrification: Profiles of a Selected Compound
CP reactor with α=3.5°; Re=930; I=122 Wm^{-2}

pretreatment is performed for more than 2 hours. This indicated some inhibition of the *Nitrobacter* group by photocatalytic intermediates. This inhibition needs further investigation, since it is an undesirable feature in wastewater treatment. Total nitrogen was approximately constant during all treatments, indicating no denitrification or other nitrogen losses were occurring. As can be seen from Figure 5-10, the unidentified target compound disappears after the nitrification tests regardless of the pretreatment conditions. There might be many reasons for this result (i.e., the selected compound being highly biodegradable, volatile, etc.). As the compound was not identified, it is difficult at this point to make further comments on this issue. Dry mass of the microbes were also performed and the results indicated no significant growth during any of the tsts.

Complete nitrification was not achieved in these tests. This may be a consequence of the type of short-term test performed, where there was no additional carbon source and no significant growth of microbes. These tests can therefore be used for only comparative purposes, but do not necessarily indicate that full nitrification is not possible. Additional longer-term tests under typical operating conditions, with a continuous-flow or sequencing batch biotreatment, would be required.

For a full scale CP reactor with a capacity of 170 Lh^{-1}, assuming a lamp efficiency of 17%, an electricity price of \$0.1/kWh, and 80% of UV incident to the reactor cover, a lamp price of \$50/50W lamp, a lamp life time of 7500 (Al-Ekabi and Serpone, 1988) hours, the operating cost for treating 1000 litres of such groundwater in 6 hours could be estimated to be approximately \$11.16, of which 70% are due to the capital cost of the lamps. Costs for pumping the water, maintaining the system, as well as purchasing the system (except for the lamps) were not included in the estimate. Since lamp-related costs can all be eliminated in a solar-powered system, solar-UV should be considered if this does not result in too great an increase in the reactor cost.

5.3 Concluding Remarks

Photocatalysis had an impact on the chemical composition of the groundwater, as evidenced by the decrease in the TOC and the pH profiles of the samples, and the peaks on the HPLC chromatograms of selected (but unidentified) species. The trends of the data indicated build-up of short chain organic acids.

Photocatalytic pretreatment was successful in removing a significant fraction of the nitrification inhibitors. Up to 60% of the ammonia nitrogen was nitrified after photocatalysis, compared to only 10% in control samples that were not pretreated. Therefore, photocatalytic pretreatment appears to be a feasible alternative to carbon adsorption for reducing nitrification inhibition for the selected groundwater.

While complete nitrification was not demonstrated, the scope of the project did not allow for extensive optimization of either the photocatalytic pretreatment, or the biological nitrification tests used here. It is possible that with further study and optimization higher ammonia removal levels can be obtained.

For rough estimation purposes, the capital and operating costs to illuminate the photoreactor using lamps corresponds to approximately $0.011 per litre of groundwater, using a 6 hour residence time.

CHAPTER 6: RADIATION FIELD SIMULATION

Radiation fields in (pseudo)homogeneous photoreactors have been described using the Local Volumetric Rate of Energy Absorption (LVREA). In heterogeneous systems, however, a new term called here the Local Area-Specific Rate of Energy Absorption (LASREA) would be more appropriate to use as a result of its direct contribution to the kinetics of surface reactions. As can be seen from Section 2.3.3, previous reports on photocatalysis gave only the lamps used, the radiation intensity on certain surfaces, or the photon flux determined according to actinometry. Rigorous radiation models resulting in the LASREA on a catalyst film surface have not been developed. Based on the fundamentals of geometric optics and certain assumptions, the LASREAs on corrugated plates were calculated in this work. The results are presented in the following sections of this chapter.

6.1 Assumptions

The following assumptions were made in developing the radiation model:

(1). Photons fall incident on the cover of the LCP reactor in a diffuse way (i.e., the specific irradiance is proportional to the angle of incidence. See Figure 6-1b). This assumption should close to the real situation since diffuse emission models have been found to be suitable for modeling fluorescent lamps (Alfano, Romero, and Cassano, 1986a).

(2). In UV-A range, solar UV possess an irradiance with a direct parallel portion of 20 Wm^{-2} and a diffuse portion of 10 Wm^{-2}. The spectral irradiance increases linearly with wavelength (see Figure A-1), being zero at 300 nm and reaching a maximum at 390 nm. This assumption is well supported by the findings of several researchers (Goswami, 1997; Curcó et al., 1996; Turchi and Mehos, 1994).

(3). The effect of refractions when photons penetrate the air/plastic and plastic/water

interfaces was neglected.

(4). Once photons strike the reactor cover, they will be either absorbed by the solid material or transmitted through it. No photon will be reflected.

(5). The TiO_2 film is opaque to UV light. This is appropriate since the thickness of the film is as high as 10 microns (See Figure 3-2c). UV light can only penetrate TiO_2 films thinner than a few microns (Schiavello, 1985).

(6). Photons incident on the TiO_2 film will be subject to either absorption or coherent reflection in a diffuse way (i.e., reflected radiation energy is proportional to the angle of reflectance regardless of the angle of incidence. See Figure 6-1b). The spectral absorption coefficients of the TiO_2 film (Figure A-2 in Appendix A) agree with the relevant information found in previous research (Zhang, 1994). The reflection function is therefore "1- $a(\lambda)$", where $a(\lambda)$ is the absorption coefficient for photons with wavelength λ. This assumption should be close to the real situation because the roughness of the TiO_2 film is greater than the wavelengths of the photons. (i.e., microscopically rough, see Figures 3-2 and 3-3).

6.2 Model Development and Solution

Specific spectral intensities on the reactor cover and the plates were calculated based on the assumed radiation pattern (i.e., diffuse), the relative power distribution of the lamps as provided by the supplier (Figure A-1 in Appendix A), and the irradiance measured with the radiometer. The spectral absorption coefficients of the reactor cover (see Figure A-2 in Appendix A) were determined based on the material's spectral UV transmission information from the supplier, the diffuse radiation pattern, and energy balances within a unit hemisphere. The radiative energy profiles on the surfaces of the catalyst films were derived using the principles of geometric optics and analytical geometry through integration over the surfaces of

the radiator (i.e., the reactor cover), the reflector (none for flat plate; conjugate wings for corrugated plates), and the wavelengths of the photons. Detailed derivation of the radiation model is provided in Appendix A.

Based on the coordinate system in Figure 6-1, the spectral radiative energy incident on any point on the upper wing (x', y', z') of the corrugated plate, due to the radiation from the reactor cover, is presented in Equation (6-1).

$$I^{cv}_{\lambda-uw}(y',z') = \frac{w}{\pi\sqrt{2\pi\sigma}} e^{\frac{(\lambda-353)^2}{2\sigma^2}} \iint_{cv} \frac{\cos\psi_2 \cos\psi_1}{d_1^2} e^{\frac{k_3\delta}{\cos\psi_2}} e^{-k_4 d_1} dydz \qquad (6\text{-}1)$$

Equation (6-2) shows the relationship between the incident and the absorbed energy at wavelength λ.

$$q^{cv}_{\lambda-uw}(y',z') = a(\lambda) I^{cv}_{\lambda-uw}(y',z') \qquad (6\text{-}2)$$

Equation (6-3) is valid since the radiation field of the upper and lower wings of the corrugated plate are symmetric to *plane: z=0.*

$$I^{cv}_{\lambda-uw}(y',z') = I^{cv}_{\lambda-lw}(y',-z') \qquad (6\text{-}3)$$

Equation (6-4) gives the spectral radiative energy incident on the upper wing (point : x', y', z') due to the first reflection from the lower wing.

$$I^{(1)}_{\lambda-uw}(y',z') = \frac{(1-a(\lambda))}{\pi} \iint_{lw} \frac{I^{cv}_{\lambda-uw}(y,-z)\cos\psi_4 \cos\psi_5}{d_2^2} e^{-k_4 d_2} dydz \qquad (6\text{-}4)$$

Equation (6-5) gives the spectral radiative energy incident on point (x', y', z') of the flat plate (see Figure 6-1) due to the radiation from the reactor cover.

$$I^{cv}_{\lambda-fl}(y',z') = \frac{w}{\pi\sqrt{2\pi\sigma}} e^{\frac{(\lambda-353)^2}{2\sigma^2}} \iint_{cv} \frac{B^2}{4d^4} e^{\frac{2dk_3\delta}{B} - k_4 d} dydz \qquad (6\text{-}5)$$

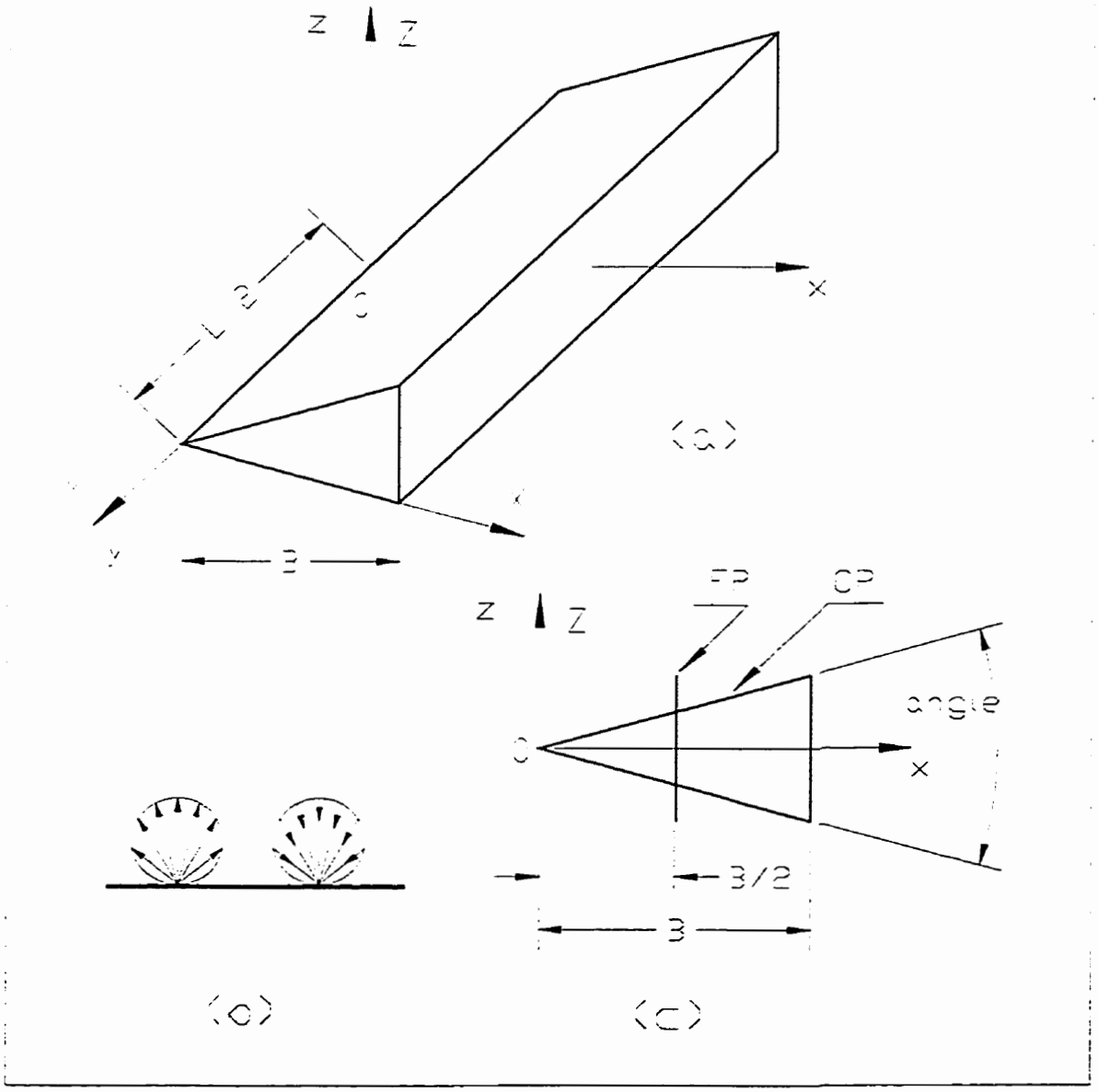

Figure 6-1: Coordinate System (a,c) for Corrugated and Flat Plates and Diffuse Incidence and Reflection Patterns (b) on a TiO_2 Film

In these equations,

$$d_1^2 = (z'\cot\alpha - B)^2 + (y'-y)^2 + (z'-z)^2$$

$$d_2^2 = \cot^2\alpha(z'+z)^2 + (y'-y)^2 + (z'+z)^2$$

$$\cos\psi_1 = (B - z\cot\alpha)/d_1$$

$$\cos\psi_2 = (B - z'\cot\alpha)/d_1$$

$$\cos\psi_4 \cos\psi_5 = 4zz'\cos^2\alpha / d_2^2, \text{ and,}$$

$$d^2 = B^2/4 + (y'-y)^2 + (z'-z)^2$$

The radiative energy profiles can be obtained from the above equations through integration over the photon wavelengths. The radiative energy profiles incident on the corrugated and flat plates were directly calculated from Equations (6-1) and (6-5). With the absorption of photons reflected from the conjugated wings (for corrugated plate) ignored, the LASREA profiles on the corrugated plates could be directly obtained from Equations (6-1) and (6-2). The LASREA of the flat plate was easy to calculate based on Equations (6-2) and (6-5) since no reflected photons can be trapped by flat plate. A special procedure was developed and used in order to consider the absorption of reflected photons in calculating the LASREA of the corrugated plates. As detailed in Appendix A, this procedure involves iteration on expressions based on Equations (6-1) through (6-4). The above equations were solved numerically using Simpson's method (Rice and Do, 1995). Fortran codes were written and run on a PC computer. Selected calculation results are presented and discussed in next section.

6.3 Results and Discussions

Figures 6-2 through 6-12 show the calculated typical radiation fields of corrugated as

well as flat plates. These figures are based on the coordinate system depicted in Figure 6-1. The radiation fields of lamp-illuminated corrugated plates are plotted in Figures 6-2 through 6-5 while those of solar-illuminated plates are given in Figures 6-6 through 6-9. The effects of the corrugated plate angle on photon absorption and on the average wavelength of the absorbed photons are depicted in Figures 6-10 and 6-11. The LASREA on the flat plate is given in Figure 6-12. The keys to these figures include:

"Incidence": the local rate of radiative energy incidences (calculated with Equation (6-1) for lamp-illuminated case),

"Absorption/no Recapture": the local rate of radiative incident energy absorption if no reflected photon could be captured (calculated with Equation (6-2) for lamp-illuminated case), and,

"LASREA": the local area-specific rate of energy absorption (calculated with the procedure described in Appendix A.5).

As can be seen from the three-dimensional plots in Figures 6-2 and 6-6, the radiation fields of the corrugated plates do not change with "Y" except near the two ends of the plates. It can also be seen that the LASREA due to solar radiation is much more uniform than that due to lamp radiation. This is because of the contribution of the direct parallel fraction of the solar UV. Since photocatalytic reactions behave lower order (usually between 0.5 and 1) dependency on radiation intensity, a uniform LASREA means higher energy efficiency if the system is not limited by mass transfer.

The results shown in Figures 6-3, 6-4, 6-7, and 6-8 indicate several things. For the same radiation intensity on the reactor cover, the average area-specific rate of photon absorption of the corrugated plates is dependent on the angles of these plates. The smaller the angle, the lower the average area-specific rate of photon absorption. By comparing the "Absorption /no Recapture" and the "LASREA" curves in these figures, we can easily see the significance of the absorption of the reflected photons. It not only enhanced photon absorption but also rendered

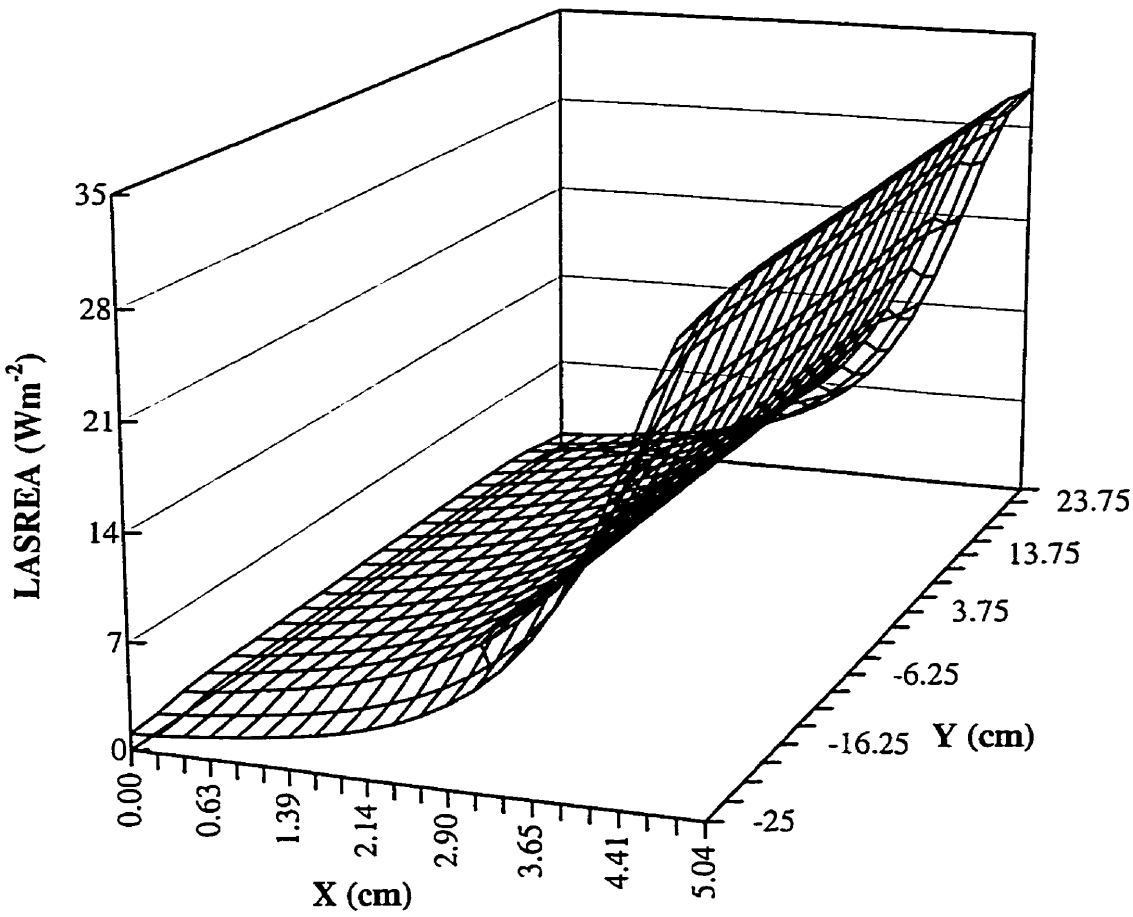

Figure 6-2: Local Area-Specific Rate of Energy Absorption on the Surface of a Corrugated Plate: Lamp-Illuminated
I= 122 Wm^{-2}; α=7°; Coordinate system: see Figure 6-1

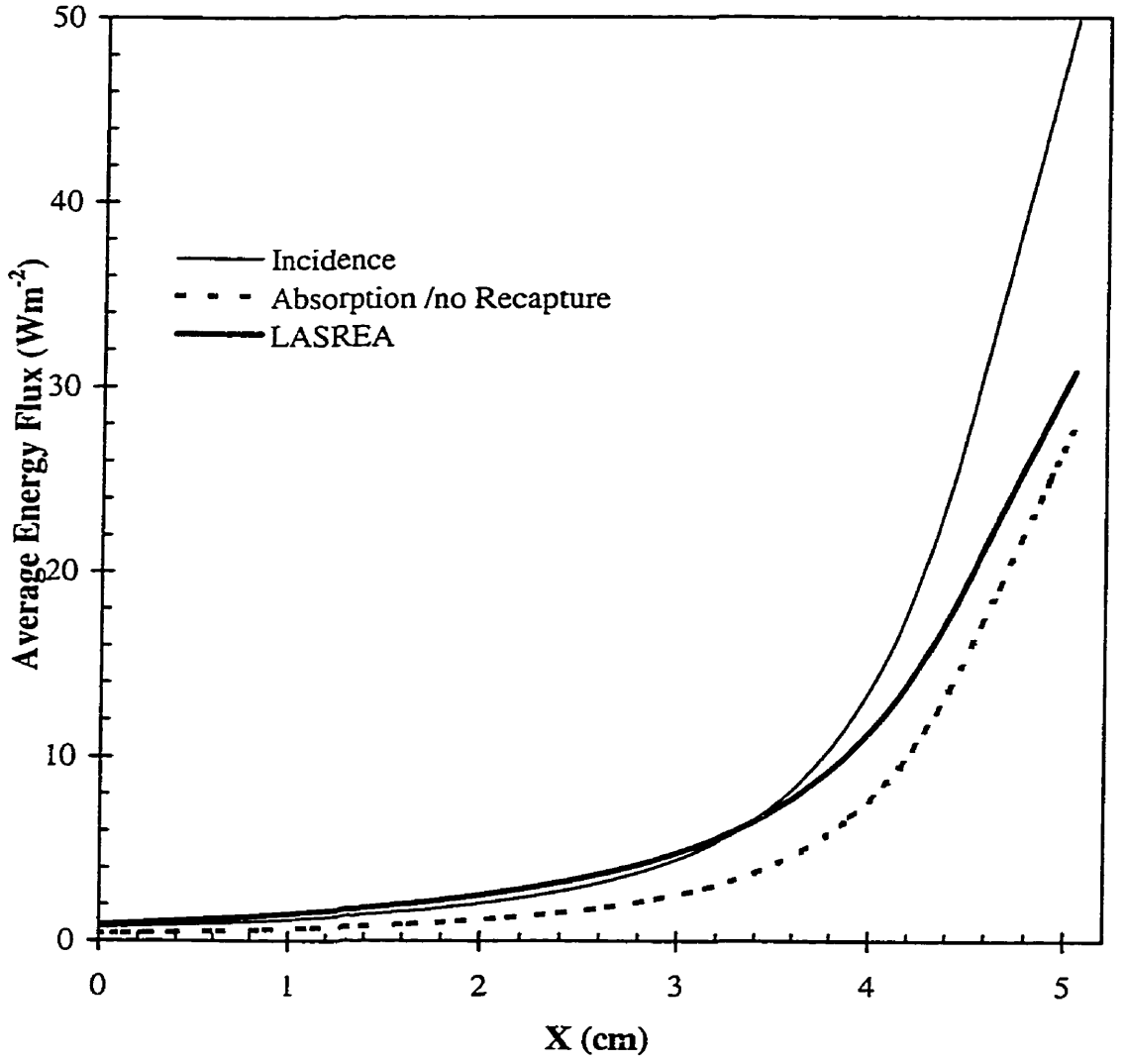

Figure 6-3: Radiation Field on the Surface of a Corrugated Plate: Lamp-Illuminated
I= 122 Wm^{-2}; α=5°; Coordinate system: see Figure 6-1

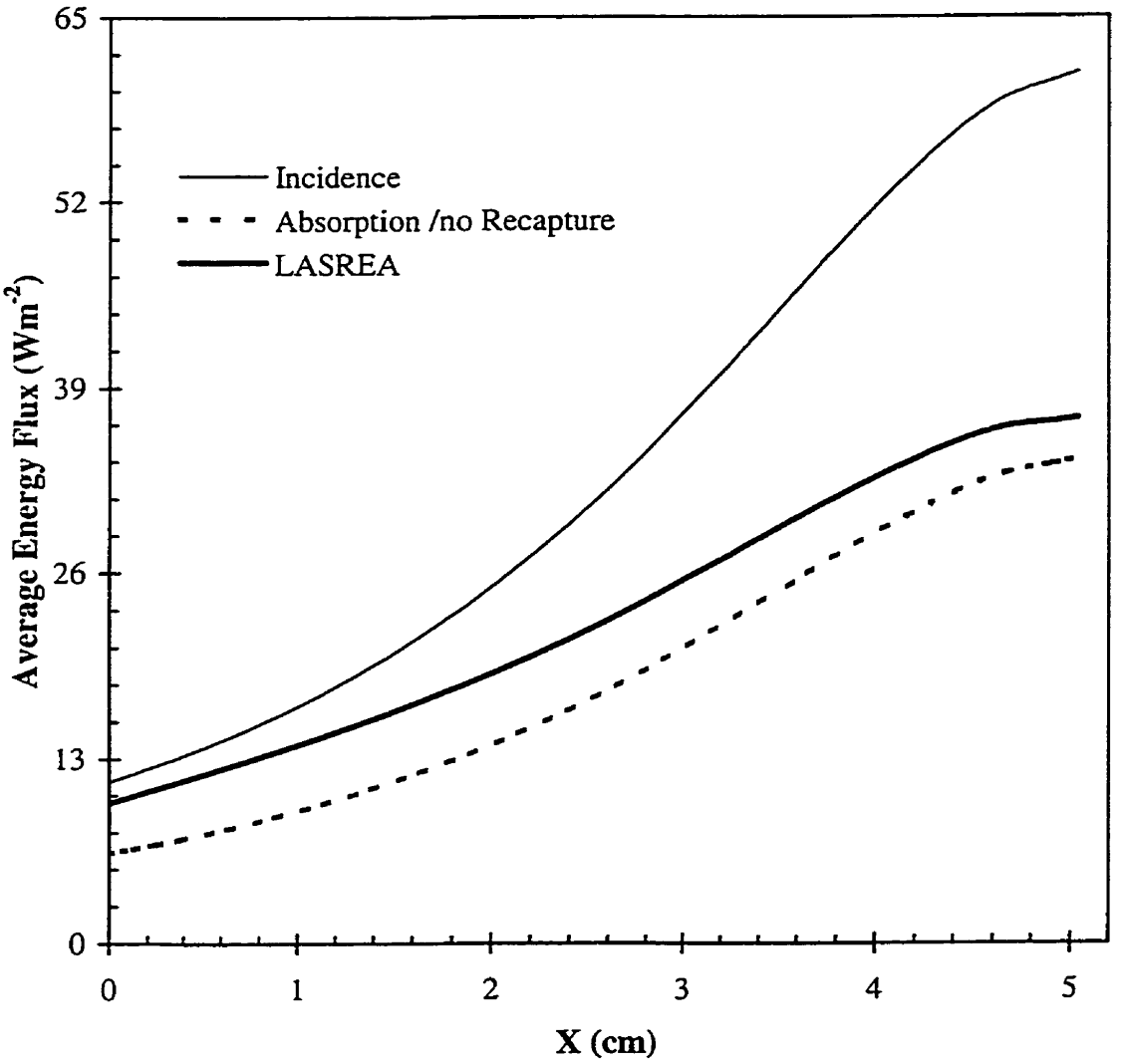

Figure 6-4: Radiation Field on the Surface of a Corrugated Plate: Lamp-Illuminated
I= 122 Wm^{-2}; α=20°; Coordinate system: see Figure 6-1

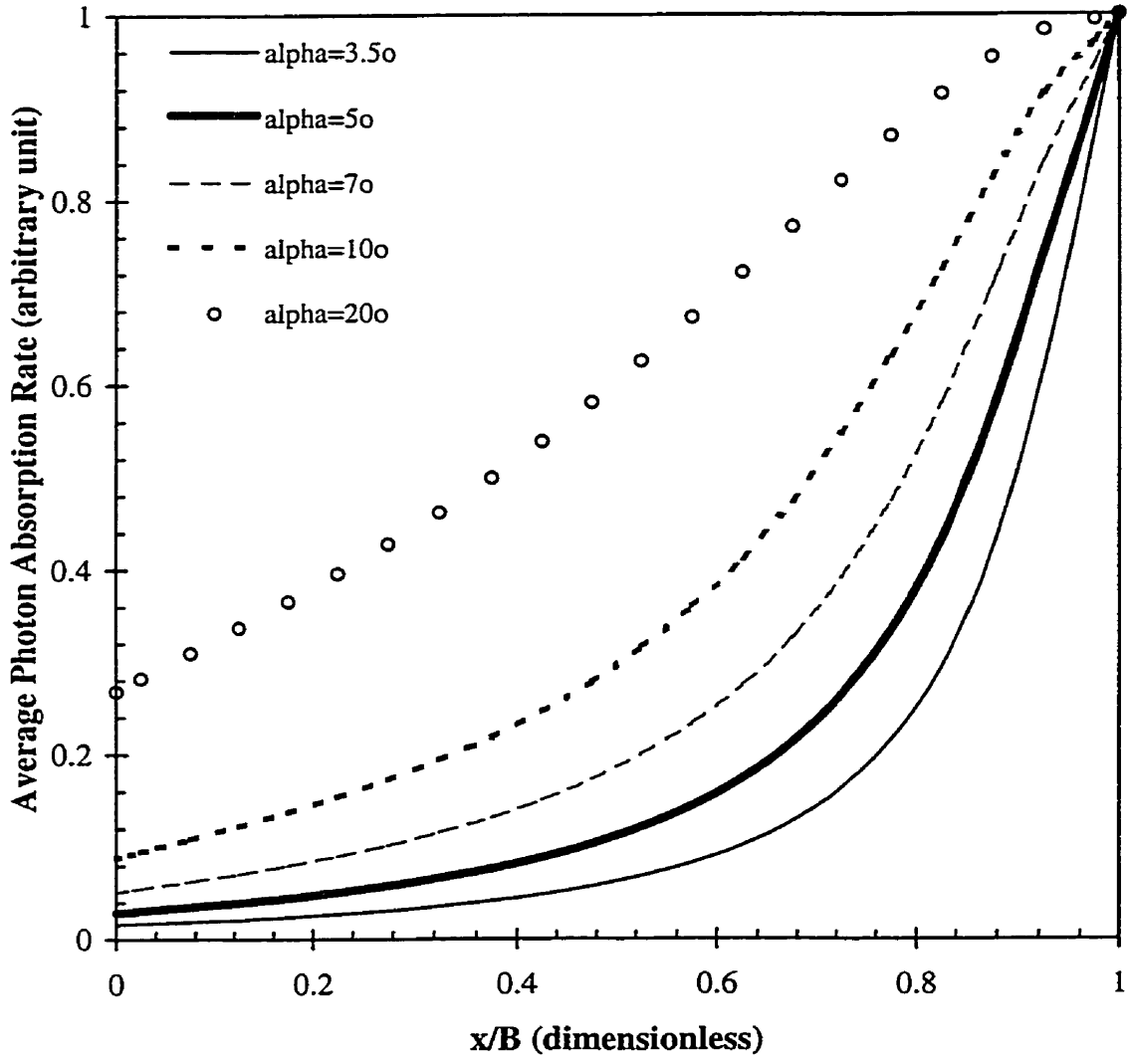

Figure 6-5: Comparison of the LASREA on the Surfaces of the Corrugated Plates with Different Angles: Lamp-Illuminated

I= 122 Wm^{-2}; Coordinate system: see Figure 6-1

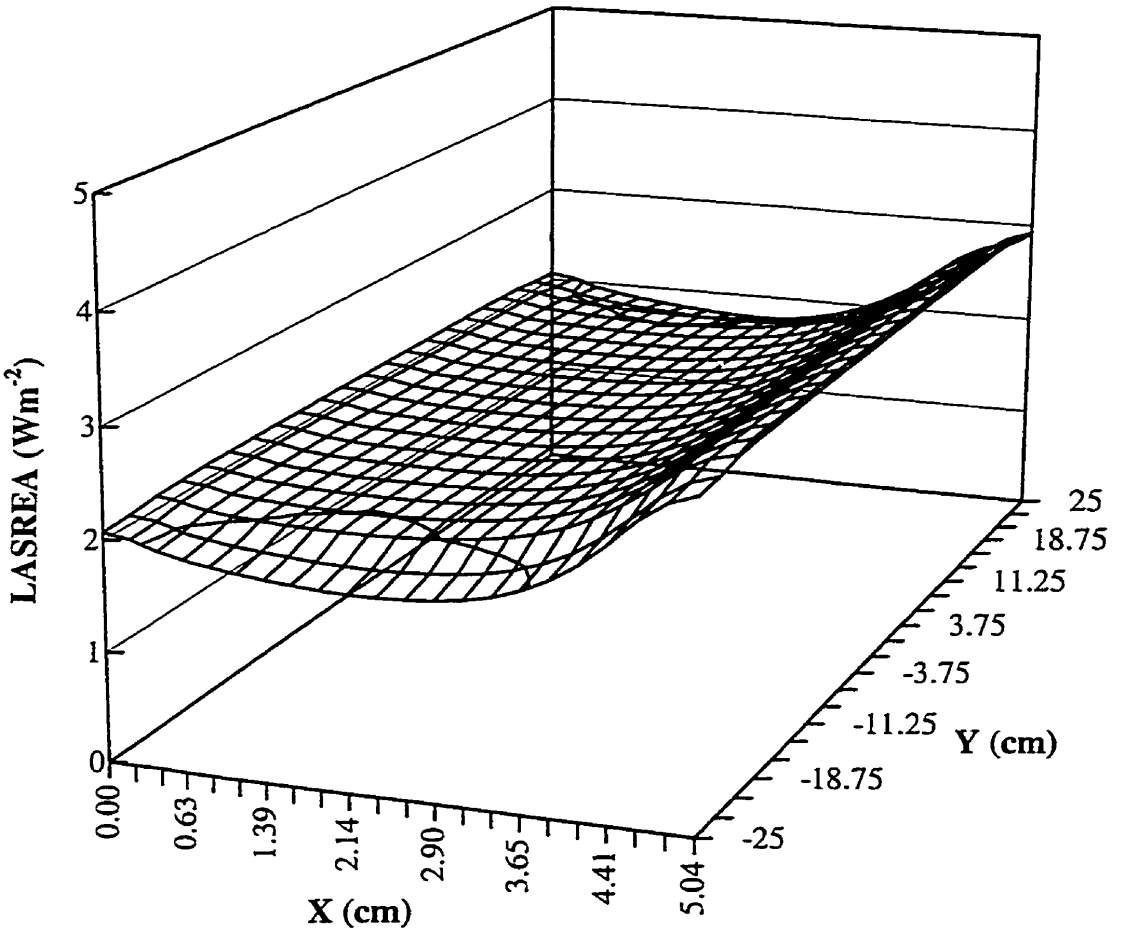

Figure 6-6: Local Area-Specific Rate of Energy Absorption on the Surface of a Corrugated Plate: Solar-Illuminated
I= 30 Wm^{-2}; α=7°; Coordinate system: see Figure 6-1

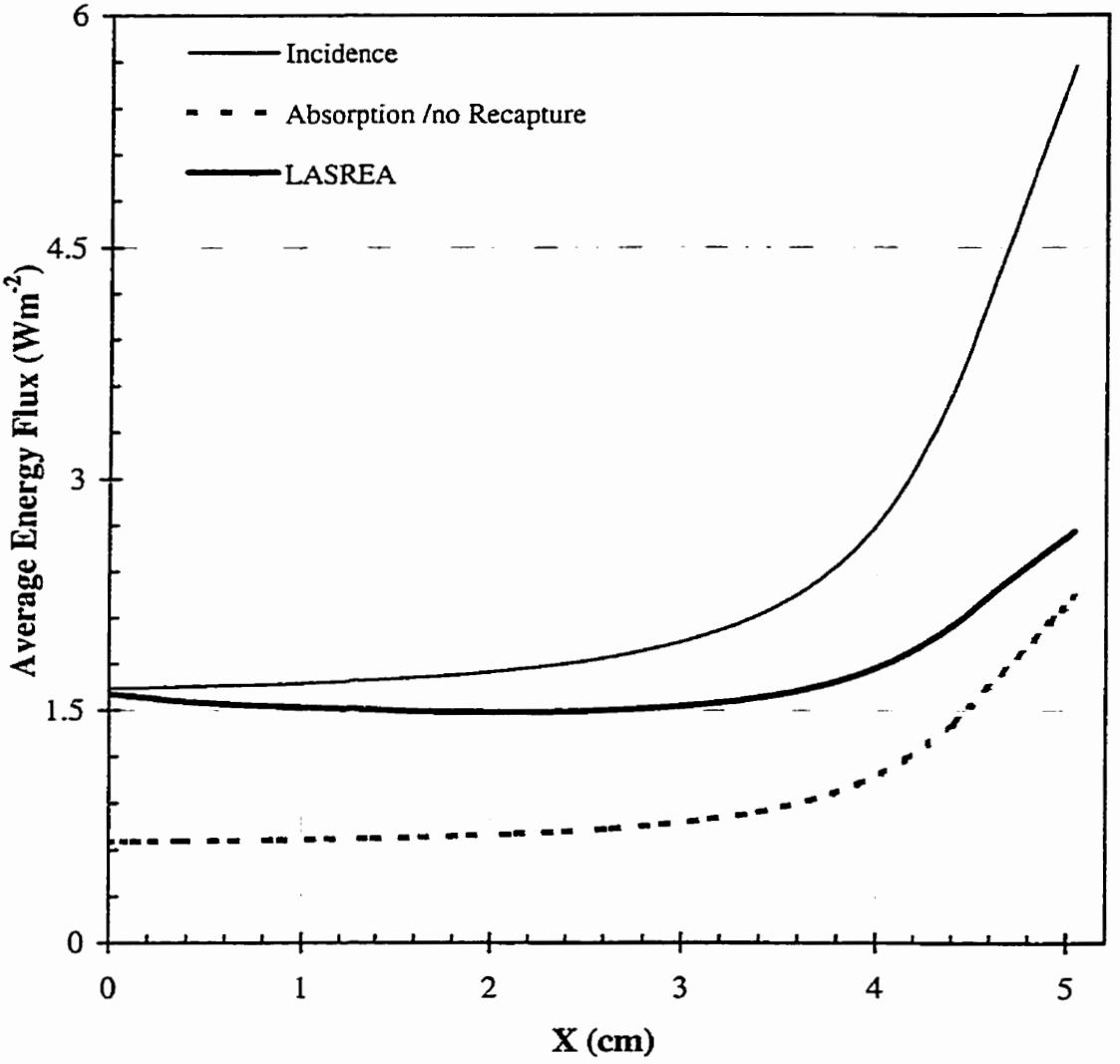

Figure 6-7: Radiation Field on the Surface of a Corrugated Plate: Solar-Illuminated
I= 30 Wm^{-2}; α=5°; Coordinate system: see Figure 6-1

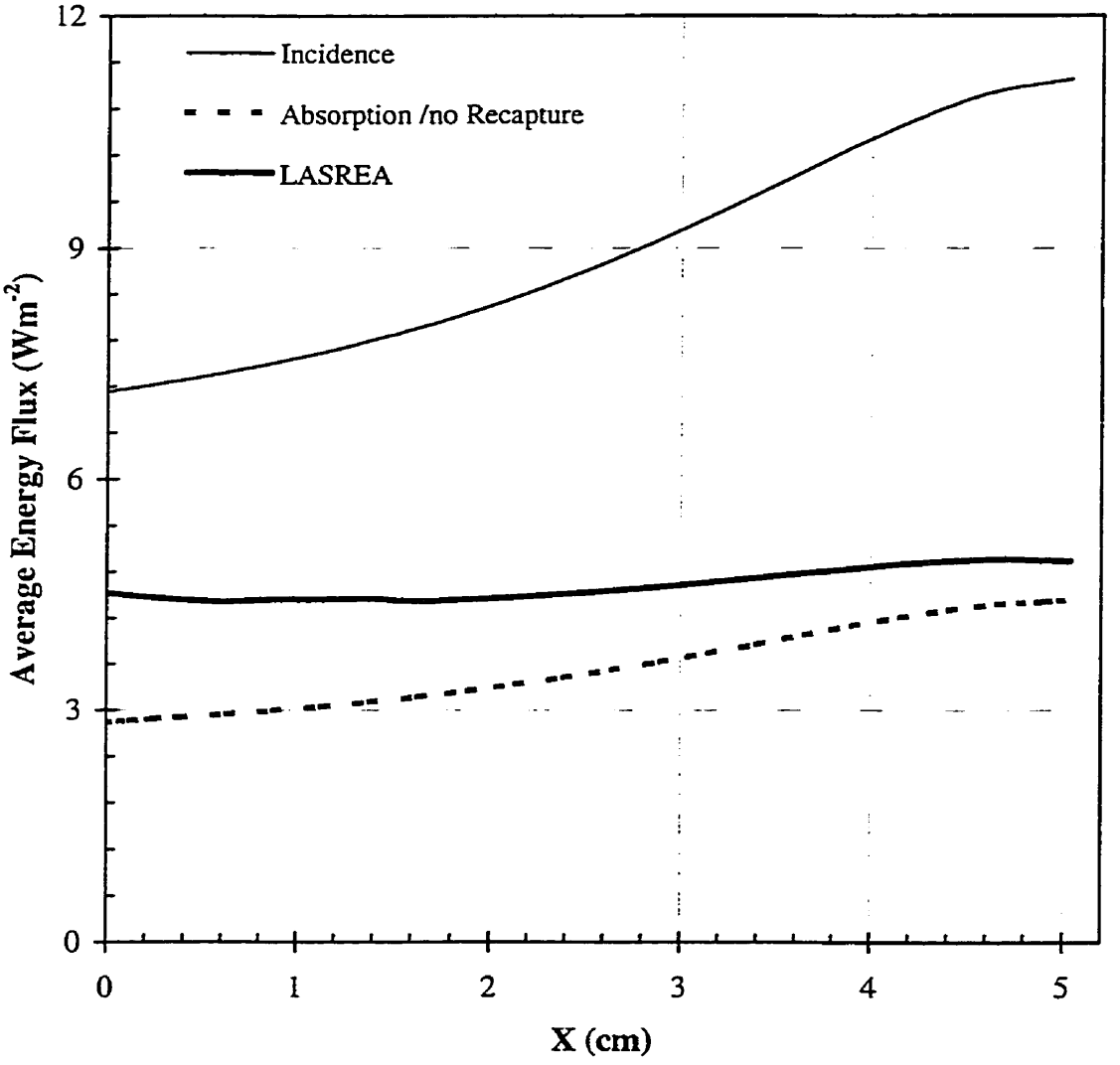

Figure 6-8: Radiation Field on the Surface of a Corrugated Plate: Solar-Illuminated
I= 30 Wm^{-2}; α=20°; Coordinate system: see Figure 6-1

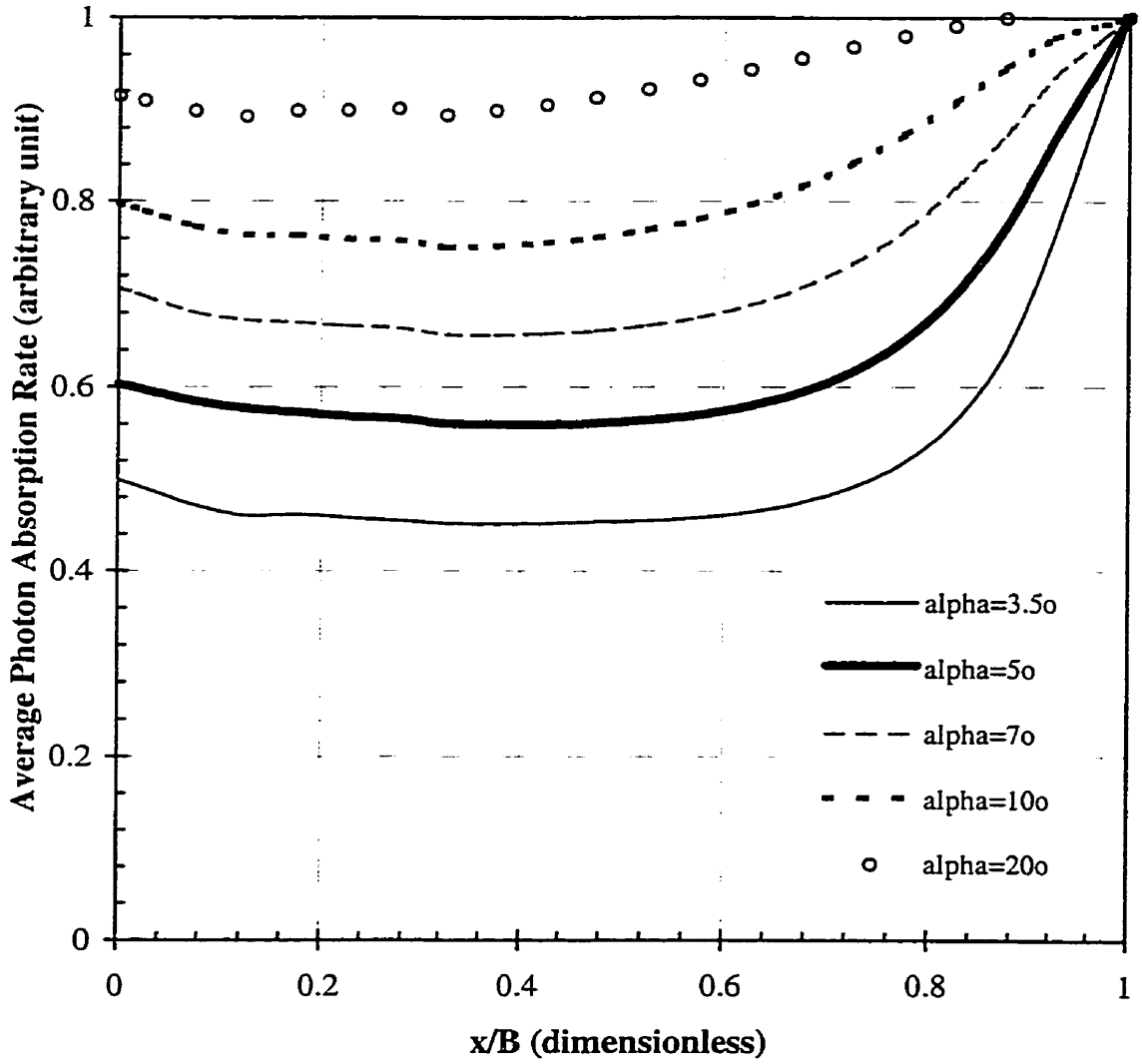

Figure 6-9: Comparison of the LASREA on the Surfaces of the TiO_2-Coated Corrugated Plates with Different Angles: Solar - Illuminated

I= 30 Wm^{-2}; Coordinate system: see Figure 6-1

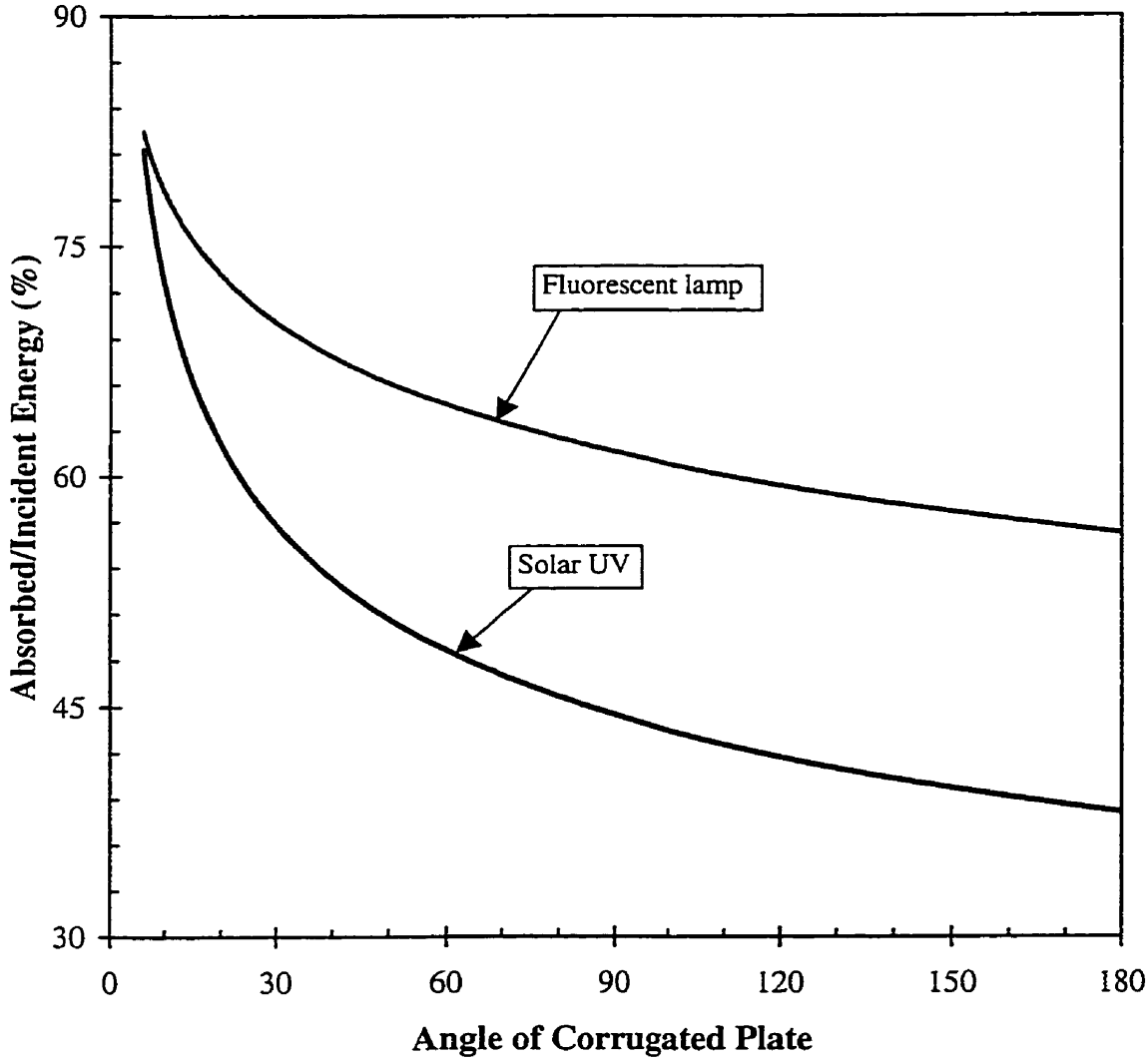

Figure 6-10: Effect of Photon Recapture on the Radiation Absorption Efficiency of the TiO_2-Coated Corrugated Plates
Angle=2α

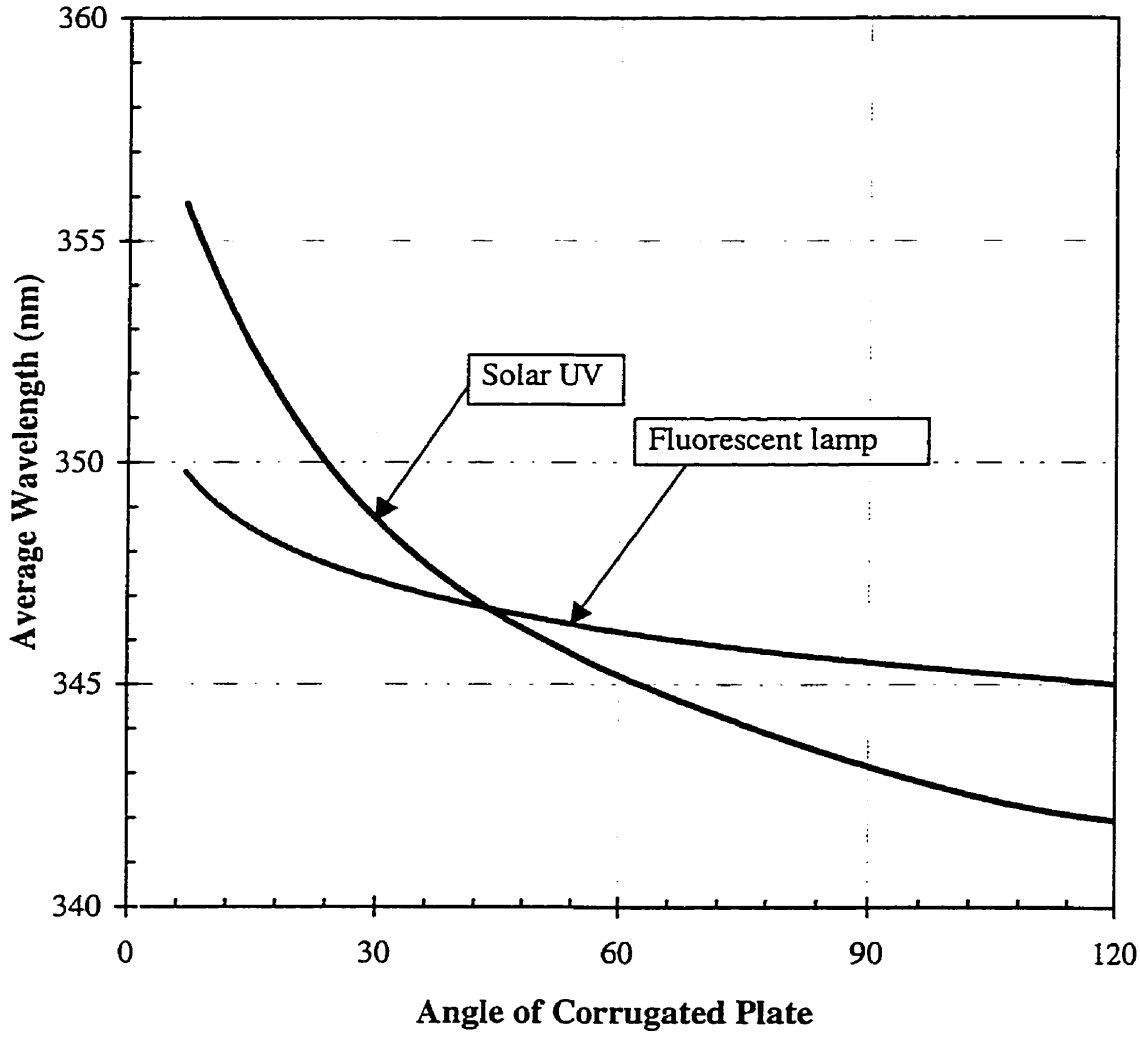

Figure 6-11: Effect of Recapture on the Average Wavelength of the Photons Absorbed by the TiO_2-Coated Corrugated Plates
Angle=2α

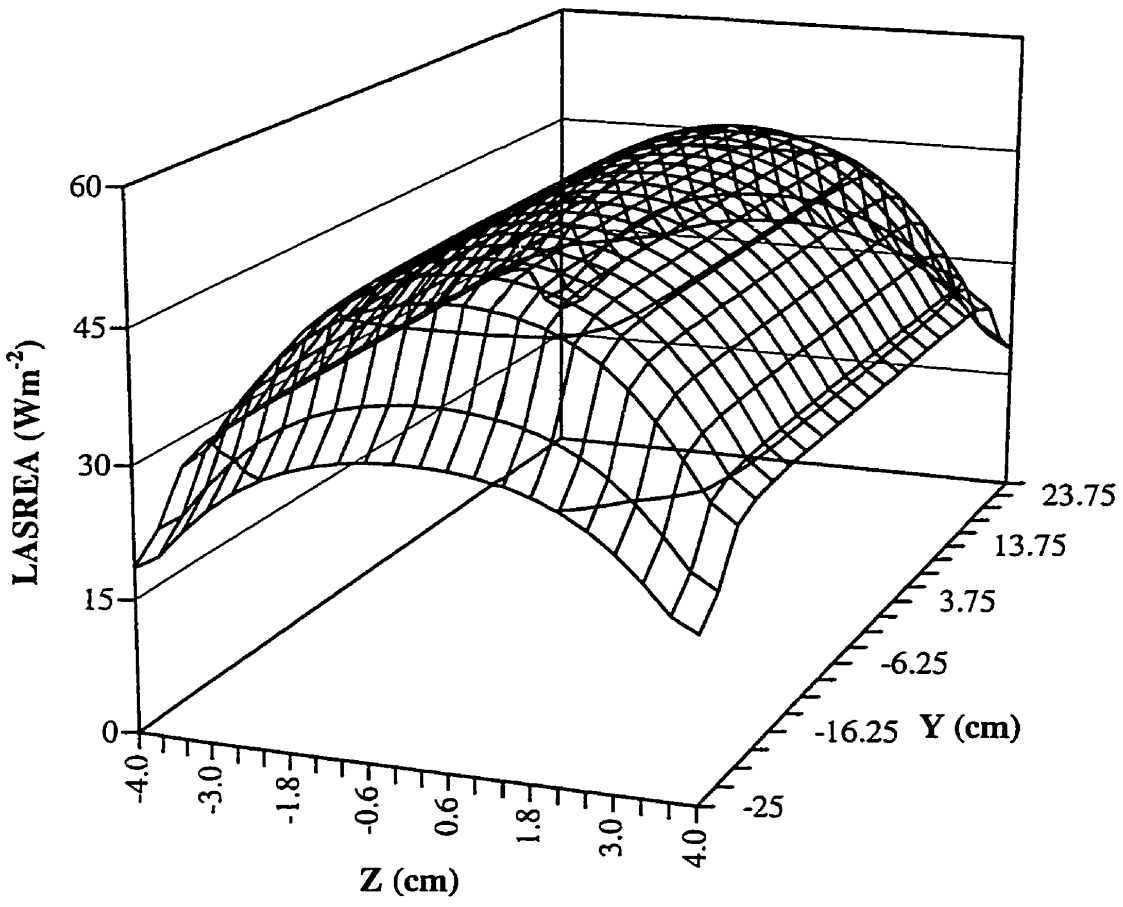

Figure 6-12: Local Area-specific Rate of Energy Absorption on the TiO_2-Coated Flat Plate: Lamp-Illuminated
I=122 Wm^{-2}; Coordinate system: see Figure 6-1

the LASREA more uniform. This enhancement is a strong function of the angle of the corrugated plates (Figures 6-3 vs. 6-4, 6-7 vs. 6-8). A small angle could result in a high photon absorption efficiency (i.e., absorbed/incident energy) but also a less uniform LASREA (Figures 6-5 and 6-9).

Figures 6-10 and 6-11 demonstrate the dependency of the photon absorption efficiency (i.e., absorbed/incident energy) and the average wavelength of absorbed photons, on the angle of the corrugated plates. As can be seen from Figure 6-10 that most of the radiative energy incident on the flat catalyst film (α=90°) will be reflected out of the reactor and dissipated as waste. This dissipation is more severe when the reactor is illuminated with sunlight. The corrugated plate can result in over 100% enhancement of the absorption efficiency of the solar UV. This enhancement is not as great in lamp-illuminated systems due to the shortage of direct parallel rays and long wavelength photons from the fluorescent lamps. Based on these two plots, the radiation field is more sensitive to angle of the corrugated plate when it is smaller than 30°.

Actinometry has been a popular method in determining the quantum yield in photoreactors. While these methods may work well for homogeneous systems, they may result in vague or even misleading results for heterogeneous systems. For example, if actinometry were used for the corrugated plate reactor, the result would show that the same amount of radiative energy is absorbed by the system regardless of the angle of the corrugated plates used. Neither the effect of multiple reflection nor the effect of the radiation field distribution can be determined. During actinometry what is measured is actually the fraction of the radiative energy that enters the reactor, not the fraction that is absorbed by the catalyst. For the system examined in this study, these methods would result in substantial (up to 150%) underestimation of the energy efficiency, depending on the radiation source and angle of the corrugated plates. Therefore, actinometry may create misleading results and tend to hide the real bottleneck in heterogeneous photoreactor systems.

6.4 Concluding Remarks

The radiation fields on corrugated and flat plates were modeled based on first principles. A special procedure was developed to calculate the effect of multiple reflection on radiative energy absorption. This allowed for the calculation of the LASREA on the corrugated plates.

Correct calculation of the LASREA is a critical step in the analysis of heterogeneous photoreactors since homogeneous actinometry can result in incorrect results.

Corrugation was proven to cause the capture of longer wavelength UV radiation that would otherwise be reflected out of some classical photoreactors (i.e., flat plate). This results in higher radiative energy absorption efficiency as well as more uniform LASREA on corrugated plate.

The angle of the corrugated plate has a profound effect on the LASREA. The smaller the angle, the higher the radiative energy absorption efficiency, but the less uniform the radiation distribution. The smaller the angle, the lower the average area-specific rates of photon absorption. The radiation field is most sensitive to the angles smaller than 30° (i.e., $\alpha<15°$).

Compared to the flat plate, the corrugated plate was shown to enhance the catalyst energy absorption efficiency for more than 100% for solar UV and 50% for rays from UV-A fluorescent lamps.

The difference of this enhancement is due to the different spectral distribution of these two types of radiation sources. Under otherwise the same conditions, the LASREAs on solar-powered corrugated plates are more uniform than those powered by UV-A lamps due to the contribution of the direct parallel fraction of the solar UV.

CHAPTER 7: MASS TRANSFER TO CORRUGATED AND FLAT PLATE SURFACES

Just as in any other heterogeneous process, mass transfer is an inherent step in photocatalysis. Mass transfer limitations in immobilized systems have been experienced and discussed in several previous studies (Assink and Koster, 1995; Turchi and Ollis, 1988). Therefore, it is imperative to examine the role of mass transfer in developing, designing, and modeling immobilized photocatalytic reactors. There exist several correlations which are capable of predicting the mass transfer coefficients in tubular, rectangular, and other types of flow channels (McCabe, Smith, and Harriott, 1993; McIsaac, 1995). But such correlations tend to be unreliable when the velocity profile is not yet established or when the flow channel possesses a cross section with too great an aspect ratio (i.e., the ratio of the largest and smallest dimension). Experiments were therefore performed in order to examine the mass transfer between the main stream and the wall of the corrugated plates. Due to the technical difficulty encountered, only average mass transfer rates were measured. Local mass transfer coefficients were estimated using a semiempirical model.

7.1 Materials and Methods

The benzoic acid dissolution method was adopted for the mass transfer experiments. This method is convenient to use and can usually offer data of good quality due to the suitable physical properties of benzoic acid (Harriott and Hamilton, 1965). For example, the magnitude of the solubility of benzoic acid in water is such that it is usually possible to keep the acid concentration at the center of the flow channel far from saturation and to saturate the fluid adjacent to the solid surface. Its diffusivity in water is also desirable for being insensitive to concentration within the low concentration range that is frequently of interest (Noulty and

Lealst, 1987). In addition, benzoic acid layers with the desired shape and roughness are easy to prepare due to the low melting point (122 °C) and the good mechanical properties of the solid benzoic acid layers.

Prior to the experiments, selected surfaces of the corrugated and flat plates were coated with a thin acid layer solidified from the molten benzoic acid poured onto these surfaces. During the experiments, tap water was pumped through the photoreactor at the desired flowrates. Water samples were taken from downstream of the reactor and analyzed for benzoic acid concentration. In order to minimize the experimental error, sampling time was kept at approximately 30 seconds and the sample was mixed completely before analysis was performed. After steady states were reached (acid concentration stops changing with time), the acid concentrations were recorded for use in calculating the average mass transfer coefficients of the acid-coated area under the corresponding flowrates or Reynolds numbers.

Reagent grade benzoic acid from BDH Inc., Toronto and tap water was used. The benzoic acid concentration was determined by measuring the UV absorbance of the sample at 226 nm and comparing it with a calibration curve. The calibration curve of the spectrophotometer was found to be: $C^{out} = 10.93\,ABS_{226nm}$. During all mass transfer measurement runs, the water temperature was kept constant at 26.6 °C. The main stream benzoic acid concentration at the exit from the reactor was assumed to be, C^{out}, the measured average concentration during data analyses. For each flow condition (Reynolds number), the mass transfer rates and coefficients were obtained based on the following relationship (McISAAC, 1995):

$$R_m = C^{out} Q = \bar{k}_L A \frac{(C^* - C^{in}) - (C^* - C^{out})}{\ln \frac{(C^* - C^{in})}{(C^* - C^{out})}} \qquad (7\text{-}1)$$

The solubility of benzoic acid in water was obtained through interpolation using the data

reported by Stevens and Mourad (1995). At 26.6 °C, its value was found to be 29.52 mmol L^{-1}. The diffusivities of benzoic acid and 4-CP were estimated to be 10^{-9} m^2s^{-1} and 8.9 $x10^{-10}$ m^2s^{-1} respectively, based on an established method (Lyman, Reehl, and Rosenblatt,1982; Hayduk and Laudie, 1974). The viscosity of the reaction medium and the diffusivity of dissolved oxygen were both obtained from Perry's Handbook (Perry, Green, and Maloney, 1984). At 26.6 °C, their values were found to be 0.876 x 10^{-3} N-s-m^{-2} and 2.61 $x10^{-9}$ m^2s^{-1} respectively.

7.2 Local Mass Transfer Rate Model

In order to estimate the mass transfer coefficients at different locations on corrugated plate surfaces, the following assumptions were made:

(1). Mass transfer rate does not change along direction of water flows (Y direction in Figure 6-1). This assumption is strictly speaking not true due to the entrance effect. However, since the change in X direct is substantially greater, it does give a good approximation of the real situation.

(2) Local mass transfer rate at any point on corrugated plates is inversely proportional to the distance from that point to the geometric center of the cross section of the corrugated plate (Figure B-1). This assumption should be close to reality when the flow is laminar and the boundary layer extends right to the center of the flow channel. Under turbulent flow conditions, the result may show noticeable deviation from the real situation.

Based on these assumptions, a single relationship, showing the local mass transfer coefficients on corrugated plates as a function of their structural parameters, was determined. This is expressed in Equation (7-2) below. The derivation procedure is given in Appendix B in detail.

$$k_L = \bar{k}_L B \Big/ \left\{ \sqrt{(x - \frac{B\cos^2\alpha}{1+\sin\alpha})^2 + (\frac{B\sin\alpha\cos\alpha}{1+\sin\alpha})^2} \bullet \ln\left| \frac{\sin\alpha(1+\sin\alpha)}{\cos\alpha(1-\cos\alpha)} (1 + \sqrt{\frac{2}{1+\sin\alpha}}) \right| \right\} \qquad (7\text{-}2)$$

Because of the entrance effect in this system, the mass transfer rate on the surface of the flat plate was expected to change along the direction the fluid flows. A linear relationship was adopted and its constants were determined using the experimental data. Under the coordinate system in Figure 6-1, the result can be written as:

$$k_{fl} = \bar{k}_{fl}[1.23 - 0.46\frac{Y}{L}] \qquad (7\text{-}3)$$

7.3 Results and Discussions

The results of the mass transfer work are summarized in Figures 7-1 through 7-6. Reynolds numbers in these figures were calculated based on the hydraulic radius (McCabe, Smith, and Harriott, 1993). Figures 7-1 through 7-3 show the Sherwood numbers calculated from the experimental data for flat as well as corrugated plates at different flow conditions. Results from two representative correlations were also plotted for comparative purposes. Although these two correlations represent the situations under well-developed flow conditions, they can still serve as the benchmarks for discussions. As indicated in Figure 7-1, the experimental data are reasonably reproducible and the general trend agrees with the correlations within the laminar flow region. Data with the flat plate (Figure 7-2) demonstrate substantial deviation from both correlations. This is probably due to the entrance effect in this system. Under completely laminar flow conditions (i.e., Re<500), the entrance effect does not exist and the data show little deviation from the correlations. As the flowrate increases (i.e., 500<Re<2100), a boundary layer starts to build up and the region affected extends toward down stream of the plate. Under turbulent flow conditions (i.e., Re>2100), mass transfer was

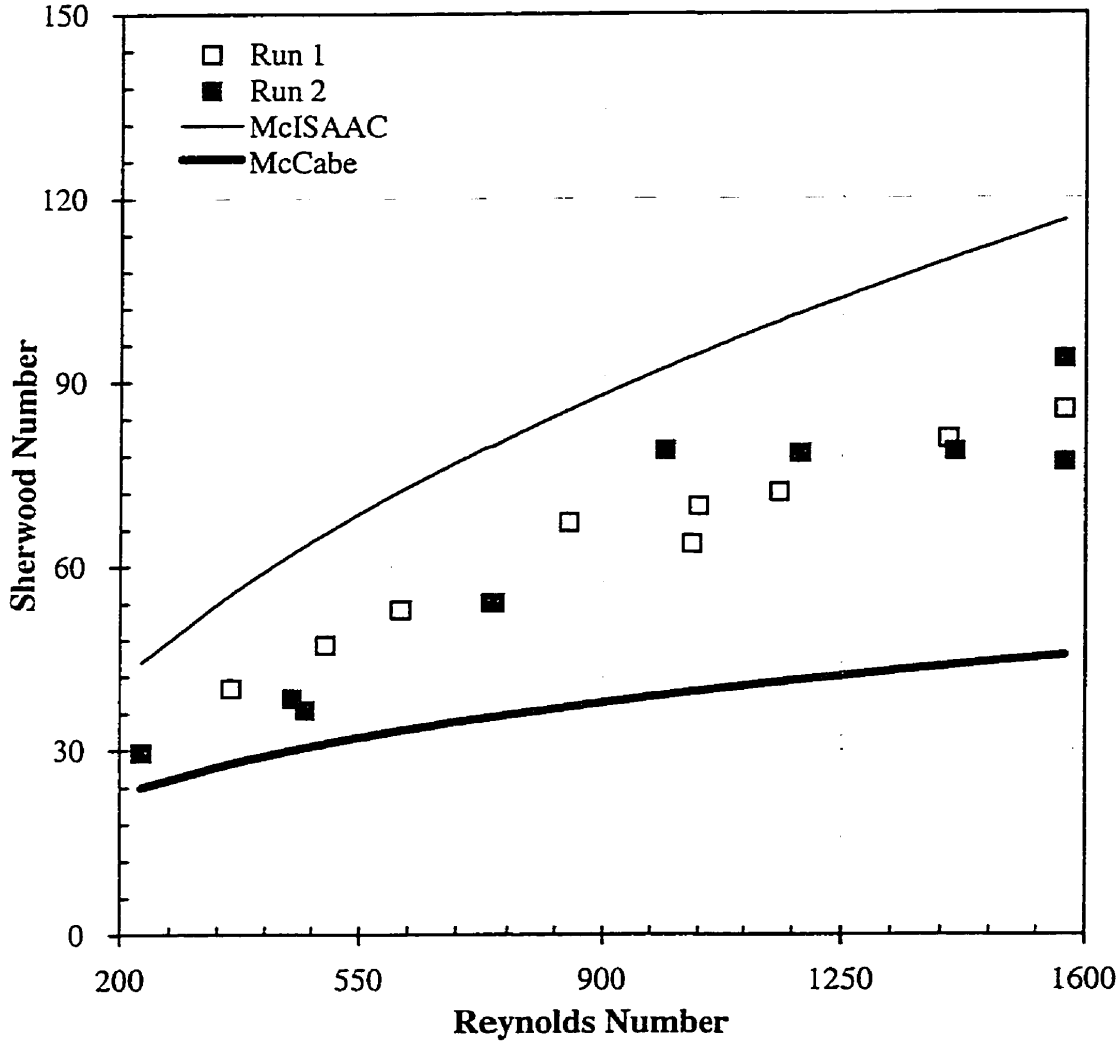

Figure 7-1: Mass Transfer from a Corrugated Plate, Compared to Correlations from McISAAC (1995) and McCabe, Smith, and Harriott (1993), Showing Reproducibility
Corrugated plate with α=5°

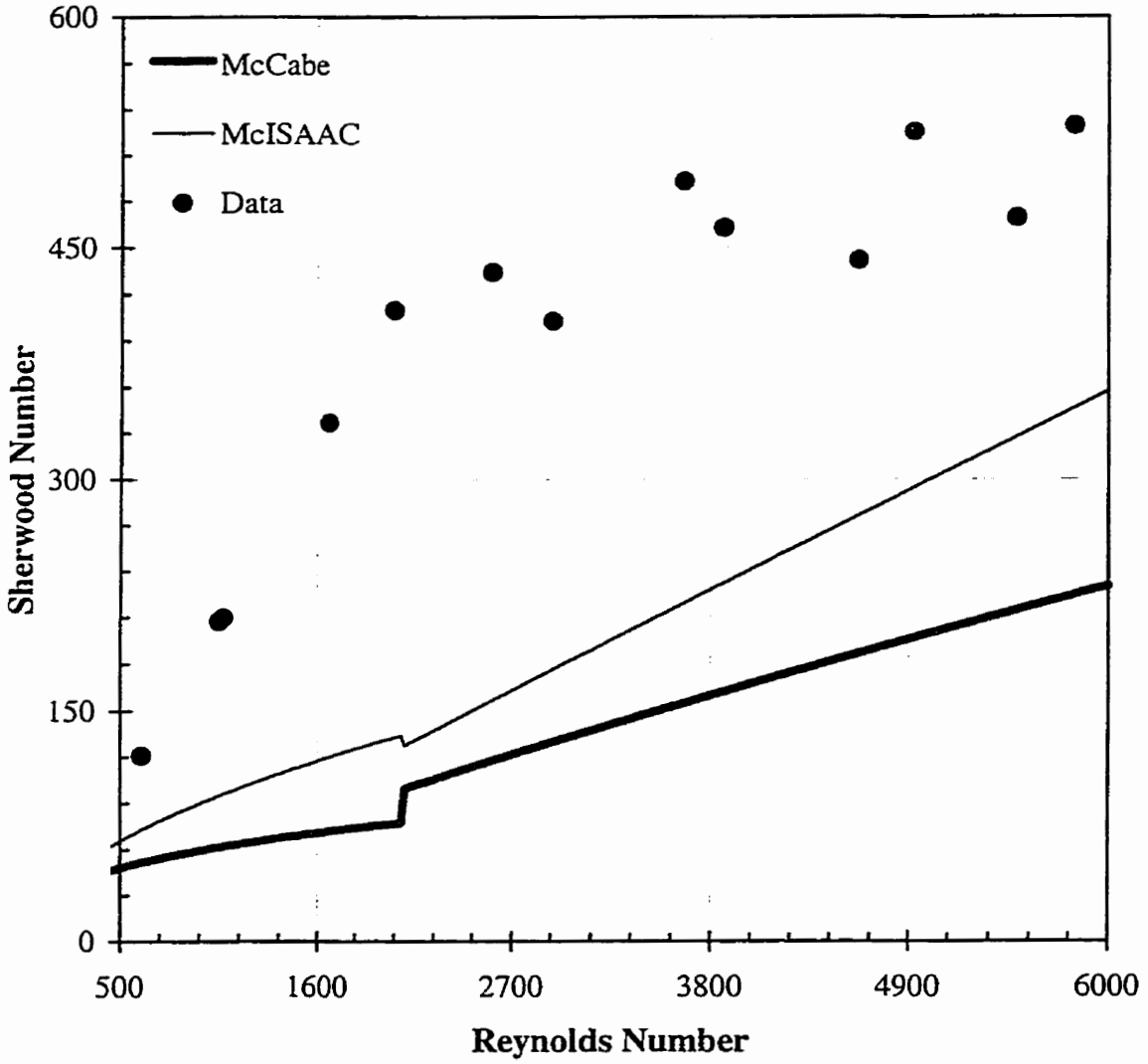

Figure 7-2: Mass Transfer from the Flat Plate, Compared to Correlations from McISAAC (1995) and McCabe, Smith, and Harriott (1993)

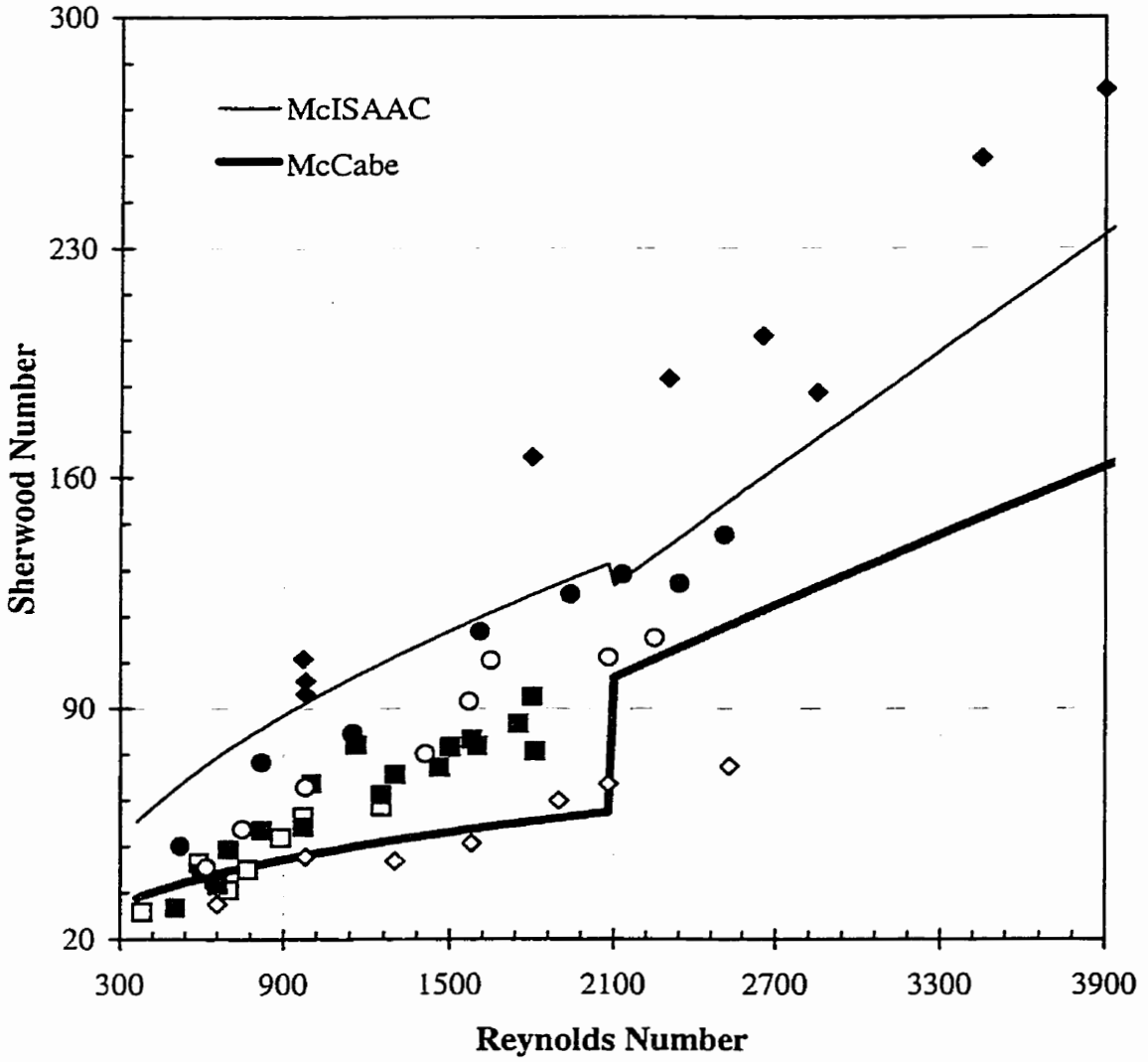

Figure 7-3: Mass Transfer from Corrugated Plates with Different Angles, Compared to Correlations from McISAAC (1995) and McCabe, Smith, and Harriott (1993)

□ α=3.5°; ■ α=5°; ○ α=7°; ● α=10°; ◆ α=20°;
◇ only the bottom half of the α=10° plate (0<x<B/2 under the coordinate system in Figure 6-1) was coated with benzoic acid

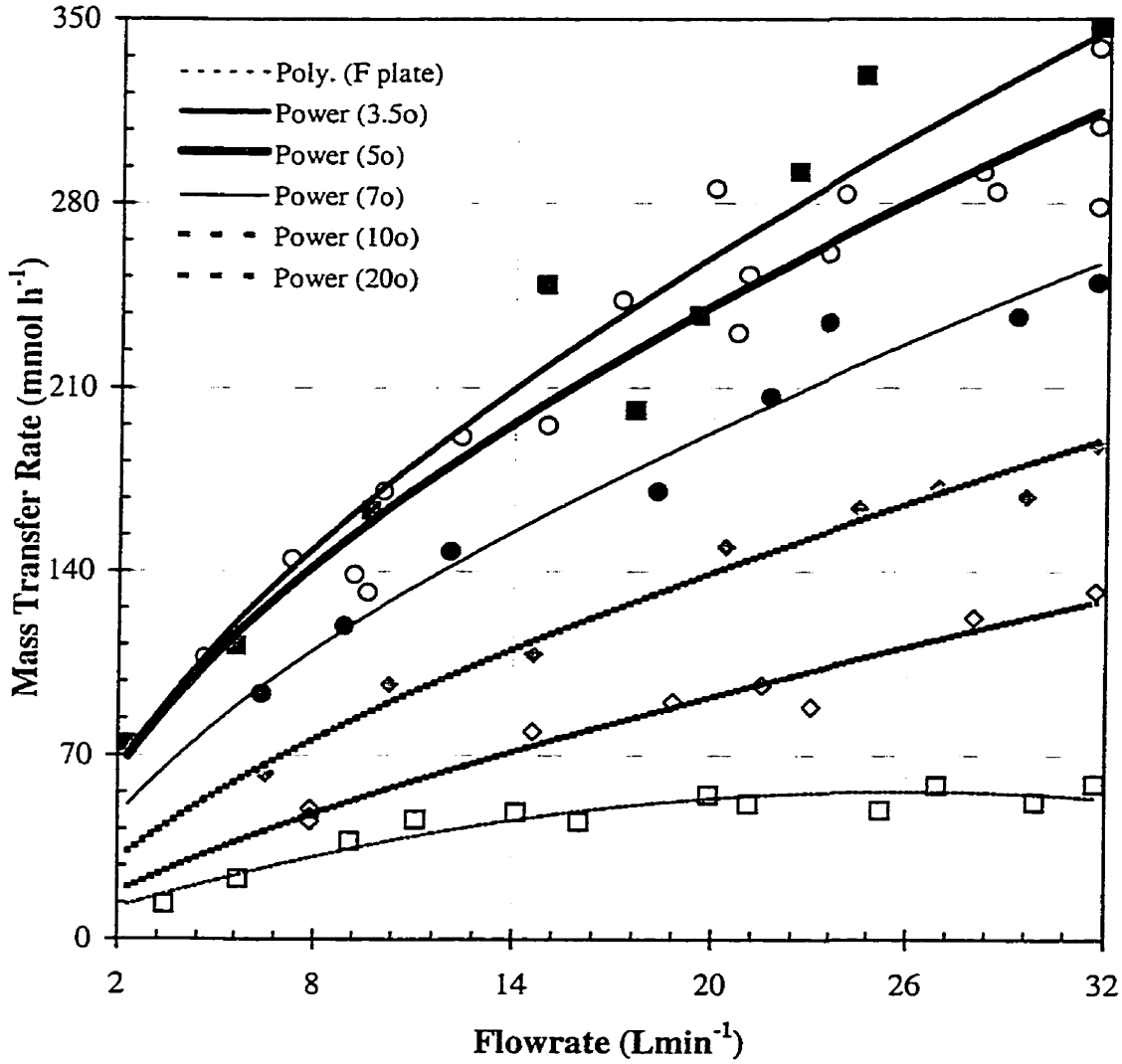

Figure 7-4: Overall Benzoic Acid Transfer Rates
□ Flat plate; ■ α=3.5°; ○ α=5°; ● α=7°; ◆ α=10°
◇ α=20°; Lines: fitted curves

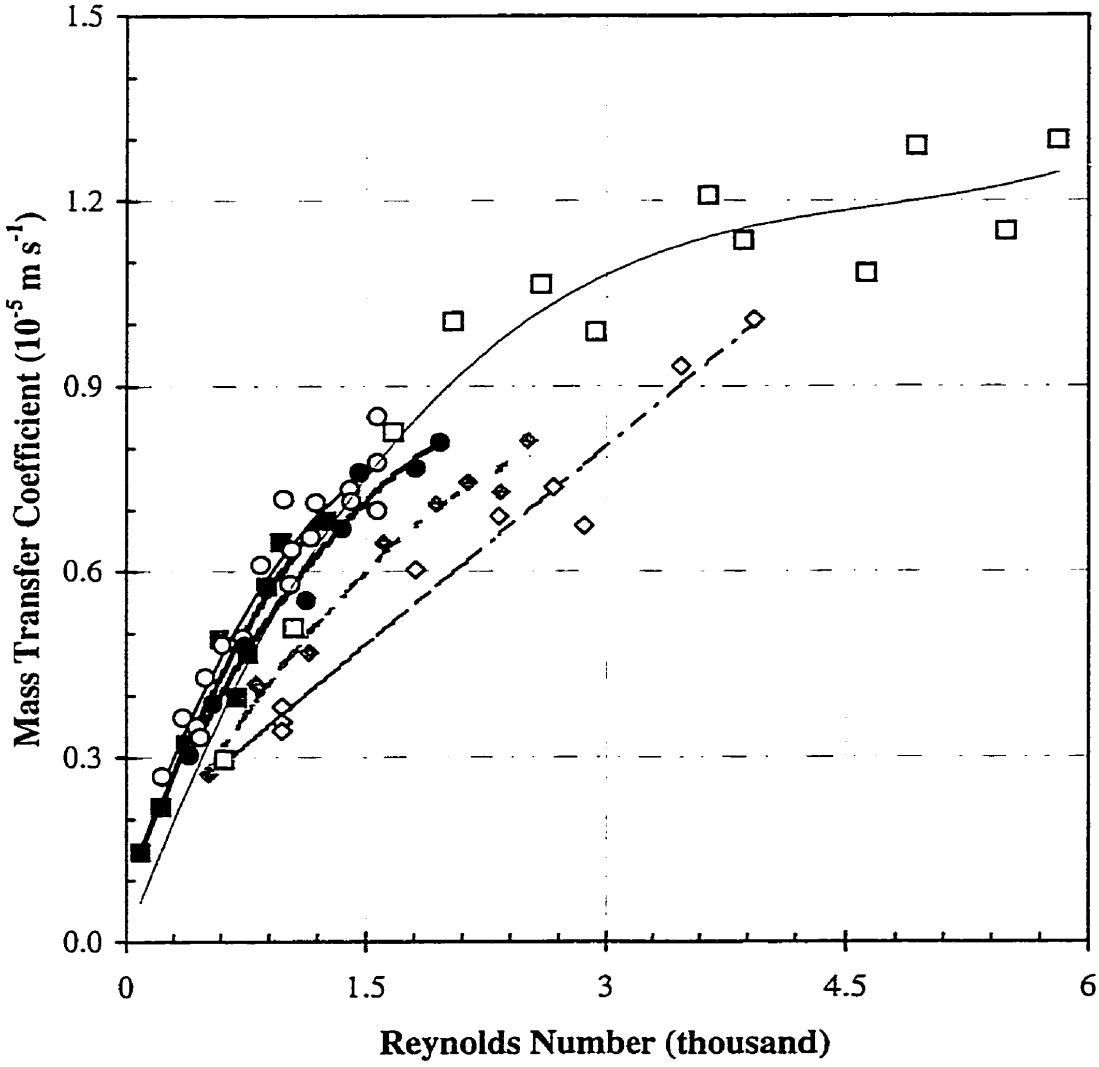

Figure 7-5: Benzoic Acid Transfer Coefficient and Fitted Curves
□ Flat plate; ■ α=3.5°; ○ α=5°; ● α=7°; ◆ α=10°
◇ α=20°; Lines: predictions of Equations 7-4 through 7-9.

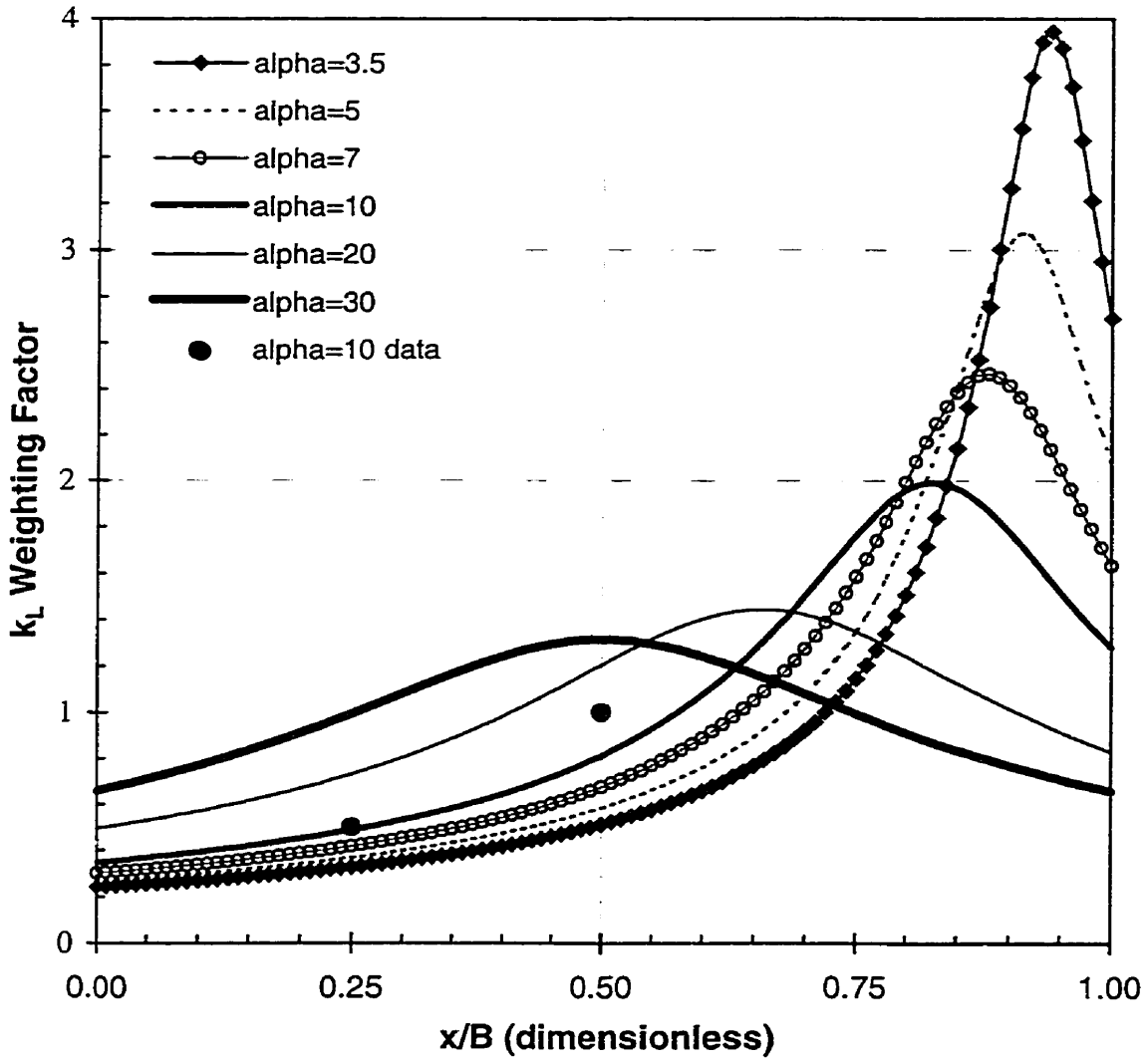

Figure 7-6: Model-Predicted Local Mass Transfer Coefficient Weighting Factor

relatively insensitive to the flowrate since the full length of the flat plate has become the entrance region and the flow is turbulent. The results shown in Figure 7-3 demonstrate a consistent decrease of the Sherwood number with the angle of the corrugated plates. Therefore, it is necessary to be cautious when extending round pipe correlations to pipes with different cross sectional shapes through the use of a hydraulic radius. We also deduce from this figure that the local mass transfer coefficients on corrugated plates change considerably with respect to "X" under the coordinate system shown in Figure 6-1.

Figure 7-4 shows the overall mass transfer capability of the flat and corrugated plates as a function of water flowrate through the reactor. It is indicated that the smaller the angle of the corrugated plates, the greater the enhancement of mass transfer over that of the flat plate. With approximately the same energy consumption of the pump (i.e., pressure drop), the corrugated plate can be 600% more efficient in mass transfer compared to the flat plate. For the purpose of reactor modeling, the mass transfer coefficients data were fitted into polynomials. The results are plotted against the Reynolds numbers as Figure 7-5. These fitted polynomials are also given in Equations (7-4) through (7-9). Figure 7-6 depicts the one-dimensional variation of the mass transfer coefficient on corrugated plates based on Equation (7-2).

$$\bar{k}_7 = 4.7\times10^{-6}[-0.117(\frac{Re}{650})^2 + 0.945(\frac{Re}{650}) + 0.208] \qquad (7\text{-}4)$$

$$300<Re<1200$$

$$\bar{k}_{10} = 6.2\times10^{-6}[-0.276(\frac{Re}{952})^2 + 1.156(\frac{Re}{952}) + 0.177] \qquad (7\text{-}5)$$

$$400<Re<1800$$

$$\bar{k}_{14} = 6.3\times10^{-6}[-0.244(\frac{Re}{1176})^2 + 1.133(\frac{Re}{1176}) + 0.168] \qquad (7\text{-}6)$$

$$500<Re<2300$$

$$\bar{k}_{20} = 6.4 \times 10^{-6}[-0.315(\frac{Re}{1630})^2 + 1.285(\frac{Re}{1630}) + 0.092] \quad (7\text{-}7)$$

$$600<Re<2500$$

$$\bar{k}_{40} = 6.82 \times 10^{-6}[-0.013(\frac{Re}{2225})^2 + 0.775(\frac{Re}{2225}) + 0.241] \quad (7\text{-}8)$$

$$1000<Re<4000$$

$$\bar{k}_{fl} = 1.0 \times 10^{-4}[0.034(\frac{Re}{3273})^3 - 0.145(\frac{Re}{3273})^2 + 0.222(\frac{Re}{3273})] \quad (7\text{-}9)$$

$$600<Re<6000$$

The subscripts refer to either the angle (in degrees) of the corrugated plates or flat plate.

7.4 Concluding Remarks

Mass transfer between the main stream and the surfaces of the corrugated as well as flat plates was examined experimentally using the benzoic acid dissolution method. Experimental results were fitted into several relationships which can be used to calculate the average mass transfer coefficients of the tested plates under different flow conditions. A mass transfer model for these plates was developed based on semi-empirical assumptions. The mass transfer fields over the surfaces of different corrugated plates can be estimated using the model.

Based on the results of the experiments, mass transfer coefficients were identified to be dependent on not only Reynolds number but also the angle of the corrugated plates. This finding revealed the apparent limitation in using the hydraulic radius method for extending round pipe correlations to flow channels with triangular cross sectional shapes. Measured mass

transfer rates on corrugated plates were found to change considerably in "X" direction of the coordinate system in Figure 6-1.

The mass transfer rate on the surface of the flat plate was found to change along the direction the fluid flows due probably to the entrance effect. A linear relationship was experimentally determined to account for this variation.

CHAPTER 8: PHOTOREACTOR MODELING

As can be seen from Section 2.3.5, very few heterogeneous photoreactor models have been presented previously. Of the few models reported in the literature, none was tested with experimental data. The objective of this work was to develop a simple model which may not be theoretically impeccable but should be usable in solving some of the engineering problems in photocatalysis. This was accomplished by fitting a semi-empirical kinetic model using data collected with the flat plate reactor, predicting the performance of CP reactors, and comparing the predictions with the experimental results. Details are described in the following sections.

8.1 Assumptions and Model Development

For the convenience of model development, the following assumptions were made:

(1). There exist only two reactants in the system (i.e., parent compound and oxygen) and intermediate compounds are kinetically negligible. Based on the results in Chapter 3, this assumption is approximately true for 4-CP.

(2) The system could be mathematically modelled as a completely mixed batch reactor and at any time reactant concentrations in the reservoir and the reactor are identical. Since conversion per pass is sufficiently low (results in Chapter 3), this assumption is appropriate (Klausner et al., 1994).

(3) Conversion of the parent compound was due entirely to photocatalytic reactions on the catalyst surface. This is supported by the results of photolysis and adsorption blank runs, discussed in Chapter 3.

(4) Degradation kinetics follows the relationship: $r_{4cp} = \dfrac{k_0 k_{O_2} C_s (q/q_0)^n}{(1 + K_1 C_s)(1 + k_{O_2} O_s)}$.

(5) The reaction kinetics expression was proposed based on the following considerations.

Surface concentrations were used because the reactions proceed primarily on the catalyst surfaces instead of in the liquid bulk. The term, $C_s/(1+K_1C_s)$, was introduced to qualitatively reflect "competitive absorption" of the water and all the organic compounds on the catalyst surface. The exponent "n" was introduced to reflect the effect of photon absorption rates. The term, $k_{o2}/(1 + k_{o2} O_s)$, was introduced to reflect the effect of mass transfer and the other reactant, oxygen, on the degradation rate.

(6) The concentration of the model compound is a function of time only and does not change with position except in the boundary layer near catalyst surfaces. Because the local area-specific rate of energy absorption (LASREA) and mass transfer rates are not uniform over the surface of the catalyst films, reactant concentrations on the catalyst surface will be dependent on both time and location.

(7) Contribution of the "caps" of the corrugated plates is negligible.

Based on the above assumptions and the principles of mass balance, mass transfer, and reaction stoichiometry, a new semi-empirical kinetic model was derived. The model is summarized in Equation (8-1). The derivation of this model is detailed in Appendix C.

$$C = C_0 - \int_0^t \{ \iint_S r_{4cp} dS \} \frac{dt}{V} \qquad (8\text{-}1)$$

where $r_{4cp} = \dfrac{k_0 k_{O_2} C_s (q/q_0)^n}{(1 + K_1 C_s)(1 + k_{O_2} O_s)} = k_{4cp}(C - C_s)$, and,

$$O_s = O_b - \frac{416}{257} \left(\frac{D_{4cp}}{D_{O_2}}\right)^{\frac{2}{3}} (C - C_s)$$

In order to determine the model parameters (i.e., k_0, K_1, and n), a nonlinear regression

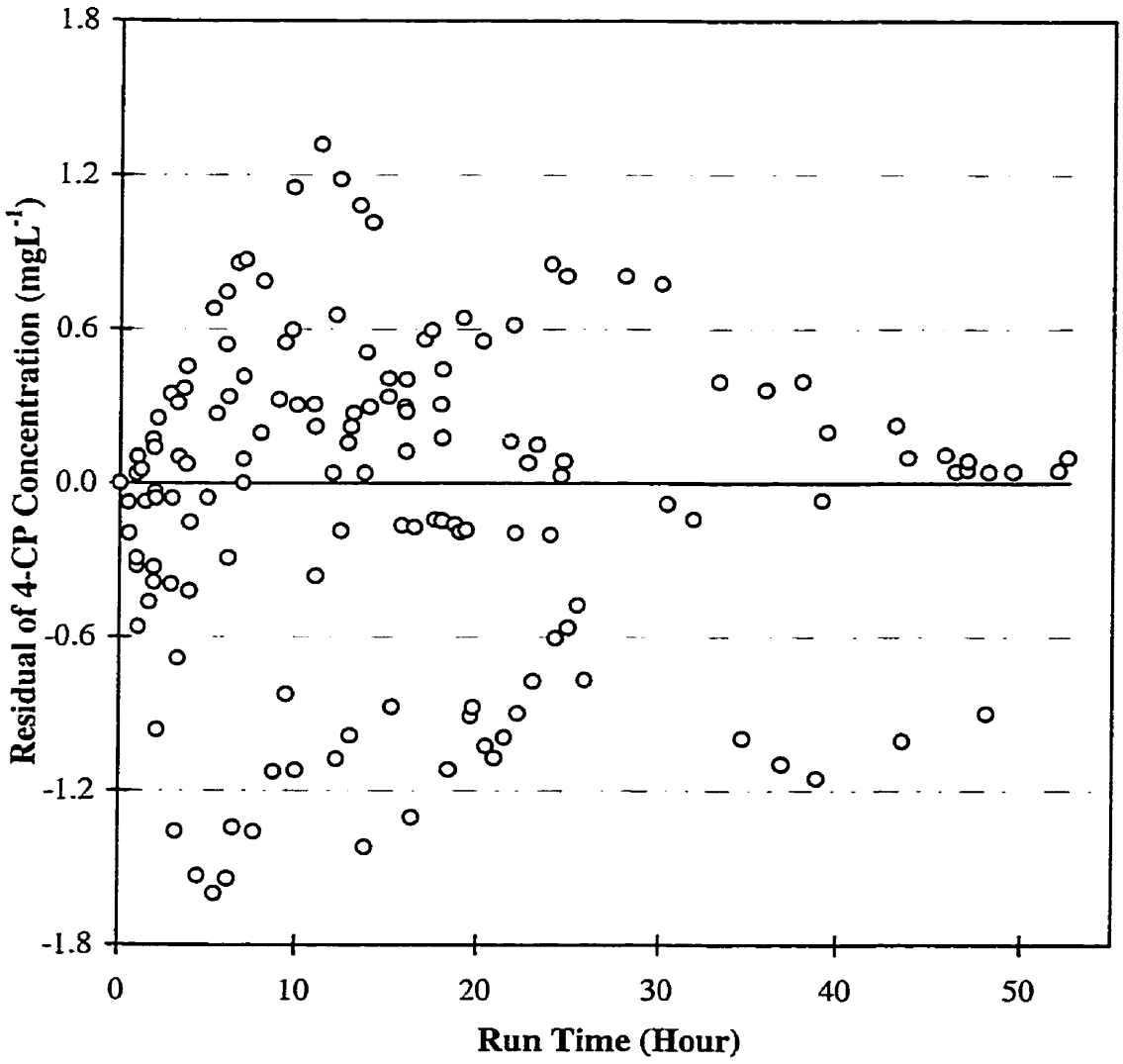

Figure 8-1: Reactor Performance Model Fitting: Residual vs. Run Time

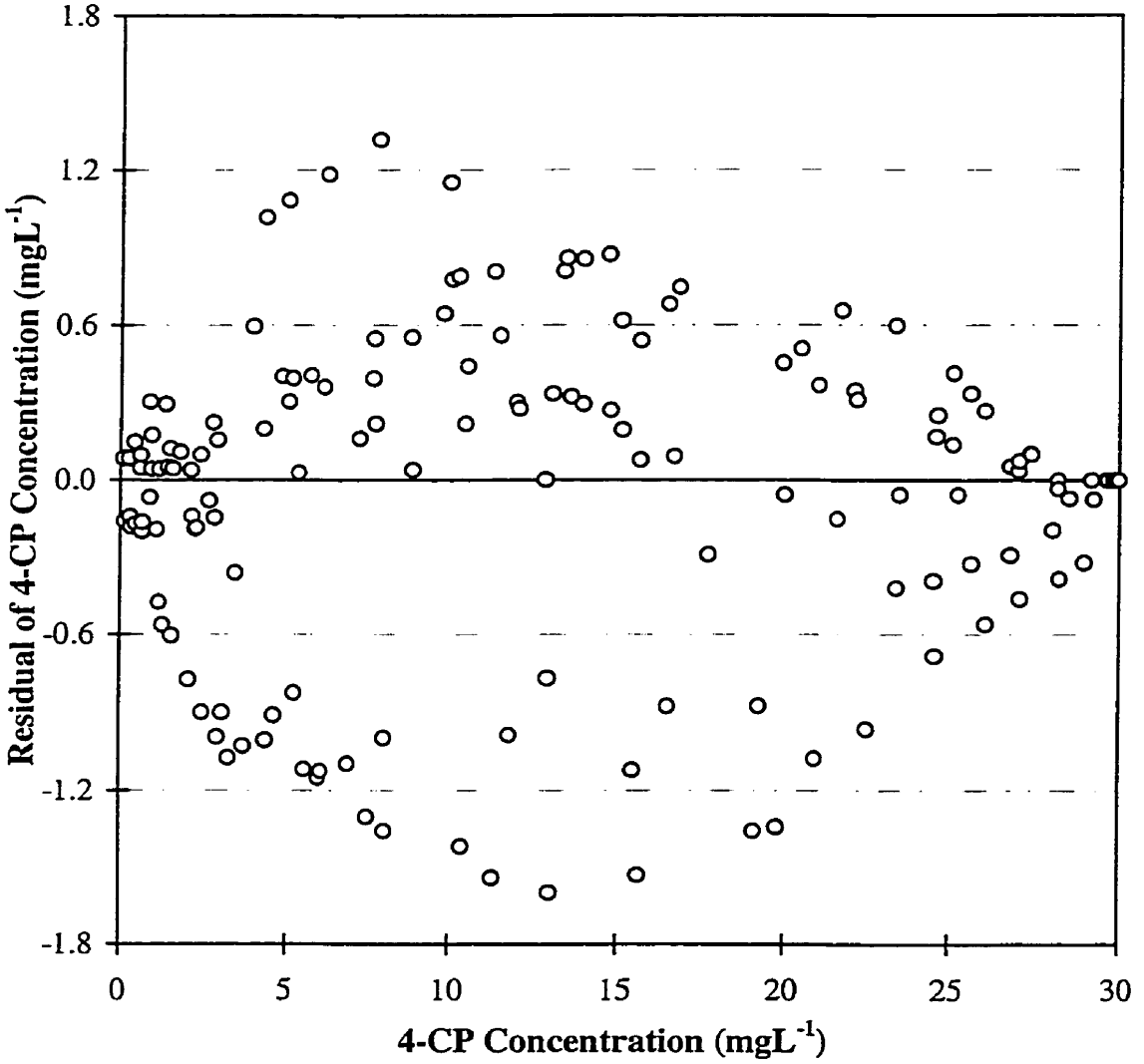

Figure 8-2: **Reactor Performance Model Fitting: Residual vs. Concentration**

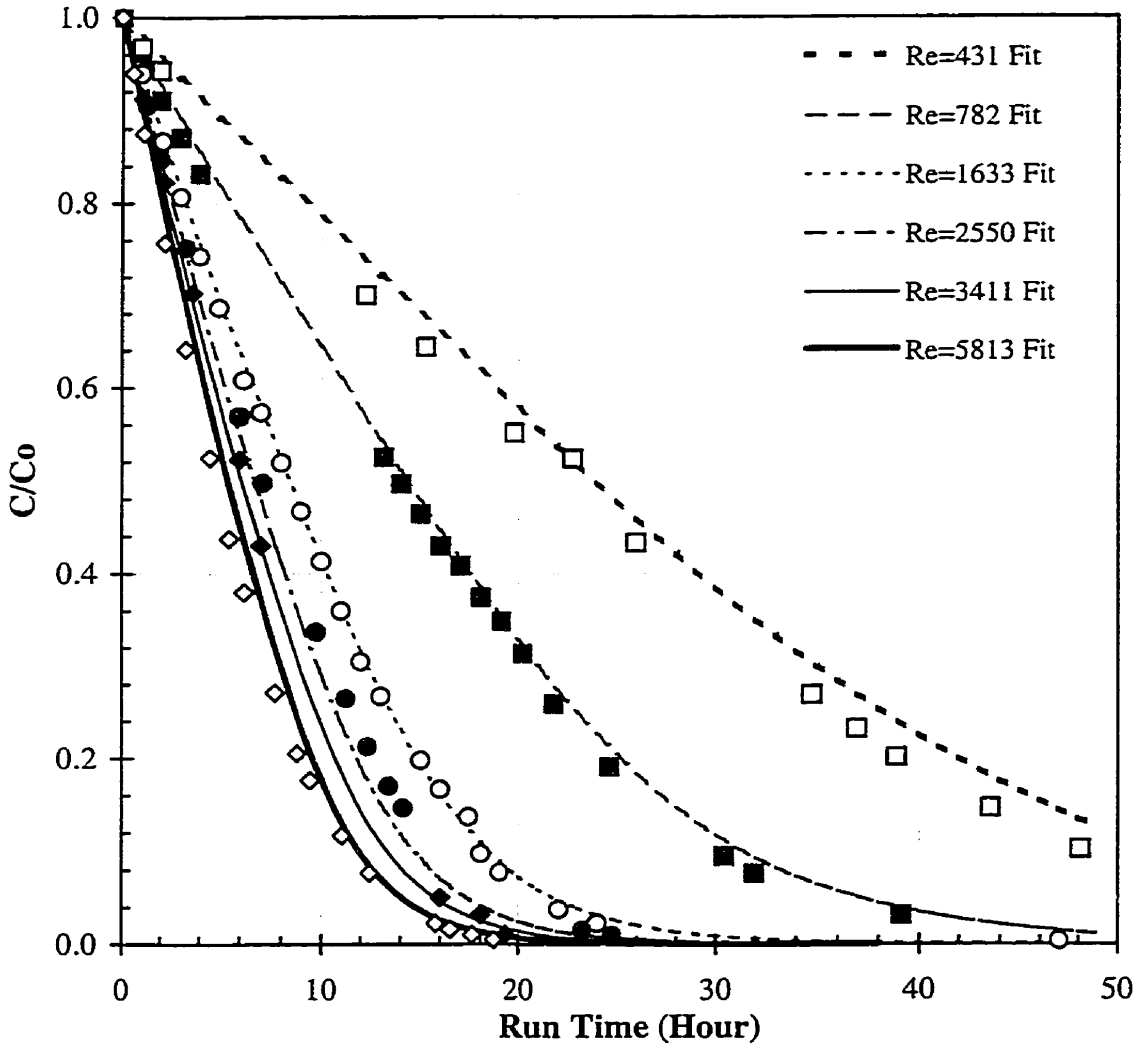

Figure 8-3: Kinetic Data and Model Fittings: Mass Transfer Effect
Flat plate; C_0=30 mgL^{-1}; I=122 Wm^{-2}; □ Re=431;
■ Re=782; ○ Re=1633; ● Re=2550; ◆ Re=3411; ◇ Re=5813
Lines: reactor model fittings

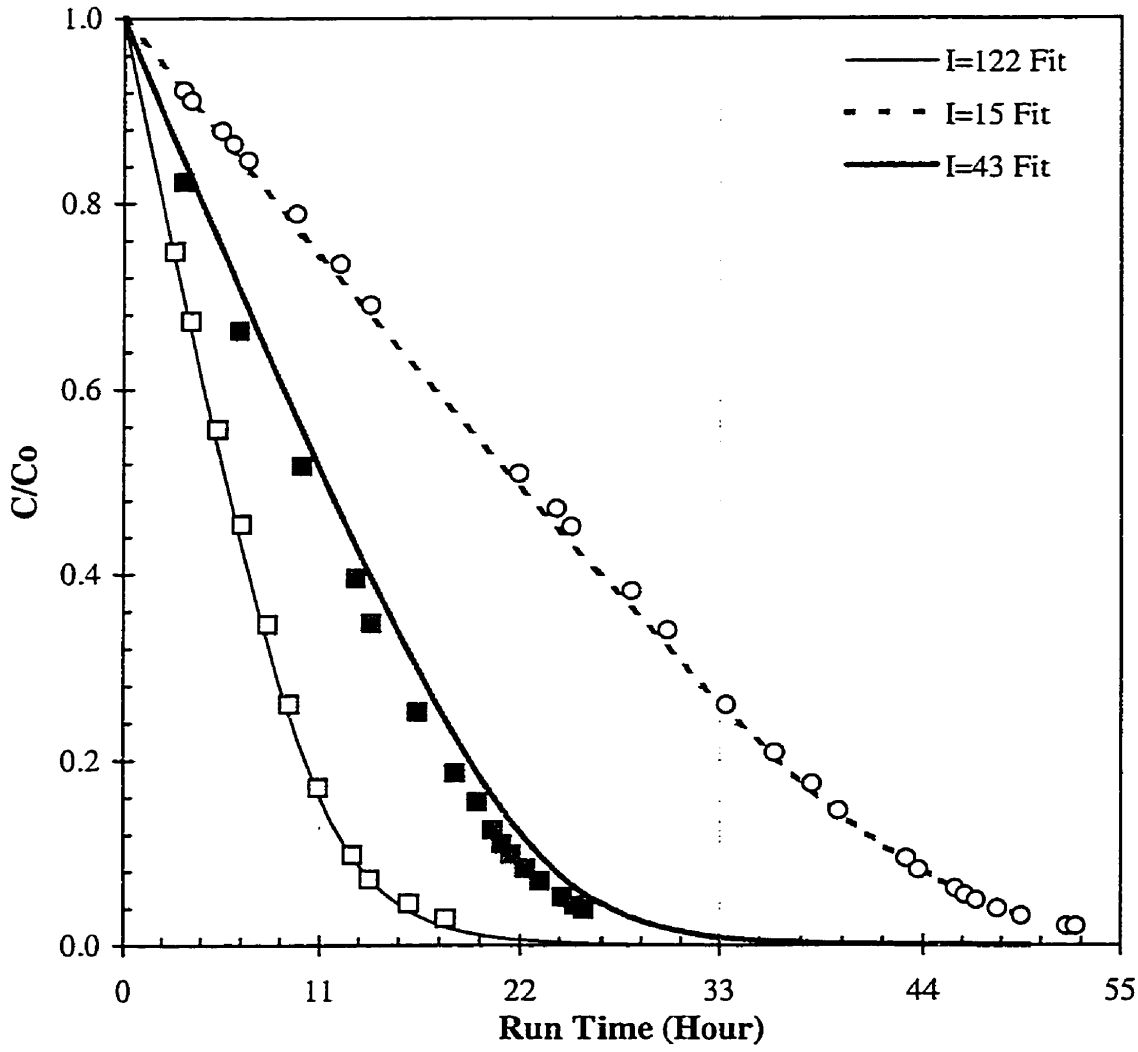

Figure 8-4: Kinetic Data and Model Fittings for Several Radiation Levels

Flat plate; C_0=30 mgL^{-1}; Re=4313; □ I=122 Wm^{-2}; ■ I=43 Wm^{-2}; ○ I=15 Wm^{-2}; Lines: reactor model fittings

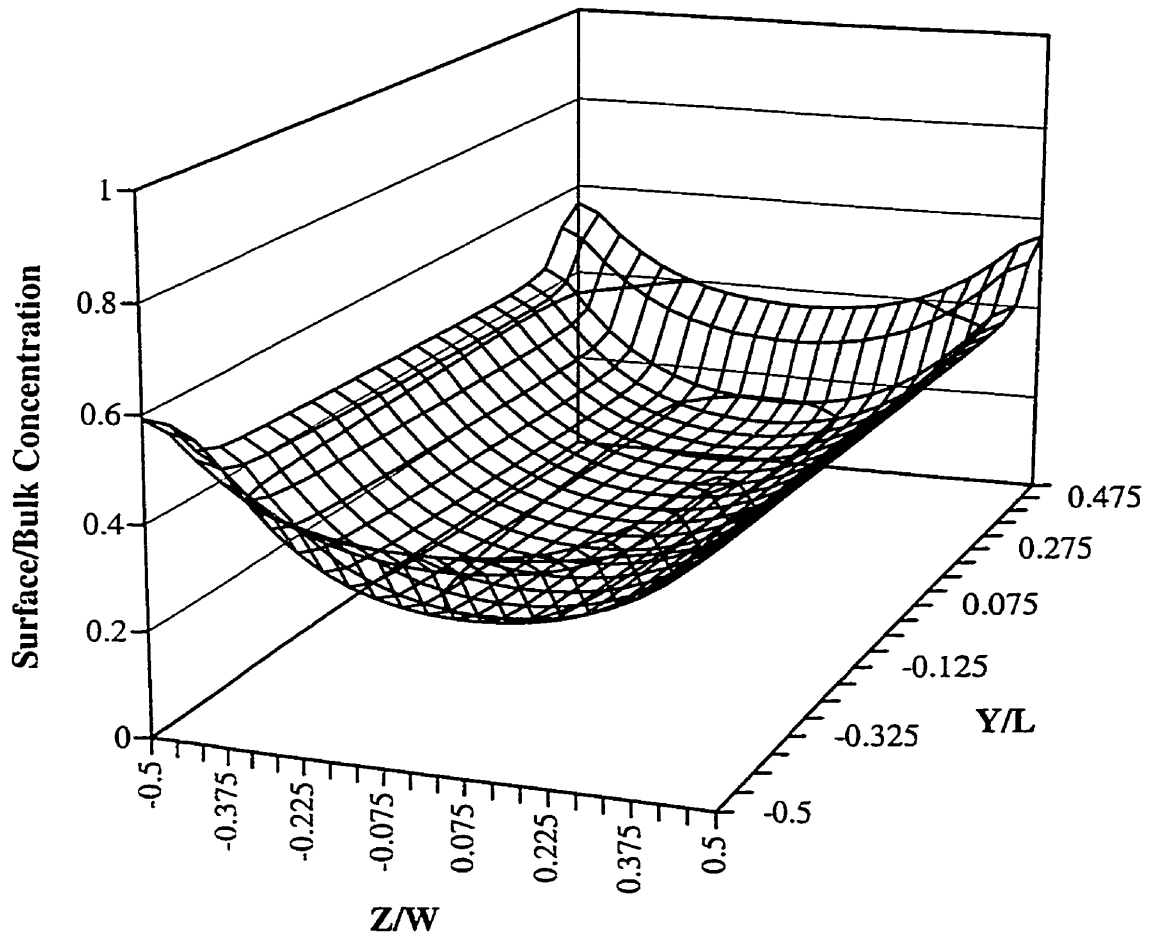

Figure 8-5: Model-Predicted Oxygen Profile on the Surface of the Flat Plate: Lamp-Illuminated
C=30 mgL^{-1}; O_b =7 mgL^{-1}; Re=4313; I=122 Wm^{-2}
Coordinate system: see Figure 6-1

was performed using the Simplex and Runge-Kutta methods (Rice and Do, 1995). All kinetic data of 4-CP degradation in the flat plate reactor (as shown in Figures 3-8 and 3-9) were used in the regression. The results are presented in the next section.

8.2 Model Regression Results and Discussions

The results of the nonlinear regression are summarized in Table 8-1 and Figures 8-1 through 8-5.

Table 8-1: Results of the Nonlinear Regression

Model Parameter	Fitted Value	R^2
k_0	0.321	0.994
K_I	0.573	
n	0.520	

The residuals are plotted in Figures 8-1 and 8-2, against run time and 4-CP concentration respectively. No apparent patterns can be observed from these two figures, indicating no significant structural deficiencies in the models. Figures 8-3 and 8-4 show the kinetic data and model fittings for different illumination and water flow conditions. As can be seen from these two figures, the model accommodated the effects of both flow condition (Reynolds number) and radiation intensity consistently well. Reactant concentrations on the catalyst film surfaces were also calculated using the fitted model parameters. Figure 8-5 shows a typical initial oxygen concentration profile on the catalyst film in the flat plate reactor. The great differences between the central region and regions near the edges of the flat plate are resulted from the non-uniformity of the LASREA on the flat plate.

Since the transfer of reactants and photons (as functions of locations on catalyst films and flow conditions) were both incorporated in Equation (8-1), this model was able to fit the all the

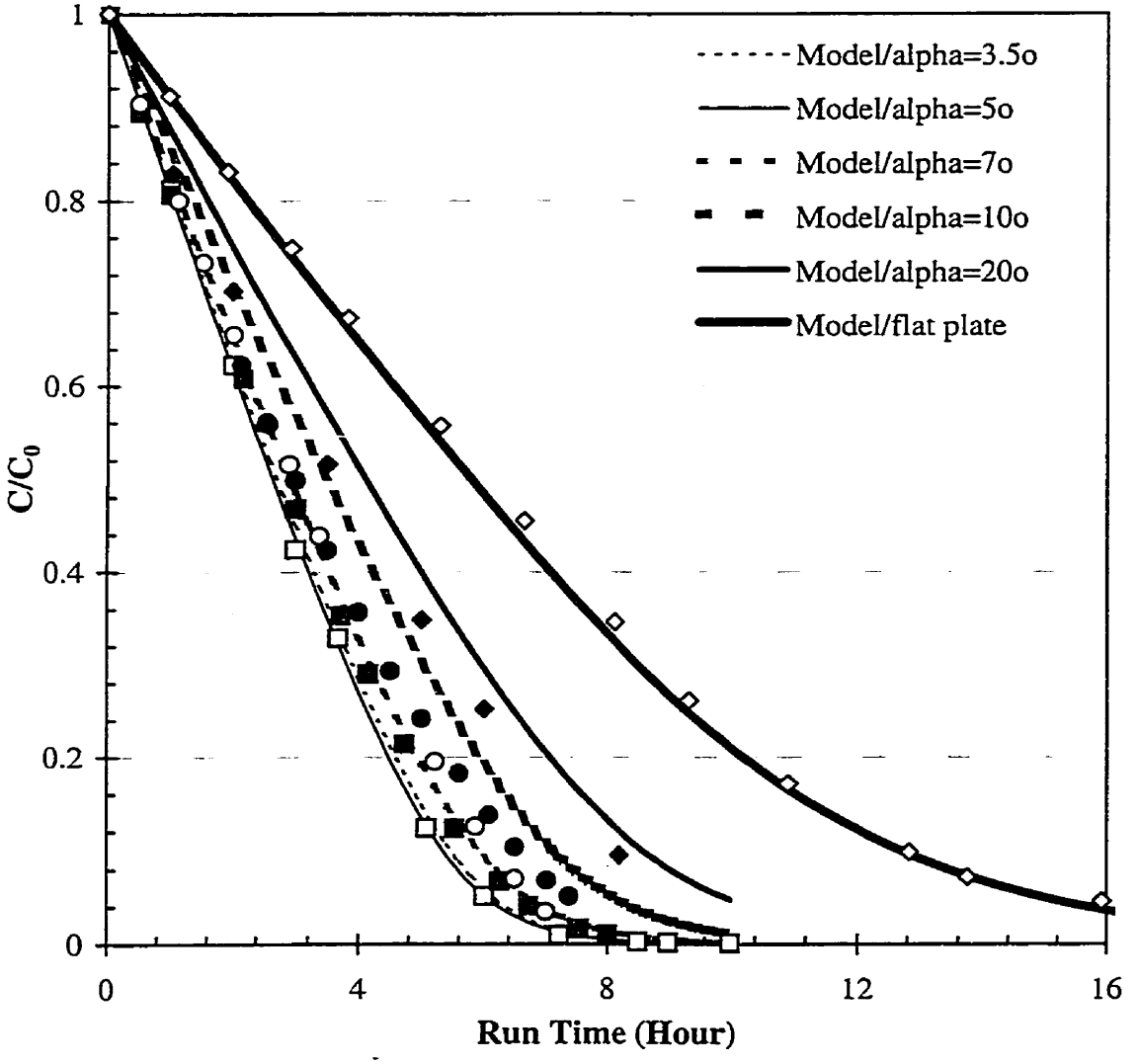

Figure 8-6: Model-Predicted Kinetic Curves and Experimental Data: Effect of Plate Geometry

C_0=30 mgL^{-1}; I=122 Wm^{-2}; Flowrate=23 $Lmin^{-1}$

Markers: experimental data; □ α=3.5°; ■ α=5°

○ α=7°; ● α=10°; ◆ α=20°; ◇ Flat plate

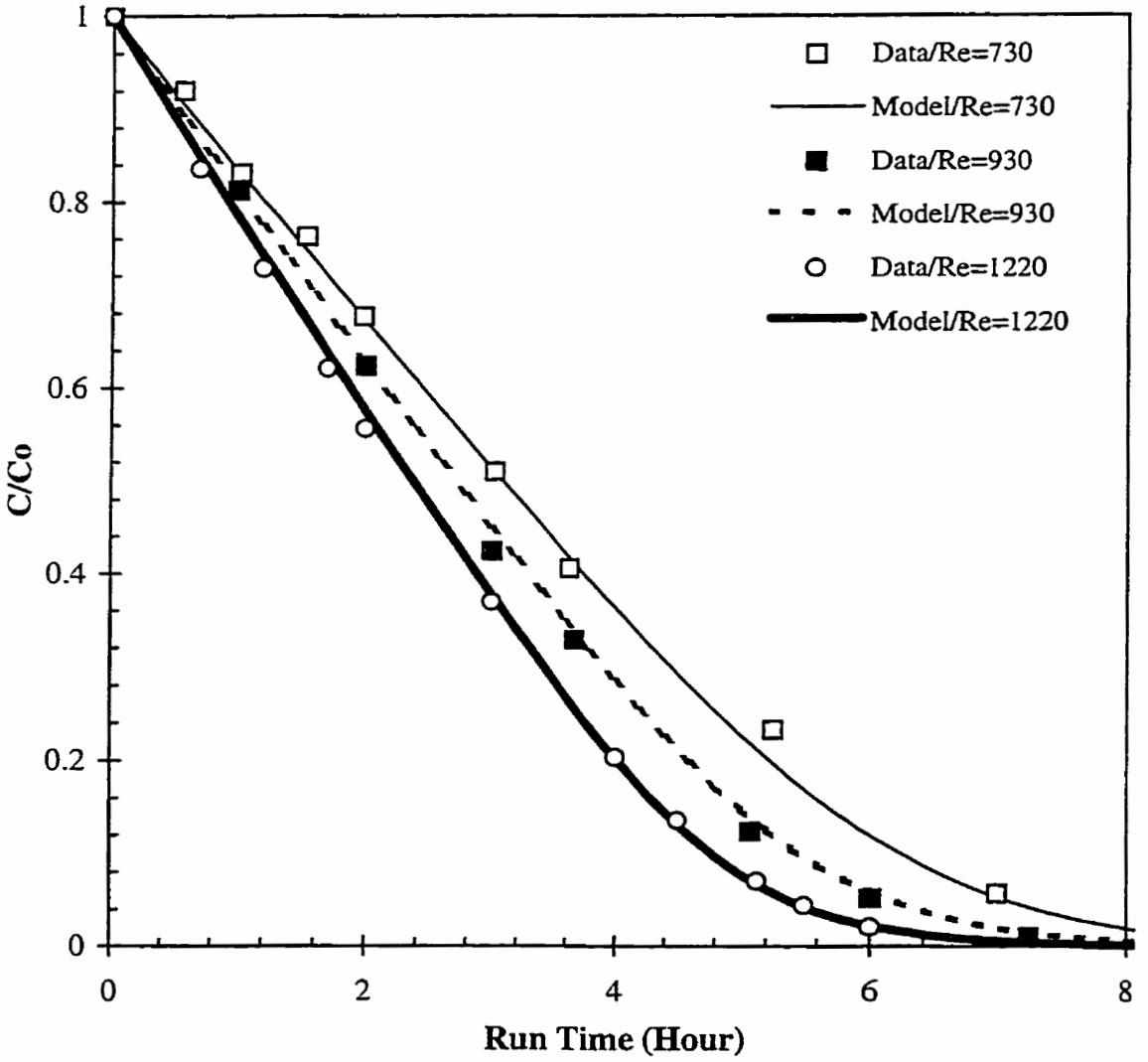

Figure 8-7: Model-Predicted Kinetic Curves and Experimental Data: Effect of Mass Transfer
C_0=30 mgL^{-1}; I=122 Wm^{-2}; Corrugated plate with α=3.5°

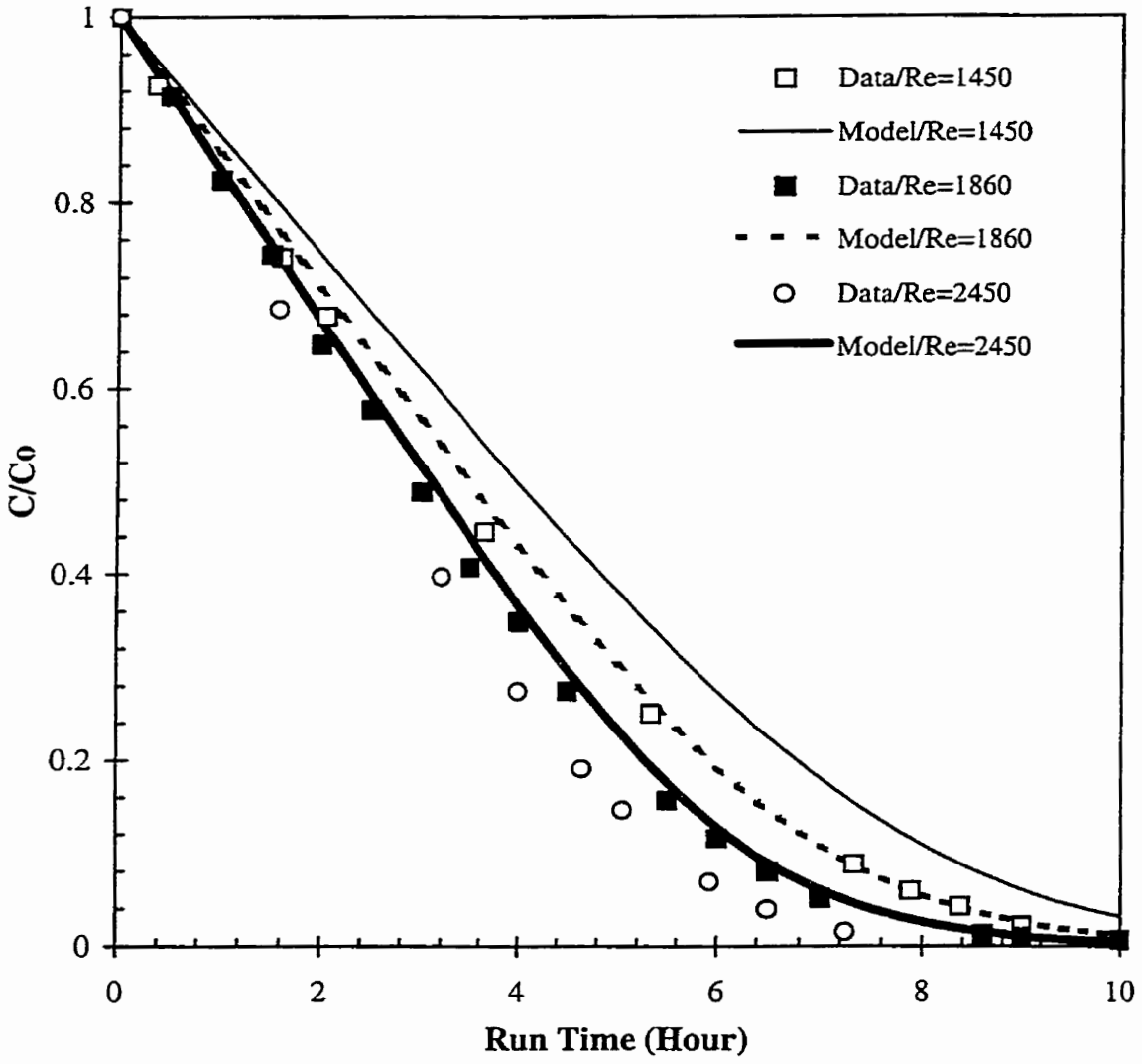

Figure 8-8: Model-Predicted Kinetic Curves and Experimental Data: Effect of Mass Transfer
C_0=30 mgL^{-1}; I=122 Wm^{-2}; Corrugated plate with α=10°

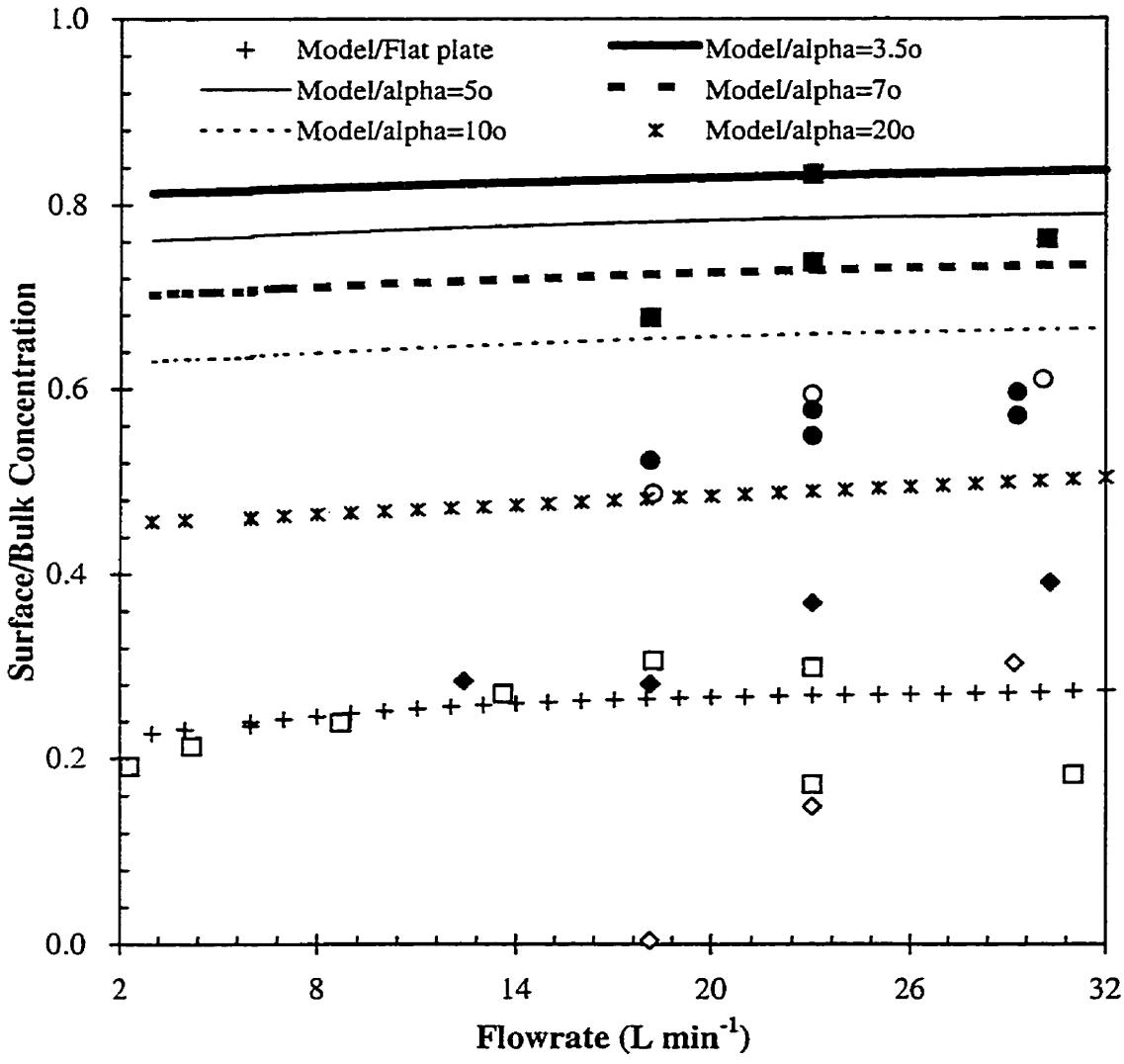

Figure 8-9: Model-Predicted Average Oxygen Concentrations on the Surfaces of the TiO_2-Coated Plates, Compared to Experimental Data

C_0=30 mgL^{-1}; I=122 Wm^{-2}; □ Flat plate

■ α=3.5°; ○ α=5°; ● α=7°; ◆ α=10°; ◇ α=20°

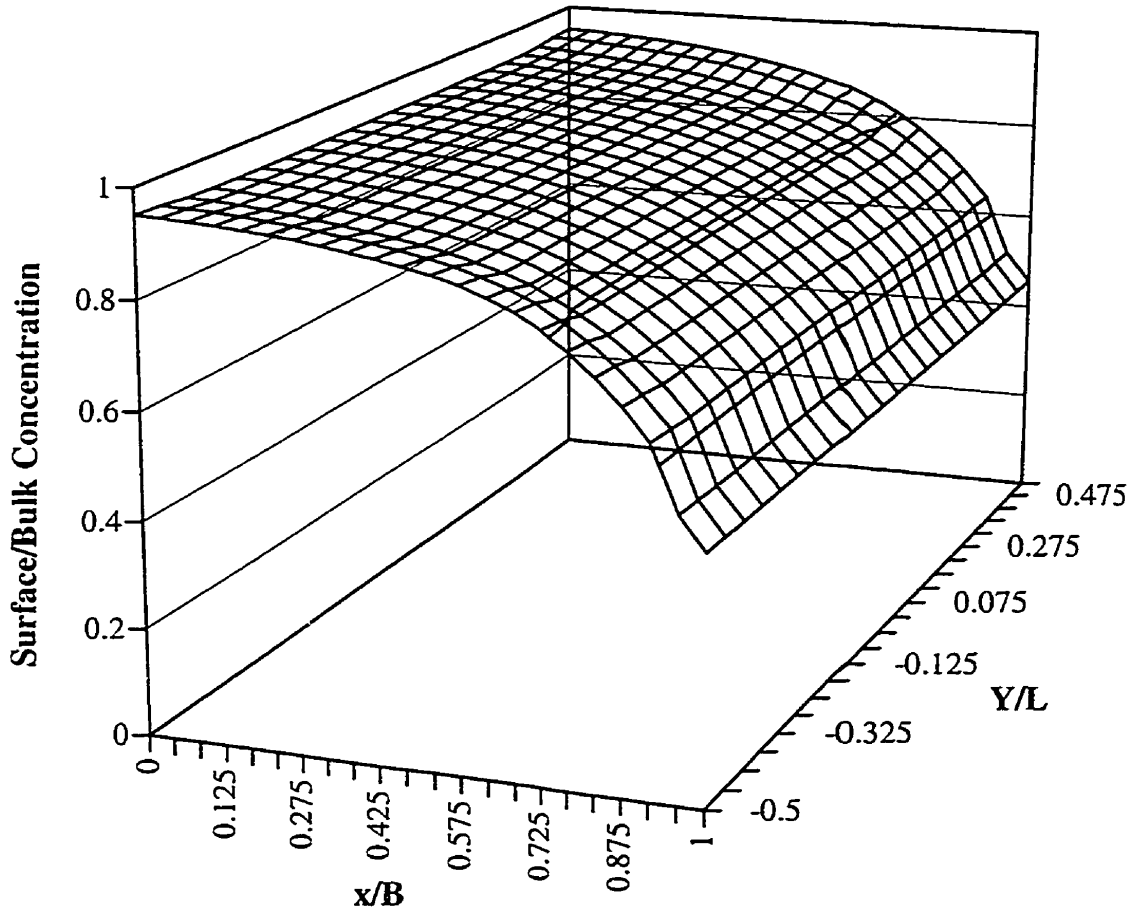

Figure 8-10: Model-Assisted Reactor Analysis: 2D Oxygen Profile on the Surface of a Lamp-Illuminated Corrugated Plate
α=3.5°; C=30 mgL^{-1}; O_b =7 mgL^{-1}; Re=930; I=122 Wm^{-2}
Coordinate system: see Figure 6-1

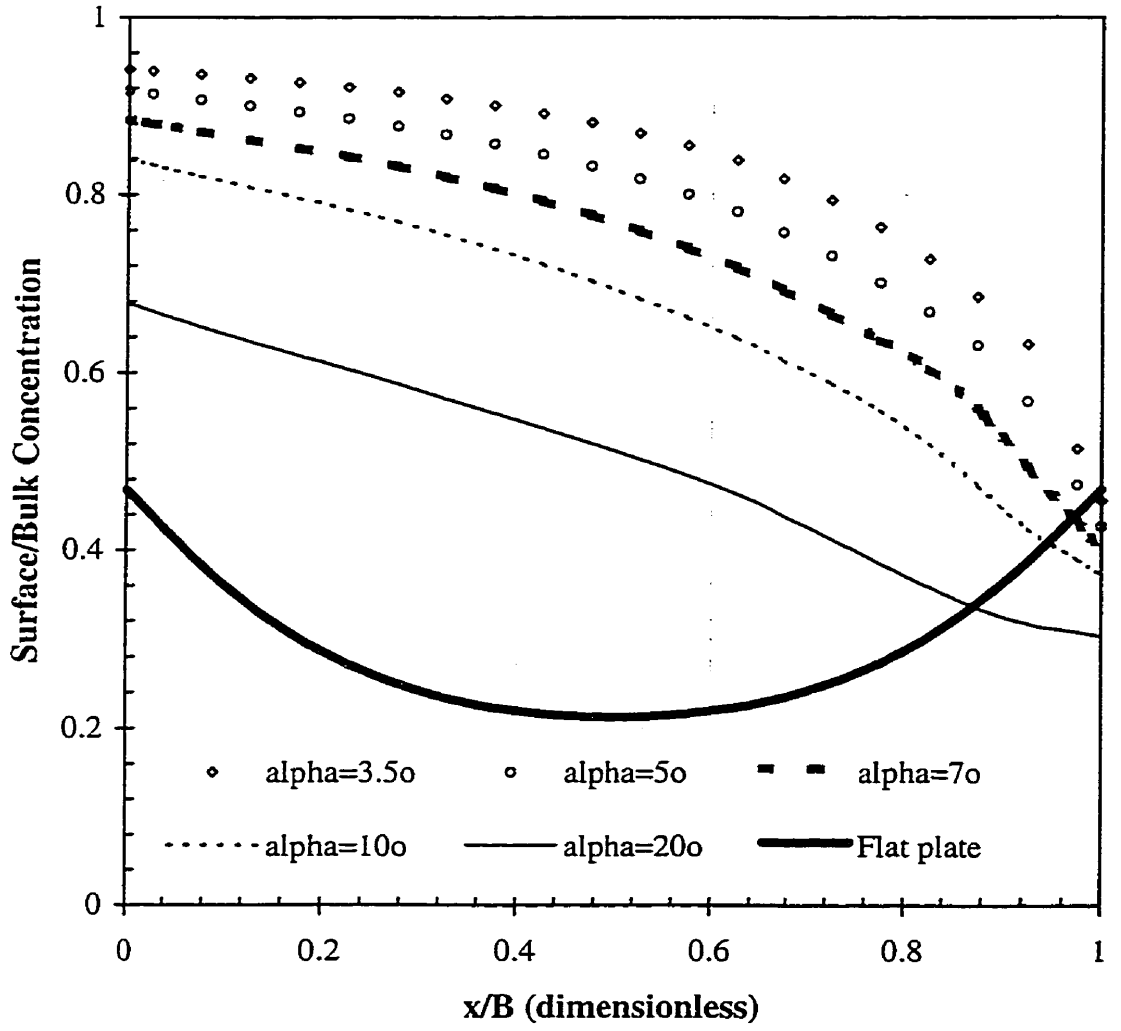

Figure 8-11: Model-Assisted Reactor Analysis: Oxygen Concentration Profiles on the Surfaces of the Lamp-Illuminated Plates
C=30 mgL^{-1}; O_b =7 mgL^{-1}; Flowrate=23 $Lmin^{-1}$; I =122 Wm^{-2}
Coordinate system: see Figure 6-1

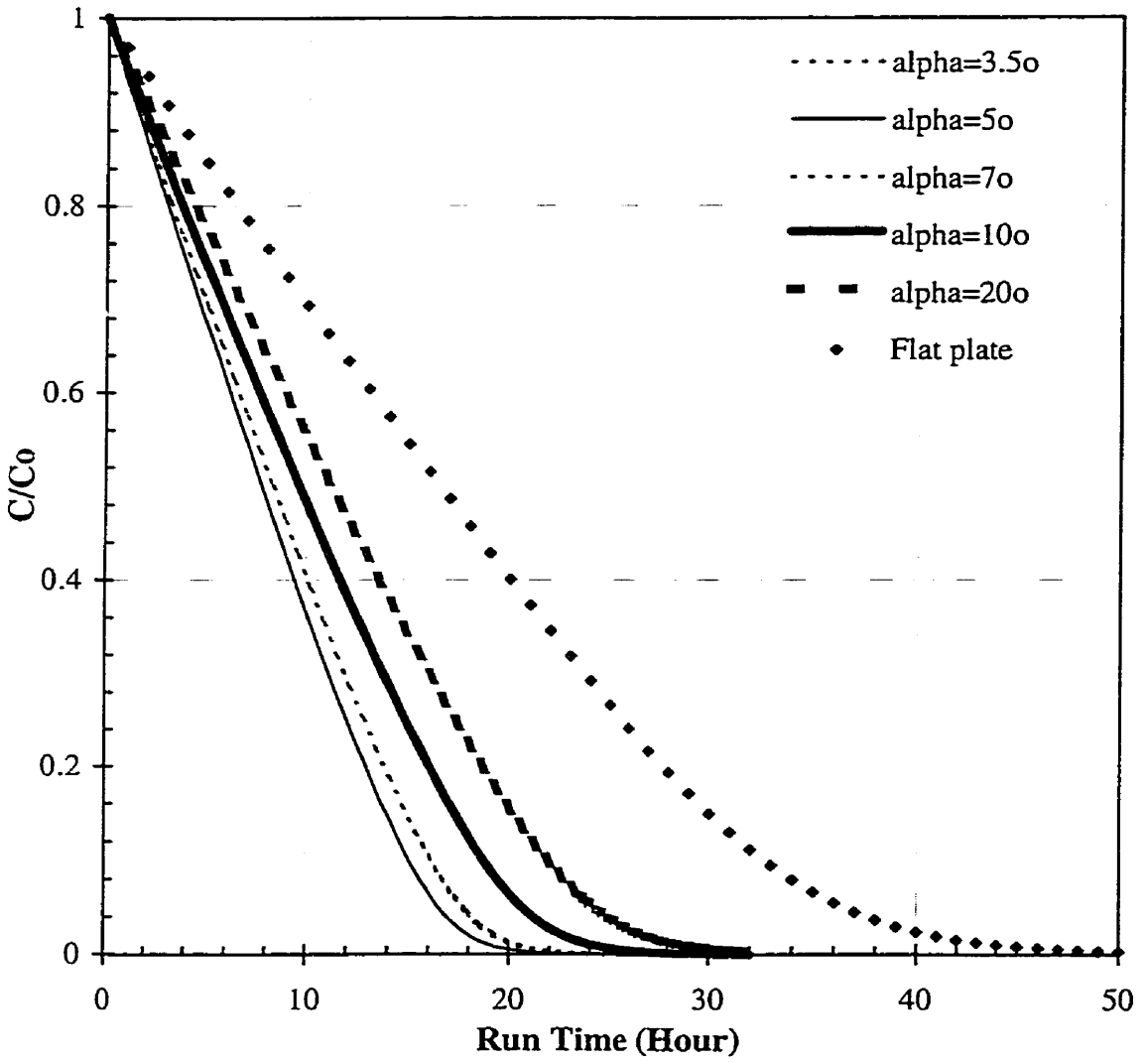

Figure 8-12: Model-Assisted Reactor Analysis: Predicted 4-CP Degradation in Solar-Powered CP and Flat Plate Reactors
C_0=30 mgL^{-1}; Solar UV=30 Wm^{-2}; Flowrate=23 $Lmin^{-1}$
Note: reactors with α=3.5° and 7° were predicted to have the same performance

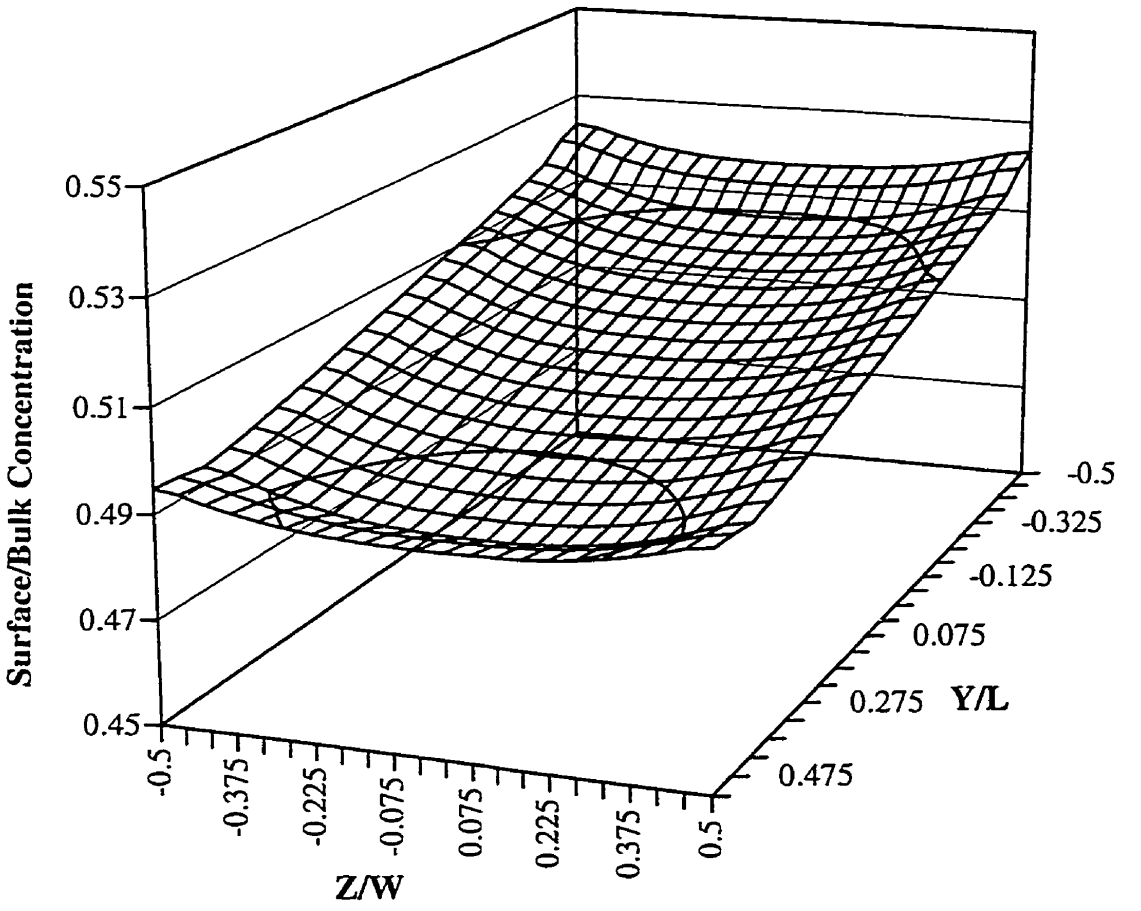

Figure 8-13: Model-Assisted Reactor Analysis: 2D 4-CP Profile on the Surface of a Solar-Illuminated Large Flat Plate
C=1 mgL^{-1}; O_b=7 mgL^{-1}; I=30 Wm^{-2}; Re=4313
Coordinate system: see Figure 6-1

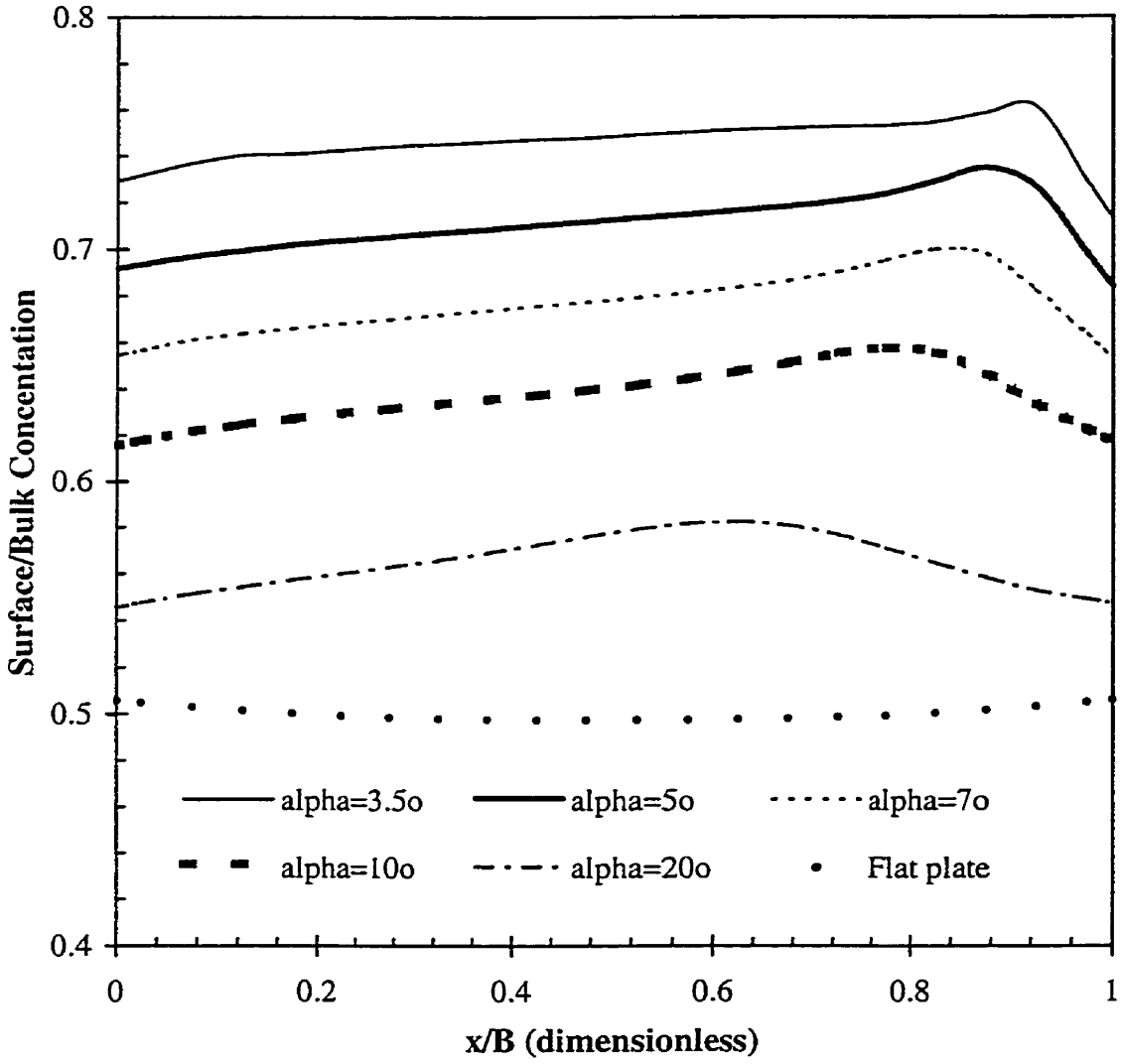

Figure 8-14: Model-Assisted Reactor Analysis: 4-CP Concentration Profiles on the Surfaces of the Solar-Illuminated Flat and Corrugated Plates

C=1 mgL^{-1}; O_b=7 mgL^{-1}; I =30 Wm^{-2}; Flowrate=23 $Lmin^{-1}$

Coordinate system: see Figure 6-1

data with only three parameters. For the same set of data, the empirical L-H type model (Equation 3-1) has to be fitted nine times. More important, the new model could be used to predict 4-CP degradation in any other immobilized reactor when mass and photon transfer to the catalyst surfaces are known. As an example, the degradation of 4-CP in the CP reactor, powered by fluorescent lamps or solar UV, was simulated with the new model. The results are presented in Sections 8.3 and 8.4.

8.3 Model Prediction Results and Discussions

Based on the local photon absorption rates (Chapter 6), the local mass transfer rates (Chapter 7), and the fitted model parameters (Table 8-1), the degradation of 4-CP in LCP reactors was estimated using the new reactor model (Equation 8-1). Selected prediction results are presented in Figures 8-6 through 8-14, together with experimental data where available. Since the model predictions were not derived from any experimental data, the degree of agreement between the model prediction and the data is indicative of the capability of the model in reactor scale-up.

Figures 8-6 through 8-11 show the performances of CP reactors powered with fluorescent lamps. As can be seen from Figure 8-6, the effect of the angle of corrugated plates was consistently reflected by the model predictions. The deviation of the model predictions from the experimental data appears to be dependent on the angle of the corrugated plates (Figures 8-6 to 8-8). For plates with small angles (i.e., α=3.5°, 5°, or 7°), the agreement between the prediction and the data was relatively good and the deviations of the model prediction from the measured concentration data were less than 3.5% of the initial value (Figure 8-6). For plates with large angles (i.e., α=10° and 20°), the model tends to underestimate the parent compound concentration by as high as 10%. The primary reason for this underestimation may well be the deviation of one mass transfer assumption (Assumption 2 in Section 7.2) from reality. For plates

with larger angles, the experimental Reynolds numbers were 1860 and 2900 respectively and turbulent flow condition must have occurred. Incorporation of the mass transfer coefficient into the model allowed the prediction of the effect of mass transfer on degradation rates (Figures 8-7 and 8-8).

The effect of water flowrate and the angle of the corrugated plates on the overall mass transfer condition in the CP reactors (expressed as the average oxygen concentration on the surface of the catalyst films) is presented in Figure 8-9. As can be seen from this figure, the model was successful in predicting the general trend of the data. As a matter of fact the same observation can be obtained from the model prediction and the experimental data, i.e., the mass transfer condition was far more sensitive to the angle of corrugated plates than to water flowrates (Reynolds number). This is due to the fact that changing the angle of the corrugated plates affects both the mass transfer capability of the reactor (Figure 7-4) and the area-specific rate of photon absorption (Figures 6-2 through 6-7) whereas flowrate affects only mass transfer.

For the convenience of discussion, we define the process as not limited by mass transfer when $O_s/O_b \geq 0.9$, slightly limited when $0.7 \leq O_s/O_b < 0.9$, moderately limited when $0.4 \leq O_s/O_b < 0.7$, severely limited when $0.2 \leq O_s/O_b < 0.4$, and controlled by mass transfer when $O_s/O_b < 0.2$. Based on this criterion and the results in Figure 8-9, reactions on corrugated plates with small angles (i.e., α=3.5°, 5°, 7°) were from lightly to moderately limited by the transfer of oxygen at the start of all the experimental runs. Reactions on 20° and 40° corrugated plates were severely limited by mass transfer and the flat plate reactor was actually mass transfer controlled.

The model-predicted local mass transfer conditions (expressed as local oxygen concentrations on the surface of the catalyst film) are plotted in Figures 8-10 and 8-11. The three-dimensional plot shown in Figure 8-10 indicates that "O_s/O_b" does not change significantly along the direction the water flows in CP reactors. Therefore, similar results for different corrugated plates are plotted against the other dimension (Figure 8-11). The following observations can be revealed from this figure:

(1). Mass transfer limitation exists in the flat plate reactors as well as CP reactors. Since it is difficult to enhance mass transfer substantially (i.e., tenfold enhancement) without sacrificing light distribution and absorption, mass transfer limitation is probably the bottleneck of aqueous phase photocatalysis in immobilized systems. Fortunately, similar obstacles do not exist for air phase photocatalysis because substances diffuse millions of times faster in air than in water (Perry, Green, and Maloney, 1984).

(2). Corrugated plates of small angles (i.e., α=3.5°) were capable of improving the overall mass transfer conditions (Figure 8-9). However, the smaller the angle of the corrugated plates, the less uniform the reactant concentrations on catalyst surfaces. Based on the model prediction, moderate level mass transfer limitation was never eliminated through the use of corrugated plates (Figure 8-11).

(3). It is traditionally believed that a uniform LASREA distribution on the catalyst surfaces offers the highest energy efficiency in heterogeneous photocatalysis (Ray and Beenackers, 1998). While this is true for slurry systems in which there is no mass transfer limitation, it does not generally hold for immobilized systems due to the interference of mass transfer. Based on Equation (8-1), the distribution of mass transfer and radiative energy absorption must be complimentary to each other in an efficient system. This is easy to understand since mass transfer and photon absorption are consecutive steps in photocatalysis. An increase in the local photon absorption rate won't result in higher reaction rates unless the reactants are transferred to the same site at an increased rate.

Based on the solar UV defined in Section 6.1 and Appendix A, the performance of solar-powered CP reactors was estimated using Equation (8-1). Selected results are presented in Figures 8-12 through 8-14. As can be observed by comparing Figure 8-12 with Figure 8-6, the

performances of CP reactors are similarly sensitive to the angles of the corrugated plates, regardless of the illumination sources used (fluorescent lamps versus solar UV). The CP reactors (i.e., α=3.5° and 5°) were predicted to be more than 100% more efficient than the flat plate reactor (Figure 8-12). The corresponding time required for 90% degradation was approximately 16 hours.

The solar UV was approximately three times weaker than the artificial UV examined (30 Wm^{-2} vs. 122 Wm^{-2}) and the mass transfer limitation was therefore slight until 4-CP concentration becomes very low. The mass transfer conditions on the catalyst surfaces (expressed as the 4-CP concentration on surface of the catalyst film at a bulk concentration of 1 mgL^{-1}) are plotted in Figures 8-13 and 8-14. The effect of the angles of the corrugated plates is again predicted to be significant. Under the specified 4-CP concentration, the degree of mass transfer limitation was from slight to moderate. Compared to the results in Figure 8-11, it is clear that the reactant concentrations on the surfaces of catalyst films are much more uniform when the plates are illuminated by solar UV. This is due to the relatively uniform local photon absorption rate under solar illumination (Figures 6-3 and 6-4).

8.4 Concluding Remarks

A semi-empirical model was developed to describe the heterogeneous photocatalytic reactions on immobilized catalyst films. With only three parameters (i.e., k_0, K_1, and n) determined by fitting experimental data, the model could potentially be used in the development, design, and optimization of heterogeneous photoreactors. The new model is superior to the prevailing simple L-H model in terms of its prediction capability.

As indicated by the results of the nonlinear regression, the model described the degradation of 4-CP in the flat plate reactor very well. The model parameters obtained in the regression could be used to predict 4-CP degradation under other mass transfer and illumination

conditions as long as the LASREA and mass transfer profile on the surfaces of the TiO_2 films are known.

The new model (together with the fitted parameters), predicted the performance of the CP reactors reasonably well. As confirmed by the experimental data, the effect of water flowrate and the angle of the corrugated plates on the overall reaction rate was clearly reflected by the model prediction. The agreement between the experimental data and the model prediction was very encouraging.

For the degradation of 4-CP, the optimal angle of the corrugated plate was predicted to be near 7° (i.e., α=3.5°), regardless of the radiation sources used (i.e., solar UV or fluorescent lamps).

Corrugated plate reactors were predicted to suffer from mass transfer limitations of different degrees, depending on the water flow rate and the angle of the corrugated plate. The most effective way to alleviate this limitation is the use of corrugated plates of small angles.

For systems illuminated by fluorescent lamps, it is essentially impossible to eliminate mass transfer limitation on corrugated plates unless a weak illumination source is used. This happens because the smaller the angle of a corrugated plate, the greater the difference of the degree of mass transfer limitation on the corrugated plate. The region near the top of the corrugated plates suffers from more severe mass transfer limitation.

The degree of mass transfer limitation on a solar-illuminated corrugated plate is relatively uniform, thanks to the direct-parallel fraction of the solar irradiation. The time required for 90% 4-CP reduction was predicted to be about 16 hours in a solar-powered CP reactor. Only slight mass transfer limitation was predicted to occur.

CHAPTER 9: GENERAL CONCLUSIONS AND CONTRIBUTIONS TO ORIGINAL RESEARCH

Based on the results presented in previous chapters, the following general conclusions can be drawn as they relate to the contributions to original research. More specific observations have been attached to the end of the corresponding chapters as Concluding Remarks.

1. The newly proposed photocatalytic reactor, the corrugated plate reactor, was found to be up to 150% faster and energy-efficient than the flat plate reactor for the degradation of 4-CP. Its EE/O was estimated to be 37 kWh m^{-3} and was close to that of the slurry system examined. The optimal angle of the corrugated plate was found to be near 7°. These experimental results, together with the expected low capital, operating, and maintenance cost, and good scale-up potential of the new reactor indicate the novelty of the design. The superior performance of the new reactor is due primarily to its large illuminated catalyst surface area and its great capability to deliver both photons and reactants to catalyst surfaces.
2. Successful application of advanced mathematical methods and geometric optics, together with the development of the special procedure allowed for the calculation of the LASREA on corrugated plates. Multiple reflection was found to result in higher photon absorption efficiency as well as more uniform LASREA, which was revealed to be dependent strongly on the dimensions of the catalyst support. The photon absorption enhancement was calculated to be up to 100% for solar UV and 50% for rays from UV-A fluorescent lamps. This work is novel since a similar approach was never reported previously and simulation is the only way to obtain the LASREA on catalyst films. Widely used actinometry can provide neither the LASREA nor the overall photon absorption rate in a heterogeneous photoreactor.
3. Within the flowrate range examined, the corrugated plate reactor showed an enhancement of overall mass transfer rates of up to 400% to 600% over that of the flat

plate reactor. In addition, local mass and photon transfer rates on the corrugated plates correlated positively and therefore are complementary to each other. This result is favourable since a higher local photon absorption rate requires a higher mass transfer rate to avoid mass transfer limitation. Uniform LASREA on the catalyst film becomes optimal only if mass transfer limitations are eliminated.

4. With only three parameters fitted with the kinetic data, the new reactor model incorporates reaction kinetics, mass transfer as well as photon transfer and possesses reactor scale-up capability. As indicated by the results of the nonlinear regression, this model described the degradation of 4-CP in the flat plate reactor very well. The new model (together with the fitted parameters), predicted the performance of the corrugated plate reactors reasonably well. As confirmed by the experimental data, the effect of water flowrate and the angle of the corrugated plates on the overall reaction rate was clearly reflected by the model predictions. The agreement between the experimental data and the model predictions was very encouraging.

5. Corrugated plate reactors were predicted to suffer from mass transfer limitations of different degrees, depending on the water flow rate and the angle of the corrugated plate. The most effective way to alleviate this limitation is the use of corrugated plates of small angles. However, it is essentially impossible to eliminate mass transfer limitations on corrugated plates unless a weak illumination source is used because the smaller the angle of the corrugated plates, the less uniform the degree of mass transfer limitation on the corrugated plates. The region near the top of the corrugated plates suffers from more severe mass transfer limitation.

6. The degree of mass transfer limitation on a solar-illuminated corrugated plate is relatively uniform, thanks to the direct-parallel fraction of the solar irradiation. The time required for 90% 4-CP reduction was predicted to be about 16 hours in a solar-powered corrugated plate reactor. Only a slight mass transfer limitation was predicted to occur.

7. Simple Langmuir-Hinshelwood kinetic model fitted the photocatalytic 4-CP degradation

data very well and was therefore used to extract reaction rate information from the kinetic data. However, this model cannot be used for photoreactor scale-up due to the shortage of the terms representing the local mass and photon transfer rates on the surfaces of catalyst films.

8. The TiO_2 films immobilized on the stainless steel plates were physically and chemically stable during the course of the experiments. It possesses a thickness of approximately 10 microns, a porosity of approximately 80%, and a trace amount of iron on its surface.

9. The degradation rate of 4-CP, 2,4-dichlorophenol, and 2,4,5-trichlorophenol were found to be similar in terms of phenol concentration or TOC, regardless of the degree of chlorination. This observation indicates the advantage in using photocatalysis to detoxify highly chlorinated phenols.

10. Photocatalytic mineralization of the contaminants in the selected groundwater was slow even after carbonate and bicarbonate were removed. However, nitrification was enhanced significantly after only short periods of pretreatment in the photoreactor. The capital and operating costs to illuminate the photoreactor was estimated to be $0.011 per litre of groundwater pretreated. This indicates the potential for using photocatalysis to remove inhibition from biological nitrification systems.

11. Quantum efficiency is not as suitable as the EE/O in evaluating the energy efficiencies of photoreactor systems as it does not incorporate the efficiency in converting electricity or sunlight to absorbed photons. However, it could be used to estimate how far the energy efficiency of any particular system is from its upper limit based on the reaction mechanisms.

12. Photocatalysis on immobilized TiO_2 films can be limited by the transfer of either the oxidant (i.e., oxygen), the substances being oxidized (i.e., 4-CP), and/or the reaction products between the reaction sites and the main flow stream.

CHAPTER 10: RECOMMENDATIONS FOR FUTURE WORK

If future work is conducted in photocatalysis, the following are the possible directions in which the project may be extended:

1. Photocatalytic air purification and disinfection. Based on the results of this study, mass transfer limitation is usually a real concern for water phase photocatalysis in immobilized systems. It is very challenging to eliminate this limitation without sacrificing in other respects (i.e., pressure drop, photon transfer). Air phase photocatalysis is less likely to suffer from mass transfer problems due to the great diffusivity of most substances in the air. In addition, simultaneous detoxification and disinfection has market potential.
2. Reactor systems suitable for treating color and/or turbid streams. These streams are absorbing and therefore demand different systems for optimal treatment. The role of photolysis may be important for some streams. There is certainly a shortage of research in this respect.
3. Combined photocatalytic and biological treatment. Based on the result of this study, work in this direction may be fruitful. However, the use of artificial wastewater is not recommended due to the difficulty in applying the results to the treatment of actual industrial wastewater.
4. Solar-powered systems. Based on the cost estimation result of this study, the cost of purchasing, replacing, and operating the artificial lamps was very high and will affect considerably the competitiveness of this technology. This observation agrees with those reported previously.
5. Reactor modeling. As indicated in the literature review, there exists a shortage of work on the development of models which can be used in the development, design, and optimization of heterogeneous photoreactors.

6. Radiation modeling. There exists a shortage of radiation models in which the effect of scattering and reflection are considered. Correct radiation models are the keys for the modeling and scale-up of heterogeneous photoreactors since the LASREA can only be obtained this way. Actinometry can only be used to measure the overall rate at which photons enter the reactor. This method cannot give the overall rate of photon absorption (by catalyst film), let alone the LASREA.

7. New mass transfer model. The mass transfer model developed in this work is semi-empirical in nature and tends to be less reliable under turbulent flow conditions. A better mass transfer model may be obtained with the help of computational fluid dynamics.

REFERENCES

Abdullah, M., G.K.C. Low, and R.W. Matthews (1990); "Effects of Common Inorganic Anions on Rates of Photocatalytic Oxidation of Organic Carbon over Illuminated Titanium Dioxide", *J. Phys. Chem.*, 94, 6820-6825.

Aguado, M.A.; M.A. Anderson, and C.G. Jr. Hill (1994); "Influence of Light Intensity and Membrane Properties on the Photocatalytic Degradation of Formic Acid over TiO_2 Ceramic Membranes", *J. of Molecular Catal.*, 89, No.1-2, 165-178.

Ahmed, S. and D.F. Ollis (1984); "Solar Photoassisted Catalytic Decomposition of the Chlorinated Hydrocarbons Trichloroethylene and Trichloromethane", *Solar Energy*, 32, 597-601.

Akehata, T. and T. Shirai (1972); "Effect of Light Source Characteristics on the Performance of a Circular Annular Photochemical Reactor", *J. Chem. Eng. Jpn*, 5, No.4, 385-391.

Alberici, R.M. and W.F. Jardim (1994); "Photocatalytic Degradation of Phenol and Chlorinated Phenols Using Ag-TiO_2 in a Slurry Reactor", *Water Res.*, 28, No.8, 1845-1849.

Al-Ekabi, H., B. Butters, D. Delany, J. Ireland, N. Lewis, T. Powell, and J. Story (1993); "TiO_2 Advanced Photo-Oxidation Technology: Effect of Electron Acceptors", in Photocatalytic Purification and Treatment of Water and Air, Edited by D.F. Ollis and H. Al-Ekabi, Elsevier: Amsterdam, 321-334.

Al-Ekabi, H., N. Serpone, E. Pelizzetti, C. Minero, M.A. Fox, and R.B. Draper (1989); "Kinetic Studies in Heterogeneous Photocatalysis 2: TiO_2-Mediated Degradation of 4-Chlorophenol Alone and in a Three Component Mixture of 4-Chlorophenol, 2,4-Dichlorophenol, and 2,4,5-Trichlorophenol in Air Equilibrated Aqueous Media", *Langmuir*, 5, 250-255.

Al-Ekabi, H. and N. Serpone (1988); "Kinetic Studies in Heterogeneous Photocatalysis. 1. Photocatalytic Degradation of Chlorinated Phenols in Aerated Aqueous Solutions over TiO_2 Supported on a Glass Matrix", *J. Phys. Chem.*, 92, 5726-5731.

Alfano, O.M., R.L. Romero, and A.E. Cassano (1986a); "Radiation Field Modelling in Photoreactors-I: Homogeneous Media", *Chem. Eng. Sci.*, 41, No.3, 421-444.

Alfano, O.M., R.L. Romero, and A.E. Cassano (1986b); "Radiation Field Modelling in Photoreactors-II. Heterogeneous Media", Chem. Eng. Sci., 41, No.5, 1137-1153.

Al-Sayyed, G., J.C. D'Oliveira, and P. Pichat (1991); "Semiconductor-sensitized Photodegradation of 4-Chlorophenol in Water", *J. Photochem. Photobiol. A: Chem.*, 58, 99-114.

Anheden, M., D.Y. Goswami, and G. Svedberg (1995); "Photocatalytic Treatment of Wastewater from 5-fluorouracil Manufacturing", *ASME-Solar Eng./95.*

Assink, J.W. and T.P.M. Koster (1995); "Mass Transfer Limitation in Heterogeneous Photocatalytic Processes; A Design Rule for Activity Measurements", Proceedings of the 2nd Int. Conf. on Advanced Oxidation Technologies for Water and Air Remediation, London, Canada, p342.

Augugliaro, V., V. M.G. Loddo, L. Palmisano, and M. Schiavello (1995); "Performance of a Continuous Flat Reactor for Phenol Degradation in Heterogeneous Photocatalytic System", *Chem. Biochem. Eng. Q.*, 9, 133-139.

Augugliaro, V., M.J. López-Muñoz, L. Palmisano, and J. Soria (1993); "Influence of pH on the Degradation Kinetics of Nitrophenol Isomers in a Heterogeneous Photocatalytic System", *Appl. Catal. A: Gen.*, 101, 7-13.

Augugliaro, V., L. Palmisano, M. Schiavello, A. Sclafani, L. Marchese, G. Martra, and F. Miano

(1991); "Photocatalytic Degradation of Nitrophenols in Aqueous Titanium Dioxide Dispersion", *Appl. Catal.*, 69, No.2, 323-340.

Bahnemann, D., I. Fornefett, A. Renwrantz, U. Siebers, and R. Dillert (1995); "Photocatalytic Treatment of TNT-Polluted Water: Mechanism and Comparison with Other AOTs", Proceedings of the 2nd Int. Conf. on Advanced Oxidation Technologies for Water and Air Remediation, London, Canada, p236.

Bahnemann, D., D. Bockelmann, and R. Goslich (1991); "Mechanistic Studies of Water Detoxification in Illuminated TiO_2 Suspensions", *Solar Energy Materials*, 24, No.1-4, 564-583.

Barbeni, M., E. Pramauro, and E. Pelizzetti (1986); "Photochemical Degradation of Chlorinated Dioxins, Biphenyls, Phenols, and Benzene on Semiconductor Dispersion", *Chemosphere*, 15, 1913-1916.

Barbeni, M., E. Pramauro, and E. Pelizzetti (1984); "Photodegradation of 4-Chlorophenol Catalyzed by Titanium Dioxide Particles", *New J. Chem.*, 8, No.8/9, 547-550.

Blake, D.M., J. Webb, C. Yurchi, and K. Magrini (1991); "Kinetic and Mechanistic Overview of TiO_2 Photocatalyzed Oxidation Reactions in Aqueous Solution", *Solar Energy Materials*", 24, No.1-4, 584-593.

Blanco, G.J. and R.S. Malato (1994); "Solar Photocatalytic Mineralization or Real Hazardous Wastewater at Pre-industrial Level", *ASME-Solar Eng./94*, 103-109.

Bockelmann, D., R. Goslich, D. Weichgrebe, and D. Bahnemann (1993); "Comparing the Efficiencies of a Parabolic Reactor and a Novel Film Fixed Bed Reactor", in Photocatalytic Purification of Water and Air, Ollis, D. and H. Al-Ekabi Eds., Elsevier, New York, p771.

Bolduc, L. and W.A. Anderson (1997); "Enhancement of the Biodegradability of Model

Wastewater Containing Recalcitrant and Inhibitory Chemical Compounds by Photocatalytic Pre-oxidation", *Biodegradation*, 8, 237-249.

Bolton, J.R., K.G. Bircher, W. Tumas, and C.A. Tolman (1996); "Fgiures-of Merit for the Technical Development and Applications of Advanced Oxidation Processes", *J. Adv. Oxid. Technol.*, 1, 13-17.

Bolton, J.R., S.R. Cater, A. Safarzadeh-Amiri (1992); "The Use of Reduction Reactions in the Photodegradation of Organic Pollutants in Waste Streams", Proceedings of the 203rd ACS National Meeting, San Francisco, U.S.A.

Bonsen, E.M., S. Schroeter, H. Jacobs, and J.A.C. Broekaert (1997); "Photocatalytic Degradation of Ammonia with TiO_2 as Photocatalyst in the Laboratory and Under the Use of Solar Radiation", *Chemosphere*, 35, No.7, 1431-1445.

Brucato, A., D. Iatridis, L. Rizzuti, and P.L. Yue (1992); "Modeling of Light Transmittance and Reflectance in Flat Fluidized Bed Photoreactors", *Can. J. Chem. Eng.*, 70, 1063-70.

Cabrera, M.I., O.M. Alfano, and A.E. Cassano (1994); "Novel Reactor for Photocatalytic Kinetic Studies", *Ind. Eng. Chem. Res.*, 33, 3031-42.

Calderbank, P.H. and M. Moo-Young (1961); "The Continuous Phase Heat and Mass Transfer Properties of Dispersions", *Chem. Eng. Sci.*, 16, 39-54.

Cermenati, L, C. Guillard, P. Pichat, and A. Albini (1995); "Investigation of the Mechanism of the TiO_2 Photocatalytic Degradation of Aromatic Pollutants in Water by Use of a Model Molecule", Proceedings of the 2nd Int. Conf. on Advanced Oxidation Technologies for Water and Air Remediation, London, Canada, p234.

Chemseddine, A. and H.P. Boehm (1990); "A Study of the Primary Step in the Photochemical

Degradation of Acetic Acid and Chloroacetic Acids on a TiO_2 Photocatalyst", *J. Mol. Catal.*, 60, 295-311.

Chen, D. and A.K. Ray (1998); "Photodegradation Kinetics of 4-Nitrophenol in TiO_2 Suspensions", *Wat Res.*, No.11, 3223-3234.

Chen, L. C. and T. C. Chou (1994); "Photodecolorization of Methyl Orange Using Silver Ion Modified TiO_2 as Photocatalyst", *Ind. Eng. Chem. Res.*, 33, 1436-1443.

Cassano, A.E., C.A. Martín, R.J. Brandi, and O.M. Alfano (1995); "Photoreactor Analysis and Design: Fundamentals and Applications", *Ind. Eng. Chem. Res.*, 34, 2155-2201.

Chester, G., M. Anderson, H. Read, and S. Esplugas (1993); "A Jacketed Annular Membrane Photocatalytic Reactor for Wastewater Treatment: Degradation of Formic Acid and Atrazine", *J. Photochem. Photobiol., A*, 71, No.3, 291-7.

Choi, W and M.R. Hoffmann (1995); "Photoreductive Degradation of CCl_4 on TiO_2", Proceedings of the 2nd Int. Conf. on Advanced Oxidation Technologies for Water and Air Remediation, London, Canada, p293.

Crittenden, J.C., Y. Zhang, D.W. Hand, and D.L. Perram (1995); "Destruction of Organic Compounds in Water Using Fixed Bed Photocatalysts", *ASME-Solar Eng./95*, 449-457.

Cunningham, J. and P. Sedlák (1994); "Interrelationships Between Pollutant Concentration, Extent of Adsorption, TiO_2-sensitized Removal, Photon Flux and Levels of Electron or Hole Trapping Additives 1: Aqueous monochlorophenol-TiO_2(P25) Suspensions", *J. Photochem. Photobiol. A: Chem.*, 77, 255-263.

Curcó, D., S. Malato, J. Blanco, and J. Giménez (1996); "Photocatalysis and Radiation Absorption in a Solar Plant", *Solar Energy Materials and Solar Cells*, 44, 199-217.

D'Oliveira, J.C., G. Al-Sayyed, and P. Pichat (1990); "Photodegradation of 2- and 3-Chlorophenol in TiO_2 Aqueous Suspensions", *Environ. Sci. Technol.*, 24, No.7, 990-996.

Domènech, X (1993); "Photocatalysis for Aqueous Phase Decontamination: Is TiO_2 the Better Choice?", in Photocatalytic Purification of Water and Air, Edited by D.F. Ollis and H. Al-Ekabi, 337-351.

Draper, R.B. and M.A. Fox (1990); "Titanium Dioxide Photosensitized Reactions Studied by Diffuse Reflectance Flash Photolysis in Aqueous Suspensions of TiO_2 Powder", *Langmuir*, 6, No.8, 1396-1402.

Enzweiler, R. J., D.L. Mowery, L.M. Wagg, and J.J. Dong (1994); "Pilot Scale Investigation of Photocatalytic Detoxification of BETX Water", *ASME-Solar Eng./94*, 155-162.

Fernández, A., G. Lassaletta, V.M. Jiménez, A. Jasto, A.R. González-Elipe, J.M. Herrmann, H. Tahiri, and Y. Ait-Ichou (1995); "Preparation and Characterization of TiO_2 Photocatalysys Supported on Various Rigid Supports (Glass, Quartz, and Stainless Steel). Comparative Studies of Photocatalytic Activity in Water Purification", *Appl. Catal. B: Environmental*, 7, 49-63.

Fox, M.A. and M.T. Dulay (1993); "Heterogeneous Photocatalysis", *Chem. Rev.*, 93, 341-357.

Freudenhammer, H., D. Bahnemann, L. Bousselmi, S.U. Geissen, A. Ghrabi, F. Saleh, A. Si-Salah, U. Siemon, and A. Vogelpohl (1997); "Detoxification and Recycling of Wastewater by Solar-Catalytic Treatment", *Wat. Sci. Tech.*, 35, No.4, 149-156.

Fu, X., L.A. Clark, Q. Yang, and M.A. Anderson (1996); "Enhanced Photocatalytic Performance of Titania-Based Binary Metal Oxides: TiO_2/SiO_2 and TiO_2/ZrO_2", *Environ. Sci. Technol.*, 30, 647-653.

Fujishima, A (1995); "Photocatalytic Reaction for Environmental Applications", Proceedings

of the 2nd Int. Conf. on Advanced Oxidation Technologies for Water and Air Remediation, London, Canada, p226.

Fujihira, M., Y. Satoh, and T. Osa (1982); "Heterogeneous Photocatalytic Reactions on Semiconductor Materials. III. Effect of pH and Cu^{++} Ions on the Photo-Fenton Type Reaction", *Bull. Chem. Soc. Jpn.*, 55, 666-671.

Gao, Y.M., W. Lee, R. Trehan, D.K. Kershaw, and A. Wold (1991); "Improvement of Photocatalytic Activity of Titanium (IV) Oxide by Dispersion of AU on TiO_2", *Mat. Res. Bull.*, 26, 1247-1254.

Gerischer, H. and A. Heller (1992); "Photocatalytic Oxidation of Organic Molecules at TiO_2 Particles by Sunlight in Aerated Water", *J. Electrochemical Society*, 139, No.1, 113-118.

Glaze, W.H., J.F. Kenneke, and J.L. Ferry (1993); "Chlorinated Byproducts from the TiO_2-Mediated Photodegradation of Trichloroethylene and Tetrachloroethylene in Water", *Environ. Sci. Technol.*, 27, No.1, 177-184.

Goswami, D. Y. (1997); "A Review of Engineering Developments of Aqueous Phase Solar Photocatalytic Detoxification and Disinfection Processes", *J. Solar Energy Eng.*, 119, 101-107.

Goswami, D. Y., D.M. Trivedi, S.S. Block (1997); "Photocatalytic Disinfection of Indoor Air", *J. Solar Energy Eng.*, 119, 92-96.

Ha, H.Y. and M. Anderson (1996); "Photocatalytic Degradation of Formic Acid via Metal-Supported Titania", *J. Environ. Eng.*, 122, 217-221.

Haarstrick, A., O.M. Kut, and E. Heinzle (1996); "TiO_2-Assisted Degradation of Environmentally Relevant Organic Compounds in Wastewater Using a Novel Fluidized Bed Photoreactor", *Environ. Sci. Technol.*, 30, 817-824.

HACH (1998); HACH Analysis Procedure.

Hacker, D.S. and J.B. Butt (1975); "Photocatalysis in a Slurry Reactor", *Chem. Eng. Sci.*, 30, 1149-1158.

Harada, K., T. Hisanaga, and K. Tanaka (1990); "Photocatalytic Degradation of Organophosphorous Insecticides in Aqueous Semiconductor Suspensions", *Water Res.*, 24, No.11, 1415-1417.

Harriott, P. and R.M. Mamilton (1965); "Solid-Liquid Transfer in Turbulent Pipe Flow", *Chem. Eng. Sci.*, 20, 1073-1078.

Harriott, P. and R.M. Hamilton (1965); "Solid-Liquid Transfer in Turbulent Pipe Flow", *Chem. Eng. Sci.*, 20, 1073-1078.

Hayduk, W. and H. Laudie (1974); "Prediction of Diffusion Coefficients for Nonelectrolytes in Dilute Aqueous Solutions", *A.I.Ch.E. J.*, 20, 611-615.

Heinzle, E., F. Geiger, M. Fahmy, and O.M. Kut (1992); "Integrated Ozonation-Biotreatment of Pulp Bleaching Effluents Containing Chlorinated Phenolic Compounds", *Biotechnol. Prog.*, 8, 67-77.

Hess, T.F., T.A. Lewis, R.L. Crawford, S. Katamneni, J.H. Wells, and R.J. Watts (1998); "Combined Photocatalytic and Fungal Treatment for the Destruction of 2,4,6-Trinitrotoluene (TNT)", *Wat. Res.*, 32, No.5, 1481-1491.

Hoffman, M.R., S.T. Martin, W. Choi, and D.W. Bahnemann (1995); "Environmental Applications of Semiconductor Photocatalysis", *Chem. Rev.*, 95, 69-96.

Hofstadler, K., R. Bauer, S. Novallc, and K. Heisler (1994); "New Reactor Design for

Photocatalytic Wastewater Treatment with TiO_2 Immobilized on Fused-Silica Glass Fibres: Photomineralization of 4-Chlorophenol", *Environ. Sci. Technol.*, 26, 670-674.

Holden, W., A. Marcellino, D. Valic, and A.C. Weedon (1993); "Titanium Dioxide Mediated Photochemical Destruction of Trichloroethylene Vapors in Air", in Photocatalytic Purification and Treatment of Water and Air, Editted by D.F. Ollis and H. Al-Ekabi, Elsevier, Amsterdam, p393-404.

Howard, P.H., (1991); Handbook of Environmental Degradation Rates, Lewis Publishers.

Hsiao, C.Y., C.L. Lee, and D.F. Ollis (1983); "Heterogeneous Photocatalysis: Degradation of Dilute Solutions of Dichloromethane(CH_2Cl_2), Chloroform($CHCl_3$), and Carbon Tetrachloride(CCl_4), with Illuminated TiO_2 Photocatalyst", *J. Catalysis*, 82, 418-23.

Izumi, I., F.R. F. Fan, and A.J. Bard (1981); "Heterogeneous Photocatalytic Decomposition of Benzoic Acid and Adipic Acid on Platinized TiO_2 Powder. The Photo-Kolbe Decarboxylative Route to the Breakdown of the Benzene Ring and to the Production of Butane", *J. Phys. Chem.*, 85, 218-223.

Izumi, I., W.W. Dunn, K. O. Wilbourn, F.R.F. Fan, and A.J. Bard, (1980); "Heterogeneous Photocatalytic Oxidation of Hydrocarbon on Platinized TiO_2 Powders", *J. Phys. Chem.*, 84, No.24, 3207-3210.

Jacob, M. (1992); Photophysical and Photochemical Properties of Aromatic Compounds, CRC Press Inc., Roca Raton, Florida.

Jaeger, C. and A. Bard (1979); "Spin Trapping and Electron Spin Resonance Detection of Radical Ion: the Photodecomposition of Water at TiO_2 Particulate Systems", *J. Phys. Chem.*, 83, No.24, 3146-3152.

Jardim, W.F., S.G. Moraes, and M.M.K. Takiyama (1997); "Photocatalytic Degradation of Aromatic Chlorinated Compounds Using TiO_2: Toxicity of Intermediates", *Water Res.*, 31, 1728-1732.

Jochimsen, J.C. and M.R. Jekel (1997); "Partial Oxidation Effect During the Combined Oxidative and Biological Treatment of Separated Streams of Tannery Wastewater", *Wat. Sci. Tech.*, 35, No.4, 337-345.

Karpel, N., V. Leitner, E. Le Bras, E. Foucault, and J.L. Bousgarbiès (1997); "A New Photochemical Reactor Design for the Treatment of Absorbing Solutions", *Wat. Sci. Tech.*, 35, No.4, 215-222.

Karrer, N.J., G. Ryhiner, and E. Heinzle (1997); "Applicability Test for Combined Biological-Chemical Treatment of Wastewaters Containing Biorefractory Compounds", *Wat. Res.*, 31, No.5, 1013-1020.

Klausner, J.F., A.R. Martin, D.Y. Goswami, and K.S. Schanze (1994); "On the Accurate Determination of Reaction Rate Constants in Batch-type Solar Photocatalytic Oxidation Facilities", *J. Solar Energy Eng.*, 116 , No.1, 19-24.

Kondo, M.M. and W. Jardim (1991); "Photodegradation of Chloroform and Urea Using Ag-loaded Titanium Dioxide as Catalyst", *Water Res.*, 25, No.7, 823-827.

Krýsová, H., J. Krýsa, K. Macounová, and J. Jirkovský (1998); "Photocatalytic Degradation of Diuron [3-(3,4-Dichlorophenyl)-1,1-dimethylurea] on the Layer of TiO_2 Particles in the Batch Mode Plate Film Reactor", *J. Chem. Technol. Biotechnol.*, 72, 169-175.

Ku, Y. and C.B. Hsieh (1992); "Photocatalytic Decomposition of 2,4-Dichlorophenol in Aqueous TiO_2 Suspensions", *Water Res.*, 26, No.11, 1451-1456.

Lawless, D., N. Serpone, and D.J. Meisel (1991); "Role of $OH^{\cdot}$ Radicals and Trapped Holes in Photocatalysis. A Pulse Radiolysis Study", *J. Phys. Chem.*, 95, 5166-5170.

Lee, C.C.H. (1995); Photocatalytic Degradation of Aqueous-Phase Organic Contaminants in a Fluidized Bed Reactor; M.A.Sc. Thesis, Chemical Engineering, University of Waterloo.

Lee, W., Y.R. Do, K. Dwight, and A. Wold (1993); "Enhancement of Photocatalytic Activity of Titanium(IV) Oxide with Molybdenum (VI) Oxide", *Materials Res. Bulletin*, 28, No.11, 1127-1134.

Legrini, O., E. Oliveros, and A.M. Braun (1993); "Photocatalysis Processes for Water Treatment", *Chem. Rev.*, 93, 671-698.

Lepore, G.P., B.C. Pant, and C.H. Langford (1993); "Limiting Quantum Yield Measurements for the Disappearance of 1-Propanol and Propanols: an Oxidative Reaction Study Employing a TiO_2 Based Photoreactor", *Can J. Chem.*, 71, 2051-2059.

Lichtin, N.N. and M. Avudaithai (1996); "TiO_2- Photocatalyzed Oxidative Degradation of CH_3CN, CH_3OH, C_2HCl_3, and CH_2Cl_2 Supplied as Vapors and in Aqueous Solution under Similar Conditions", *Environ. Sci. Technol.*, 30, 2014-2020.

Lin, W.Y. and K. Rajeshwar (1997); "Photocatalytic Removal of Nickel from Aqueous Solutions Using Ultraviolet-Irradiated TiO_2", J. Electrochem. Soc., 144, 2751-2756.

Lindner, M., J. Theurich, and D.W. Bahnemann (1997); "Photocatalytic Detoxification of Organic Compounds: Accelerating the Process Efficiency", *ASME- Solar Eng./95*, 399-408.

Lindner, M., D.W. Bahnemann, B. Hirthe, and W.D. Griebler (1995); "Solar Water Detoxification: Novel TiO_2 Powders as Highly Active Photocatalysts", *ASME- Solar Eng./95*, 399-408.

Linsebigler, A.L., G. Lu, and J.T. Yates, (1995); "Photocatalysis on TiO_2 Surfaces: Principles, Mechanisms, and Selected Results", *Chem. Rev.*, 93, 735-758.

Low, G.K.C., S.R. McEovy, and R.W. Matthews (1991); "Formation of Nitrate and Ammonium Ions in Titanium Dioxide Mediated Photocatalytic Degradation of Organic Compounds Containing Nitrogen Atoms", *Environ. Sci. Technol.*, 25, 460-467.

Low, G. and R.W. Matthews (1990); "Flow-Injection Determination of Organic Contaminants in Water Using an Ultraviolet Mediated Titanium Dioxide Film Reactor", *Analytica Chimica Acta*, 231, No.1, 13-20.

Luo, Y. (1994); Reactor Analysis for Heterogeneous Photocatalytic Air Purification Processes, Ph.D. Dissertation, North Carolina State University.

Lyman, W.J. , W.F. Reehl,, and D.H. Rosenblatt (1982); Handbook of Chemical Property Estimation Methods, McGraw-Hill, New York, USA.

Malato, S., J. Blanco, C. Richter, D. Curcó, and J. Giménez (1997); "Low- Concentration CPC Collectors for Photocatalytic Water Detoxification: Comparison with a Medium Concentrating Solar Collector", *Wat. Sci. Tech.*, 35, No.4, 157-164.

Manilal, V.B., A. Haridas, R. Alexander, and G.D. Surender (1992); "Photocatalytic Treatment of Toxic Organics in Wastewater: Toxicity of Photodegradation Products", *Water Res.*, 26, No.8, 1035-1038.

Mao, Y., C. Schöneich, and K.D. Asmus (1991); "Identification of Organic Acids and Other Intermediates in Oxidative Degradation of Chalrinated Ethanes on TiO_2 Surfaces en Route to Mineralization: a Combined Photocatalytic and Radiation Chemical Study", *J. Phys. Chem.*, 95, No.24, 10080-10089.

March, M., A. Martin, and C. Saltiel (1995); "Performance Modeling of Nonconcentrating Solar Detoxification Systems", *Solar Energy*, 54, No.3, 143-15.

Marinangeli, R.E. and D.F. Ollis (1980); "Photo-assisted Heterogeneous Catalysis with Optical Fibres: II. Nonisothermal Single Fibre and Fibre Bundle", *A.I.Ch.E. J.*, 26, No.6, 1000-1008.

Marinangeli, R.E. and D.F. Ollis (1977); "Photo-assisted Heterogeneous Catalysis with Optical Fibres: I. Isolated Single Fibre", *A.I.Ch.E. J.*, 23, No.4, 415-426.

Martin, S.T., A.T. Lee, and M.R. Hoffman (1995); "Chemical Mechanism of Inorganic Oxidants in the TiO_2/UV Process: Increased Rates of Degradation of Chlorinated Hydrocarbons", *Environ. Sci. Technol.*, 29, 2567-2573.

Martin, S.T., H. Herrmann, W. Choi, and M.R. Hoffmann (1995); "Photochemical Destruction of Chemical Contaminants on Quantum-Sized Semiconductro Particles", *ASME-Solar Eng./95*, 409-413.

Maruyama, T. and T. Nishimoto (1992); "Light Intensity Profile in Heterogeneous Photochemical Reactor", *Chem. Eng. Comm.*, 117, 111-116.

Matthews, R. W. and S.R. McEvoy (1992); "Destruction of Phenol in Water with Sun, Sand, and Photocatalysis", *Solar Energy*, 49 , No.6, 507-513.

Matthews, R.W (1991); "Photooxidative Degradation of Colored Organics in Water Using Supported Catalysts. TiO_2 on Sand", *Water Res.*, 25, No.10, 1169-1176.

Matthews, R.W. (1990); "Purification of Water with near-UV Illuminated Suspensions of Titanium Dioxide", *Water Res.*, 24, No.5, 653-660.

Matthews, R.W. (1988); "Kinetics of Photocatalytic Oxidation of Organic Solutes over Titanium

Dioxide", *J. Catalysis*, 111, 264-272.

Matthews, R.W. (1987a); "Solar-Electric Water Purification Using Photocatalytic Oxidation with TiO_2 as a Stationary Phase", *Solar Energy*, 38, No.6, 405-413.

Matthews, R.W. (1987b); "Photooxidation of Organic Impurities in Water Using Thin Films of Titanium Dioxide", *J. Phys. Chem.*, 91, 3328-33.

Matthews, R.W. (1984); "Hydroxylation Reactions Induced by Near-ultraviolet Photolysis of Aqueous Titanium Dioxide Suspensions", *J. Chem. Soc. Faraday Trans. I.*, 80, 457-471.

McCabe, W.L., J.C. Smith, and P. Harriott (1993); Unit Operations of Chemical Engineering, 5th Edition, McGrw-Hill Inc.

McISAAC, L.J. (1995); Mass Transfer at Rough Surfaces in the Transitional Regime, M.A.Sc. Thesis, University of Waterloo, Canada.

Mehos, M.S. and C.S. Turchi (1993); "Field Testing Solar Photocatalytic Detoxification on TCE-Contaminated Groundwater", *Environ. Prog.*, 12, No.3, 194-199.

Mehrvar, M. (1998); Kinetic Modeling and a Novel Packed Bed Photocatalytic Reactor, Ph.D. Dissertation, Univ. of Waterloo, Canada.

Mikesell, M.D. and S.A. Boyd (1985); "Reductive Dechlorination of the Pesticides 2,4-D, 2,4,5-T, and Pentachlorophenol in Anaerobic Sludges", *J. Environ. Quality*, 14, No.3, 337-340.

Mills, G. and M.R. Hoffmann (1993); "Photocatalytic Degradation of Pentachlorophenol on TiO_2 Particles: Identification of Intermediates and Mechanism of Reaction", *Environ. Sci. Technol.*, 27, No.8, 1681-1689.

Mills, A. and S. Morris (1993); "Photo-mineralization of 4-Chlorophenol Sensitized by Titanium Dioxide: a Study of the Initial Kinetics of Carbon Dioxide Photo-generation", *J. Photochem. Photobiol. A: Chem.*, 71, 75-83.

Munuera, G., V. Rives-Arnau and A. Saucedo (1979); "Photo-adsorption and Photo-desorption of Oxygen on Highly Hydroxylated TiO_2 Surfaces", *J. Chem. Soc. Faraday Trans. I.*, 75, 736-747.

Murabayashi, M., K. Itoh, K. Kawashima, R. Masuda, and S. Suzuki (1993); "Photocatalytic Degradation of Chloroform with TiO_2-Coated Glass Fibre Cloth", in Proceedings of the 1st Int. Conf. on TiO_2 Photocatalytic Purification and Treatment of Water and Air, Elsevier Science Publishers B.V., Amsterdam, The Netherland, 783-788.

Noulty, R.A. and D.G. Lealst (1987); "Diffusion Coefficient of Aqueous Benzoic Acid at 25 °C", *J. Chem. & Engng Data*, 32, No.4, 418-420.

Ogata, I, I. Urakami, T. Inaba, R. Masuda, I. Kitamura, K. Itoh, and M. Murabayashi (1995); "Effect of Thickness of TiO_2 Layer Supported on Glass Fibre on the Rate and Selectivity of Photocatalytic Decomposition of Organic Compounds in Water", Proceedings of the 2nd Int. Conf. on Advanced Oxidation Technologies for Water and Air Remediation, London, Canada, p269.

Ohko, Y., K. Hashimoto, and A. Fujishima (1997); "Kinetics of Photocatalytic Reactions Under Extremely Low-Intensity UV Illumination on Titanium Dioxide Thin Films", *J. Phys. Chem.*, 101, 8057-8062.

Okamoto, K., Y. Yamamoto, H. Tanaka, M. Tanaka, and A. Itaya (1985a); "Heterogeneous Photocatalytic Decomposition of Phenol over TiO_2 Powder", *Bull. Chem. Soc. Jpn.*, 58, 2015-2022.

Okamoto, K., Y. Yamamoto, H. Tanaka, M. Tanaka, and A. Itaya (1985b); "Kinetics of Heterogeneous Photocatalytic Decomposition of Phenol over Anatase TiO_2 Powder", *Bull. Chem. Soc. Jpn.*, 58, 2023-2038.

Ollis, D. F., E. Pelizzetti, and N. Serpone (1991); "Destruction of Water Contaminants", *Environ. Sci. Technol.*, 25, No.9, 1523-1529.

Ollis, D.F. (1991); Photochemical Conversion and Storage of Solar Energy, Edited by E. Pelizzetti and M. Schiavello, Kluwer Academic, Dordrecht, The Netherlands, p593-622.

Ollis, D.F. and C. Turchi (1990); "Heterogeneous Photocatalysis for Water Purification: Contaminant Mineralization Kinetics and Elementary Reactor Analysis", *Environ. Prog.*, 9, No.4, 229-234.

Ollis, D.F., E. Pelizzetti, and N. Serpone (1989); "Heterogeneous Photocatalysis in the Environment: Application to Water Purification", in Photocatalysis: Fundamentals and Applications, Edited by N. Serpone and E. Pelizzetti, John Wiley & Sons, p603-637.

Ollis, D. F. (1988); "Process Economics for Water Purification: Comparative Assessment", in Photocatalyis and Environment, M. Schiavello (ed.), 663-677, Kluwer Academic Publishers.

Ollis, D.F. (1985); "Contaminant Degradation in Water", *Environ. Sci. Technol.*, 19, No.6, 480-484.

Ollis, D. F., C.Y. Hsiao, L. Budiman, and C.L. Lee (1984); "Heterogeneous Photoassisted Catalysis: Conversions of Perchloroethylene, Dichloroethane, Chloroacetic Acids, and Chlorobenzenes", *J. Catal.*, 88, 89-96.

Pacheco, J.E., M.R. Prairie, and L. Yellowhorse (1993); "Photocatalytic Destruction of Chlorinated Solvents in Water with Solar Energy", *J. Solar Energy Eng.*, 115, No.3, 123-129.

Pacheco, J., A.S. Watt, and C.S. Turchi (1993); "Solar Detoxification of Water: Outdoor Testing of Prototype Photoreactors", *ASME-Solar Eng./93*, 43-49.

Palmisano, L., V. Augugliaro, M. Schiavello, and A. Sclafani (1989); "Influence of Acid-base Properties on Photocatalytic and Photochemical Processes", *J. Molecular Catal.*, 56 , No.1-3, 284-295.

Papp, J., H.S. Shen, R. Kershaw, K. Dwight, and A. Wold (1993); "Titanium (IV) Oxide Photocatalysts with Palladium", *Chemistry of Materials*, 5, No.3, 284-288.

Parent, Y., D. Blake, B.K. Magrini, C. Lyons, C. Turchi, A. Watt, E. Wolfrum, and M. Prairie (1996); "Solar Photocatalytic Processes for the Purification of Water: State of Development and Barriers to Commercialization", *Solar Energy,* 56, 429-437.

Pasquali, M., F. Santarelli, J.F. Porter, and P.L. Yue (1996); "Radiative Transfer in Photocatalytic Systems", *A.I.Ch.E. J.*, 42, 532-537.

Peill, N. J. and M.R. Hoffmann (1997); "Solar-Powered Photocatalytic Fiber-Optic Cable Reactor for Waste Stream Remediation", *J. Solar Energy Eng.*, 119, 229-236.

Peill, N.J. and M.R. Hoffmann (1996); "Chemical and Physical Characterization of a TiO_2-Coated Fibre-Optic Cable Reactor", *Environ. Sci. Technol.*, 30, 2806-2812.

Peill, N.J. and M.R. Hoffmann (1995); "Development and Optimization of a TiO_2-Coated Fibre-Optic Cable Reactor: Photocatalytic Degradation of 4-Chlorophenol", *Environ. Sci. Technol.*, 29, 2974-2981.

Pelizzetti, E., V. Carlin, C. Minero, and M. Gräzel (1991); "Enhancement of the Rate of Photocatalytic Degradation on TiO_2 of 2-Chlorophenol, 2,7-Dichlorobibenzodioxin, and Atrazine by Inorganic Oxidizing Species", *New J. Chem.*, 15, 351-359.

Pelizzetti, E., V. Maurino, C. Minero, V. Carlin, E. Pramauro, O. Zerbinati, and M.L. Tosato (1990); "Photocatalytic Degradation of Atrazine and Other s-triazine Herbicides", *Environ. Sci. Technol.*, 24, No.10, 1559-1565.

Perry, R.H., D.W. Green, and J.O. Maloney (1984); Perry's Chemical Engineers' Handbook, 6th Edition, McGraw-Hill, New York, USA.

Peyton, G.R. and W.H. Glaze (1988); "Destruction of Pollutants in Water with Ozone in Combination with Ultraviolet Radiation 3: Photolysis of Aqueous Ozone", *Environ. Sci. Technol.* 22, 761-767.

Philip Lighting Company (1998); Specialty Catalog, Sommerset, New Jersey.

Prairie, M.R., L. R. Evans, B.M. Stange, and S.L. Martinez (1993); "An Investigation of TiO_2 Photocatalysis for the Treatment of Water Contaminated with Metals and Organic Chemicals", *Environ. Sci. Technol.*, 27, 1776-1782.

Preis, S., M. Krichevskaya, and A. Kharchenko (1997); "Photocatalytic Oxidation of Aromatic Aminocompounds in Aqueous Solutions and Groundwater from Abandoned Military Bases", *Wat. Sci. Tech.*, 35, No.4, 265-272.

Pugh, K.C., D.J. Kiserow, J.M. Sullivan, and J.H. Grinstead Jr. (1995); "Photocatalytic Destruction of Atrazine Using TiO_2 Mesh", in Emerging Technologies in Hazardous Waste Management V, 174-194.

Puma, G.L. and P.L. Yue (1994); "Effects of Radiation Wavelength on the Rate of Mineralization of Organics by Heterogeneous Photocatalysis", Proceedings of the 1st Int. Conf. on Advanced Oxidation Technologies for Water and Air Remediation, London, Canada, p308.

Rabek, J.F. (1983); Experimental Methods in Photochemistry and Photophysics, John Wiley &

Sons.

Ray, K. and A.C.M. Beenackers (1998); "Development of a New Photocatalytic Reactor for Water Purification", *Catalysis Today*, 40, 73-83.

Ray, K. and A.C.M. Beenackers (1997); "Novel Swirl-Flow Reactor for Kinetic Studies of Semiconductor Photocatalysis", *AIChE J.*, 43, 2571-2578.

Reeves, P., R. Ohlhausen, D. Sloan, K. Pamplin, T. Scoggins, C. Clark, B. Hutchinson, and D. Green (1992); "Photocatalytic Destruction of Organic Dyes in Aqueous Suspensions Using Concentrated Simulated and Natural Solar Energy", *Solar Energy*, 48 , No.6, 413-420.

Rice, R.G. and D.D. Do (1995); Applied Mathematics and Modeling for Chemical Engineers, John Wiley & Sons Inc.

Rizzuti, L., 1985; "Absorption of Light Energy in Photoreactors", in Photoelectrochemistry, Photocatalysis and Photoreactors, Edited by M. Schiavello, D. Reidel Publishing, 587-604.

Nair, M.L., Z. Luo, and A. Heller (1993); "Rates of Photocatalytic Oxidation of Crude Oil on Salt Water on Buoyant, Cenosphere-attached Titanium Dioxide", *I&EC Chem. Res.*, 32, No.10, 2318-2323.

Roche, W.J. (1993); "High Temperature Behaviour of Compact Fluorescent Lamps", *J. Illumin. Eng. Soc.*, 97-103.

Roger, M. and J. Villermaux (1979); "Modelling of Light Absorption in Photoreactors: Part I. General Formulation Based on the Laws of Photometry", *Chem. Eng. J.*, 17, 219-226.

Rohm and Haas Company (1985); Ultraviolet Filtering and Transmitting Formulations of Plexiglas Acrylic Plastic, Product Manual.

Romero, R. L. , O.M. Alfano, and A.E. Cassano (1997); "Cylindrical Photocatalytic Reactors. Radiation Absorption and Scattering Effects Produced by Suspended Fine Particles in an Annular Space", *Ind. Eng. Chem. Res.*, 36, 3094-3109.

Sabate, J., Anderson, M.A., Kikkawa, H., Edwards, M., and Hill Jr., C.G. (1991); "A Kinetic Study of the Photocatalytic Degradation of 3-Chlorosalicylic Acid over TiO_2 Membranes Supported on Glass", *J. Catalysis*, 127, 167-77.

Sabin, F., T. Turk, A. Vogler (1992); "Decontamination of Industrial Waste Water by Photocatalytic Oxidation of Organic Components: A Model Study", *Zeitschrift fuer Wasser - und Abwasser Forschung*, 25, No. 3, 163-167.

Saltiel, C., A. Martin, and D.Y. Goswami (1992); "Performance Analysis of Solar Water Detoxification Systems by Detailed Simulation", *ASME-Solar Eng./92*, 21-28.

Sclafani, A., L. Palmisano, and E. Davì (1990); "Photocatayltic Degradation of Phenol by TiO_2 Aqueous Dispersions: Rutile and Anatase Activity", *New J. Chem.*, 14, 265-268.

Scott, J.P. and D.F. Ollis (1996); "Engineering Models of Combined Chemical and biological Processes", *J. Environ. Eng.*, 122, 1110-1114.

Scott, J.P. and D.F. Ollis (1995); "Integration of Chemical and Biological Oxidation Processes for Water Treatment: Review and Recommendations", *Environ. Prog.*, 14, No.2, 88-103.

Sczechowski, J.G. (1995); "Applying Controlled Periodic Illumination in a Taylor Vortex Reactor to Increase the Photoefficency in Heterogeneous Photocatalysis", *ASME-Solar Eng./95*, 459-466.

Serpone, N., E. Borgarello, R. Harris, P. Cahill, M. Borgarello, and E. Pelizzetti (1986); "Photocatalysis over TiO_2 Supported on a Glass Substrate", *Solar Energy Materials*, 14, 121-7.

Serrano, B. and H. de Lasa (1997); "Photocatalytic Degradation of Water Organic Pollutants. Kinetic Modeling and Energy Efficiency", *Ind. Eng. Chem. Res,* 36, 4705-4711.

Siegel, R. and J.R. Howell (1992); Thermal Radiation Heat Transfer, 3rd ed., Hemisphere Publishing Co.: Bristol, PA.

Stafford, U., K.A. Gray, and P.V. Kamat (1997a); "Photocatalytic Degradation of 4-Chlorophenol: The Effects of Varying TiO_2 Concentration and Light Wavelength", *J. of Catal.*, 167, 25-32.

Stafford, U., K.A. Gray, and P.V. Kamat (1997b); "Photocatalytic Degradation of 4-Chlorophenol: A Mechanically-Based Model", *Res. Chem. Intermed.*, 23, 355-388.

Stephen, H. and T. Stephen (1963); Solubilities of Inorganic and Organic Compounds: Binary Systems Part I, p470, The Macmillan Company, New York.

Stevens, R.D.S. and B. Mourad (1995); "All Watts Are not Created Equal: the Importance of Lamp Output on UV/Oxidation System Performance", Proceedings of the 2nd Int. Conf. on Advanced Oxidation Technologies for Water and Air Remediation, London, Canada, p255.

Suri, R., J. Liu, D.W. Hand, J.C. Crittenden, D.L. Perram, and M.E. Mullins, (1993); "Heterogeneous Photocatalytic Oxidation of Hazardous Organic Contaminants in Water", *Water Environ. Res.*, 65 , No.5, 665-673.

Tada, H., and M. Tanaka (1997); "Dependence of TiO_2 Photocatalytic Activity Upon Its Film Thickness", *Langmuir*, 13, 360-364.

Tanaka, K. and T. Hisanaga (1994); "Photodegradation of Chlorofluorocarbon Alternatives on Metal Oxide", *Solar Energy*, 52, No.5, 447-450.

Tanaka, S. and T. Ichikawa (1993); "Effects of Photolytic Pretreatment on Biodegradation and Detoxification of Surfactants in Anaerobic Digestion", *Wat. Sci. Tech.*, 28, No.7, 103-110.

Tanaka, K., M.F.V. Capule, and T. Hisanaga (1991); "Effect of Crystallinity of TiO_2 on Its Photocatalytic Action", *Chem. Phys. Lett.*, 187, No.1-2, 73-76.

Tanaka, K., T. Hisanaga, and K. Harada (1989); "Photocatalytic Degradation of Organohalide Compounds in Semiconductor Suspension with Added Hydrogen Peroxide", *New J. Chem.*, 13, No.1, 5-7.

Terzian, R., N. Serpone, R.B. Draper, M.A. Fox, and E. Pelizzetti (1991); *Langmuir*, 7, 3081-3089.

Trillas, M., J. Peral, and X. Domènech (1996); "Photocatalyzed Degradation of Phenol, 2,4-Dichlorophenol, Phenoxyacetic Acid, and 2,4-dichlorophenoxyacetic Acid Over Supported TiO_2 in a Flow System", *J. Chem Technol. & Biotechnol.*, 67, 237-242.

Tsekov, R. and P.G. Smirniotis (1997); "Radiation Field in Continuous Annular Photocatalytic Reactors: Role of the Lamp Finite Size", *Chem. Eng. Sci.*, 52, 1667-1671.

Tseng, J.M., and C.P. Huang (1991); "Removal of Chlorophenols from Water by Photocatalytic Oxidation", *Wat. Sci. Tech.*, 23, 377-387.

Turchi, C. S., M.S. Mehos (1994); "Solar Photocatalytic Detoxification of Groundwater: Developments in Reactor Design", *Chem. Oxid.*, 2, 301-14.

Turchi, C.S. (1990); Heterogeneous Photocatalytic Degradation of Organic Water Contaminants: Kinetics and Hydroxyl Radical Mechanism, Ph.D. Dissertation, Chemical Engineering, North Carolina State University.

Turchi, C.S. and D.F. Ollis (1990); "Photocatalytic Degradation of Organic Water Contaminants: Mechanisms Involving Hydroxyl Radical Attack", *J. Catal.*, 122, 178-92.

Turchi, C.S. and D.F. Ollis (1989); "Mixed Reactant Photocatalysis: Intermediates and Mutual Rate Inhibition", *J. Catal.*, 119, 483-96.

Turchi, C.S., L. Edmundson, and D.F. Ollis (1989); "Application of Heterogeneous Photocatalysis for the Destruction of Organic Contaminants from a Paper Mill Alkali Extraction Process", paper Presented at TAPPI 5th Int. Symp. On Wood and Pulping Chemistry, Raleigh, NC.

Turchi, C.S. and D.F. Ollis (1988); "Photocatalytic Reactor Design: An Example of Mass-Transfer Limitations with an Immobilized Catalyst", *J. Phys. Chem.*, 92, 6852-6853.

Uchida, H., S. Itoh, and H. Yoneyama (1993); "Photocatayltic Degradation of Propyzamide Using TiO_2 Supported on Activated Carbon", *Chem. Lett.*, 12, 1995-1998.

Valladares, J.E. (1995); A New Photocatalytic Reactor for the Degradation of Organic Contaminants in Water, Ph.D. Dissertation, Chemistry, University of Western Ontario.

Valladares, J.E. and J. R. Bolton, (1993); "A Method for the Determination of Quantum Yields in Heterogeneous Systems: the TiO_2 Photocatalyzed Bleaching of Methylene Blue", in Photocatalytic Purification of Water and Air, Ollis, D. and H. Al-Ekabi Eds., Elsevier, New York, p111.

Vandevivere, P.C., R. Bianchi, and W. Verstraete (1998); "Treatment and Reuse of Wastewater from the Textile Wet-Processing Industry: Review of Emerging Technologies", *J. Chem. Technol. Biotechnol.*, 72, 289-302.

Verschueren, K. (1983); Environmental Data on Organic Chemicals, Van Nostrand Reinhold

Company.

Vinodgopal, K., U. Stafford, K.A. Gray, and P.V. Kamat (1994); "Electrochemically Assisted Photocatalysis. 2. Role of Oxygen and Reaction Intermediates in the Degradation of 4-Chlorophenol on Immobilized TiO_2 Particle Films", *J. Phys. Chem.*, 98, 6797-6803.

Vohra, M.S. and A. Davis (1993); "Photocatalytic Oxidation: the Process and Its Practical Applications", Hazardous and Industrial Wastes - Proceedings of the Mid-Atlantic Industrial Waste Conference, p 275-282.

Wang, S. (1989); Fundamentals of Semiconductor Theory and Device Physics, 1st ed., Eaglewood Cliffs, NJ: Printice-Hall Publishers.

Watts, R.J., S. Kong, M.P. Orr, and G.C. Miller (1994); "Titanium Dioxide-Mediated Photocatalysis of a Biorefractory Chloroether in Secondary Wastewater Effluent", *Environ. Technol.*, 15, No.5, 469-475.

Wei, T. Y. and C. C. Wan (1991); "Heterogeneous Photocatalytic Oxidation of Phenol with Titanium Dioxide Powders", *Ind. Eng. Chem. Res.*, 30, No.6, 1293-1300.

Well, M.V., R.H.G. Dillert, D.W. Bahnemann, and V.W. Benz, and M.A. Müller (1996); "A Novel Non-Concentrating Reactor for Solar Water Detoxification", *ASME-Solar Eng./96*, 43-52.

Wilkinson, S.L. (1994); Heterogeneous Photocatalysis in a Flat Plate Reactor, M.A.Sc. Thesis, Chemical Engineering, University of Waterloo.

World Health Organization (1976); Polychlorinated Biphenyls and Terphenyls.

Yokota, T., T. Iwano, and T. Tadaki (1976); "Light Intensity in an Annular Photochemical Reactor", *Kagaku Kogaku*, 2, 298-303.

Yoneyama, H., H. Uchida, S. Kuwabata, and S. Itoh (1994); "Enhancement of Photodegradation Rate of Dilute Organic Pollutants on TiO_2 Photocatalyst with Use of Inert Adsorbent as the Support", Proceedings of the 1st Int. Conf. on Advanced Oxidation Technol. for Water and Air Remediation, London, Canada, 112-113.

Yu, Y.H. and S.T. Hu (1994); "Preoxidation of Chlorophenolic Wastewaters for Their Subsequent Biological Treatment", *Wat. Sci. Tech.*, 29, 313-320.

Yue, P.L. (1993); "Modeling of Kinetics and Reactor for Water Purification by Photo-oxidation", *Chem. Eng. Sci.*, 48, No.1, 1-11.

Zaidi, A.H., D.Y. Goswami, and A.C. Wilkie (1993); "Solar Photocatalytic Post-Treatment of Anaerobically Digested Distillery Effluent", Proceedings of the American Solar Energy Society Annual Conference, Minneapolis, MN, p51-56.

Zeltner, W.A., C.G. Hill, Jr., and M.A. Anderson (1993); "Supported Titania for Photodegradation", *CHEMTECH*, 21-28.

Zhang, Yin (1994); Detoxification of Water Using Fixed-Bed Photocatalysts, Ph.D. Dissertation, Environmental Engineering, Michigan Technological University.

Zhang, Y., J.C. Crittenden, D.W. Hand, and D.L. Perram (1994); "Fixed Bed Photocatalysts for Solar Decontamination of Water", *Environ. Sci. Technol.*, 28, 435-442.

US PATENT

Berman, E. and A. Grayfer (1998); "Fibrous Matte Support for the Photopromoted Catalyzed Degradation of Compounds in a Fluid Stream", US Patent No. 5,766,455.

Bischoff, B.L., E. Fain, and J.A.D. Stockdale (1999); "Photocatalytic Reactor", US Patent No. 5,862,449.

Butters, B.E. and A.L. Powell (1995); "Method and System for Photocatalytic Decontamination", US Patent No. 5,462,674.

Cooper, G. (1998); "Cartridge for Photocatalytic Purification of Fluids", US Patent No. 5,736,055.

de Lasa, H.I. and J. Valladares (1997); "Photocatalytic Reactor", US Patent No. 5,683,589.

Dong, J. and E. Berman (1996); "Apparatus and Method for the Photopromoted Catalyzed Degradation of Compounds in a Fluid Stream", US Patent No. 5,516,492.

Gonzalez-Martin, A., O.J. Murphy, and D. Hodko (1998); "Photocatalytic Oxidation of Organics Using a Porous Titanium Dioxide Membrane and an Efficient Oxidant", US Patent No. 5,779,992.

Kennedy, III and C. James (1996); "Method and Apparatus for Optimizing Control of an Immobilized Film Photoreactor", US Patent No. 5,494,643.

Langford, C.H., G.P. Lepore, and L. Persaud (1997); "Photocatalyst with Modified Alkyl Silicate Ester Support and Process for Production Thereof", US Patent No. 5,685,372.

Raupp, G.B. and L.A. Dibble (1991); "Gas-Solid Photocatalytic Oxidation of Environmental Pollutants", US Patent No. 5,045,288.

Robertson, M.K. and R.B. Henderson (1990); "Fluid Purification", US Patent No. 4,966,759.

Say, J., R. Bonnecaze, A. Heller, S. Sitkiewitz, E. Heller, and P. Haugsja (1998); "Apparatus

for Photocatalytic Fluid Purification", US Patent No. 5,790,934.

Sczechowski, J.G., C.A. Koval, and R.D. Noble (1995); "Use of Controlled Periodic Illumination for an Improved Method of Photocatalysis and an Improved Reactor Design", US Patent No. 5,439,652.

APPENDIX A: RADIATION MODEL DEVELOPMENT

A.1: Calculation of the Spectral Specific Irradiance

Lamp Radiation:

Figure A-1 shows the manufacture's data on the relative spectral power of the fluorescent lamps used in this study. As shown in this figure, a normal distribution function (σ=15.75 nm, λ_{avg}= 353 nm) was found to fit these data quite well. The lamps were arranged such that the UV-A reading of the radiometer was constant (let it be "w") over the entire reactor cover. Therefore, the spectral irradiance at any point of the reactor cover can be expressed as:

$$w_\lambda = \frac{w}{\sqrt{2\pi\sigma}} e^{-\frac{(\lambda-353)^2}{2\sigma^2}} \qquad \text{(A-1)}$$

Based on radiation energy balance over a unit hemisphere and Assumption (1) in Section 6.1, the spectral specific irradiance at any point of the reactor cover can be expressed as:

$$w_{\lambda\psi} = \frac{w_\lambda}{\pi}\cos\psi = \frac{w\cos\psi}{\pi\sqrt{2\pi\sigma}} e^{-\frac{(\lambda-353)^2}{2\sigma^2}} \qquad \text{(A-2)}$$

Solar Radiation:

Based on Assumption (2) in Section 6.1, the spectral specific irradiance due to the direct parallel fraction of the solar UV was derived through energy balance. The result can be expressed as:

$$w_\lambda^p = \begin{cases} 4.884\times10^{-3}(\lambda-300)\cdots\cdots for\ \psi=0 \\ 0\cdots\cdots\cdots\cdots\cdots\cdots for\ \psi\neq0 \end{cases} \qquad \text{(A-3)}$$

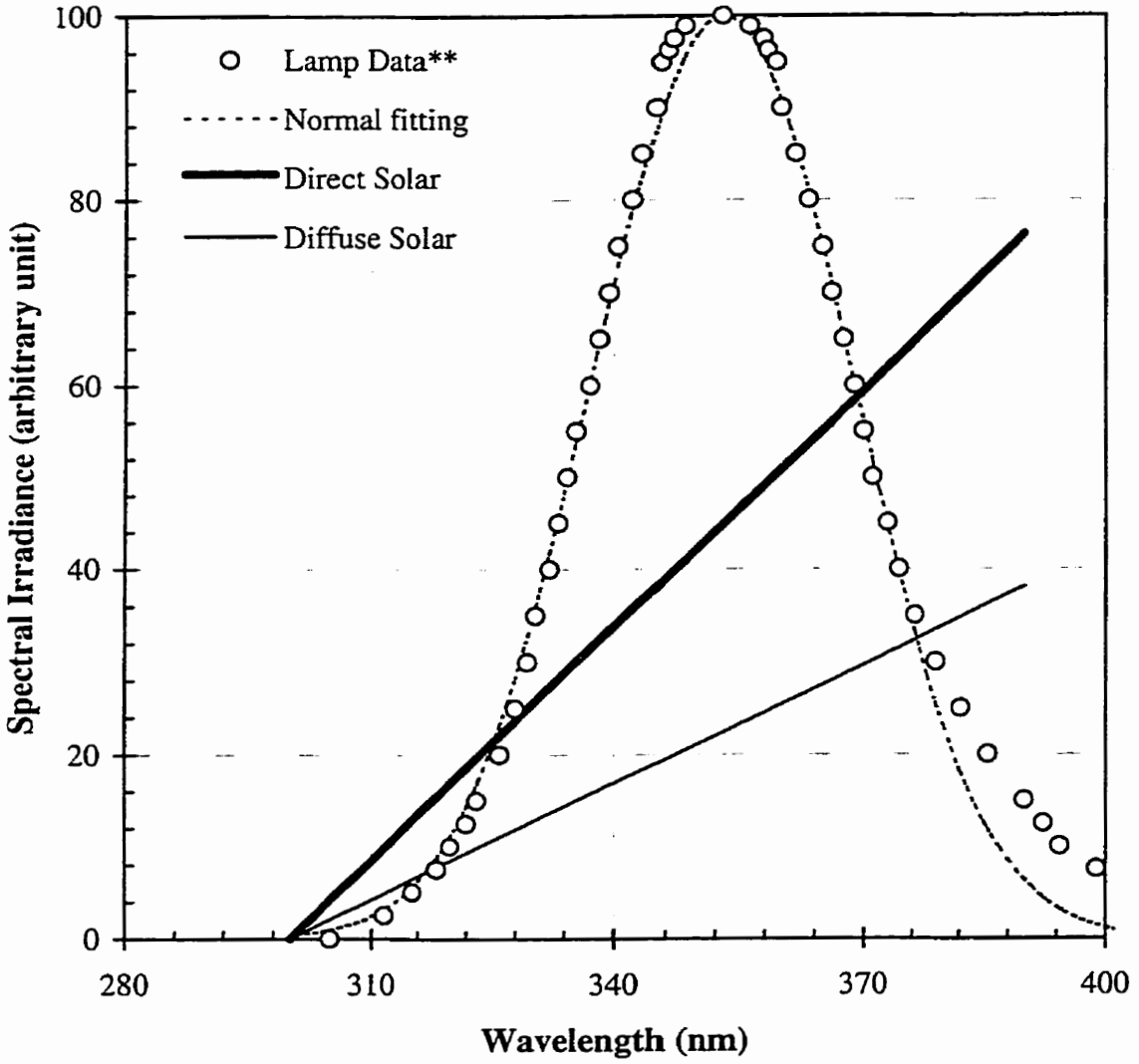

Figure A-1: Spectral Irradiance of Fluorescent Lamps and the Solar UV
**Philip Lighting Co., 1998

The spectral specific irradiance of the diffuse solar UV was also derived using the same method. The result is presented in Equation (A-4). The units in Equations (A-3) and (A-4) are both $W/m^2/Sr$.

$$w^{d}_{\lambda\psi} = \frac{2.442 \times 10^{-3}}{\pi}(\lambda - 300)\cos\psi \qquad \text{(A-4)}$$

A.2: Spectral Extinction Coefficient of the UV Transmitting Plexiglas

The UV transmission property of the Plexiglas used as the reactor cover was provided by the supplier. This information was given as the fraction of transmission through a quarter inch plate at different wavelengths. However, it was not clear what type of radiation pattern (i.e., direct parallel, diffuse, or spherical) the information was based on. Irradiance of the fluorescent lamps at 365 nm before and after penetrating the reactor cover was therefore measured with the radiometer. The experimental data approximately agreed with the supplier's specification. Therefore, diffuse radiation pattern should be an appropriate assumption to use in calculating the extinction coefficients of plastic material at different wavelengths.

After penetrating the Plexiglas plate, the spectral specific irradiance becomes:

$$w^{pn}_{\lambda\psi} = \frac{w_{\lambda}}{\pi}\cos\psi\, e^{-\frac{k_3\delta}{\cos\psi}} \qquad \text{(A-5)}$$

Integrating Equation (A-5) over all solid angles, we have:

$$fn_{\lambda}w_{\lambda} = \int_0^{\pi/2} w^{pn}_{\lambda\psi} 2\pi \sin\psi d\psi = w_{\lambda}\int_0^{\pi/2} e^{-\frac{k_3\delta}{\cos\psi}} 2\cos\psi \sin\psi d\psi \qquad \text{(A-6)}$$

The known spectral transmission information, fn_λ (from the plastic supplier for δ=0.25*2.54 cm), can therefore be used to calculate the spectral extinction coefficient, k_3, through Equation (A-7) below:

$$fn_\lambda = \int_0^{\pi/2} e^{-\frac{2.54 k_3}{4\cos\psi}} \sin 2\psi d\psi \qquad \text{(A-7)}$$

Extinction coefficient as a function of wavelength was obtained by solving Equation (A-7) with Maple V. The results are presented in Figure A-2.

A.3: Radiation Fields Under Lamp Radiation

Corrugated Plate:

Equations (A-8) through (A-16) are obtained based on the principles of analytical geometry. Under the coordinate system shown in Figure 6-1, the upper wing of the corrugated plate (uw) can be expressed as:

$$x - z\,tan\alpha = 0 \qquad \text{(A-8)}$$

where $0 \le x \le B$ and $-L/2 \le y \le L/2$

the lower wing (lw) can be expressed as:

$$x + z\,tan\alpha = 0 \qquad \text{(A-9)}$$

where $0 \le x \le B$ and $-L/2 \le y \le L/2$

and the reactor cover (cv) can be expressed as:

$$x = B \qquad \text{(A-10)}$$

where $-L/2 \le y \le L/2$ and $-B\,tan\alpha \le z \le B\,tan\alpha$

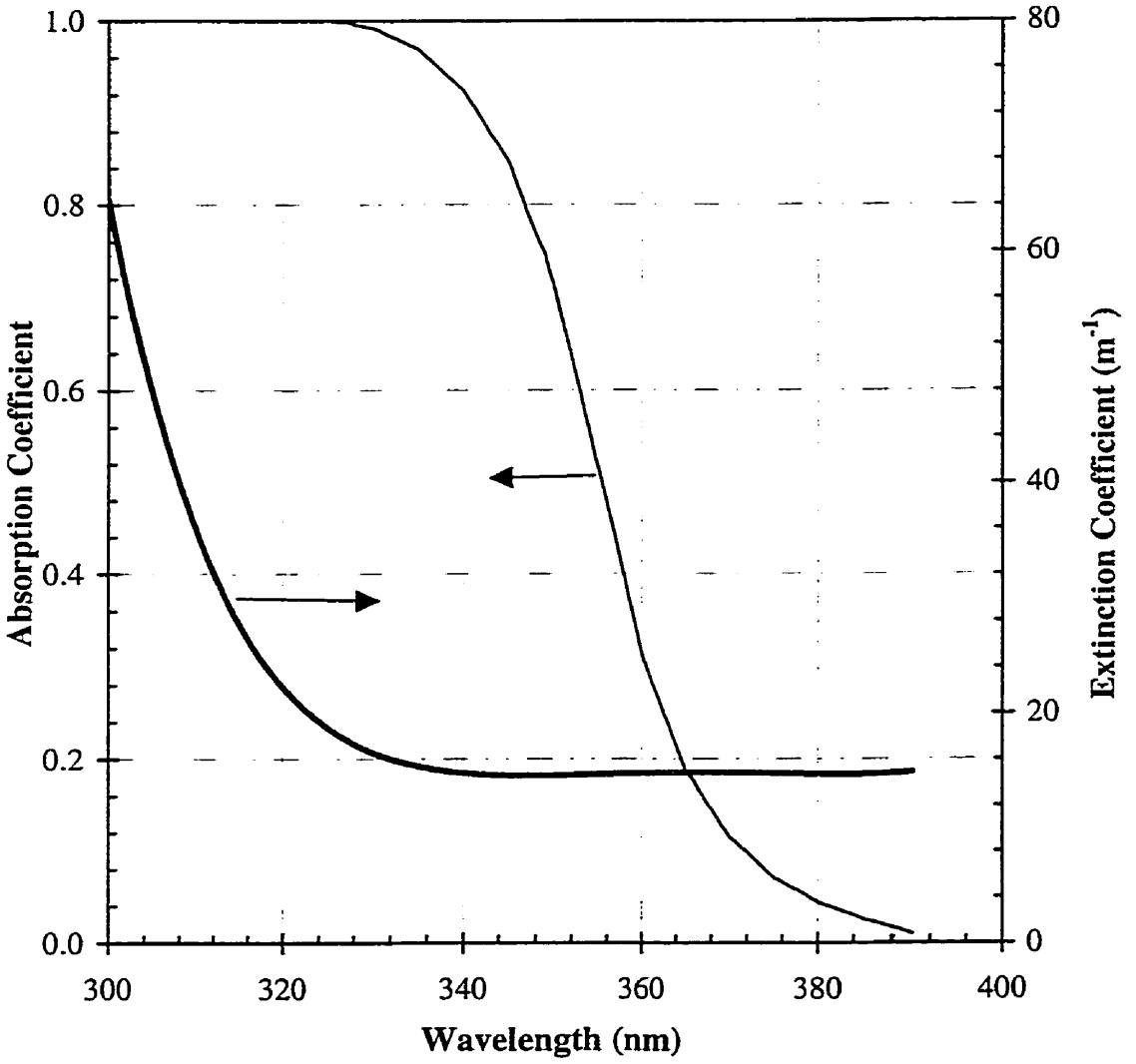

Figure A-2: Absorption Coefficient of the TiO_2 Film (Crittenden et al., 1995) and Extinction Coefficient of the UVT Acrylic

For points P'(x', y', z') on ***uw***, P"(x", y", z") on ***lw***, and P(x, y, z) on ***cv***, the square of the distance from P to P′ can be expressed as:

$$d_1^2 = (z'\cot\alpha - B)^2 + (y'-y)^2 + (z'-z)^2 \qquad \text{(A-11)}$$

and the square of the distance from P′′ to P′ can be expressed as:

$$d_2^2 = (\cot\alpha)^2(z'+z'')^2 + (y'-y'')^2 + (z'-z'')^2 \qquad \text{(A-12)}$$

The *cosine* of the angle between ***cv*** vector and line PP′ can be expressed as:

$$\cos\psi_2 = (B - z'\cot\alpha)/d_1 \qquad \text{(A-13)}$$

and the *cosine* of the angle between ***uw*** vector and line PP′ can be written as:

$$\cos\psi_1 = \sin\alpha\,(B - z\cot\alpha)/d_1 \qquad \text{(A-14)}$$

The *cosine* of the angle between ***lw*** vector and line P′′P′ can be expressed as:

$$\cos\psi_4 = 2z'\cos\alpha/d_2 \qquad \text{(A-15)}$$

and the *cosine* of the angle between ***uw*** vector and line P′′P′ can be written as:

$$\cos\psi_5 = 2z''\cos\alpha/d_2 \qquad \text{(A-16)}$$

Based on the principles of geometric optics, the spectral radiative energy incident on point P'(x',y',z'), due to the radiation from the reactor cover, can be written as:

$$I^{cv}_{\lambda-uw}(y',z') = \iint_{cv} \frac{w_\lambda}{\pi} \frac{\cos\psi_1 \cos\psi_2}{d_1^2} e^{-\frac{k_3\delta}{\cos\psi_2} - k_4 d_1}\, dydz \qquad \text{(A-17)}$$

Within the wavelength range in question, the extinction coefficient of the reaction medium, k_4, is zero for the artificial wastewater used in this study.

If the photons reflected from the lower wing could be ignored, the relationship between the incident energy and the absorbed one at wavelength λ could then be expressed by Equation (A-18).

$$q_{\lambda-uw}(y',z') = a(\lambda) I_{\lambda-uw}(y',z') \qquad \text{(A-18)}$$

Actually, as a results of the absorption of the photons reflected from the lower wing, neither Equation (A-17) nor Equation (A-18) give the LASREA on the upper wing. In order to calculate the LASREA, a special procedure has been developed and presented in next section.

Flat Plate:

The radiation field on the flat plate was modeled similarly. The spectral radiative energy incident on any point on the flat plate (x',y',z') was derived to be:

$$I^{cv}_{\lambda-fl}(y',z') = \iint_{cv} \frac{w_\lambda B^2}{4\pi d^4} e^{-\frac{2dk_3\delta}{B} - k_4 d} dydz \qquad \text{(A-19)}$$

Where is the distance between the reference point on the flat plate (x',y',z') and the reactor cover (x,y,z) and can be found based on the equation below:

$$d^2 = B^2/4 + (y'-y)^2 + (z'-z)^2 \qquad \text{(A-20)}$$

Since no photon will be reflected back to the flat plate, the LASREA can be conveniently calculated using:

$$q_{\lambda-fl}(y',z') = a(\lambda) I_{\lambda-fl}(y',z') \qquad \text{(A-21)}$$

A.4: Radiation Field Under Solar Radiation

Contributions from the diffuse part of the solar UV can be modeled using the equations in Section A.3, except that $w^d_{\lambda\psi}$ from Equation (A-4) should be used in stead of $w_{\lambda\psi}$ from Equation (A-2). Based on geometric optics, the spectral radiative energy incident on point

P'(x',y', z'), due to the direct parallel part of the solar UV from the reactor cover, has been derived to be:

$$I_{\lambda}^{p} = w_{\lambda\psi}^{p} \sin\alpha\, e^{-k_{\lambda}\delta} \qquad \text{(A-22)}$$

This equation holds for both corrugated and flat ($\alpha=\pi/2$) plates.

A.5: Procedure for the Calculation of the LASREA

Step (1): Imagine at time "t" photons have just contacted on the two wings of the corrugated plate from the reactor cover and no reflection occurred yet. The spectral radiative energy incident on any location of the upper wing [i.e., $I_{\lambda-uw}^{cv}(y',z')$] can be calculated from Equations (A-5), (A-11), (A-13), (A-14), and (A-17). Let:

$$I_{\lambda-uw}^{(0)}(y',z') = I_{\lambda-uw}^{cv}(y',z') \qquad \text{(A-23)}$$

and

$$q_{\lambda-uw}^{(0)}(y',z') = a(\lambda) I_{\lambda-uw}^{(0)}(y',z') \qquad \text{(A-24)}$$

Since the radiation field of the upper and lower wings of the corrugated plate are symmetric to *plane: z=0*,

$$I_{\lambda-lw}^{(0)}(y',z') = I_{\lambda-uw}^{(0)}(y',-z') \qquad \text{(A-25)}$$

Step (2): Imagine at time "t+Δt" photons on the two wings of the corrugated plate just finished their first reflection (to conjugated wing and to reactor cover). The spectral radiative energy incident on any location of the upper wing due to this

reflection can be calculated based on:

$$I^{(1)}_{\lambda-uw}(y',z') = \frac{(1-a(\lambda))}{\pi}\iint_{lw}\frac{I^{(0)}_{\lambda-uw}(y,-z)\cos\psi_4\cos\psi_5}{d_2^2}e^{-k_\lambda d_2}\,dydz \qquad \text{(A-26)}$$

The fraction that can be absorbed is:

$$q^{(1)}_{\lambda-uw}(y',z') = a(\lambda)I^{(1)}_{\lambda-uw}(y',z') \qquad \text{(A-27)}$$

Since the radiation field of the upper and lower wings of the corrugated plate are symmetric to *plane: z=0*,

$$I^{(1)}_{\lambda-lw}(y',z') = I^{(1)}_{\lambda-uw}(y',-z') \qquad \text{(A-28)}$$

Step (3): Imagine at time "t+2Δt" photons on the two wings of the corrugated plate just finished their second reflection (to conjugated wing and to reactor cover). The spectral radiative energy incident on any location of the upper wing due to this reflection can be calculated based on:

$$I^{(2)}_{\lambda-uw}(y',z') = \frac{(1-a(\lambda))}{\pi}\iint_{lw}\frac{I^{(1)}_{\lambda-uw}(y,-z)\cos\psi_4\cos\psi_5}{d_2^2}e^{-k_\lambda d_2}\,dydz \qquad \text{(A-29)}$$

The absorbed part can be calculated using:

$$q^{(2)}_{\lambda-uw}(y',z') = a(\lambda)I^{(2)}_{\lambda-uw}(y',z') \qquad \text{(A-30)}$$

Since the radiation field of the upper and lower wings of the corrugated plate are symmetric to *plane: z=0*,

$$I^{(2)}_{\lambda-lw}(y',z') = I^{(2)}_{\lambda-uw}(y',-z') \qquad \text{(A-31)}$$

••••••••••••••••

Step (n+1): Imagine at time "t+nΔt" photons on the two wings of the corrugated plate just finished their "n" th reflection (to conjugated wing and to reactor cover). The spectral radiative energy incident on any location of the upper wing due to this reflection can be calculated based on:

$$I^{(n)}_{\lambda-uw}(y',z') = \frac{(1-a(\lambda))}{\pi}\iint_{lw} \frac{I^{(n-1)}_{\lambda-uw}(y,-z)\cos\psi_4\cos\psi_5}{d_2^2} e^{-k_\lambda d_2}\, dydz \quad \text{(A-32)}$$

The absorbed part can be calculated using:

$$q^{(n)}_{\lambda-uw}(y',z') = a(\lambda) I^{(n)}_{\lambda-uw}(y',z') \quad \text{(A-33)}$$

Since the radiation field of the upper and lower wings of the corrugated plate are symmetric to *plane: z=0*,

$$I^{(n)}_{\lambda-lw}(y',z') = I^{(n)}_{\lambda-uw}(y',-z') \quad \text{(A-34)}$$

After sufficient times of reflections, the calculation stopped based on the criterion:

$$\iint_{uw} I^{(n)}_{\lambda-uw}(y',z')dy'dz' \le \iint_{uw} 0.01 \times I^{(1)}_{\lambda-uw}(y',z')dy'dz' \quad \text{(A-35)}$$

The LASREA was calculated with:

$$q_{uw}(y',z') = q_{lw}(y',-z') =$$
$$\int_{300}^{390} \{q^{(0)}_{\lambda-uw}(y',z') + q^{(1)}_{\lambda-uw}(y',z') + \ldots\ldots + q^{(n)}_{\lambda-uw}(y',z')\}d\lambda \quad \text{(A-36)}$$

APPENDIX B: MODEL FOR LOCAL MASS TRANSFER RATE ON CORRUGATED PLATES

Under the coordinate system shown in Figure B-1, consider the projection of the corrugated plate on *plane: y=0*. Point P on the projection of *UW* can be expressed as P{x, xtanα}. The geometric center of the triangle formed by *UW*, *LW*, and *CV*, A, can be located with A{B[1-tanαtan(π/4-α/2)], 0} or {B/(1+sinα), 0}. The distance from the geometric center to any point on *UW* is then:

$$|P'\Omega| = \sqrt{(x - \frac{B}{1+\sin\alpha})^2 + x^2\tan^2\alpha} = \frac{1}{\cos\alpha}\sqrt{(x - \frac{B}{1+\sin\alpha})^2 + (\frac{B\sin\alpha\cos\alpha}{1+\sin\alpha})^2} \qquad \text{(B-1)}$$

According to the assumptions in Section 7.2, there exist:

$$\int_0^B k\,dx = \int_0^B \frac{\bar{k}\cdot Const}{|P'\Omega|}dx = \bar{k}B \qquad \text{(B-2)}$$

The integration constant, *Const*, can be determined from Equation (B-2) to be:

$$Const = \frac{B}{\cos\alpha \bullet \ln\left|\frac{\sin\alpha(1+\sin\alpha)}{\cos\alpha(1-\cos\alpha)}(1+\sqrt{\frac{2}{1+\sin\alpha}})\right|} \qquad \text{(B-3)}$$

Substituting Equation (B-3) into Equation (B-2), we have:

$$k_L = \bar{k}_L B \Big/ \left\{\sqrt{(x - \frac{B\cos^2\alpha}{1+\sin\alpha})^2 + (\frac{B\sin\alpha\cos\alpha}{1+\sin\alpha})^2} \bullet \ln\left|\frac{\sin\alpha(1+\sin\alpha)}{\cos\alpha(1-\cos\alpha)}(1+\sqrt{\frac{2}{1+\sin\alpha}})\right|\right\} \qquad \text{(B-4)}$$

This is identical with Equation (7-2).

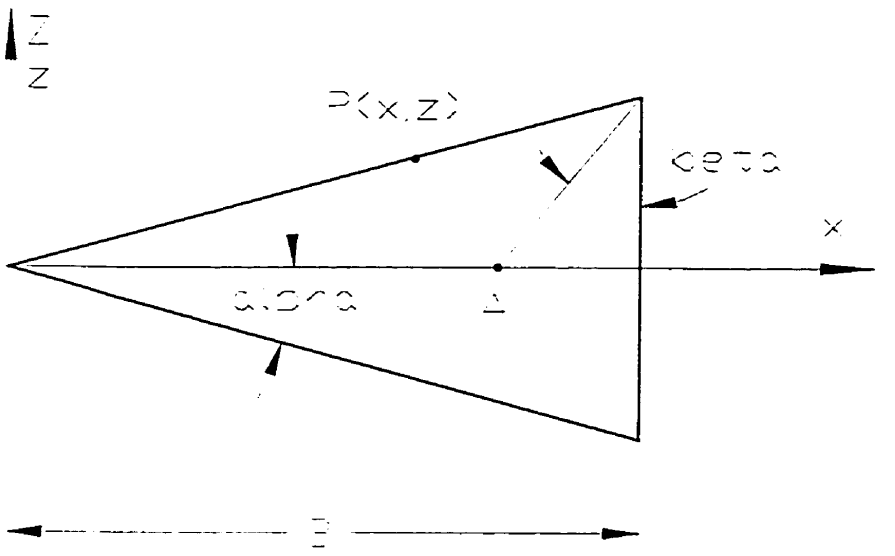

$\beta=45°-\alpha/2$; **P**(x, x *tan*α); **A**[B(1-*tan*α *tan* β), 0]

Figure B-1: Coordinate System Used in Mass Transfer Model Development

APPENDIX C: NEW KINETIC MODEL DEVELOPMENT

Based on Assumption 3 in Chapter 8, parent compound consumption rate can be calculated with Equation (C-1) below. The integration is over the whole catalyst surface.

$$V\frac{dC}{dt} = -\iint_S r_{4cp}\,dS \tag{C-1}$$

Since all reactants are transferred from the liquid bulk to catalyst surfaces, Equations (C-2) and (C-3) are applicable.

$$r_{4cp} = k_{4cp}(C - C_s) \tag{C-2}$$

$$r_{O_2} = k_{O_2}(O_b - O_s) \tag{C-3}$$

According to Assumption 1 in Chapter 8, the reaction stoichiometry can be written as Equation (C-4), from which the ratio of 4-chlorophenol and oxygen consumption rates can be determined to be 257/416 (by mass).

$$2\ C_6H_4ClOH + 12\ O_2 = 12\ CO_2 + 4\ H_2O + 2\ HCl \tag{C-4}$$

Based on the film theory in mass transfer (McCabe, Smith, and Harriott, 1993), the effect of diffusivity can be expressed by Equation (C-5).

$$\frac{k_{4cp}}{k_{O_2}} = \left(\frac{D_{4cp}}{D_{O_2}}\right)^{\frac{2}{3}} \tag{C-5}$$

Applying Assumption (4) into Equation (C-2), there exist:

$$k_0(q/q_0)^n\left(\frac{D_{O_2}}{D_{4cp}}\right)^{\frac{2}{3}}C_s = (1 + K_1C_s)(1 + k_{O_2}O_s)(C - C_s) \tag{C-6}$$

Oxygen concentration on the catalyst surfaces can be solved from Equations (C-2) through (C-5) to be:

$$O_s = O_b - \frac{416}{257}\left(\frac{D_{4cp}}{D_{O_2}}\right)^{\frac{2}{3}}(C - C_s) \qquad \text{(C-7)}$$

Due to Assumption 2 and Equation (C-1), parent compound concentration in the reservoir at any run time can be derived to be:

$$C = C_0 - \int_0^t \{\iint_S r_{4cp}\, dS\}\frac{dt}{V} \qquad \text{(C-8)}$$

Since bulk oxygen concentration (O_b), local mass transfer coefficients (k_{4cp} and k_{O_2}), LASREA (q), diffusivities of the reactants (D_{4cp} and D_{O_2}), and total water volume (V) are all known, Equations (C-6), (C-7), (C-2), and (C-8) form a complete model.

The derivatives of the local reaction rate with respect to the model parameters were obtained based on Assumption (4). They are:

$$\frac{\partial r_{4cp}}{\partial k_0} = \frac{r_{4cp}}{k_0} \qquad \text{(C-9)}$$

$$\frac{\partial r_{4cp}}{\partial K_1} = -\frac{C_s r_{4cp}}{(1 + K_1 C_s)} \qquad \text{(C-10)}$$

$$\frac{\partial r_{4cp}}{\partial n} = \frac{n r_{4cp}}{q} \qquad \text{(C-11)}$$

APPENDIX D: CALIBRATION CURVES

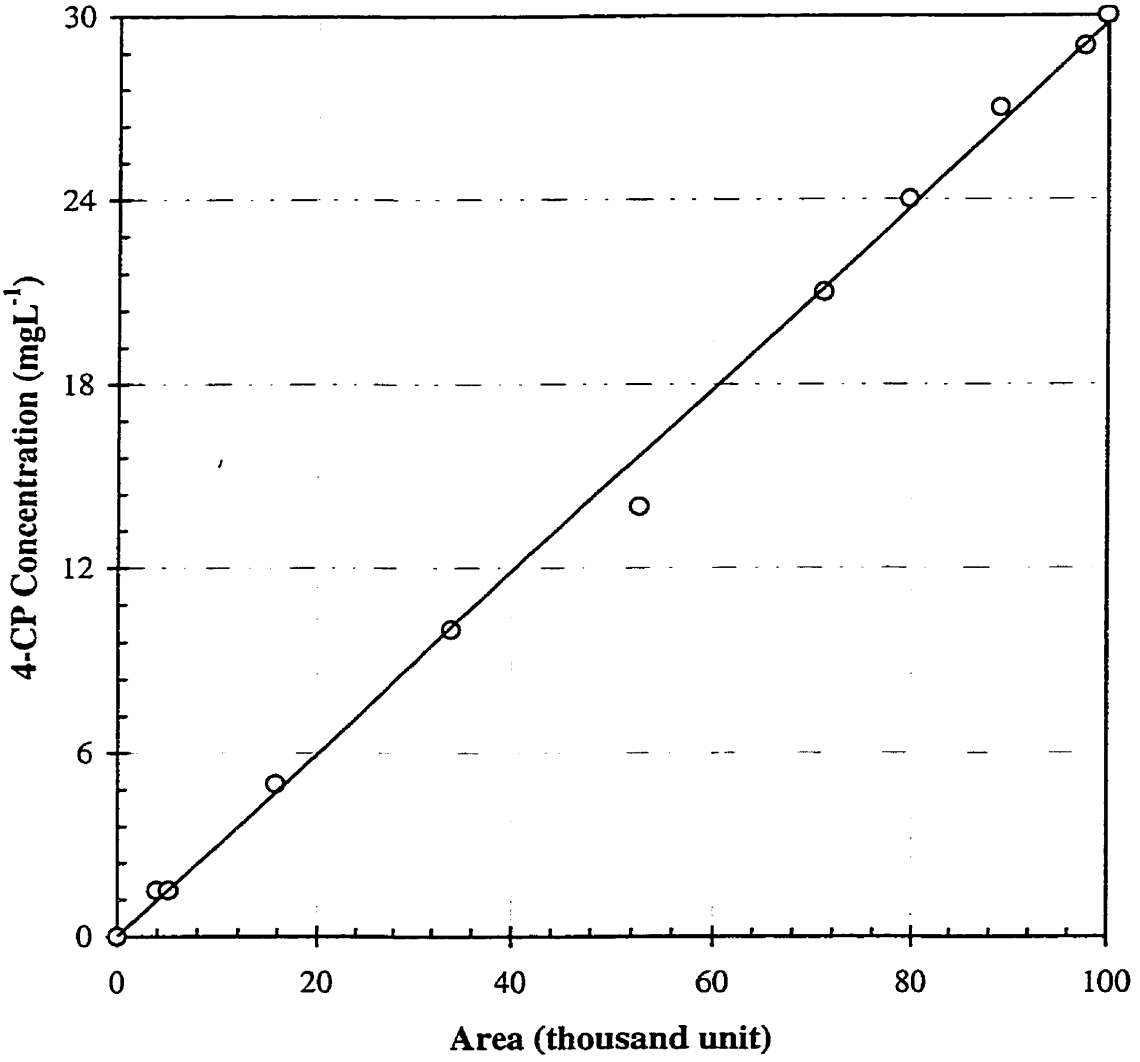

Figure D-1: HPLC Calibration Curve: 4-CP Concentration

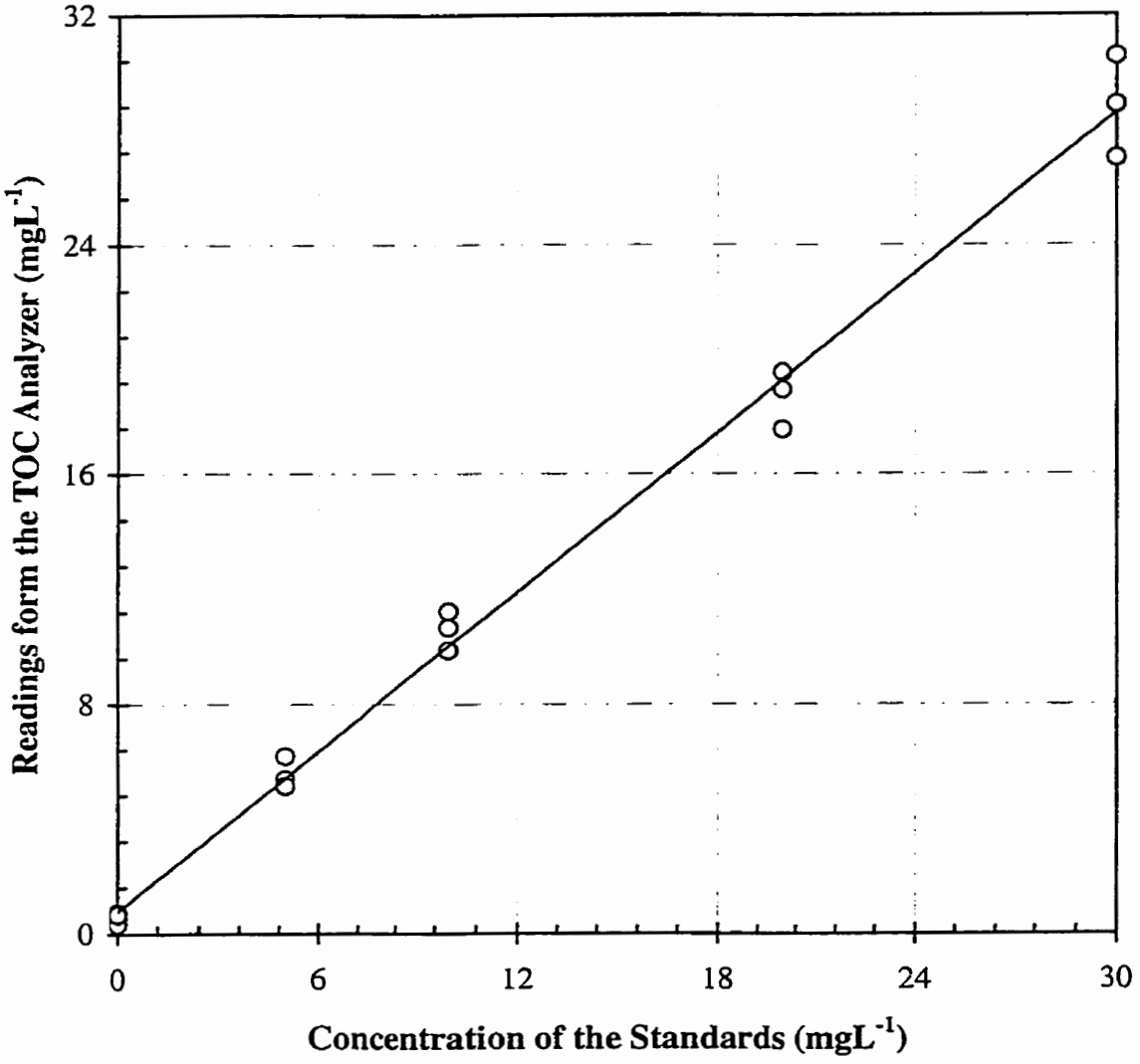

Figure D-2: A Typical Calibration Curve for TOC Measurement

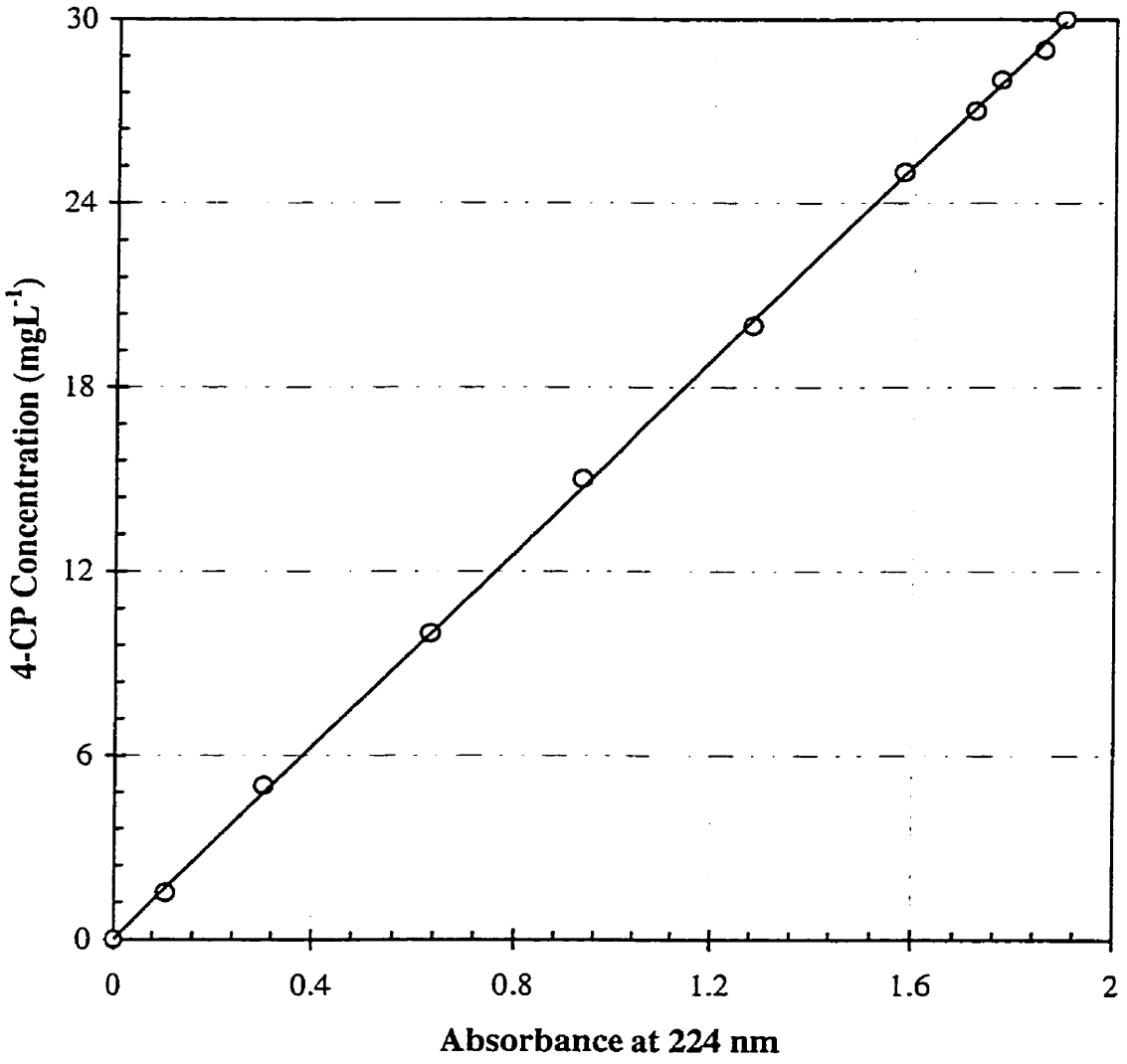

Figure D-3: Spectrophotometer Calibration Curve: 4-CP Concentration

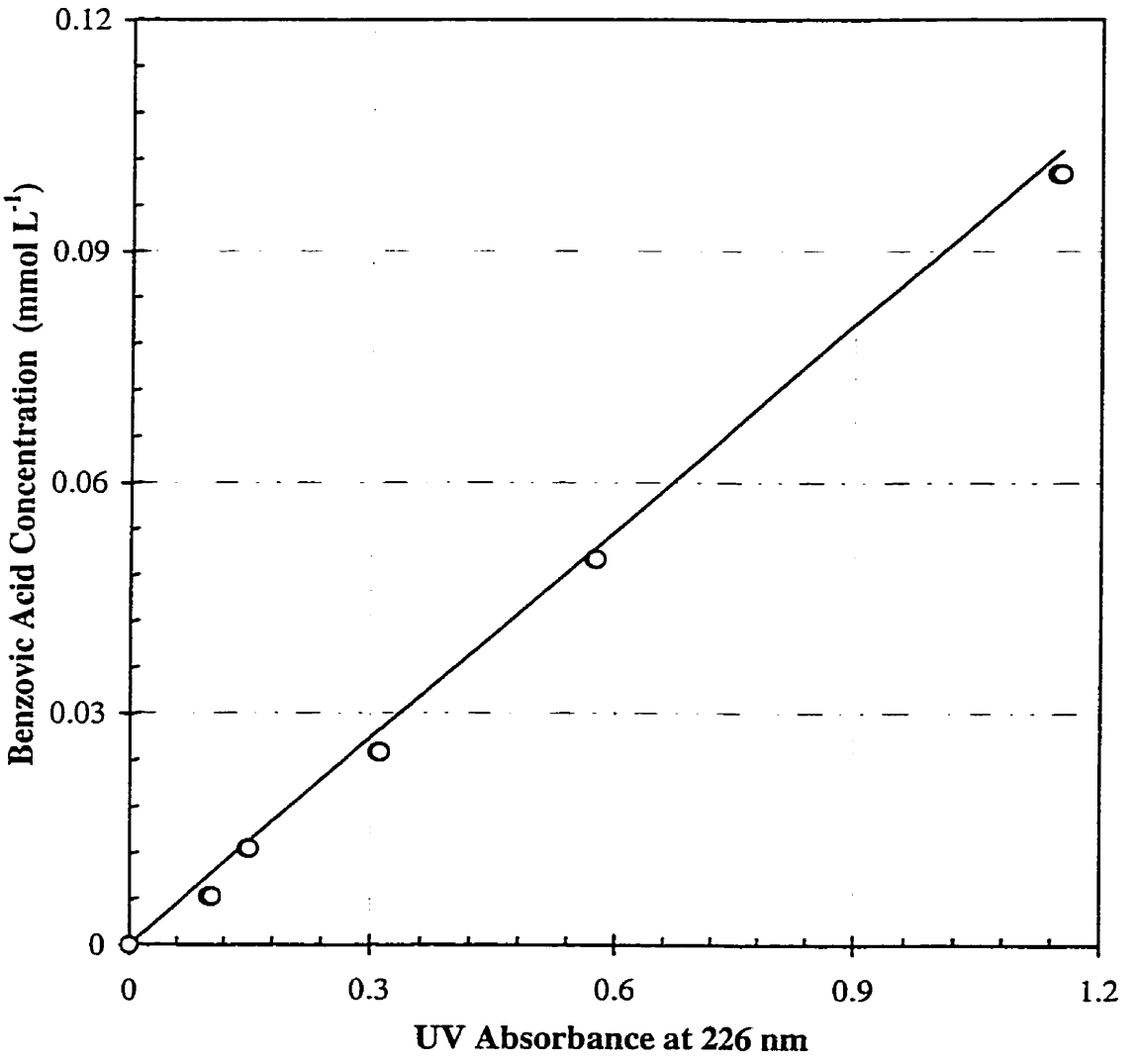

Figure D-4: Spectrophotometer Calibration Curve: Benzoic Acid Concentration

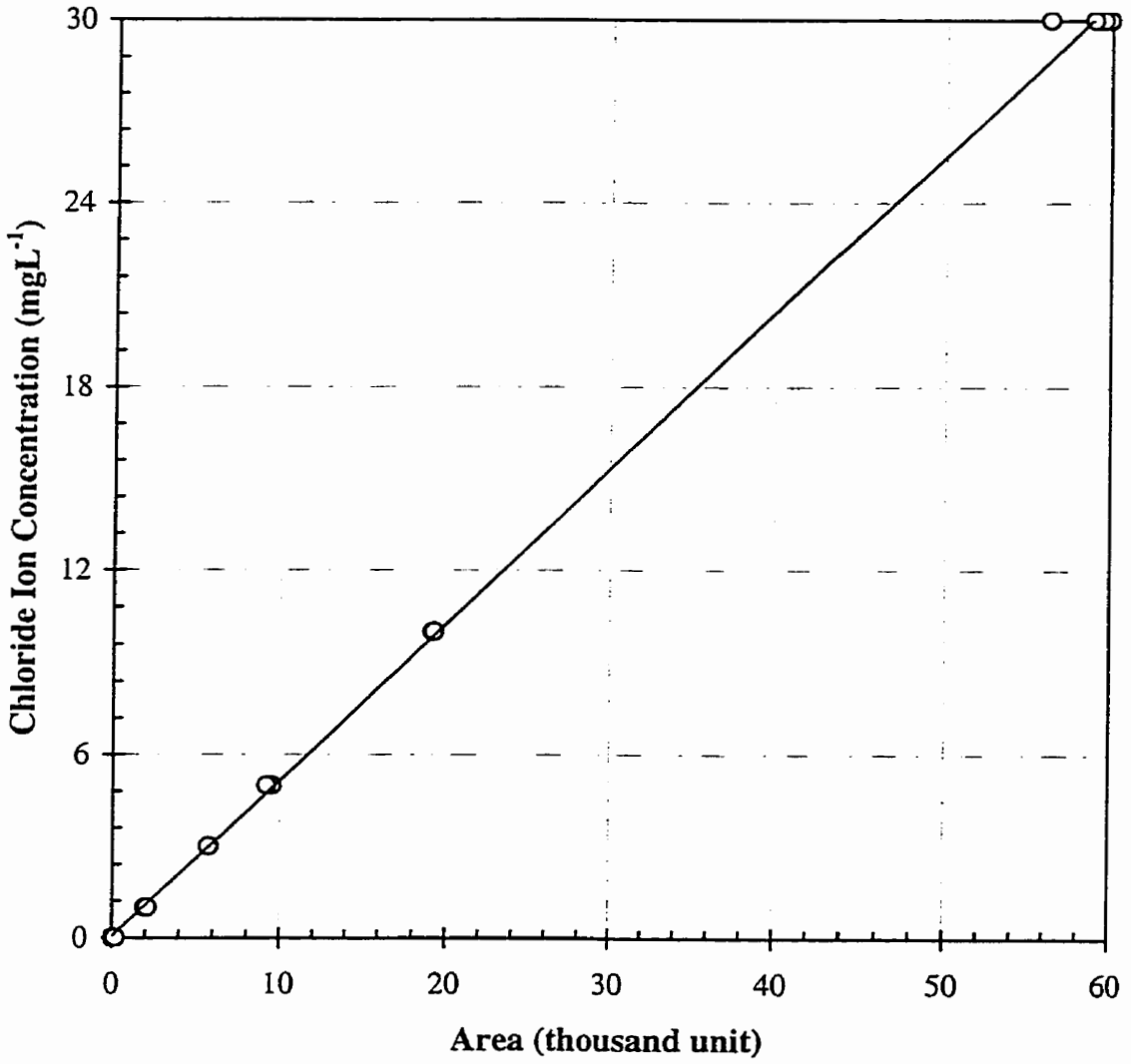

Figure D-5: Ion Chromatography Calibration Curve: Chloride Ion